Catalysis Communications 9 (2008) 2297–2302

Contents lists available at ScienceDirect

Catalysis Communications

journal homepage: www.elsevier.com/locate/catcom

Selective hydrogenation of acetylene over Pd catalysts supported on nanocrystalline α-Al_2O_3 and Zn-modified α-Al_2O_3

Suthana Chinayon [a], Okorn Mekasuwandumrong [b], Piyasan Praserthdam [a], Joongjai Panpranot [a,*]

[a] Center of Excellence on Catalysis and Catalytic Reaction Engineering, Department of Chemical Engineering, Faculty of Engineering, Chulalongkorn University, Bangkok 10330, Thailand

[b] Department of Chemical Engineering, Faculty of Engineering and Industrial Technology, Silpakorn University, Nakorn Pathom 73000, Thailand

ARTICLE INFO

Article history:
Received 18 December 2007
Received in revised form 7 March 2008
Accepted 17 March 2008
Available online 20 March 2008

Keywords:
Selective acetylene hydrogenation
Pd/α-Al_2O_3
Zn-modified α-Al_2O_3
Sol–gel
Solvothermal
Nanocrystalline α-Al_2O_3

ABSTRACT

The catalytic performance of Pd catalysts supported on nanocrystalline α-Al_2O_3 and Zn-modified α-Al_2O_3 prepared by sol–gel and solvothermal methods was studied in the selective hydrogenation of acetylene. Acidity of the nanocrystalline α-Al_2O_3 was significantly decreased by incorporation of Zn atoms in the α-Al_2O_3. Both of acetylene conversions and ethylene selectivities were improved in the order: Pd/Zn-modified α-Al_2O_3-sol–gel > Pd/Zn-modified α-Al_2O_3-solvothermal > Pd/α-Al_2O_3-sol–gel ≈ Pd/α-Al_2O_3-solvothermal >> Pd/α-Al_2O_3-commerical. As revealed by thermal gravimetric and differential temperature analysis (TG-DTA), Pd catalysts on the nanocrystalline Zn-modified α-Al_2O_3 also showed less deactivation by coke formation.

1. Introduction

Pd-based catalyst supported on Al_2O_3 with low Pd loading (0.1–0.3 wt.%) is typically employed for selective hydrogenation of acetylene in ethylene feedstock [1–3]. Removal of acetylene is a crucial process in polyethylene production since acetylene poisons the polymerization catalysts [4,5]. The Al_2O_3 used as Pd catalyst support in this reaction contains mostly the α-phase Al_2O_3 since it possesses relatively low specific surface area and low acidity compared to other 'transition' alumina (such as β-, γ-, η-, χ-, κ-, δ-, θ-phase Al_2O_3). With respect to selectivity changes, catalysts with low dispersion were suggested to give better selectivity toward ethylene [1,2].

In recent years, nanocrystalline materials have gained considerable interest in the field of catalysis because they show significant differences in terms of catalytic activity and selectivity compared with those synthesized in micron scale. Several techniques have been reported for preparation of nanocrystalline Al_2O_3 such as sol–gel method [6], hydrothermal synthesis [7], microwave synthesis [8], emulsion evaporation [9], precipitation from solution [10], and solvothermal synthesis [11]. The sol–gel method is widely used due to its simplicity, however, the precipitated powders obtained are amorphous in nature and further heat treatment is required for crystallization. Solvothermal method is an alternative route for one-step synthesis of nanocrystalline materials.

In the present study, nanocrystalline α-Al_2O_3 and Zn-modified α-Al_2O_3 have been synthesized via sol–gel and solvothermal methods and employed as supports for Pd catalysts for selective hydrogenation of acetylene. Modification of nanocrystalline α-Al_2O_3 with zinc is studied because it can form $ZnAl_2O_4$ spinel which is an interesting material with low acidity that can exhibit the strong metal-support interaction (SMSI) with noble metal [12–14]. Based on the work reported by Moon et al. [15], addition of TiO_2 to Pd/SiO_2 catalysts has shown improvement in ethylene selectivity and less catalyst deactivation during selective acetylene hydrogenation. The origin of the improvement in catalyst performance was proposed to be due to strong interaction between the added TiO_2 and Pd. Thus, the presence of $ZnAl_2O_4$ in the Pd/α-Al_2O_3 catalyst may improve the catalytic performance in the selective acetylene hydrogenation as well. The molar ratio of Zn/Al = 0.1 was selected in order to avoid the formation of $ZnAl_2O_4$ alone so that surface area of the Zn-modified supports were not much different from that of the unmodified α-Al_2O_3. The catalysts were characterized by X-ray diffraction (XRD), N_2 physisorption, ammonia temperature program desorption (NH_3-TPD), CO chemisorption, transmission electron microscope (TEM), and thermal gravimetric and differential temperature analysis (TG/DTA).

* Corresponding author. Tel.: +66 2 2186883; fax: +66 2 2186877.
E-mail address: joongjai.p@eng.chula.ac.th (J. Panpranot).

1566-7367/$ - see front matter © 2008 Elsevier B.V. All rights reserved.
doi:10.1016/j.catcom.2008.03.032

2. Experimental

2.1. Catalyst preparation

Nanocrystalline α-Al_2O_3 were prepared by sol–gel and solvothermal methods. In the sol–gel method, 24 g of aluminum nitrate was dissolved in 50 ml of ethanol at room temperature. The solution was then heated to 70–80 °C in the reflux-condenser reactor and held for 18 h, after which the urea solution was added to adjust pH of sol. The mixture was rested at the same temperature for 24 h to be gelled at neutral condition. The obtained product was calcined with two steps heating rate to avoid overflowing of gel during calcinations, i.e. 3 °C/min from room temperature to 500 °C and continue heating at 5 °C/min to 1150 °C and held at that temperature for 3 h. The solvothermal-derived α-Al_2O_3 were prepared according to the method described in Ref. [16] using aluminum isopropoxide and toluene. For the preparation of Zn-modified α-Al_2O_3 by sol–gel and solvothermal method, an appropriate amount of zinc (II) nitrate hexahydrate and zinc (II) acetylacetonate (Zn/Al molar ratio = 0.1) were added to the precursor mixture of each method, respectively.

Approximately 0.3 wt.% Pd on α-Al_2O_3 and Zn-modified α-Al_2O_3 were prepared by the incipient wetness impregnation technique using an aqueous solution of the desired amount of $Pd(NO_3)_2$ (Aldrich). The catalysts were dried overnight at 110 °C and then calcined in N_2 flow 60 ml/min with a heating rate of 10 °C/min until the temperature reached 500 °C and them in air flow 100 ml/min at 500 °C for 2 h. For comparison purposes, a commercial α-Al_2O_3 (JRC-ALO2) was also employed as Pd catalyst support.

2.2. Catalyst characterization

X-ray diffraction patterns of the catalyst samples were obtained with a SIEMENS D5000 X-ray diffractometer using Cu Kα radiation with a Ni filter. The BET surface area measurements were carried out by nitrogen adsorption in a Micromeritic Chemisorb 2750 system. Each sample was degassed at 200 °C for 2 h. The analysis gas consisting of 30% N_2 in helium was adsorbed on the samples at low temperature by dipping cell into liquid nitrogen dewar. Ammonia temperature program desorption (NH_3-TPD) was performed in a Micromeritic Chemisorb 2750 automated system attached with ChemiSoft TPx software. Approximately 0.1 g of catalyst was placed in a quartz tube in a temperature-controlled oven. The amounts of CO chemisorbed on the catalyst were measured using a Micromeritic Chemisorb 2750 automated system attached with ChemiSoft TPx software at room temperature. Prior to chemisorption, the sample was reduced in a H_2 flow at 150 °C for 2 h then cooled down to ambient temperature in a He flow. The distribution of palladium on catalyst supports were observed using JEOL Model JEM-2010 transmission electron microscope operated at 200 keV. Thermal gravimetric and differential temperature analysis (TG/DTA) were performed using an SDT Analyzer Model Q600 from TA Instruments, USA.

2.3. Reaction study

Selective acetylene hydrogenation was performed in a pyrex tube reactor (i.d. 10.1 mm). Prior to the start of each experimental run, the catalyst was reduced in H_2 at 150 C for 2 h. Then the reactor was purged with Ar and cooled down to the reaction temperature. Feed gas was composed of 1.5% C_2H_2, 1.7% H_2 and balanced C_2H_4 (TIG Co., Ltd.) with a GHSV of 16,901 h^{-1}. The composition of products and feeds were analyzed by a Shimadzu GC 8A equipped with TCD and FID detectors (molecular sieve-5A and carbosieve S2 columns, respectively). The temperature dependence of the catalytic performance was observed during the range of 40–100 C in 20 C increments.

Acetylene conversion is defined as moles of acetylene converted with respect to acetylene in feed. Ethylene selectivity is defined as the percentage of acetylene hydrogenated to ethylene over totally hydrogenated acetylene. However, due to the difficulty in precise measurement of the ethylene change in the feed and product, the indirect calculation using the difference in the hydrogen amount (hydrogen consumed) was used. The ethylene being hydrogenated to ethane is the difference between all the hydrogen consumed and all the acetylene totally hydrogenated.

$$\text{Selectivity of } C_2H_4\ (\%) = \frac{100 \times [dC_2H_2 - (dH_2 - dC_2H_2)]}{dC_2H_2} \quad (1)$$

where dC_2H_2 = mole of acetylene in feed − mole of acetylene in product, dH_2 = mole of hydrogenation in feed − mole of hydrogen in product.

3. Results and discussion

The XRD patterns of Pd/α-Al_2O_3 and Pd/Zn-modified α-Al_2O_3 are shown in Fig. 1. The diffraction patterns were not different from those of the corresponding unmodified α-Al_2O_3 and Zn-modified α-Al_2O_3 supports. The characteristic peaks of α-Al_2O_3 were evident for Pd/α-Al_2O_3 samples while the diffraction lines of both spinel-type $ZnAl_2O_4$ structure and α-Al_2O_3 were apparent for the Pd/Zn-modified α-Al_2O_3 catalysts. The average crystallite sizes of each crystal phase were calculated from the Scherrer equation and are given in Table 1. The crystallite sizes α-Al_2O_3 and $ZnAl_2O_4$ were calculated from the full width at half maximum of the XRD peaks at $2\theta = 43°$ and 37°, respectively. The average crystallite sizes of the α-Al_2O_3 prepared by sol–gel and solvothermal method were 31 and 69.5 nm, respectively while the crystallite sizes of $ZnAl_2O_4$ formed in the Zn-modified Al_2O_3 prepared by sol–gel and solvothermal method were 28 and 14.9 nm, respectively. The surface areas of the catalysts prepared by sol–gel were ranged from 1.6 to 2.3 m^2/g while those prepared by solvothermal were ranged from 10.5 to 14.9 m^2/g. The surface areas were quite low probably due to high agglomeration of these nanocrystalline particles during calcination at high temperature. The nitrogen adsorption–desorption isotherms and the pore size distribution plots are shown in Figs. 2 and 3, respectively. Based on the nitrogen adsorption–desorption isotherms at 77 K, all the samples exhibited Type IV adsorption isotherms according to Brunauer Deming, Deming and Teller (BDDT) classification [17]. The sol–gel Al_2O_3, however, pos-

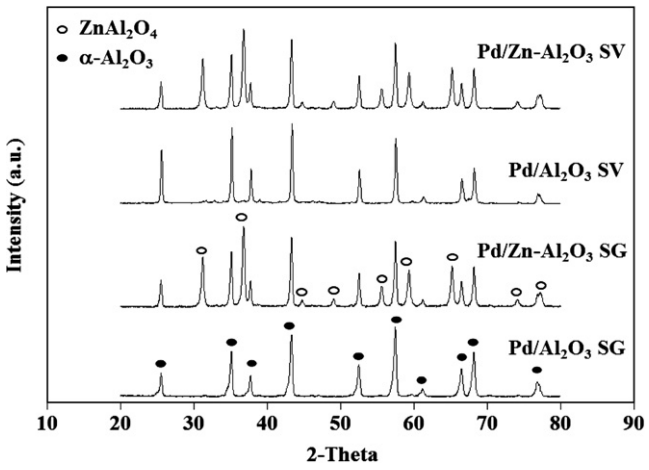

Fig. 1. XRD patterns of the Pd/α-Al_2O_3 and Pd/Zn-modified α-Al_2O_3 supports prepared by sol–gel (SG) and solvothermal (SV) methods.

Table 1
Characteristics of the various Pd/α-Al_2O_3 and Pd/Zn-modified α-Al_2O_3 catalysts

Sample	Crystallite size (nm)		BET surface area (m^2/g)	Pore volume (cm^3/g)	Average pore diameter (nm)	Pd active sites ($\times 10^{-17}$ molecule CO/g cat.)	Pd dispersion (%)	d_P Pd^0 (nm)
	α-Al_2O_3	$ZnAl_2O_4$						
Pd/Al_2O_3 SG	31.0	n.d.[a]	1.6	0.011	20.4	11.3	8.8	13
Pd/Zn–Al_2O_3 SG	40.4	28	1.9	0.020	11.8	4.9	3.9	29
Pd/Al_2O_3 SV	69.5	n.d.	14.9	0.075	13.6	32.9	20.8	5
Pd/Zn–Al_2O_3 SV	32.8	14.9	10.7	0.100	22.4	22.8	16.6	7

[a] n.d. = not determined.

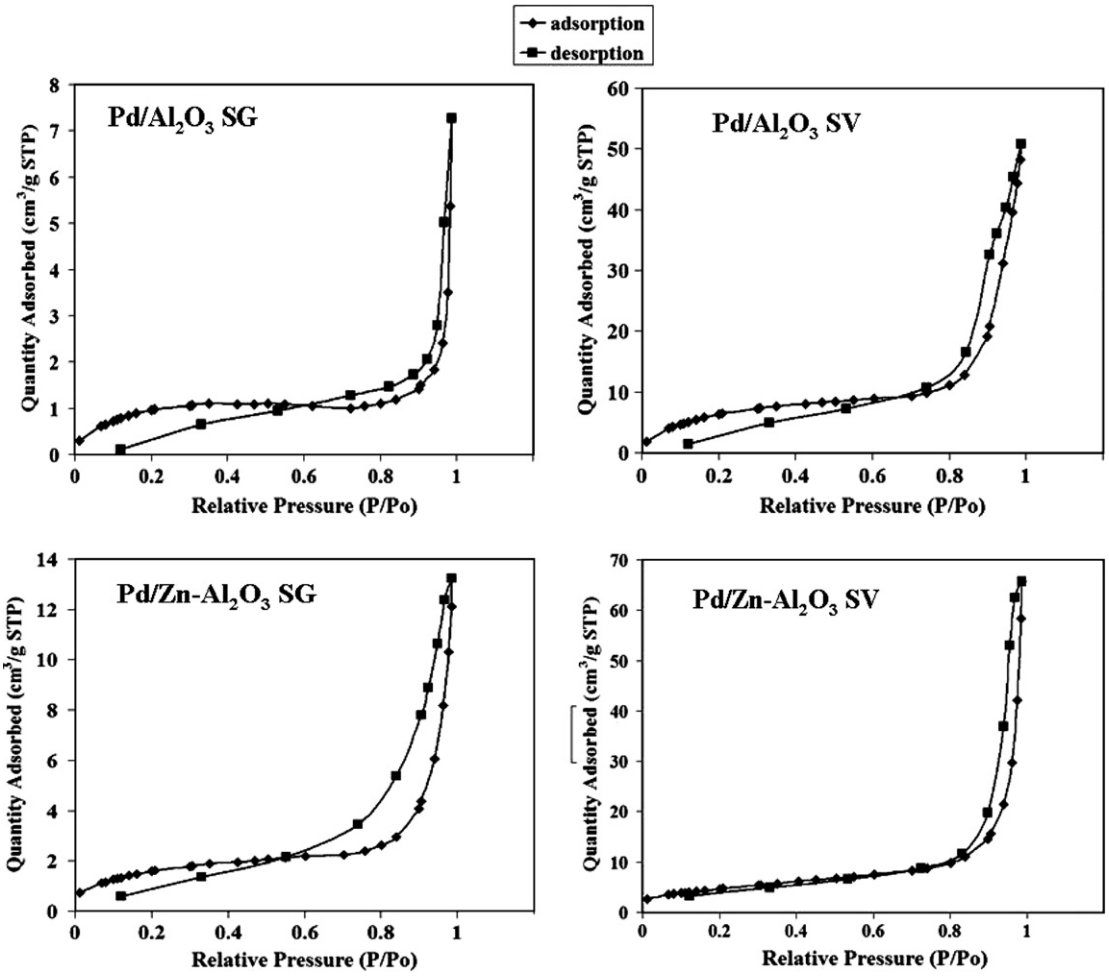

Fig. 2. N_2 adsorption–desorption isotherms of the Pd/α-Al_2O_3 and Pd/Zn-modified α-Al_2O_3 supports prepared by sol–gel (SG) and solvothermal (SV) methods.

sessed much less pore volume than the samples prepared by the solvothermal method. Incorporation of Pd particles by impregnation did not alter the textural properties of the supports as shown by similar pore size distributions in Fig. 3.

Fig. 4 shows the TEM micrographs with SAED patterns of Pd/α-Al_2O_3 and Pd/Zn-modified α-Al_2O_3 prepared by sol–gel and solvothermal methods. It can be seen that the sol–gel made catalysts consisted of agglomerated particles with primarily irregular shape structure (average particle size around 0.5–1 μm) whereas for those prepared by solvothermal method, agglomeration of finger-like particles were observed. The finger-like α-Al_2O_3 particles are normally obtained by calcination of the solvothermal-made α-Al_2O_3 powders at high temperature [18,19]. For Pd/Zn-modified α-Al_2O_3, the corresponding selected area diffraction patterns shows rings match d-spacing for the $ZnAl_2O_4$ confirmed the structure of $ZnAl_2O_4$ [20]. The large particles observed maybe the secondary particles formed by agglomeration of the primary nano-particles due to heat treatment during calcinations step. Based on TEM analysis, palladium particles/clusters with average particle size ca. 5–10 nm were found to be deposited on both of the alumina supports.

The metal active sites, the Pd dispersion, and the average Pd metal particle sizes from CO chemisorption experiment are also summarized in Table 1. The technique is based on the assumption that only one CO molecule adsorbed on one metal active site [21] and it is known that CO did not chemisorb on Al_2O_3 support [22–24]. Without Zn addition on the Al_2O_3 supports, Pd/Al_2O_3 sol–gel and Pd/Al_2O_3 solvothermal possessed the amounts of Pd active sites 11.3×10^{17} and 32.8×10^{17} sites/g cat., respectively. The Pd active sites significantly decreased when the catalysts were supported on Zn-modified α-Al_2O_3. The Pd/Zn–Al_2O_3 SG and Pd/Zn–

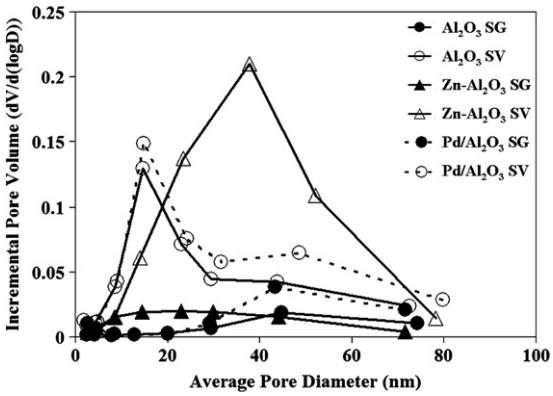

Fig. 3. Pore size distributions of the α-Al_2O_3, Zn-modified α-Al_2O_3, and Pd/α-Al_2O_3.

Al_2O_3 SV possessed the amounts of Pd active sites 4.86×10^{17} and 22.7×10^{17} sites/g cat., respectively. Thus, the catalysts on Zn-modified Al_2O_3 had lower Pd dispersion and larger Pd particle size (as determined from CO chemisorption experiments). Comparing the samples prepared by different techniques, the catalysts prepared by sol–gel method showed lower amount of Pd active sites and Pd dispersion than the catalysts prepared by solvothermal method due probably to more agglomeration of the α-Al_2O_3 supports as noticed from TEM measurements.

NH_3 temperature program desorption was a commonly used technique for the titration of surface acid sites [25]. The strength of an acid site could be related to the corresponding desorption temperature, while the total amount of ammonia desorption after saturation coverage permits quantification of the number of acid sites at the surface. The temperature-programmed desorption profiles for the nanocrystalline α-Al_2O_3 and Zn-modified α-Al_2O_3 supports are shown in Fig. 5. It was found that the desoprtion peak areas of the α-Al_2O_3 samples prepared by sol–gel method were lower that prepared by solvothermal method. Moreover, regardless of the preparation method used, the desorption peak areas of Zn-modified α-Al_2O_3 decreased. It is suggested that formation of $ZnAl_2O_4$ species resulted in a decrease of surface acidity of α-Al_2O_3 [26].

The catalytic properties of Pd/α-Al_2O_3 and Pd/Zn-modified α-Al_2O_3 catalysts were evaluated in the selective hydrogenation of acetylene using a fixed bed flow reactor with a GHSV of 16,901 h^{-1}. Study of temperature dependence of Pd/α-Al_2O_3 and Pd/Zn-modified α-Al_2O_3 catalysts on acetylene conversion and selectivity toward ethylene in the temperature range between 40 and 100 °C are shown in Fig. 6. For comparison purposes, selective acetylene hydrogenation using Pd catalysts supported commercial

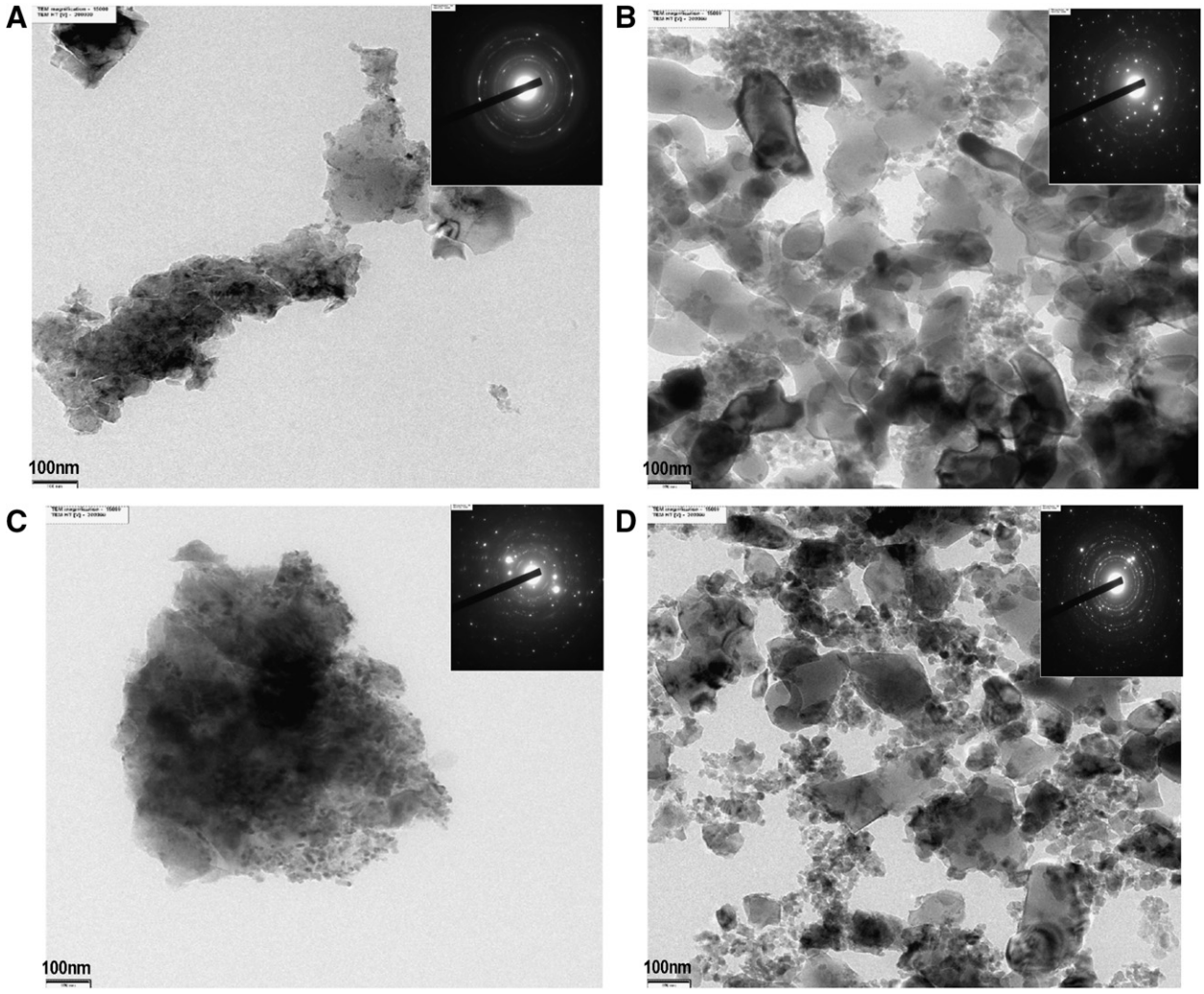

Fig. 4. TEM micrographs of Pd/α-Al_2O_3 and Pd/Zn-modified α-Al_2O_3 catalysts prepared by sol–gel (SG) and solvothermal (SV) methods with SAED pattern: (A) Pd/Al_2O_3 SG (B) Pd/Al_2O_3 SV (C) Pd/Zn–Al_2O_3 SG (D) Pd/Zn–Al_2O_3 SV.

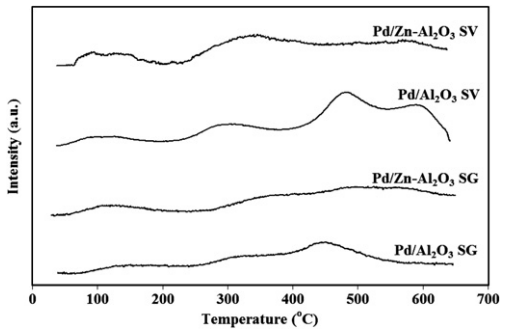

Fig. 5. NH_3 temperature program desorption profiles for the Pd/α-Al_2O_3 and Pd/Zn-modified α-Al_2O_3 supports prepared by sol–gel (SG) and solvothermal (SV) methods.

α-Al_2O_3 was also carried out. In all cases, acetylene conversion increased with increasing temperature while ethylene selectivity decreases due to the fact that the ethylene is produced as an intermediate in acetylene hydrogenation reaction. Acetylene conversion as well as ethylene selectivity was found to be in the order: Pd/Zn-modified α-Al_2O_3-sol–gel > Pd/Zn-modified α-Al_2O_3-solvothermal > Pd/α-Al_2O_3-sol–gel ≈ Pd/α-Al_2O_3-solvothermal >> Pd/α-Al_2O_3-commerical. It was clearly seen that the use of nanocrystalline α-Al_2O_3 prepared by sol–gel or solvothermal method resulted in much better catalyst performance compared to the commercial one. It can be noticed that Pd/Al_2O_3-SV had the largest Pd active sites; however, it exhibited the lowest activity. This can probably be explained by the dependent of acetylene hydrogenation activity on Pd particle size. Many researchers have shown that the specific activity of Pd decreased by an order of magnitude when the size of palladium particles were very small (1–5 nm) [27–29]. Modification of Pd/α-Al_2O_3 catalysts with Zn, however, resulted in significantly improvement of both acetylene conversion and ethylene selectivity. Comparing the samples prepared by the different techniques, the catalysts prepared by sol–gel method showed better catalytic properties than the catalysts prepared by solvothermal method.

After reaction, the amounts of carbonaceous deposits on the catalyst samples were measured by thermal gravimetric analysis and the results are shown in Fig. 7. A small weight loss (<1%) observed in the TGA profiles (Fig. 5A) below 200 °C was probably due to the removal of physisorbed water and/or chemisorbed hydroxyl groups. The weight loss at higher temperature was due to oxidation of the carbonaceous deposited on the surface of used catalysts [30]. As shown by the exothermic peaks in Fig. 5B, the type of coke species occurred during reaction was probably "soft coke" since it could be removed from the used catalysts by oxidation at a relative lower temperature (~350 °C) as suggested by Xiangjing et al. [31]. Based on TGA results, the amount of coke deposits on the catalysts prepared by sol–gel method were lower than those prepared by solvothermal method while Pd/Zn-modified α-Al_2O_3 prepared by sol–gel method showed the lowest value (2.33 wt.%) and Pd/α-Al_2O_3 prepared by solvothermal method showed the highest valve (6.39 wt.%). For Pd/α-Al_2O_3-commerical, the amount

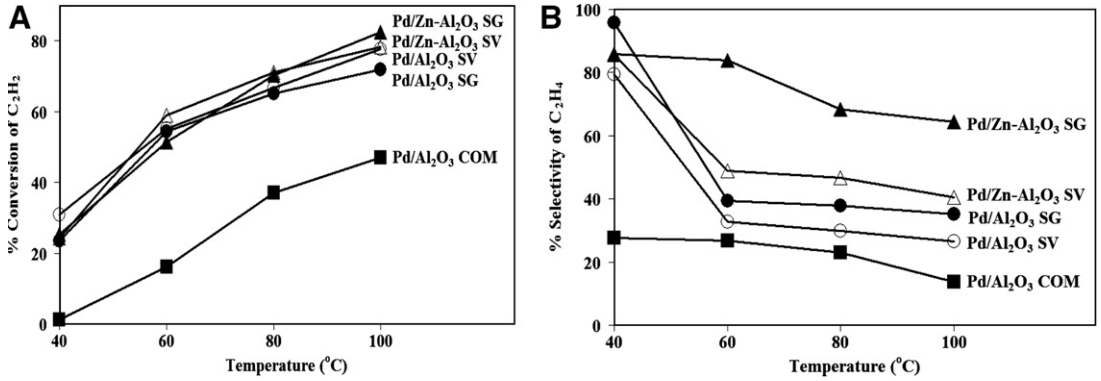

Fig. 6. Temperature dependence of the catalytic performance of Pd/α-Al_2O_3 and Pd/Zn-modified α-Al_2O_3 catalysts; (A) in terms of % conversion of C_2H_2 (B) in terms of % selectivity of C_2H_4.

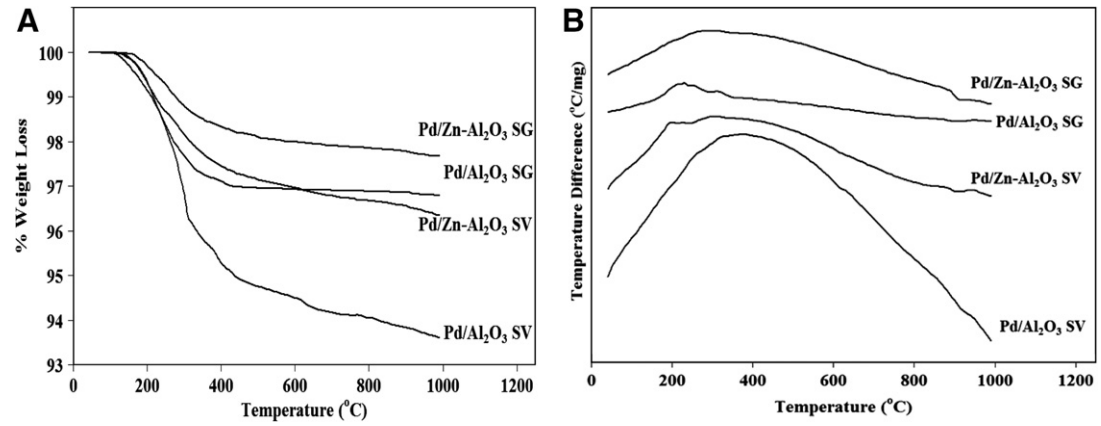

Fig. 7. Thermal gravimetric and differential temperature analysis (TG/DTA) of Pd/α-Al_2O_3 and Pd/Zn-modified α-Al_2O_3 catalysts after reaction; (A) in terms of temperature (°C) and weight loss (%), (B) in terms of temperature (°C) and temperature difference (°C/mg).

of coke deposits on the catalysts was 3.53 wt.% The results were in good agreement with acidity of the Al_2O_3 supports measured from NH_3 TPD technique. Based on the mechanisms in the literature [32,33], acetylene hydrogenation was suggested to take place on the active sites on Pd surface while most of the carbonaceous deposits were found to be accumulated on the support. The carbon deposits acted as a hydrogen bridge for the hydrogen spillover from Pd to the support facilitating ethylene hydrogenation to ethane. The low concentration of acid sites on the Al_2O_3 surface considerably reduced coke deposition thus ethylene selectivity was improved.

4. Conclusions

Modification of α-Al_2O_3 supports by Zn drastically decreased surface acidity of Al_2O_3 due to formation of $ZnAl_2O_4$ species. When used as the supports for Pd catalysts in selective acetylene hydrogenation, the catalysts exhibited lower Pd dispersion and larger Pd particle size (as determined from CO chemisorption experiments) compared to those on the unmodified ones. The Pd/Zn-modified α-Al_2O_3 catalysts showed higher acetylene conversion and ethylene selectivity and less amount of carbonaceous deposits than Pd on the unmodified and commercial α-Al_2O_3. Comparing the samples prepared by the different techniques, the catalysts prepared by sol–gel method showed better catalytic properties than those prepared by solvothermal method due to larger Pd particle size and lower amount of acid sites obtained.

Acknowledgements

Financial supports from the National Research Council of Thailand (NRCT), the Thailand Research Fund (TRF), the Commission on Higher Education, Ministry of Education, and the Graduate School of Chulalongkorn University are gratefully acknowledged.

References

[1] S. Hub, L. Hilaire, R. Touroude, Appl. Catal. 36 (1988) 307.
[2] J.P. Boitiaux, J. Cosyns, S. Vasudevan, Appl. Catal. 6 (1983) 41.
[3] Á. Sárkány, A.H. Weiss, L. Guczi, J. Catal. 98 (1986) 550.
[4] Y.-J. Huang, C.F. Shun, L.G. Daniel, E.L. Mohundro, J.E. Hartgerink, US Patent 5,332,705, 1994.
[5] Q. Zhang, J. Li, X. Liu, Q. Zhu, Appl. Catal. A 197 (2000) 221.
[6] C.J. Brinker, G.W. Scherrer, Sol–gel Science: The Physics and Chemistry of Sol–gel Processing, Academic Press, San Diego, 1990.
[7] W.H. Dawson, Am. Ceram. Soc. Bull. 67 (1988) 1673.
[8] S.G. Deng, Y.S. Lin, J. Mater. Sci. Lett. 16 (1997) 1291.
[9] Y. Sarikaya, I. Sevinc, M. Akinc, Powder Technol. 116 (2001) 109.
[10] W.B. Scott, E. Matijevic, J. Colloid Interf. Sci. 66 (1978) 447.
[11] M. Inoue, H. Kominami, T. Inui, J. Am. Ceram. Soc. 73 (1990) 1100.
[12] M.A. Valenzuela, J.P. Jacobs, P. Bosch, Appl. Catal. A 148 (1997) 315.
[13] M. Zawadzki, J. Wrzyszcz, J. Mater. Res. Bull. 35 (2000) 109.
[14] M. Zawadzki, W. Miśta, L. Kępński, J. Vacuum 63 (2001) 291.
[15] J.H. Kang, E.W. Shin, W.J. Kim, J.D. Park, S.H. Moon, J. Catal. 208 (2002) 310.
[16] O. Mekasuwandumrong, P. Praserthdam, M. Inoue, V. Pavarajarn, W. Tanakulrungsank, J. Mater. Sci. 39 (2004) 2417.
[17] S.J. Gregg, K.S.W. Sing, Adsorption Surface Area and Porosity, Academic Press, London, 1969.
[18] O. Mekasuwandumrong, V. Pavarajarn, M. Inoue, P. Praserthdam, Mater. Chem. Phys. 100 (2006) 445.
[19] O. Mekasuwandumrong, P.L. Silveston, P. Praserthdam, M. Inoue, V. Pavarajarn, W. Tanakulrungsank, Inorg. Chem. Commun. 6 (2003) 930.
[20] Z. Mirosław, J. Solid State Sci. 8 (2006) 14.
[21] J.R. Anderson, K.C. Pratt, Australia Press, Australia, 1985.
[22] Y. Soma-Noto, W.M.H. Sachtler, J. Catal. 32 (1974) 315.
[23] D. Cormack, J. Pritchard, R.L. Moss, J. Catal. 37 (1975) 548.
[24] B. Heinrichs, P. Delhez, J.-P. Schoebrecht, J.-P. Pirard, J. Catal. 172 (1997) 322.
[25] M.C. Kung, H.H. Kung, Catal. Rev. Sci. Eng. 27 (3) (1985) 425.
[26] C. Otero Areán, B. Sintes Sintes, G. Turnes Palomino, C. Mas Carbonell, E. Escalona Platero, J.B. Parra Soto, J. Micropor. Mater. 8 (1997) 187.
[27] C.E. Gigola, H.R. Aduriz, P. Bodnariuk, Appl. Catal. 27 (1986) 133.
[28] Y.A. Ryndin, M.V. Stenin, A.I. Boronin, V.I. Bukhtiyarov, V.I. Zaikovskii, Appl. Catal. 54 (1989) 277.
[29] J. Panpranot, K. Phandinthong, T. Sirikajorn, M. Arai, P. Praserthdam, J. Mol. Catal. 261 (2007) 29–35.
[30] R.W. Soares, V.J. Menezes, M.V.A. Fonseca, J. Dweck, J. Therm. Anal. 49 (1997) 657–661.
[31] Z. Xiangjing, W. Yan, X. Feng, Appl. Catal. A 307 (2006) 222.
[32] A. Sarkarny, L. Guczi, A.H. Weiss, Appl. Catal. 10 (1984) 369.
[33] S. Asplund, J. Catal. 158 (1996) 267.

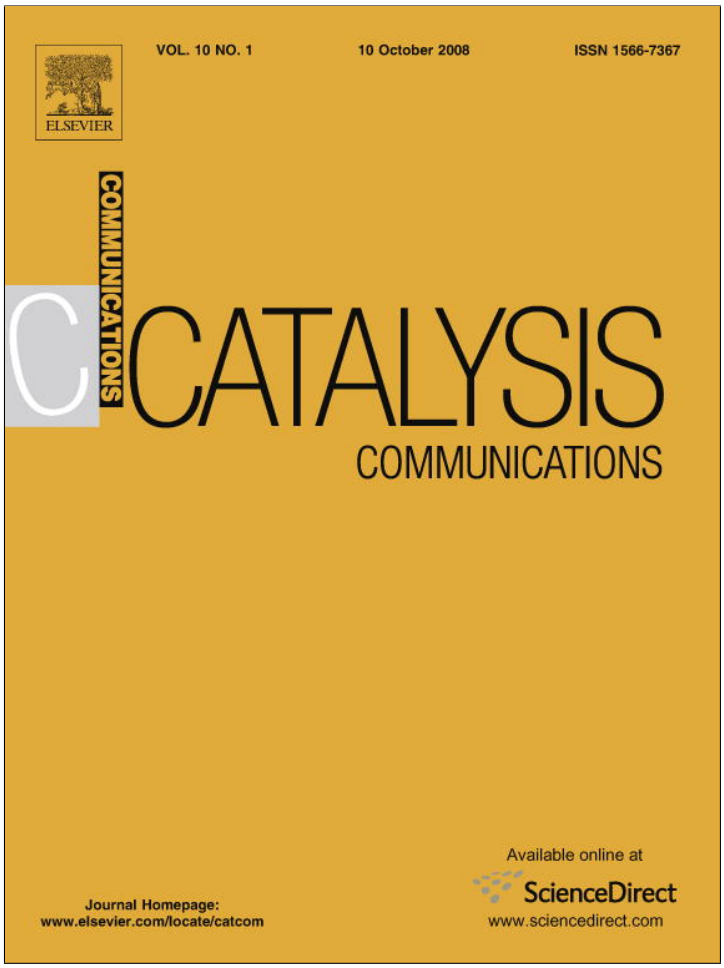

Catalysis Communications 10 (2008) 86–91

Contents lists available at ScienceDirect

Catalysis Communications

journal homepage: www.elsevier.com/locate/catcom

Improvement of Pd/Al_2O_3 catalyst performance in selective acetylene hydrogenation using mixed phases Al_2O_3 support

Sataporn Komhom [a], Okorn Mekasuwandumrong [b], Piyasan Praserthdam [a], Joongjai Panpranot [a,*]

[a] Center of Excellence on Catalysis and Catalytic Reaction Engineering, Department of Chemical Engineering, Faculty of Engineering, Chulalongkorn University, Bangkok 10330, Thailand
[b] Department of Chemical Engineering, Faculty of Engineering and Industrial Technology, Silpakorn University, Nakhonphatom 73000, Thailand

ARTICLE INFO

Article history:
Received 13 February 2008
Received in revised form 24 July 2008
Accepted 29 July 2008
Available online 7 August 2008

Keywords:
Selective acetylene hydrogenation
Mixed phases
Pd/Al_2O_3
α-Al_2O_3

ABSTRACT

The catalytic performances of Pd catalysts supported on γ-Al_2O_3, α-Al_2O_3, and mixed phases Al_2O_3 were investigated in the selective hydrogenation of acetylene in ethylene feed stream. It was found that the use of mixed phases Al_2O_3 with approximately 64% of α-phase resulted in significant improvements in both acetylene conversion and ethylene selectivity. The presence of small amount of transition phase in the alumina supports brought about higher BET surface area and Pd dispersion as well as improvement of reduction ability of the Pd/Al_2O_3 catalysts. On the other hand, significant amount of α-Al_2O_3 is necessary for high ethylene selectivity due to the lower amount of ethylene adsorbed.

1. Introduction

The effective removal of trace amount of acetylene in ethylene feedstock via selective hydrogenation using supported Pd-based catalysts is of particular challenge in the production of polyethylene since acetylene acts as a poison to the polymerization catalysts. The Pd/α-Al_2O_3 catalyst commonly used for selective acetylene hydrogenation is typically macroporous with a relatively small surface area of approximately 0.1–2 m^2/g. In general, α-Al_2O_3 provides low dispersion of active metal than γ-Al_2O_3 due to its lower surface area; however, it is desirable in this reaction because Pd/α-Al_2O_3 catalyst possesses less active sites for direct ethane formation than Pd/γ-Al_2O_3 catalyst [1]. Moreover, α-Al_2O_3 is less acidic than γ-Al_2O_3 thus less oligomer/green oil was formed during acetylene hydrogenation reaction. However, the catalysts are suffered from runaway ethylene hydrogenation especially at high levels of acetylene conversion [2]. Several attempts have been made to improve the selectivity of Pd/Al_2O_3 catalysts and also reduce green oil formation in selective hydrogenation of acetylene such as promotion with a second component such as Ag [3], SiO_2 [4], TiO_2 [5] and pre-treatment of catalysts using oxygen-containing compounds [6–8]. However, development of new efficient catalysts for selective hydrogenation of acetylene has still received much attention and has been reported continuingly including Pd on nano-sized TiO_2 [9,10], Pd on Ni modified Al_2O_3 [11], and zeolite-supported Pd–Ag catalysts [12,13].

In general, the more acidic, high surface area alumina hydrates are produced at relatively low temperatures by precipitation from either acidic or basic solutions and are transformed to 'transition' β-, γ-, η-, χ-, κ-, δ-, θ-, and α-Al_2O_3 by dehydration and treatment at high temperatures [14]. Differences in crystalline phases may result in changes in physical and chemical properties of Al_2O_3 supports and could play an important role on the catalytic performance of Al_2O_3 supported catalysts. For example, Chary et al. [15] reported that dispersion of vanadium oxide on Al_2O_3 supports as well as their catalytic activities in partial oxidation decreased with increasing calcination temperature due to the transformation of γ-Al_2O_3 into θ-, δ-, and α-Al_2O_3. Moya et al. [16] studied silver nanoparticles supported on α-, η-, and δ-Al_2O_3 prepared by colloidal processing route. It was found that silver particle sizes varied between 1 and 100 nm depending on the Al_2O_3 phases.

In this study, the effect of mixed phases Al_2O_3 (i.e. γ-, θ-, and α-Al_2O_3) on the properties of Pd/Al_2O_3 catalysts was investigated in the gas-phase selective hydrogenation of acetylene in ethylene feed stream. The weights (%) of α-phase were 0, 14, 47, 64, and 100 depending on the calcination conditions of the starting γ-Al_2O_3. The catalysts were characterized by means of X-ray diffraction (XRD), N_2 physisorption, CO pulse chemisorption, H_2-temperature programmed reduction (TPR), X-ray photoelectron spectroscopy (XPS), transmission electron microscope (TEM) and temperature programmed desorption of ethylene (C_2H_4-TPD).

* Corresponding author. Tel.: +66 2 2186869; fax: +66 2 2186877.
E-mail address: joongjai.p@eng.chula.ac.th (J. Panpranot).

1566-7367/$ - see front matter © 2008 Elsevier B.V. All rights reserved.
doi:10.1016/j.catcom.2008.07.039

2. Experimental

2.1. Catalysts preparation

γ-Al_2O_3 used in this study was the commercial available alumina JRC-ALO-2 (JRC Co., Ltd. Japan). The mixed phases with various phase compositions were prepared by calcination of the γ-Al_2O_3 at 1100 °C for 120, 200, or 240 min. The α-Al_2O_3 was obtained by calcination of the γ-Al_2O_3 at 1175 °C for 120 min. In this paper, the alumina samples consisting of 0, 14, 47, 64, and 100% α-phase are referred to as Al-α0, Al-α14, Al-α47, Al-α64, and Al-α100, respectively. The percentage of alpha phase was calculated using a calibration curve from XRD results of the physically mixed γ-, and α-Al_2O_3 (not shown here).

The Pd/Al_2O_3 catalysts with weight (%) of Pd approximately 1% were prepared by the incipient wetness impregnation technique using an aqueous solution of $Pd(NO_3)_2$ (Wako, Japan) as the palladium precursor. The catalysts were subsequently dried at 110 °C for 12 h and calcined in air at 550 °C for 2 h.

2.2. Catalyst characterization

The X-ray diffraction (XRD) pattern of the Al_2O_3 supports and Pd/Al_2O_3 catalysts were carried out using an X-ray diffractometer, SIEMENS XRD D5000, with Cu Kα radiation with a Ni filter. The BET surface areas of the Al_2O_3 supports were measured by N_2 physisorption using a Micrometritics ASAP 2000 automated system. The samples were degassed at 200 °C for 1 h prior to N_2 physisorption. The amounts of CO chemisorbed on the Pd/Al_2O_3 catalysts were measured at room temperature by using a Micromeritic Chemisorb 2750 automated system attached with ChemiSoft TPx software at room temperature. Prior the measurement, 30 ml/min of He gas was introduced into the sample cell in order to remove the remaining air. The system was switched to 50 ml/min of hydrogen and heated to 150 °C with a heating rate of 10 °C/min. The temperature was kept constant for 2 h and then cooled down to the room temperature. Temperature program experiments were carried out in a Micromeritic Chemisorb 2750 automated system. The temperature ramping was controlled by temperature controller, Furnace Power 48 VAC 8A MAX. The XPS analysis was performed using an AMICUS photoelectron spectrometer equipped with an Mg Kα X-ray as primary excitation and KRATOS VISION2 software. XPS elemental spectra were acquired with 0.1 eV energy step at a pass energy of 75 kV. The C 1s line was taken as an internal standard at 285.0 eV. The distribution of palladium on catalyst supports were observed using JEOL Model JEM-2010 transmission electron microscope operated at 200 keV. A mixture of 10% H_2 in Ar with a flow rate of 15 cm^3/min was used in TPR experiment. Prior the experiment, the sample was treated in N_2 flow at 200 °C for 1 h in order to remove any adsorbed gas. The TPR was performed with a constant heating rate of 10 °C/min from 35 to 200 °C. For ethylene-TPD experiments, the samples were pre-reduced at 150 °C in H_2 for 2 h (flow rate 50 cm^3/min) and cooled down to room temperature. Then adsorption of ethylene was performed at room temperature for 3 h. The temperature programmed desorption was performed with a constant heating rate of 10 °C/min from 35 to 800 °C. The amount of desorbed ethylene was measured by analyzing the effluent gas with a thermal conductivity detector.

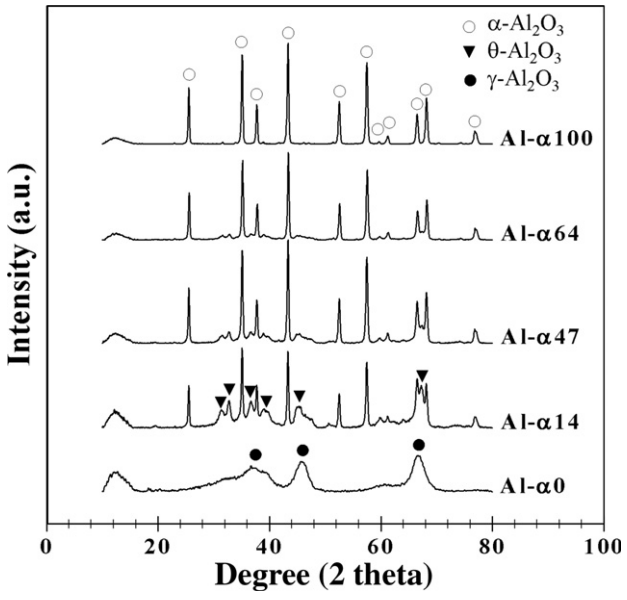

Fig. 1. The XRD patterns of the Al_2O_3 supports containing various % of α-phase.

2.3. Reaction study

The catalyst performances in selective hydrogenation of acetylene were evaluated using a 10 mm (id) pyrex reactor. Prior to the start of each experimental run, the catalyst was reduced *in situ* with hydrogen by heating from room temperature to 150 °C at a heating rate of 10 °C/min. Then the reactor was purged with argon and cooled down to the reaction temperature 40 °C. The reaction was carried out using a feed composition of 1.5% C_2H_2, 1.7% H_2, and balanced C_2H_4 with a vary GHSV of 52,580, 32,577, 22,534 and 12,385 h^{-1}. The products and feeds were analyzed by

Table 1
The physical properties of alumina with various phase compositions

Samples	α-Phase (%)	BET surface area (m^2/g)	Crystallite size (nm)[a]		Pore volume[b] (cm^3/g)	Average pore dameter[b] (Å)
			γ-Phase	α-Phase		
Al-α100	100	12.3	n.d.	44.5	0.03	90.1
Al-α64	64	36.1	28.3	45.8	0.14	129.6
Al-α47	47	45.4	17.8	48.9	0.20	151.9
Al-α14	14	67.3	11.8	46.0	0.30	143.8
Al-α0	0	244.1	3.7	n.d.	0.66	78.9

n.d. = Not determined.
[a] Calculated from XRD results.
[b] Based on BJH method.

Table 2
Physiochemical properties of Pd supported on alumina with various phase compositions

Samples	Pd active sites[a] ($\times 10^{-18}$ CO molecule/g-cat)	% Pd dispersion[b]	dp[c] (Pd^0) (nm)	Pd $3d_{5/2}$ [d]		Atomic concentration[d] Pd/Al
				BE (eV)	FWHM	
Pd/Al-α100	7.4	12.5	8.9	336.9	1.8	0.034
Pd/Al-α64	11.0	18.5	6.1	336.9	2.0	0.027
Pd/Al-α47	25.4	42.9	2.6	336.4	2.4	0.020
Pd/Al-α14	31.7	53.5	2.1	336.4	2.3	0.011
Pd/Al-α0	35.1	59.2	1.9	336.4	2.2	0.001

V_{ads}, volume adsorbed; V_g, molar volume of gas at STP; S_f, stoichiometry factor, CO on Pd; MW, molecular weight of the metal; %M, %metal loading.
[a] Pd active sites = $(V_{ads}/V_g) \times (6.02 \times 10^{23})$. Error of measurement = ±5%.
[b] % Pd dispersion = [Pd active sites $\times S_f \times$ (M.W./% M) $\times$ 100% $\times$ 100%]/(6.02×10^{23}).
[c] Based on $d_p = 1.12/D$ (nm), where D = % Pd dispersion [25].
[d] Based on XPS results.

a two gas chromatographs equipped with a FID detector (SHIMADZU FID GC 9A, carbosieve column S-2) and TCD detector (SHIMADZU TCD GC 8A, molecular sieve-5A).

3. Results and discussion

The mixed phases Al_2O_3 supports used for preparation of the Pd/Al_2O_3 catalysts in this study were obtained by varying the calcination conditions of the γ-Al_2O_3 (calcination temperature 1100–1175 °C and holding time 2–4 h). The XRD patterns of Al_2O_3 are shown in Fig. 1. The weight (%) of α-phase in these samples were calculated to be 0%, 14%, 47%, 64% and 100% using a calibration from XRD results of the physically mixed γ-, and α-Al_2O_3 (not shown here) and were designated herein as Al-α0, Al-α14, Al-α47, Al-α64, and Al-α100, respectively.

Table 1 summarizes physical properties of the various Al_2O_3 supports. The crystallite size of transition phase was increased from 3.7 to 28.3 nm as the weight (%) of α-phase content increased from 0% to 64%, while the crystal size of α-phase remained constant at around 45 nm. The specific surface area and total pore volume calculated from BJH method decreased from 244 to 12 m^2/g and 0.66 to 0.03 cm^3/g with increasing amount of α-phase alumina. A drastically decrease in BET surface area and total pore volume of alumina during phase transformation can be explained by the rapidly increase of alumina crystal size. It is generally known that calcination of γ-Al_2O_3 at high temperature results in phase transformation from γ- to θ- and then α-Al_2O_3.

The XRD characteristic peaks of all the Pd/Al_2O_3 catalysts were not different from the Al_2O_3 supports after Pd loading. No XRD peaks for PdO or Pd^0 metal were observed due probably to the low loading of palladium (results not shown). The CO chemisorption results such as the number of active Pd atoms, Pd dispersion (%), and average Pd metal particle size are summarized in Table 2. Palladium dispersion was estimated from the amount of CO chemisorbed assuming a stoichiometry of CO/Pd = 1 [17]. The number of Pd active sites decreased from 35.1 to 7.4×10^{18} sites/

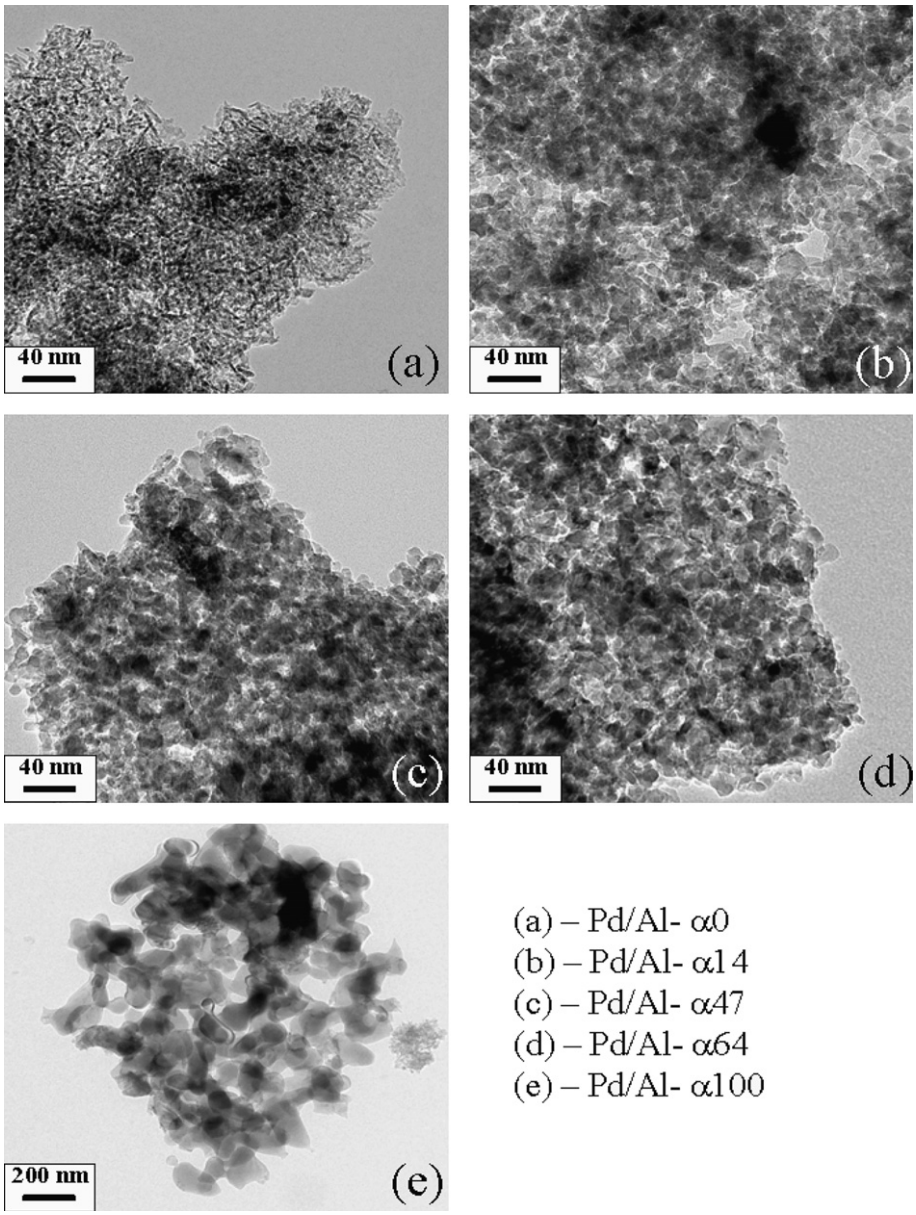

Fig. 2. Transmission electron micrographs of the Pd/Al_2O_3 catalysts.

g-catalyst corresponding to a decrease in Pd dispersion (%) from 59.5 to 12.5 and an increase in Pd metal particle size from 1.9 to 8.9 nm as the weight (%) of α-phase contents increased from 0% to 100%.

In order to verify the Pd particle size, TEM micrographs have been acquired and are shown in Fig. 2. The Pd supported on pure γ-Al_2O_3 consisted of particles with primarily spherical shape with some needlelike structure. The particle shape appeared more uniformly spheroidal for those supported on mixed phases Al_2O_3. Large fingerlike shape particles were observed for the catalysts containing 100% α-phase Al_2O_3. Increasing α-phase content of the alumina supports from 0 to 100% resulted in an increase of Pd cluster/particle size from about 2 to 10 nm.

XPS is used to determine the surface compositions of the catalysts and the interaction between Pd and the Al_2O_3 supports. The deconvoluted XPS photoelectron spectra for the Pd 3d core level region of all the catalysts are shown in Fig. 3. From the figure, the Pd doublet was clearly evident. A small shoulder at the binding energy around 335.1–335.8 eV was present in every sample and was attributed to metallic Pd^0 [18]. Such results indicated that partial reduction occurred during analysis. PdO species was observed at the binding energies in the range of 336.9–336.4 eV which was consistent to the values reported in the literature [19,20]. The percentages of atomic concentration, the binding energy, and FWHM of Pd 3d are also given in Table 2. The atomic concentration ratios for Pd/Al decreased with the decrease in α-phase Al_2O_3 contents. The results were consistent with the CO chemisorption results that larger Pd particle sizes were obtained on α-Al_2O_3. The FWHM values larger than two for Pd $3d_{5/2}$ may be due to some differential charging that contributed to the widening of the palladium peaks [21,22].

Reduction behavior and reducibility of the catalysts were investigated by means of H_2-temperature programmed reduction and the results are shown in Fig. 4. All the Pd/Al_2O_3 catalysts exhibited TPR profiles with one main reduction peak which can be assigned to the reduction of PdO to Pd^0 metal. This peak remained constant at around 55 °C for those with the weight (%) of α-phase contents between 0% and 64%. The reduction peak was slightly shifted to

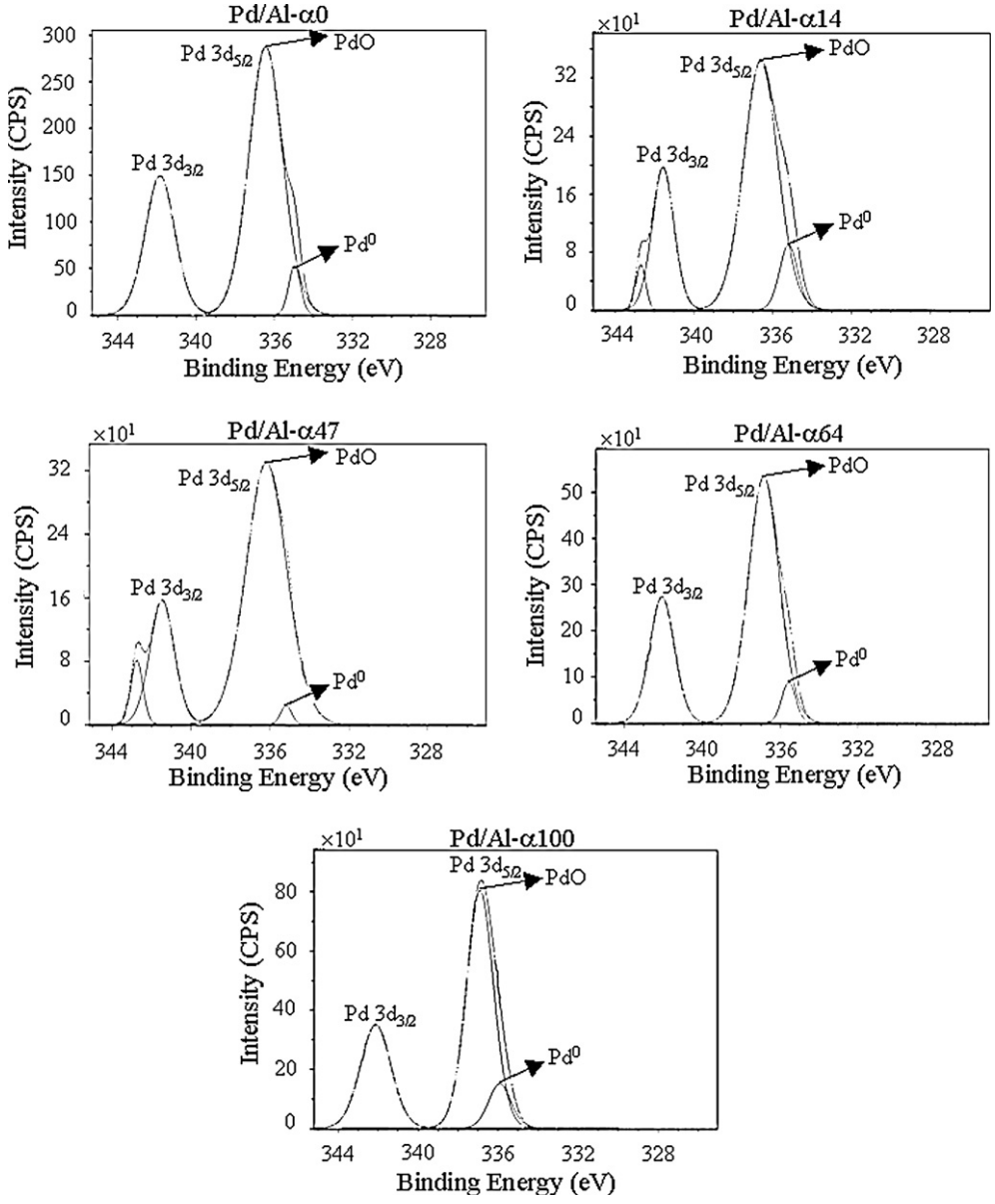

Fig. 3. The XPS deconvoluted spectra of the Pd/Al_2O_3 catalysts.

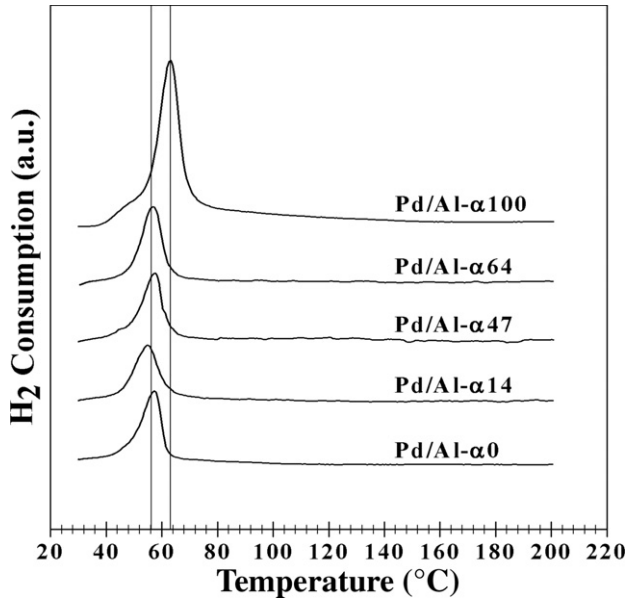

Fig. 4. TPR profiles of the Pd/Al_2O_3 catalysts.

65 °C for the Pd/Al-α100 catalyst (100% α-phase). It is suggested that the existence of transition phase Al_2O_3 (either γ- or θ-Al_2O_3) in the Al_2O_3 supports facilitated reduction at low temperature. However, the hydrogen consumptions during the transformation of PdO to metallic Pd as determined from the areas of the reduction peak for all the catalysts were essentially the same.

Ethylene-temperature programmed desorption (C_2H_4-TPD) was performed in order to obtain an information about ethylene adsorption behavior on the catalyst surfaces. The C_2H_4-TPD experiments were carried out at 35–800 °C after the samples were reduced in H_2 at 150 °C and purged with He at the same adsorption temperature. The temperature programmed study profiles of the catalysts are shown in Fig. 5. Two main desorption peaks at ca. 80–105 °C and 275–300 °C were observed for all the catalyst samples. As suggested by Moon et al. [23], the lower temperature desorption peak was assigned to π-bonded ethylene species while the higher temperature was assigned to di-σ-bonded ethylene. The latter species were suggested to be the species that recombined with surface hydrocarbon and produced ethane. In some cases, the third peak at temperature range around 450–650 °C was observed. It was suggested to be due to decomposition of C_2 hydrocarbons adsorbed on Pd surface [24]. In the present study, the intensities of the TCD signals during ethylene temperature programmed desorption was significantly decreased when the content of α-phase in the Al_2O_3 supports increased from 0 to 100%. In other words, the amount of ethylene adsorbed was much lower when the Al_2O_3 supports contained significant amounts of α-Al_2O_3.

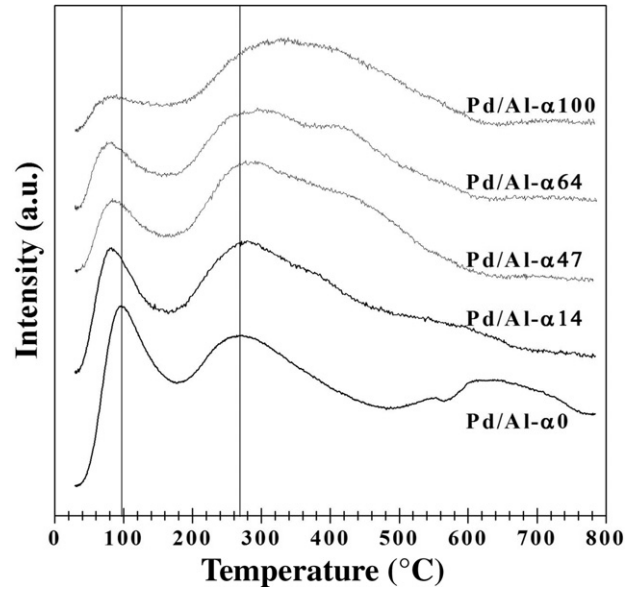

Fig. 5. Ethylene TPD results of the Pd/Al_2O_3 catalysts.

The catalytic performances of Pd/Al_2O_3 catalysts containing α-Al_2O_3, γ-Al_2O_3, or mixed phases alumina were evaluated in the selective hydrogenation of acetylene at 40 °C under various feed flow rates (GHSV 52,580, 32,577, 22,534, and 12,385 h^{-1}). Acetylene conversion is defined as moles of acetylene converted with respect to acetylene in feed. Ethylene gain is defined as the percentage of acetylene hydrogenated to ethylene over totally hydrogenated acetylene. The ethylene being hydrogenated to ethane (ethylene loss) is the difference between all the hydrogen consumed and all the acetylene which has been totally hydrogenated. The plots of acetylene conversion and ethylene selectivity versus GHSV are shown in Figs. 6 and 7, respectively. In general, acetylene conversion decreased with increasing GHSV while ethylene gain increased. Since ethylene is produced as an intermediate in

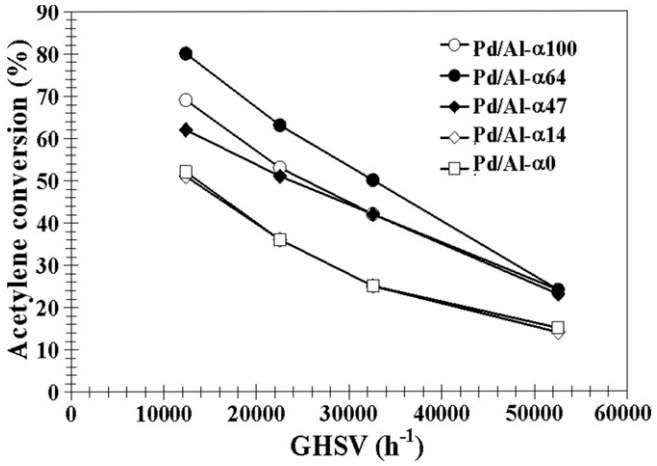

Fig. 6. Catalyst performances in selective hydrogenation of acetylene in terms of GHSV values and acetylene conversion (%).

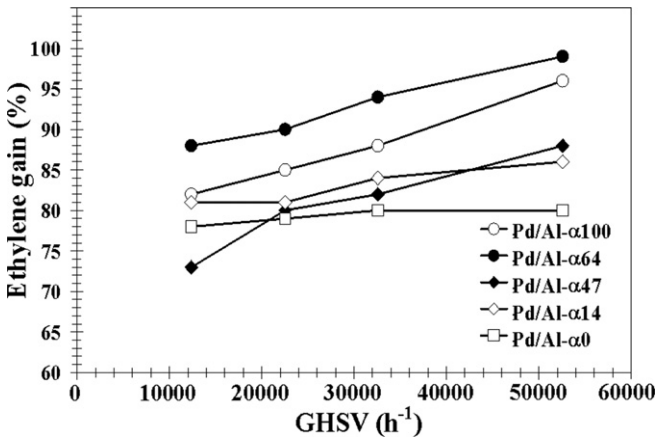

Fig. 7. Catalyst performances in selective hydrogenation of acetylene in terms of GHSV values and ethylene gain (%).

acetylene hydrogenation, which is a typical consecutive reaction, the ethylene selectivity decreases with acetylene conversion [5]. The performance of Pd/Al_2O_3 catalysts was improved in the order of Pd/Al-α64 > Pd/Al-α100 > Pd/Al-α47 > Pd/Al-α14 > Pd/Al-α0. It is clearly shown that the Pd catalyst supported on mixed phase Al_2O_3 that contained 64% of α-phase (Pd/Al-α64) exhibited the best catalytic performance among the five catalysts studied.

Based on the characterization results, the presence of the transition phase in α-Al_2O_3 supports increased the specific surface area, total pore volume, Pd active sites and the dispersion of Pd on Al_2O_3 supports and facilitated the reduction of PdO at lower temperature, which promoted acetylene conversion. However, the TPD profiles suggest that the amount of ethylene adsorbed on the catalyst surface decreased with increasing α-phase content. The feature is important for the improvement of ethylene gain especially at high acetylene conversion. The results in this study revealed that the beneficial properties of both α-Al_2O_3 and transition alumina can be combined to give the best catalytic performance of Pd/Al_2O_3 catalyst in selective acetylene hydrogenation. Among the five catalysts studied, the optimum amount of α-phase content was found to at 64 wt%.

4. Conclusions

The catalytic performances of Pd/Al_2O_3 catalysts in selective hydrogenation of acetylene were significantly improved when the Al_2O_3 support consisted of mixed transition- Al_2O_3 and α-Al_2O_3 with ca. 64% of α-Al_2O_3. The presence of transition phase Al_2O_3 in α-Al_2O_3 resulted in combined properties of the transition Al_2O_3 such as higher BET surface area, higher Pd dispersion, improved reduction ability and the beneficial properties of α-Al_2O_3 for selective acetylene hydrogenation such as lower amount of ethylene adsorbed. Among the five crystalline phase compositions of alumina used in this study, the one containing 64% α-Al_2O_3 was found to be the best (optimum) composition to prepare Pd/Al_2O_3 catalysts with high acetylene conversion and high ethylene selectivity.

Acknowledgements

The authors would like to thank the Commission for Higher Education, Ministry of Education, Thailand and the Thailand Research Fund (TRF) for the financial supports of this project.

References

[1] M.J. Vincent, R.D. Gonzalez, Appl. Catal. A: Gen. 217 (2001) 143.
[2] S. LeViness, V. Nair, A. Weiss, J. Mol. Catal. A: Chem. 25 (1984) 131.
[3] Y. Jin, A.K. Datye, E. Rightor, R. Gulotty, W. Waterman, M. Smith, J. Catal. 203 (2001) 292.
[4] E.W. Shin, C.H. Choi, K.S. Chang, Y.H. Na, S.H. Moon, Catal. Today 44 (1998) 137.
[5] J.H. Kang, E.W. Shin, W.J. Kim, J.D. Park, S.H. Moon, J. Catal. 208 (2002) 310.
[6] P. Praserthdam, B. Ngamsom, N. Bogdanchikova, S. Phatanasri, M. Pramotthana, Appl. Catal. A: Gen. 230 (2002) 41.
[7] R.N. Lamb, B. Ngamsom, D.L. Trimm, B. Gong, P.L. Silveston, P. Praserthdam, Appl. Catal. A: Gen. 268 (2004) 43.
[8] B. Ngamsom, N. Bogdanchikova, M.A. Borja, P. Praserthdam, Catal. Commun. 5 (2004) 243.
[9] J. Panpranot, K. Kontapakdee, P. Praserthdam, Appl. Catal. A: Gen. 314 (2006) 128.
[10] J. Hong, W. Chu, M. Chen, X. Wang, T. Zhang, Catal. Commun. 8 (2007) 593.
[11] N. Wongwaranon, O. Mekasuwandumrong, P. Praserthdam, J. Panpranot, Catal. Today 131 (2008) 553.
[12] W. Huang, J.R. McCormick, R.F. Lobo, J.G. Chen, J. Catal. 246 (2007) 40.
[13] W. Huang, W. Pyrz, R.F. Lobo, J.G. Chen, Appl. Catal. A: Gen. 333 (2007) 254.
[14] R.J. Farrauto, C.H. Bartholomew, Fundamentals of Industrial Catalytic Process, third ed., Blackie Academic and Professional, New York, 2002.
[15] K.V.R. Chary, G. Kishan, C.P. Kumar, G.V. Sagar, Appl. Catal. A: Gen. 246 (2003) 335.
[16] A. Esteban-Cubillo, C. Díaz, A. Fernández, L.A. Díaz, C. Pecharromán, R. Torrecillas, J.S. Moya, J. Eur. Ceram. Soc. 26 (2006) 1.
[17] V.H. Sandoval, C.E. Gigola, Appl. Catal. A: Gen. 148 (1996) 81.
[18] J.F. Moulder, W.W. Stickle, P.E. Sobol, K.D. Bomber, in: J. Chastain (Ed.), Handbook of X-ray Photoelectron Spectroscopy, Perkin Elmer, Eden Praine, USA, 1992.
[19] P. Legare, F. Finck, R. Roche, G. Maire, J. Surf. Sci. 217 (1989) 167.
[20] M. Brun, A. Berthet, J.C. Bertolini, J. Electron Spectrosc. Relat. Phenom. 104 (1999) 55.
[21] A.M. Venezia, A. Rossi, L.F. Liotta, A. Martorana, G. Deganello, Appl. Catal. A: Gen. 147 (1996) 81.
[22] A.B. Gaspar, L.C. Dieguez, Appl. Catal. A: Gen. 201 (2000) 241.
[23] I.Y. Ahn, W.J. Kim, S.H. Moon, Appl. Catal. A: Gen. 308 (2006) 75.
[24] E.W. Shin, J.H. Kang, W.J. Kim, J.D. Park, S.H. Moon, Appl. Catal. A: Gen. 223 (2002) 161.
[25] N. Mahata, V. Vishwanathan, J. Catal. 196 (2000) 262.

Catal Lett
DOI 10.1007/s10562-008-9621-3

Effect of Support Crystallite Size on Catalytic Activity and Deactivation of Nanocrystalline $ZnAl_2O_4$-Supported Pd Catalysts in Liquid-Phase Hydrogenation

Terachai Sirikajorn · Okorn Mekasuwandumrong · Piyasan Praserthdam · James G. Goodwin Jr. · Joongjai Panpranot

Received: 21 November 2007 / Accepted: 28 March 2008

Abstract The catalytic activity and deactivation of nanocrystalline $ZnAl_2O_4$-supported Pd catalysts were investigated for the liquid-phase hydrogenation under mild conditions. Nanocrystalline $ZnAl_2O_4$ spinels with average crystallite size between 8 and 33 nm were synthesized by the solvothermal method in toluene. Higher turnover frequencies for 1-heptyne hydrogenation and less deactivation due to Pd leaching were obtained for the Pd/$ZnAl_2O_4$-33 nm catalyst. XPS and ESR results suggest that the presence of defects in larger crystallite size $ZnAl_2O_4$ resulted in higher Pd dispersion and stronger interaction between Pd and the support.

Keywords $ZnAl_2O_4$ spinel · Solvothermal · Nanocrystals · Pd catalyst · Liquid-phase hydrogenation · 1-heptyne hydrogenation

T. Sirikajorn · P. Praserthdam · J. Panpranot (✉)
Center of Excellence on Catalysis and Catalytic Reaction Engineering, Department of Chemical Engineering, Faculty of Engineering, Chulalongkorn University, Bangkok 10330, Thailand
e-mail: joongjai.p@eng.chula.ac.th

O. Mekasuwandumrong
Department of Chemical Engineering, Silpakorn University, Sanam Chandra Palace Campus, Nakorn Pathom 73000, Thailand

J. G. Goodwin Jr.
Department of Chemical and Biomolecular Engineering, Clemson University, Clemson, SC 29634, USA

1 Introduction

Supported Pd catalysts are widely used in liquid-phase selective alkyne hydrogenation especially for the synthesis of fine chemicals and bio-active compounds [1–4]. The notable advantages of supported noble metal catalysts under heterogeneous conditions are relatively high activity, mild process conditions, easy separation, and better handling properties. The commonly used supports for Pd catalysts include activated carbon [5, 6], silica [7], alumina [8], and to a lesser extent, polymer [9] and zeolite [10]. It is known that the choice of an efficient support can significantly improve the activity, selectivity, recycling, and reproducibility of Pd catalyst systems [11–13]. Recently, spinel type oxides like $ZnAl_2O_4$ have been used as supports for Pt and Pd catalysts and a distinct metal-support interaction was found [14, 15]. It has also been reported that Rh complexes were effectively and stably bound to hydrothermally synthesized $ZnAl_2O_4$ better than to Al_2O_3 [16].

The solvothermal method is one of the most interesting methods for preparation of nanocrystalline materials. It has been used to successfully synthesize various types of nano-sized metal oxides with large surface areas, high crystallinities, and high thermal stabilities [17, 18]. The products obtained by solvothermal synthesis usually show uniform morphology, well-controlled chemical composition, and narrow particle size distribution. As catalyst supports, solvothermal-derived nanocrystalline oxides have been shown to provide better catalytic properties of the corresponding supported metal catalysts compared to commercially available supports [19–21]. In this study, nanocrystalline $ZnAl_2O_4$ spinels were prepared by the solvothermal method using toluene as the solvent and were employed as Pd catalyst supports. The effect of support crystallite size in the range of 8–33 nm on the catalytic

activities, selectivities, and catalyst deactivation due to metal leaching of the nanocrystalline $ZnAl_2O_4$-supported Pd catalysts were investigated by X-ray diffraction (XRD), N_2 physisorption, transmission electron microscopy with selected area electron diffraction (TEM with SAED), CO pulse chemisorption, electron spin resonance (ESR), X-ray photoelectron spectroscopy (XPS), and atomic absorption spectroscopy (AAS). Liquid-phase hydrogenation of 1-heptyne under mild reaction conditions was used as a test reaction.

2 Experimental

2.1 Preparation of $ZnAl_2O_4$ and $Pd/ZnAl_2O_4$

Zinc aluminate spinel ($ZnAl_2O_4$) was prepared by the solvothermal technique using aluminium isopropoxide (Aldrich) and zinc (II) acetylacetonate (Merck) (Zn/Al molar ratio = 0.5) as reactants suspended in toluene (Carlo Erba Reagenti). First, the mixture of aluminium isopropoxide, 15.0 g and appropriate amount of zinc (II) acetylacetonate (Zn/Al molar ratio = 0.5) was prepared in 100 cm^3 toluene in a 1.5-dm^3 autoclave reactor. The suspension was heated to 300 °C at the rate of 2.5 °C/min and held at that temperature for 2 h. The resulting products were washed with methanol and dried in air and then calcined in a furnace at various temperatures (500, 700, 900, or 1,150 °C) for 1 h. The as-synthesized $ZnAl_2O_4$ was referred to as $ZnAl_2O_4$-as-syn and the calcined $ZnAl_2O_4$ supports were denoted as $ZnAl_2O_4$-500, $ZnAl_2O_4$-700, $ZnAl_2O_4$-900, $ZnAl_2O_4$-1150 according to the calcination temperature used.

$Pd/ZnAl_2O_4$ catalysts were prepared by the incipient wetness impregnation method using $Pd(NO_3)_2$ (Aldrich) as the palladium precursor. The support was impregnated to incipient wetness with an aqueous solution containing sufficient palladium to result in 1 wt% Pd catalysts. The catalyst samples were dried in an oven at 100 °C overnight and calcined in air at 400 °C for 6 h prior to characterization.

2.2 Catalyst Characterization

The specific surface areas, pore volumes, and average pore diameters were determined by N_2 physisorption using a Micromeritics ASAP 2000 automated system and the Brunauer-Emmet-Teller (BET) method. Each sample was degassed under vacuum at <10 μm Hg in the Micromeritics system at 150 °C for 4 h prior to N_2 physisorption. The XRD patterns of the catalysts were measured from 10° to 80° 2θ using a SIEMENS D5000 X-ray diffractometer and Cu K_α radiation with a Ni filter. Catalyst crystallite sizes and diffraction patterns of supports were obtained using the JEOL JEM 2010 transmission electron microscope that employed a LaB_6 electron gun in the voltage range of 80–200 kV with an optical point-to-point resolution of 0.23 nm. The amounts of CO chemisorbed on the catalysts were measured at room temperature using a Micromeritic Chemisorb 2750 automated system with ChemiSoft TPx software. Prior to chemisorption, the sample was reduced in a H_2 flow at 500 °C for 2 h and then cooled down to ambient temperature in a He flow. The bulk compositions of palladium in the catalysts before and after reaction were determined using a Varian Spectra A800 atomic absorption spectrometer. Electron spin resonance spectroscopy (ESR) was conducted using a JEOL JESRE2X-electron spin resonance spectrometer. The intensity of ESR was calculated using a computer software program ES-PRIT ESR DATA SYSTEM (version 1.6).

2.3 Reaction Study

Liquid-phase partial hydrogenation of 1-heptyne was carried out in a 50-cm^3 stainless steel autoclave. Approximately 0.02 g of supported Pd catalyst was placed in the reactor with 10 cm^3 of 2 vol% of 1-heptyne in toluene. Afterward the reactor was filled with hydrogen at 1 bar pressure. Stirring was switched on to start the reaction, and reaction was carried out for 5 min. The products were analyzed by gas chromatography with a flame ionization detector.

3 Results and Discussion

3.1 Catalyst Characteristics

Figure 1 shows the XRD patterns of the as-synthesized and calcined $ZnAl_2O_4$ powders. Reaction of the mixture of aluminum isopropoxide (AIP) and zinc acetylacetonate (ZnAcAc) in toluene yielded the nanocrystalline spinel $ZnAl_2O_4$ powders with no other impurities. Increasing calcination temperature resulted in a subsequent increase in the degree of crystallinity and in the crystallite size. The average crystallite size of $ZnAl_2O_4$ powders calculated from the Scherrer equation was found to increase linearly from 8 to 33 nm with increasing calcination temperature to 1,150 °C. The average crystallite sizes, BET surface areas, pore volumes, and average pore diameters of the solvothermal-derived $ZnAl_2O_4$ are given in Table 1. The BET surface areas gradually decreased with increasing calcination temperature suggesting that sintering occurred during the calcination process corresponding to the increase of crystallite size. The pore size distributions of the $ZnAl_2O_4$ supports are shown in Fig. 2. It was found that the calcined

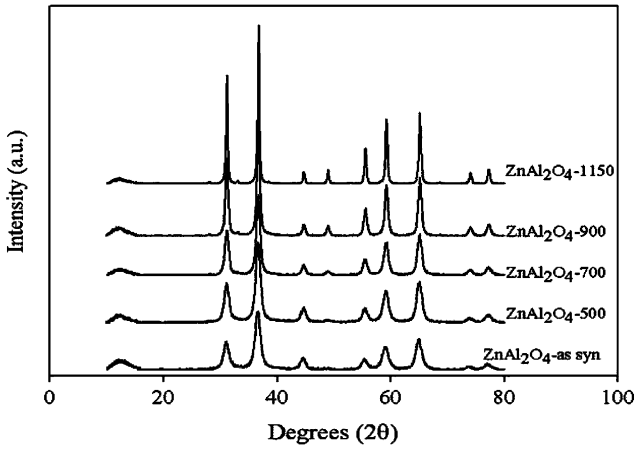

Fig. 1 XRD patterns of the as-synthesized and the calcined $ZnAl_2O_4$

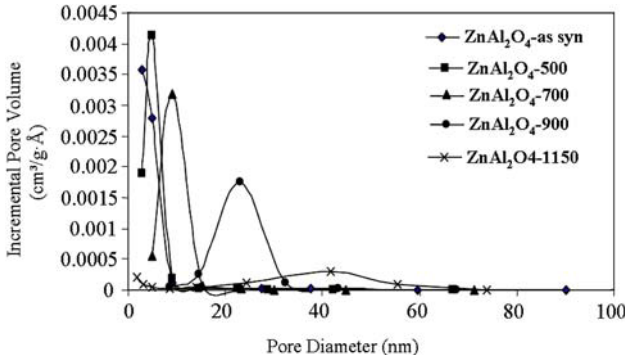

Fig. 2 Pore size distribution of the as-synthesized and the calcined $ZnAl_2O_4$

$ZnAl_2O_4$ samples retained their large pore volume and narrow pore size distribution during high temperature calcination up to 700 °C. Significant loss of pore volume was found for the sample calcined at 1,150 °C ($ZnAl_2O_4$-33 nm).

Figure 3 shows the transmission electron micrographs with selective area electron diffraction (SAED) pattern of various $ZnAl_2O_4$ spinels. The crystallites of $ZnAl_2O_4$ consisted of particles which were agglomerates of smaller crystallites with primarily spherical shapes. The average crystal sizes of the as-prepared and the calcined samples determined from TEM were similar to those measured from the XRD line broadening. The corresponding selected area diffraction patterns confirmed the structure of $ZnAl_2O_4$ and there was no significantly difference in SAED patterns of the as-synthesized and the calcined samples (not shown), indicating that all the samples contained only crystalline $ZnAl_2O_4$.

The presence of defect sites on the nanocrystalline supports was detected using electron spin resonance spectrometry. ESR is known as an effective method for investigating of the electron spin state and the structure of the surface of nano-sized crystallites. The ESR signals from the various solvothermal-derived nanocrystalline $ZnAl_2O_4$ are shown in Fig. 4. It is shown that only the $ZnAl_2O_4$-33 nm sample exhibited very strong and stable ESR signals. These ESR signals may arise from O^{2-} vacancies on the surface and/or incorporation of trace impurities in their crystal structure during high temperature calcination resulting in crystal distortion. Moreover, it has been reported that nano-sized $ZnAl_2O_4$ possesses inverse structure when calcined at temperatures <900 °C [22]. The highly crystalline nature (regular spinel structure) of $ZnAl_2O_4$ was obtained at calcination temperatures ≥1,000 °C. The result in this study, however, was in agreement with literature that larger crystallites of nanocrystalline materials synthesized by the solvothermal method contain more defects than smaller ones [23].

3.2 Characteristics and Catalytic Properties of Nanocrystalline $ZnAl_2O_4$-Supported Pd Catalysts

The physicochemical properties of Pd supported on as-synthesize and calcined nanocrystalline $ZnAl_2O_4$ are shown in Table 2. For the as-synthesized ones, the BET surface areas were slightly decreased after impregnation with Pd suggesting pore blockage by Pd/PdO clusters. However, for the calcined $ZnAl_2O_4$ supportd ones, there were less differences in BET surface areas of the supports and of the supported Pd catalysts suggesting that much of the Pd/PdO may have been located on the external surfaces. The relative amounts of active surface Pd metal atoms on the catalyst samples were calculated from CO chemisorption experiments at room temperature. The calculation of Pd active sites was based on the assumption that

Table 1 N_2 physisorption results[a] and XRD determined average crystallite sizes of the as-synthesized and the calcined $ZnAl_2O_4$ supports prepared by the solvothermal method

Sample	BET S.A. (m^2/g)	Pore volume (m^3/g)	Avg. pore diameter (nm)	Avg. XRD crystallite size (nm)
$ZnAl_2O_4$-as-syn	130	0.18	4.2	8.2
$ZnAl_2O_4$-500	116	0.19	4.6	9.0
$ZnAl_2O_4$-700	63	0.20	8.5	10.9
$ZnAl_2O_4$-900	28	0.19	22.0	17.6
$ZnAl_2O_4$-1150	15	0.08	36.6	33.3

[a] Error of measurements as determined directly were ±10%

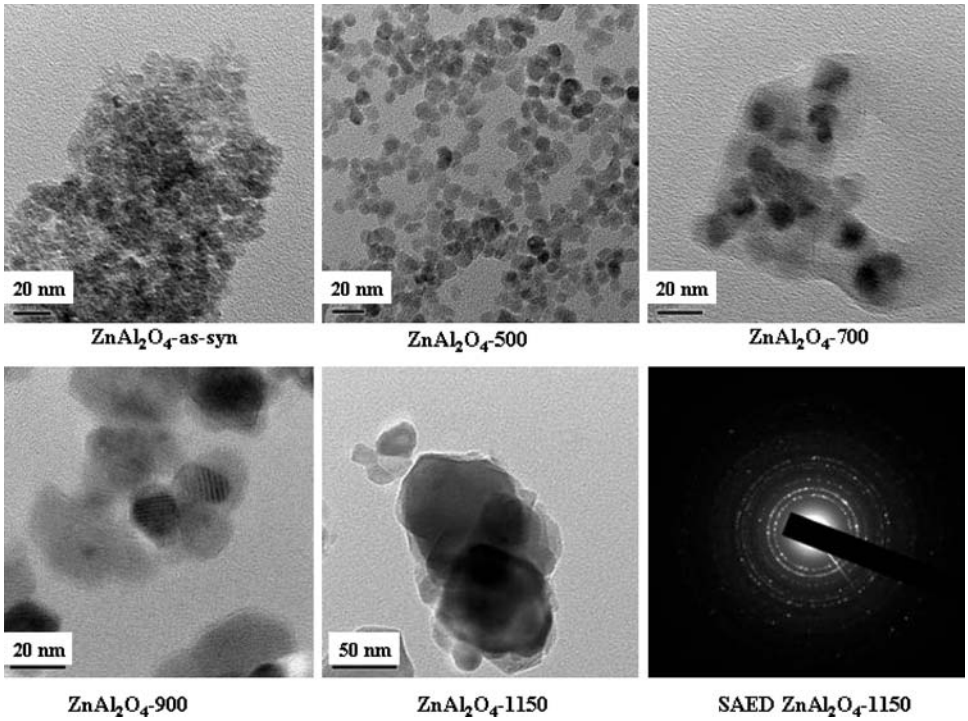

Fig. 3 TEM micrographs and selected area electron diffraction of various $ZnAl_2O_4$ samples

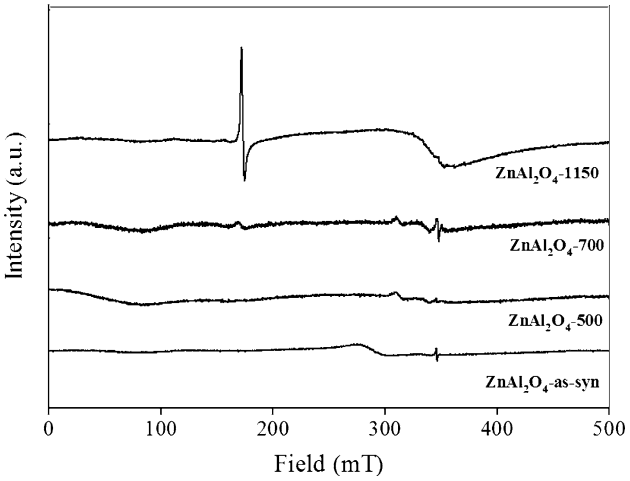

Fig. 4 ESR results of the solvothermal-derived $ZnAl_2O_4$

one carbon monoxide molecule adsorbs on one palladium surface atom or site [24]. It is surprising that the amounts of CO chemisorption were essentially similar for the Pd catalysts supported on $ZnAl_2O_4$ with the average crystallite sizes in the range of 8–18 nm. The amount of CO chemisorption was increased for the one supported on $ZnAl_2O_4$-33 nm. The percentages of Pd dispersion and corresponding Pd^0 particle sizes were calculated based on the CO chemisorption results and are also given in Table 2.

The catalytic properties of all the catalyst samples were investigated for the liquid-phase hydrogenation of 1-heptyne under mild conditions using a stirred batch reactor. The results are summarized in Table 3. The conversions of 1-heptyne for various $Pd/ZnAl_2O_4$ catalysts were in the range of 45–66% with $Pd/ZnAl_2O_4$-33 nm exhibiting the highest conversion. There were no appreciable influences on 1-heptene selectivity since all the catalysts exhibited high selectivities for 1-heptene (97–100%). The specific activities of the $Pd/ZnAl_2O_4$ catalysts are also expressed in terms of turnover frequency (TOF) which is defined as mole of product/mole of surface metal atoms/time. This is not a perfect measure of TOF since it is for reaction with a high conversion and therefore affected by changing reactant concentration. However, it is given here as a rough comparison of specific rate.

The actual amounts of palladium loading before and after reaction were determined by atomic adsorption spectroscopy and the %Pd leached for each catalyst is given in Table 3. Before reaction, palladium loading on all the catalyst samples was approximately 1.2 wt%. After one batch reaction period, the amount of palladium loading decreased to 0.6–1.1 wt% indicating that leaching of palladium occurred during reaction for most of the catalysts. Leaching of the active metal is one of the main causes of catalyst deactivation in liquid phase reactions. It depends upon the reaction medium (pH, oxidation potential, chelating properties of molecules) and upon bulk and surface properties of the metal [25]. The percentages of palladium leaching were found to be much lower when Pd catalysts were supported on $ZnAl_2O4$-33 nm compared to those on smaller crystallite size ones.

Table 2 Physicochemical properties of the various Pd catalysts

Catalysts	BET S.A.[a] (m^2/g)	Pore volume[a] (m^3/g)	Avg. pore diameter[a] (nm)	CO chemisorption[b] (10^{18} molecules CO/g cat.)	Dispersion(%)[c]	Pd^0 d_P[d] (nm)
$Pd/ZnAl_2O_4$-as-syn	106	0.20	4.6	7.4	13.0	7.8
$Pd/ZnAl_2O_4$-500	104	0.21	4.8	7.4	13.1	7.8
$Pd/ZnAl_2O_4$-700	66	0.21	8.9	7.2	12.8	7.4
$Pd/ZnAl_2O_4$-900	28	0.18	21.5	7.3	12.8	8.0
$Pd/ZnAl_2O_4$-1150	16	0.10	29.2	8.7	15.3	6.7

[a] Determined from N_2 physisorption. Error of measurements as determined directly were ±10%

[b] Error of measurements for CO chemisorption as determined directly were ±5%

[c] Based on total palladium loading and an assumption of CO/Pd = 1

[d] Based on d = (1.12/*D*) nm [24], where *D* = fractional metal dispersion

Table 3 Catalytic properties for liquid-phase 1-heptyne hydrogenation[a]

Catalysts	Conversion of 1-heptyne (%)	1-Heptene selectivity (%)	Estimated TOF[b] (s^{-1})[c]	%Pd leached[d]
$Pd/ZnAl_2O_4$-as-syn	52	97	0.24	36
$Pd/ZnAl_2O_4$-500	51	100	0.23	38
$Pd/ZnAl_2O_4$-700	45	100	0.22	30
$Pd/ZnAl_2O_4$-900	49	100	0.24	35
$Pd/ZnAl_2O_4$-1150	66	100	0.32	6

[a] Reaction conditions were 105 kPa, 30 °C, 5 min, and catalyst/substrate molar ratio = 1,600

[b] TOF = mole product/mole Pd metal surface atoms/s. Based on the amount of potentially active Pd atoms measured by CO chemisorption

[c] Estimated since at high conversion

[d] Based on atomic absorption spectroscopy results. Error of measurement as determined directly was ±10%

The mechanism of metal leaching usually involves metal compounds that are formed and are soluble in the reaction mixture. However, it is unlikely that 1-heptyne forms a compound with Pd at room temperature, unless it is some hydrido-organic complex. It is likely that Pd was leached in the form of Pd hydride phase. Under certain conditions, Pd-β-hydride can appear as a soft material with higher mechanical abrasion [26]. Moreover, leaching of Pd may depend on Pd particle size, larger particles are more likely to be leached since larger particles formed Pd-β-hydride more easily [27, 28]. Similar results have been reported previously by our group for the deactivation of Pd/SiO_2 catalysts during liquid-phase hydrogenation [29, 30]. The leached Pd species, however, appeared to be inactive for the present hydrogenation since the catalyst recycling test showed minimal loss of activity after it was reused for several cycles. Moreover, Pd-β-hydride is expected to have a different catalytic activity from that of metallic palladium [31].

The interaction between Pd and the nanocrystalline supports was also studied by XPS analysis, the Pd $3d_{5/2}$ core level binding energy of the various catalyst samples are shown in Fig. 5. It can be seen that the Pd $3d_{5/2}$ binding energy for Pd catalyst supported on the $ZnAl_2O_4$-33 nm shifted towards higher binding energy suggesting a stronger interaction between Pd and the highly crystalline supports. Among the various $ZnAl_2O_4$ samples in this

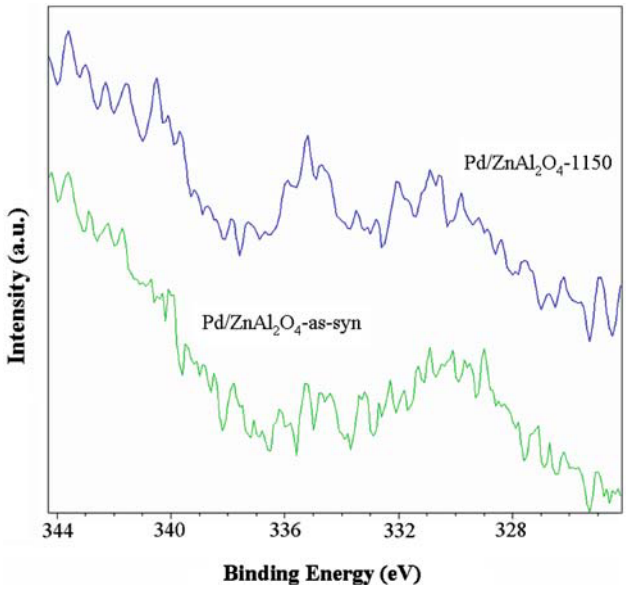

Fig. 5 XPS spectra of Pd $3d_{5/2}$ for $Pd/ZnAl_2O_4$ catalysts

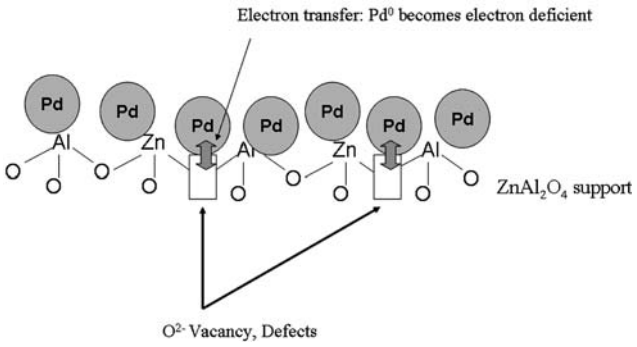

Fig. 6 A conceptual model for stronger metal-support interaction induced by defect sites of the nanocrystalline material

study, only the $ZnAl_2O_4$-33 nm possessed significant amount of defects. Thus, it is hypothesized that electron transfer occurred at the defective points of the nanocrystalline materials from Pd to the support, and, as a consequence, Pd^0 surface atoms became electron deficient and their catalytic properties were modified. A conceptual model for stronger metal-support interaction induced by defective sites of $ZnAl_2O_4$-33 nm is illustrated in Fig. 6.

4 Conclusions

The catalytic activities and deactivation of Pd catalysts supported on the solvothermal-derived nanocrystalline $ZnAl_2O_4$ in liquid-phase hydrogenation of 1-heptyne were investigated. Higher turnover frequencies and less Pd leaching were obtained on the Pd catalyst supported on larger crystallite size $ZnAl_2O_4$ that contained significant amounts of defects (as shown by strong and stable ESR signals). It is suggested that the presence of defects on these nanocrystalline materials induced stronger metal-support interaction between Pd and the supports thus their catalytic properties were modified.

Acknowledgments Financial supports from the Thailand Research Fund (RMU50-Joongjai Panpranot), the Graduate School of Chulalongkorn University (the 90th Anniversary of Chulalongkorn University-the Golden Jubilee Fund), and the Commission on Higher Education, Ministry of Education, Thailand are gratefully acknowledged.

References

1. Guczi L, Horvath A, Beck A, Sarkany A (2003) Stud Surf Sci Catal 145:351
2. Dominguez-Quintero O, Martinez S, Henriquez Y, D'Ornelas L, Krentzien H, Osuna J (2003) J Mol Catal A 197:185
3. Stanger KJ, Tang Y, Anderegg J, Angelici RJ (2003) J Mol Catal A 202:147
4. Nijhuis TA, van Koten G, Moulijn JA (2003) Appl Catal A 238:259
5. Chou P, Vannice MA (1987) J Catal 107:129
6. Jackson SD, Shaw LA (1996) Appl Catal A 134:91
7. Cherkashin GM, Shuikina LP, Parengo OP, Frilov VM (1985) Kinet Katal 26:1110
8. L'Argentiere PL, Liprandi DA, Cagnola EA, Figoli NS (1997) Catal Lett 44:101
9. Mathew JP, Srinivasan M (1995) Eur Polym J 31:835
10. Choudary BM, Kantam ML, Reddy NM, Rao KK, Haritha Y, Bhaskar V, Figueras F, Tuel A (1999) Appl Catal A 181:139
11. Shen WJ, Okumura M, Matsumura Y, Haruta M (2001) Appl Catal A 213:225
12. Pinna F, Menegazzo F, Signoretto M, Canton P, Fagherazzi G, Pernicone N (2001) Appl Catal A 219:195
13. Panpranot J, Pattamakomson K, Praserthdam P, Goodwin JG Jr (2004) Ind Eng Chem Res 43:6014
14. Wrzyszcz J, Zawadzki M, Trawczynski J, Grabowska H, Mista W (2001) Appl Catal A 210:263
15. Zawadzki M, Mista W, Kepinski L (2001) Vacuum 63:291
16. Wrzyszcz J, Zawadzki M, Trzeciak AM, Ziolkowski JJ (2002) J Mol Catal A 189:203
17. Inoue M, Kondo Y, Inui T (1988) Inorg Chem 27:215
18. Inoue M, Kominami H, Inui T (1992) J Am Ceram Soc 75:2597
19. Panpranot J, Taochaiyaphoom N, Praserthdam P (2005) Mater Chem Phys 94:207
20. Panpranot J, Nakkararuang L, Ngamsom B, Praserthdam P (2005) Catal Lett 103:53
21. Panpranot J, Taochaiyaphum N, Jongsomjit B, Praserthdam P (2006) Catal Commun 7:192
22. Mathur S, Veith M, Haas M, Shen H, Lecerf N, Huch V, Hufner S, Haberkorn R, Beck HP, Jilavi M (2001) J Am Ceram Soc 84:1921
23. Kongsuebchart W, Praserthdam P, Panpranot J, Sirisuk A, Supphasrirongjaroen P, Satayaprasert C (2006) J Crystal Growth 297:234
24. Mahata N, Vishwanathan V (2000) J Catal 196:262
25. Besson M, Gallezot P (2003) Catal Today 81:547
26. Albers P, Pietsch J, Parker SF (2001) J Mol Catal A 173:275
27. Shen WJ, Okumura M, Matsumura Y, Haruta M (2001) Appl Catal A 213:225
28. Neri G, Musolino MG, Milone C, Pietropaolo D, Glavagno S (2001) Appl Catal A 208:307
29. Panpranot J, Tangjitwattakarn O, Praserthdam P, Goodwin JG Jr (2005) Appl. Catal 292:322
30. Panpranot J, Pattamakomson K, Praserthdam P, Goodwin JG Jr (2004) Ind Eng Chem Res 43:6014
31. Walter J, Heiermann J, Dyker G, Hara S, Shioyama H (2000) J Catal 189:449

Journal of Catalysis 262 (2009) 199–205

Contents lists available at ScienceDirect

Journal of Catalysis

www.elsevier.com/locate/jcat

Effect of strong metal–support interaction on the catalytic performance of Pd/TiO_2 in the liquid-phase semihydrogenation of phenylacetylene

Patcharaporn Weerachawanasak [a], Okorn Mekasuwandumrong [b], Masahiko Arai [c], Shin-Ichiro Fujita [c], Piyasan Praserthdam [a], Joongjai Panpranot [a,*]

[a] Center of Excellence on Catalysis and Catalytic Reaction Engineering, Department of Chemical Engineering, Faculty of Engineering, Chulalongkorn University, Bangkok 10330, Thailand
[b] Department of Chemical Engineering, Faculty of Engineering and Industrial Technology, Silpakorn University, Nakhonpathom 73000, Thailand
[c] Division of Chemical Process Engineering, Graduate School of Engineering, Hokkaido University, Sapporo, Japan

ARTICLE INFO

Article history:
Received 15 October 2008
Revised 28 November 2008
Accepted 16 December 2008
Available online 22 January 2009

Keywords:
Pd/TiO_2
Solvothermal synthesis
Liquid-phase semihydrogenation
Phenylacetylene
Strong metal–support interaction
TiO_2 crystallite size

ABSTRACT

Liquid-phase semihydrogenation of phenylacetylene under mild conditions has been investigated on a series of solvothermal-derived nano-TiO_2 supported Pd catalysts with various TiO_2 crystallite sizes in the range of 9–23 nm. As revealed by CO chemisorption and transmission electron microscopy, all the catalysts exhibited strong metal–support interaction (SMSI) when reduced at 500 °C. The catalysts with SMSI show remarkably high catalytic performance in terms of both hydrogenation activities (turnover frequencies (TOFs) 9.1–21.4 s^{-1}) and moderate-high selectivities to styrene (86–90%) at complete conversion of phenylacetylene. Without SMSI effect (the catalysts reduced at 40 °C), styrene selectivity and catalytic activity depended largely on the Pd particle size in which small Pd particles (formed on small crystallite size TiO_2 supports) exhibited lower phenylacetylene conversion and poor styrene selectivity. Moreover, the TOF values of the non-SMSI catalysts were similar to those reported in the literature for other supported Pd catalysts in liquid-phase semihydrogenation of phenylacetylene under mild conditions (TOFs 1.3–2.8 s^{-1}).

1. Introduction

Phenylacetylene removal by selective hydrogenation is a process of great industrial importance because phenylacetylene is a poisoning impurity in styrene feedstocks that causes deactivation of the styrene polymerization catalyst and degrades polystyrene properties [1]. From academic points of view, semihydrogenation of phenylacetylene has often been employed as a model reaction for evaluation of selective hydrogenation catalysts under very mild conditions. New heterogeneous catalysts for the liquid-phase semihydrogenation of phenylacetylene with high styrene selectivity have been continuously developed and reported. Most recent studies focus on preparation of Pd nanoparticles in the forms of dispersed colloids [2] and supported systems [3,4]. The latter, however, may be more commercially attractive for industrial applications due to their better handling properties and low separation problems. In the past, different inorganic and organic materials have been studied as Pd catalyst supports in liquid-phase semihydrogenation of phenylacetylene including carbon [2,5–7], SiO_2 [8,9], γ-Al_2O_3 [10], pumice [11,12], zeolites [4], polymers [1,13], organic matrices [14], pillared clays [15,16], mesostructured silica such as MCM-41, HMS, MSU-X [4,17,18], and TiO_2 [19].

Despite a number of studies on support effects on the reactivity of Pd in such a reaction, controversy regarding structure sensitivity of the reaction still exists. Typically, the turnover frequencies (TOFs) were determined based on the number of palladium sites measured by irreversible CO or H_2 chemisorption. Comparing the results obtained under mild reaction conditions (ambient temperature and low H_2 pressure), the TOF values of Pd catalysts in most of the aforementioned references fall into the same range (about 1–3 s^{-1}) suggesting structure insensitive characteristic of the reaction. Nevertheless, significant increase of the TOFs of Pd nanoparticles by at least fourfold to an order of magnitude has recently been reported on some specially prepared supported Pd catalysts [4,17]. In those studies, the hydrogenation of phenylacetylene was suggested to be structure-sensitive because the TOFs were found to increase with increasing Pd nanoparticle diameter. However, it is noticed that the remarkable high activities of supported Pd catalysts coincidently reported by the two different groups were obtained when Pd nanoparticles were supported on MCM-41 via simultaneous synthesis (simultaneous self-assembling of the MCM-41 and Pd incorporation). Conventional impregnation of palladium on MCM-41 gave similar activities compared to the others [4,18]. We speculate that by simultaneous synthesis, the Pd nanoparticles

* Corresponding author. Fax: +66 2218 6877.
E-mail address: joongjai.p@eng.chula.ac.th (J. Panpranot).

0021-9517/$ – see front matter
doi:10.1016/j.jcat.2008.12.011

may be surrounded by support matrices resulting in the inhibition of CO chemisorption and as a consequence high TOF values being calculated. Such phenomenon was probably similar to the decoration of metal surface by partially reducible metal oxides after high temperature reduction or so-called "the strong metal–support interaction" (SMSI) effect [20].

Thus, it was of interest in this study to verify the effect of SMSI on the catalytic activities and selectivities of Pd catalysts in the liquid phase semihydrogenation of phenylacetylene to styrene. Nanocrystalline TiO_2 powders with various crystallite sizes in the range of 9 to 23 nm were synthesized via solvothermal method and employed as supports for Pd catalysts. It is well-known that TiO_2 manifests SMSI with group VIII transition metals (e.g. Pd, Pt, Ni, and Ir) after high temperature reduction. Significant improvement of catalyst performance due to the SMSI effect has been reported in many catalytic reactions such as CO oxidation [21], methanol synthesis [22], selective acetylene hydrogenation [23–25], and liquid-phase hydrogenation [19,26–33]. Moreover, the degree of SMSI effect on Pd/TiO_2 has been shown to depend largely on both the TiO_2 crystal structure (anatase and rutile) [25–27] and TiO_2 crystallite size [19]. The reduction by H_2 at 200 °C resulted in SMSI for anatase titania supported palladium catalyst, but not for the rutile sample [27]. A very recent study from our group shows the absence of SMSI effect on Pd/TiO_2 when the crystallite size of TiO_2 was fairly large ($\geqslant$0.1 μm) [19]. Therefore, in order to ensure the occurrence of SMSI, the TiO_2 supports used in this study were pure anatase TiO_2 with average crystallite sizes in the nanometer range. The Pd/TiO_2 catalysts were characterized by X-ray diffraction (XRD), N_2 physisorption, scanning electron microscopy (SEM), transmission electron microscopy (TEM), and pulse CO chemisorption. Furthermore, the catalytic properties of the Pd/TiO_2 catalysts were evaluated in the liquid-phase semihydrogenation of phenylacetylene to styrene under mild conditions.

2. Experimental

2.1. Preparation of TiO_2 and Pd/TiO_2 catalysts

The solvothermal-derived nano-TiO_2 was prepared according to the method described in [34] using 15–25 g of titanium(IV) *n*-butoxide (TNB) 97% from Aldrich. The starting material was suspended in 100 ml of 1,4-butanediol in a test tube and then set up in an autoclave. In the gap between the test tube and autoclave wall, 30 ml of solvent was added. After the autoclave was completely purged with nitrogen, it was heated to the desired temperature (300–340 °C) at a rate of 2.5 °C min^{-1} and held at that temperature for 0.5–12 h. Autogenous pressure during the reaction gradually increased as the temperature was raised. After the reaction, the autoclave was cooled to room temperature. The resulting powders were collected by centrifugation after repeated washing with methanol. They were then air-dried at room temperature.

The 1%Pd/TiO_2 catalysts were prepared by the incipient wetness impregnation technique using an aqueous solution of the desired amount of $Pd(NO_3)_2{\cdot}6H_2O$ (Aldrich). The catalysts were dried overnight at 110 °C and then calcined in air at 450 °C for 3 h.

2.2. Catalyst characterization

The specific surface areas, pore volumes, and average pore diameters were determined by N_2 physisorption using a Micromeritics ASAP 2020 automated system and the Brunauer–Emmet–Teller (BET) method. Each sample was degassed under vacuum at $<$10 μm Hg in the Micromeritics system at 150 °C for 4 h prior to N_2 physisorption. The average pore size was calculated using the BJH desorption method. The XRD patterns of the catalysts were measured from 10° to 80° 2θ using a SIEMENS D5000 X-ray diffractometer and CuK_α radiation with a Ni filter. The catalyst morphology was obtained using a JEOL JSM-35CF scanning electron microscope (SEM) operated at 20 kV. Metal crystallite sizes were obtained using the JEOL JEM 2010 transmission electron microscope that employed a LaB_6 electron gun in the voltage range of 80–200 kV with an optical point to point resolution of 0.23 nm. The amounts of CO chemisorbed on the catalysts were measured using a Micromeritics Chemisorb 2750 automated system with ChemiSoft TPx software. Prior to chemisorption, the sample was reduced in a H_2 flow at the desired temperature for 2 h and then cooled down to ambient temperature in a He flow.

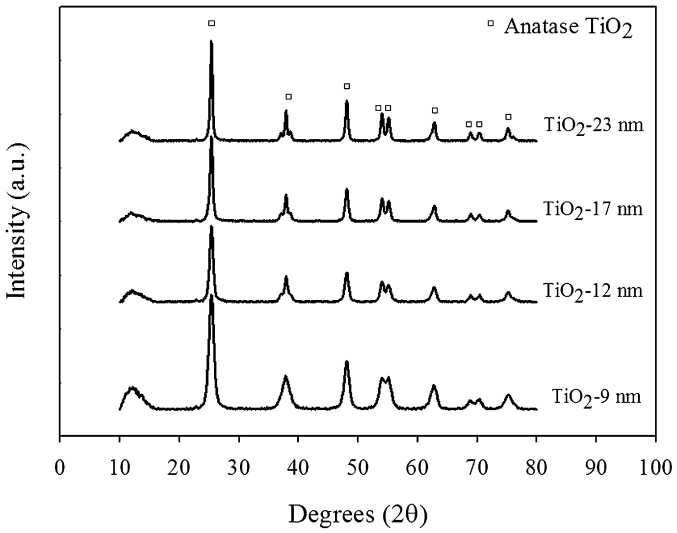

Fig. 1. XRD patterns of the solvothermal-derived TiO_2 with different crystallite sizes.

2.3. Reaction study

Approximately 0.05 g of 1%Pd/TiO_2 catalyst was placed into a 50 ml autoclave. 0.5 ml of phenyl acetylene and 4.5 ml of ethanol (solvent) were mixed in a volumetric flask before being introduced into the autoclave reactor. Afterward the reactor is purged with hydrogen gas. The liquid phase hydrogenation was carried out with H_2 pressure of 1–5 bar and at room temperature for 5–60 min. After the reaction, the vent valve was slowly opened to prevent the loss of product. The product mixture was analyzed by gas chromatography with flame ionization detector (FID) and a GS-alumina capillary column. GC analysis of the reactant after being purged with hydrogen prior to a start of run confirmed that no catalytic reaction occurred before the actual experiment took place.

3. Results and discussion

3.1. Catalyst characterization

In this study, the crystallite size of solvothermal-derived nano-TiO_2 was varied in the range of 9–23 nm by changing the synthesis conditions such as the amount of TNB, reaction temperature, and holding time. Increasing the amount of TNB, reaction temperature, or holding time resulted in an increase of TiO_2 crystallite size. Fig. 1 shows the XRD patterns of the various nano-TiO_2 samples prepared. The characteristic peaks of pure anatase phase titania were observed at $2\theta = 25$, 38, and 48° [35] without contamination of other phases such as rutile and brookite. The average crystallite sizes of TiO_2 were calculated from the full width at half maximum of the XRD peak at $2\theta = 25°$ using the Scherrer equation. The synthesis conditions and the average crystallite size, BET surface

Table 1
Synthesis conditions and physical properties of the nanocrystalline TiO_2.

Sample	TNB (g)	Temp. (°C)	Holding time[a] (h)	XRD crystallite size (nm)			BET surface area[c] (S_1) (m^2/g)	Pore volume[c] (cm^3/g)	Avg. pore diameter[c] (nm)
				As-syn	Reduced[b] at 40 °C	Reduced[b] at 500 °C			
TiO_2-9 nm	15	300	0.5	9	9	11	145	0.42	8.1
TiO_2-12 nm	25	300	2	12	12	13	88	0.37	12.5
TiO_2-17 nm	25	320	6	17	17	18	65	0.38	17.9
TiO_2-23 nm	25	340	12	23	23	23	51	0.32	20.2

[a] Holding time during the solvothermal synthesis of TiO_2 (after the autoclave was heated to 320 °C at a rate of 2.5 °C min^{-1}).
[b] After Pd was impregnated and calcined.
[c] As-syn TiO_2 samples.

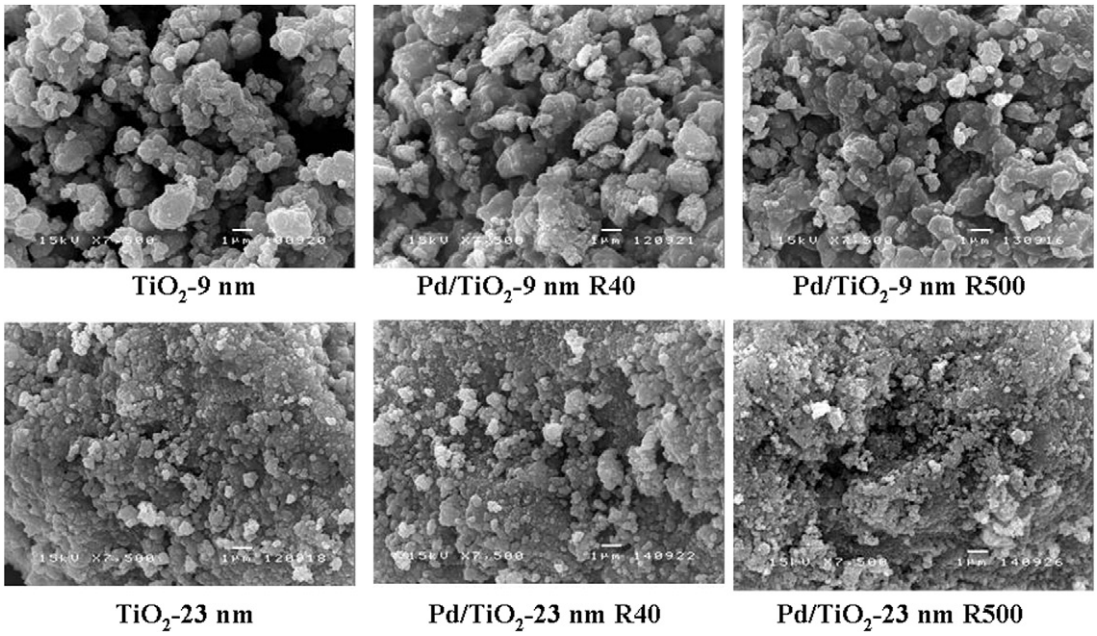

Fig. 2. SEM micrographs of calcined and reduced Pd/TiO_2 catalysts. Reduction temperature = 40 °C (R40), 500 °C (R500).

area, pore volume, and average pore diameter of the obtained TiO_2 samples are given in Table 1. As the average TiO_2 crystallite size increased from 9 to 23 nm, the BET surface area decreased monotonically from 145 to 51 m^2/g. The pore size distribution of various crystallite sizes of TiO_2 supports indicated that the pores of all TiO_2 samples were mesopores (results not shown). After impregnated with approximately 1 wt% Pd, calcined, and reduced at 40 or 500 °C, the crystallite sizes of all the TiO_2 samples as determined by XRD were essentially unaltered except that of the smallest crystallite size TiO_2 (TiO_2-9 nm) in which a slight increase of the TiO_2 crystallite size from 9 to 11 nm was observed. It is generally found that the crystals of small crystallite size show less thermal stability than the crystals of large crystallite size [36].

Fig. 2 shows the SEM micrographs of TiO_2-9 nm and TiO_2-23 nm supports and the corresponding 1 wt% Pd/TiO_2 catalysts after reduced at 40 and 500 °C. The nano-TiO_2 was consisted of irregular shape of very fine particles agglomerated. Morphologies of the reduced 1%Pd/TiO_2 catalysts were not significantly different from the corresponding TiO_2 supports. The particle size and shape of the catalyst particles were also not affected by impregnation of palladium (no changes in the particle size/shape). TEM analysis has been carried out in order to physically measure the TiO_2 crystallite size as well as Pd particle/cluster sizes on the various Pd/TiO_2 catalysts. The TEM results are shown in Fig. 3. The crystallite sizes of the TiO_2 supports were consistent to those obtained from XRD results. The presence of small palladium particles/clusters with an average particle size around 5–6 nm were apparent only on the Pd/TiO_2-23 nm.

The BET surface area, pore volume, average pore diameter, and CO chemisorption results of the various Pd/TiO_2 catalysts are shown in Table 2. The decreases in BET surface areas and pore volumes of the Pd/TiO_2 catalysts compared to the TiO_2 supports suggested that palladium was deposited in some of the pores of the TiO_2. From the CO chemisorption results, it can be seen that for the Pd/TiO_2 catalysts reduced at 40 °C, the amount of CO chemisorption decreased from 18.1×10^{18} to 9.73×10^{18} molecule CO/g cat. as the TiO_2 crystallite size increased from 9 to 23 nm. This was probably due to the lower specific surface area of the larger crystallite size TiO_2 supports that resulted in lower Pd dispersion. For the same catalyst, the amount of CO chemisorption was much lower when reduced at 500 °C. The amounts of CO chemisorption were in the range of 0.9 to 1.31×10^{18} molecule CO/g cat. However, the CO chemisorbed on all the R500 catalysts can be totally restored indicating that the palladium particles did not sinter during high temperature reduction at 500 °C and all the catalysts exhibited the SMSI effect. The Pd^0 metal particles calculated from CO chemisorption results for the catalysts reduced at 40 °C were found to be 3.2–5.9 nm depending on the TiO_2 crystallite size. The results were consistent with TEM analyses. For the catalysts reduced at 500 °C, the Pd^0 metal particle sizes were not determined since it would result in an over-estimation of the particle size. Low amounts of CO or H_2 chemisorption and an over-estimation of Pd particle size have occasionally been reported in other supported

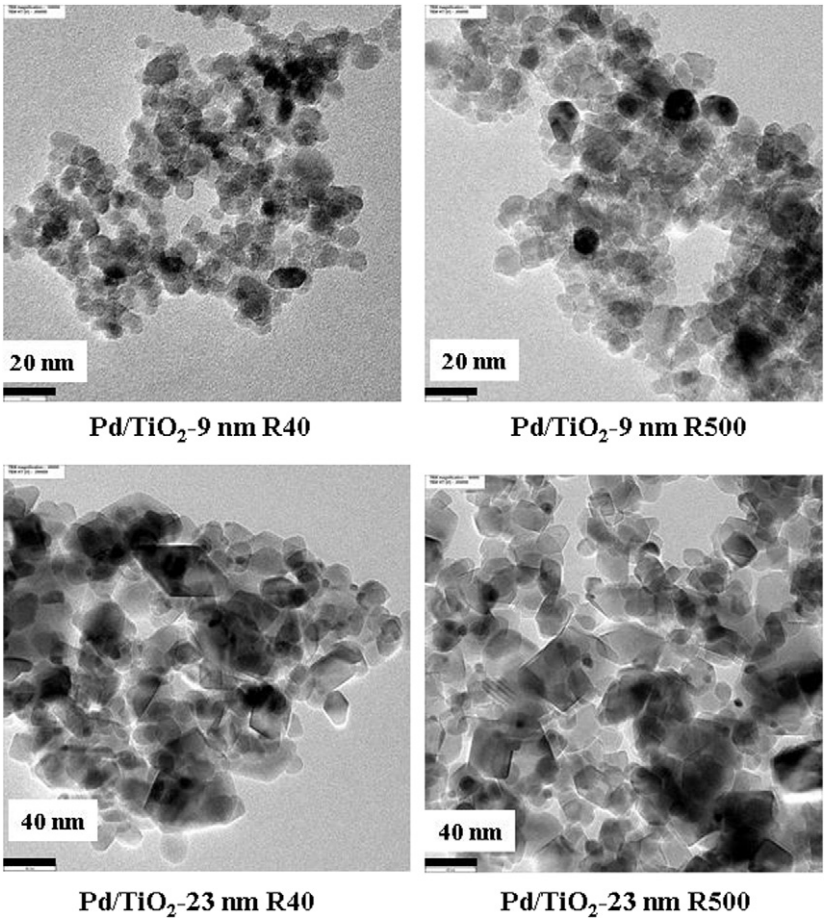

Fig. 3. TEM micrographs of Pd/TiO_2-9 nm and Pd/TiO_2-23 nm reduced at 40 °C (R40) and 500 °C (R500).

Table 2
N_2 physisorption and CO chemisorption results of the Pd/TiO_2 catalysts.

Catalyst	BET surface area (m^2/g)	Pore volume (cm^3/g)	Avg. pore diameter (nm)	CO chemisorption[a] ($\times 10^{-18}$ molecule CO/g cat.)	%Pd dispersion	d_P[d] Pd^0 (nm)
Pd/TiO_2-9 nm R40	135	0.30	6.3	18.1	35.5	3.2
Pd/TiO_2-9 nm R500	89	0.20	6.2	1.31 (18.4)[b]	n.d.[c]	n.d.
Pd/TiO_2-12 nm R40	84	0.31	11.1	15.6	30.5	3.7
Pd/TiO_2-12 nm R500	75	0.30	10.7	1.02 (16.1)	n.d.	n.d.
Pd/TiO_2-17 nm R40	62	0.30	14.3	12.1	23.8	4.7
Pd/TiO_2-17 nm R500	60	0.30	14.2	0.9 (12.0)	n.d.	n.d.
Pd/TiO_2-23 nm R40	47	0.28	19.8	9.73	19.1	5.9
Pd/TiO_2-23 nm R500	42	0.29	19.7	1.11 (11.8)	n.d.	n.d.

[a] Experimental error as determined directly from the measurements = ±5%.
[b] The number in parenthesis indicated the amount of CO chemisorption after the R500 catalyst was re-calcined and re-reduced at 40 °C.
[c] n.d. = not determined.
[d] Based on $d = (1.12/D)$ nm [47], where D = fractional metal dispersion.

Pd catalyst systems such as Pd/MCM-41 prepared via simultaneous synthesis [4,17] and Pd/SiO_2 prepared by one-step flame spray pyrolysis [37]. In those studies, the synthesis of support phase occurred simultaneously with the formation of Pd nanoparticles so the Pd particles may be surrounded by support matrix (i.e., in the form of Si–O group). This could result in the inhibition of CO chemisorption. Such phenomena were somewhat similar to the SMSI effect on Pd/TiO_2. It is generally known that SMSI occurs after reduction at high temperature due to the decoration of the metal surface by partially reducible metal oxides [38,39] and/or by an electron transfer between the support and the metals [40,41] resulting in CO and H_2 chemisorption suppression.

3.2. Catalytic tests

The performance of Pd/TiO_2 catalysts was evaluated in the liquid-phase semihydrogenation of phenylacetylene to styrene in a batch-type stainless steel reactor under mild reaction conditions (H_2 pressure 5 bar and 30 °C). Fig. 4 shows the change in product distribution with reaction time from 5–60 min. In all cases, phenylacetylene was hydrogenated up to nearly 100% conversion within 20 min under the reaction conditions used. The hydrogenation of styrene to ethylbenzene occurred when the concentration of phenylacetylene was sufficiently low indicating a slower parallel reaction pathway for the direct hydrogenation of pheny-

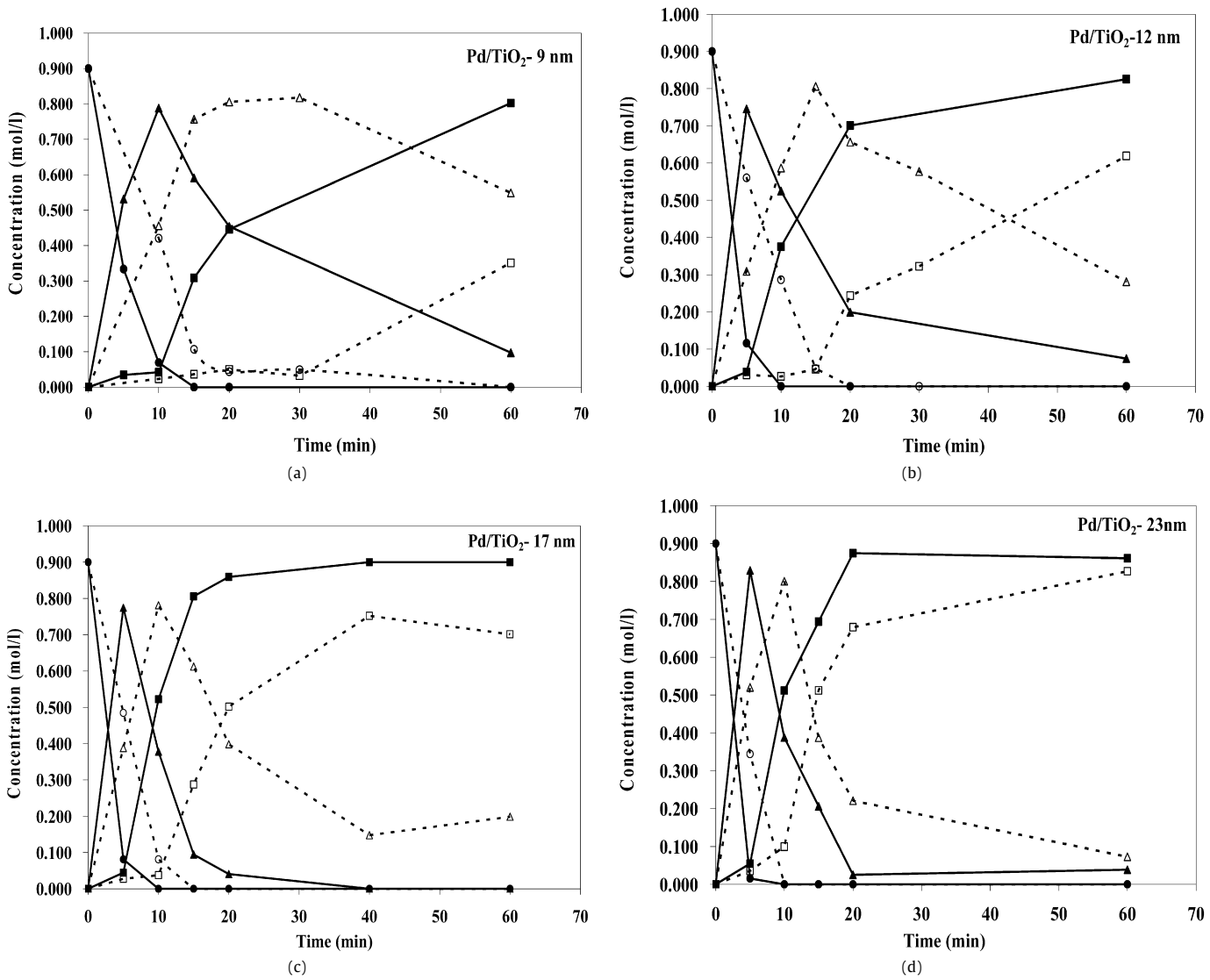

Fig. 4. Liquid-phase semihydrogenation of phenylacetylene over the Pd/TiO_2 catalysts: ○ = phenylacetylene △ = styrene □ = ethylbenzene, solid symbols = Pd/TiO_2 catalysts reduced at 40 °C and open symbols = Pd/TiO_2 catalysts reduced at 500 °C (a) Pd/TiO_2-9 nm, (b) Pd/TiO_2-12 nm, (c) Pd/TiO_2-17 nm, (d) Pd/TiO_2-23 nm (reaction conditions were H_2 pressure = 5 bar and 30 °C).

lacetylene to ethylbenzene. Similar profiles were found for other Pd catalyst systems reported in the literature such as Pd/SiO_2, Pd/C, and commercial Lindlar catalyst in semihydrogenation reaction of alkynes to alkenes [6,42]. The catalyst performance plots (styrene selectivity versus conversion of phenylacetylene) for the various Pd/TiO_2 catalysts are shown in Fig. 5. As can be observed, the catalyst performance was significantly improved when reduced at 500 °C. High styrene selectivity (around 86–90%) was achieved at complete conversion of phenylacetylene for all the catalysts reduced at 500 °C while for the non-SMSI catalysts, the selectivity for styrene significantly dropped to 20–60% when conversion of phenylacetylene reached 100%. Such results confirm the beneficial effect of SMSI in Pd/TiO_2 catalysts on the catalyst performance [8,19]. Charge transfer from the TiO_2 support to Pd during high temperature reduction caused electron enrichment of Pd particles which favored rapid desorption of styrene molecules. Similar results have also been observed for the Pd catalysts supported on organic matrices such as *oligo-p-phenylenterephthalamide* (OPTA) which induces electron transfer from support to metal surface [14]. In gas-phase selective hydrogenation of acetylene to ethylene on Pd/TiO_2 catalysts, the charge transfer from Ti species to Pd weakened the adsorption strength of ethylene on the Pd surface and,

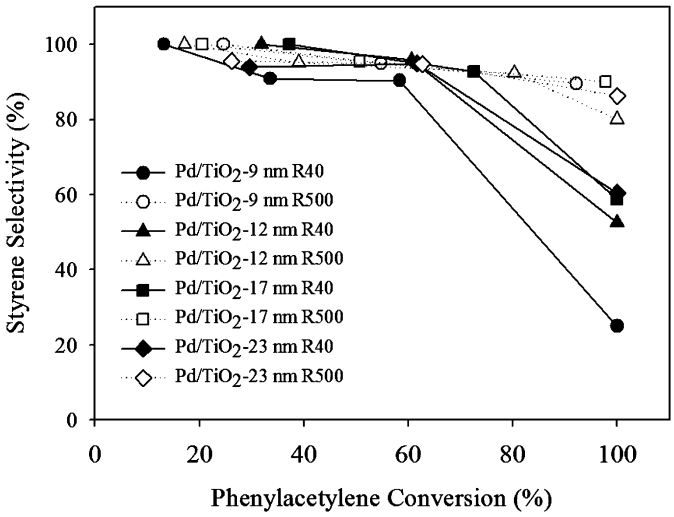

Fig. 5. Performance curves of the various Pd/TiO_2 for selective hydrogenation of phenylacetylene.

Table 3
Catalytic activity of the Pd/TiO_2 catalysts in liquid-phase semihydrogenation of phenylacetylene.

Catalyst	Initial rate[a] (mole products/g cat. s)	TOF[b] (s^{-1})	TOF_{R40}/TOF_{R500}
Pd/TiO_2-9 nm R40	0.14	1.3	
Pd/TiO_2-9 nm R500	0.07	9.1	7.2
Pd/TiO_2-12 nm R40	0.18	1.9	
Pd/TiO_2-12 nm R500	0.09	15.2	8.1
Pd/TiO_2-17 nm R40	0.20	2.8	
Pd/TiO_2-17 nm R500	0.11	20.3	7.3
Pd/TiO_2-23 nm R40	0.16	2.8	
Pd/TiO_2-23 nm R500	0.14	21.4	7.6

[a] Reaction conditions were H_2 pressure = 1 bar, $T = 30\,^{\circ}C$, and reaction time = 10 min.
[b] Based on CO chemisorption results.

hence, higher ethylene selectivity was obtained [23–25]. However, among the R40 series catalysts, the Pd/TiO_2-9 nm R40 exhibited the lowest styrene selectivity at complete conversion of phenylacetylene despite its highest Pd dispersion. This could probably be attributed to longer residence time of styrene on small metal particles [10]. Low dispersed palladium catalysts also showed to be more selective to partial hydrogenation than highly dispersed ones [43].

The initial rates of phenylacetylene hydrogenation and the corresponding TOF values for the eight catalyst samples are given in Table 3. The measured TOF values were based on the experimental results obtained under the reaction conditions that yielded phenylacetylene conversion less than 50% for all the catalysts (H_2 pressure 1 bar 30 °C and reaction time 10 min). For the R40 series (non-SMSI catalysts), the TOFs were not significantly different ranging from 1.3 to 2.8 s^{-1}. The values were very close to those reported in the literature for supported Pd catalysts in liquid-phase hydrogenation of phenylacetylene under mild conditions as summarized in Table 4. The relatively low activity of Pd/TiO_2-9 nm R40 can be attributed to the very small Pd particles being formed on the small crystallite size TiO_2 support. There has been an establishing trend in the literature that specific activity (turnover frequencies) of Pd in selective hydrogenation decreases as Pd particle size decreases especially when the average Pd particle size is very small ($\leqslant$3–5 nm) [4,8,44]. Diminishing activity of small metal particles was probably due to the different band structure characteristics of nano-sized metal compared to bulk metals and that they appear to be electron deficient [45].

For the R500 series, (SMSI catalysts), all the catalysts exhibited very high TOFs (9.1–21.4 s^{-1}). The catalyst performance was proved in terms of both hydrogenation activity and selectivity to styrene. It may be assumed that the presence of SMSI effect favors the formation of active Pd species participating in the reaction. The strong interaction between metal and support and the formation of interfacial Pd–TiO_x sites have also been found in the Pd/TiO_2 catalysts prepared by sol–gel method [28]. They were suggested to be the reasons for the catalysts exhibiting high conversion and high yield towards butyric acid in liquid-phase hydrogenation of maleic anhydride. Remarkable high activities in the hydrogenation of alkynes were also reported for the Pd/MCM-41 catalysts prepared via simultaneous synthesis [4,17] and Pd/SiO_2 prepared by one-step flame spray pyrolysis [37]. It was suggested that simultaneous formation of Pd nanoparticles in the support matrices resulted in the formation of active ensembles for the reaction. In the present study, largest improvement on the catalytic performance for Pd/TiO_2 catalysts reduced at 500 °C was observed on the smallest crystallite size TiO_2 (Pd/TiO_2-9 nm) probably because the formation of substoichiometric TiO_x species was more facile over small crystallite size TiO_2 [46]. The ratios of TOF values of the SMSI and non-SMSI catalysts for the Pd/TiO_2 with different TiO_2 crystallite sizes (see Table 3), however, were quite similar, implying that the degree of SMSI effect on the hydrogenation rate did not depend on the Pd particle size.

4. Conclusions

The presence of SMSI on Pd/TiO_2 catalysts when reduced at 500 °C has proven to produce great beneficial effect on both catalytic hydrogenation activities and selectivities to styrene in liquid-phase semihydrogenation of phenylacetylene under mild conditions (ambient temperature and low H_2 pressure). Without SMSI effect, the turnover frequencies of Pd/TiO_2 were similar to those of other supported Pd catalysts reported in the literature and the catalyst performance depended largely on Pd particle size. In the range of Pd particle size studied (3.2–5.9 nm), the TOF values and styrene selectivity at complete conversion of phenylacetylene increased with increasing Pd particle size.

Acknowledgments

Financial supports from the Thailand Research Fund (TRF) contract RMU50-80030 for Joongjai Panpranot, and the Commission on Higher Education, Thailand are gratefully acknowledged.

Table 4
Comparison of the catalytic activities of supported Pd catalysts in liquid-phase semihydrogenation of phenylacetylene under mild conditions.

Catalyst	BET surface area (m^2/g)	Reactant: Pd molar ratio	Reaction conditions[a]	Pd^0 particle size (nm)	TOFs (s^{-1})	Source
Pd/TiO_2 reduced 40 °C	42–135	1000	$T = 298$ K, $P = 1$ bar	3.2–5.9	1.3–2.8	This work
Pd/TiO_2 reduced 500 °C					9.1–21.4	
Pd/C	136–1343	n/a[b]	$T = 323$ K, $P = 1$ bar	2.5–5.6	0.81–0.96	[3]
Pd/MCM-41	875–970	7300	$T = 323$ K, $P = 1$ bar	2.5–6.8	1.0–4.0	[4]
Pd/Al-MCM-41	928–1066			2.4–7.6	1.0–6.5	
Pd/Al_2O_3	54			2.1	1.0	
Pd/beta zeolite	390			2.4	1.0	
Pd/SiO_2	234–248	1000	$T = 303$ K, $P = 1$ bar	10–12	1.2–1.6	[8]
Pd/pumice	5	1000	$T = 298$ K, $P = 1$ bar	6.3–11.0	6.0–7.7	[11,12]
Pd/organic matrices	n/a	n/a	$T = 283$ K	2.0–12.8	1.3–2.7	[14]
Pd/Al_2O_3, Pd/C	n/a	2500	$T = 298$ K, $P = 1$ bar	1.9, 5.2	0.9, 2.2	[15]
Pd/MCM-41	806–1099	2000	$T = 298$ K, $P = 1$ bar	10–23	5.1–12.9	[17]
Pd/mesostructured silica	910–1469	2500	$T = 298$ K, $P = 1$ bar	0.7–3.2	2.0–4.0	[18]

[a] T = reaction temperature, $P = H_2$ pressure.
[b] n/a = not available.

References

[1] B.R. Maurer, M. Galobardes, US Patent 4,822,936, 1989.
[2] S. Dominguez-Dominguez, A. Berenguer-Murcia, D. Cazorla-Amoros, A. Linares-Solano, J. Catal. 243 (2006) 74.
[3] S. Dominguez-Dominguez, A. Berenguer-Murcia, B.K. Pradhan, D. Cazorla-Amoros, A. Linares-Solano, J. Phys. Chem. C 112 (2008) 3827.
[4] S. Dominguez-Dominguez, A. Berenguer-Murcia, A. Linares-Solano, D. Cazorla-Amoros, J. Catal. 257 (2008) 87.
[5] R.V. Chaudhari, R. Jaganathan, D.S. Kolhe, Ind. Eng. Chem. Prod. Res. Dev. 25 (1986) 375.
[6] S.D. Jackson, L.A. Shaw, Appl. Catal. 134 (1996) 91.
[7] F.M. Bautista, J.M. Campelo, A. Garcia, D. Luna, J. Marinas, R.A. Quiros, A.A. Romero, Catal. Lett. 52 (1998) 205.
[8] J. Panpranot, K. Phandinthong, T. Sirikajorn, M. Arai, P. Praserthdam, J. Mol. Catal. 261 (2007) 29.
[9] S.S. Mahmoud, I.M. Arafa, O.I. Sheikha, Asian J. Chem. 12 (2000) 1047.
[10] C. Del Angel, J.L. Benitez, React. Kinet. Catal. Lett. 51 (1993) 547.
[11] L. Guczi, Z. Schay, Gy. Stefler, L.F. Liotta, G. Deganello, A.M. Venezia, J. Catal. 182 (1999) 456.
[12] D. Duca, L.F. Liotta, G. Deganello, J. Catal. 154 (1995) 69.
[13] M. Terasawa, H. Yamamoto, K. Kaneda, T. Imanaka, S. Teranishi, J. Catal. 57 (1979) 315.
[14] F. Arena, G. Cum, R. Gallo, A. Parmaliana, J. Mol. Catal. A 110 (1996) 235.
[15] A. Mastalir, Z. Király, J. Catal. 220 (2003) 372.
[16] A. Mastalir, Z. Király, F. Berger, Appl. Catal. A 269 (2004) 161.
[17] A. Papp, A. Molnar, A. Mastalir, Appl. Catal. A 289 (2005) 256.
[18] N. Marin-Astorga, G. Pecchi, T.J. Pinnavaia, G. Alvez-Manoli, P. Reyes, J. Mol. Catal. A 247 (2006) 145.
[19] P. Weerachawanasak, P. Praserthdam, M. Arai, J. Panpranot, J. Mol. Catal. A 279 (2007) 133.
[20] S.J. Tauster, S.C. Fung, R.L. Garten, J. Am. Chem. Soc. 100 (1978) 170.
[21] H. Zhu, Z. Qin, W. Shan, W. Shen, J. Wang, J. Catal. 233 (2005) 41.
[22] N. Tsubaki, K. Fujimoto, Top. Catal. 22 (2003) 325.
[23] H.K. Jung, W.S. Eun, J.K. Woo, D.P. Jae, H.M. Sang, J. Catal. 208 (2002) 310.
[24] J. Panpranot, K. Kontapakdee, P. Praserthdam, J. Phys. Chem. B 110 (2006) 8019.
[25] J. Panpranot, K. Kontapakdee, P. Praserthdam, Appl. Catal. A 314 (2006) 128.
[26] Y. Li, B. Xu, Y. Fan, N. Feng, A. Qiu, J. Miao, J. He, H. Yang, Y. Chen, J. Mol. Catal. A 216 (2004) 107.
[27] P.S. Kumbhar, Appl. Catal. A 96 (1993) 241.
[28] J. Xu, K. Sun, L. Zhang, Y. Ren, X. Xu, Catal. Commun. 6 (2005) 462.
[29] P. Reyes, H. Rojas, J.L.G. Fierro, Appl. Catal. A 248 (2003) 59.
[30] U.K. Singh, M.A. Vannice, Stud. Surf. Sci. Catal. 130 (2000) 497.
[31] P. Reyes, H. Rojas, G. Pecchi, J.L.G. Fierro, J. Mol. Catal. A 179 (2002) 293.
[32] U.K. Singh, M.A. Vannice, J. Mol. Catal. A 163 (2000) 233.
[33] J. Xiong, J. Chen, J. Zhang, Catal. Commun. 8 (2007) 345.
[34] W. Payakgul, O. Mekasuwandumrong, V. Pavarajarn, P. Praserthdam, Ceram. Int. 31 (2005) 391.
[35] S.S. Watson, D. Beydoun, J.A. Scott, R. Anal, Chem. Eng. J. 95 (2003) 213.
[36] H. Kominami, M. Kohno, Y. Takada, M. Inoue, T. Inui, Y. Kera, Ind. Eng. Chem. Res. 38 (1999) 3925.
[37] S. Somboonthanakij, O. Mekasuwandumrong, J. Panpranot, T. Nimmanwudtipong, R. Strobel, S.E. Pratsinis, P. Praserthdam, Catal. Lett. 119 (2007) 346.
[38] J. Santos, J. Phillips, J.A. Dumesic, J. Catal. 81 (1983) 147.
[39] G.B. Raupp, J.A. Dumesic, J. Catal. 95 (1985) 587.
[40] J.M. Herrmann, M. Gravelle-Rumeau-Maillot, P.C. Gravelle, J. Catal. 104 (1987) 136.
[41] P. Chou, M.A. Vannice, J. Catal. 104 (1987) 1.
[42] T.A. Nijhuis, G. van Koten, J.A. Moulijn, Appl. Catal. A 238 (2003) 259.
[43] G. del Angel, J.L. Benitez, J. Mol. Catal. A 94 (1994) 409.
[44] N. Semagina, A. Renken, L. Kiwi-Minsker, J. Phys. Chem. C 111 (2007) 13933.
[45] A. Molnar, A. Sarkany, M. Varga, J. Mol. Catal. 173 (2001) 185.
[46] P. Panagiotopoulou, A. Christodoulakis, D.I. Kondarides, S. Boghosian, J. Catal. 240 (2006) 114.
[47] N. Mahata, V. Vishwanathan, J. Catal. 196 (2000) 262.

Article

Preparation of Nano-Pd/SiO by One-Step Flame Spray Pyrolysis and Its Hydrogenation Activities: Comparison to the Conventional Impregnation Method

Okorn Mekasuwandumrong, Sirima Somboonthanakij, Piyasan Praserthdam, and Joongjai Panpranot

Ind. Eng. Chem. Res., **2009**, 48 (6), 2819-2825• DOI: 10.1021/ie8012055 • Publication Date (Web): 03 February 2009

Preparation of Nano-Pd/SiO_2 by One-Step Flame Spray Pyrolysis and Its Hydrogenation Activities: Comparison to the Conventional Impregnation Method

Okorn Mekasuwandumrong

Department of Chemical Engineering, Faculty of Engineering and Industrial Technology, Silpakorn University, Nakorn Pathom 73000, Thailand

Sirima Somboonthanakij, Piyasan Praserthdam, and Joongjai Panpranot*

Center of Excellence on Catalysis and Catalytic Reaction Engineering, Department of Chemical Engineering, Faculty of Engineering, Chulalongkorn University, Bangkok 10330, Thailand

Characteristics and catalytic properties of the nano-Pd/SiO_2 catalysts synthesized in one-step flame spray pyrolysis (FSP) were compared to those prepared on the flame-made SiO_2 supports by conventional impregnation method. Pd^0 metal particles/clusters <3 nm in size were obtained directly from a single-step flame process, whereas the conventional impregnation method resulted in PdO with larger crystallite sizes (in the range of 5−12 nm). Although there was little difference in the turnover frequency (TOF) values for 1-heptyne hydrogenation on the different Pd/SiO_2 catalysts prepared by impregnation, the TOF values of the flame-made catalysts decreased from 66.2 s^{-1} to 4.3 s^{-1} as the palladium loading increased from 0.5 wt % to 10 wt %, which suggested changes in the catalytic properties when palladium nanoparticles were formed simultaneously in the support matrices by FSP method. For both preparation methods, the palladium particle sizes remained unaltered after liquid-phase hydrogenation reaction.

1. Introduction

Catalytic hydrogenation is one of the most useful, versatile, and environmentally acceptable reaction routes available for organic synthesis, because the scope of the reaction type is very broad and many functional groups can be hydrogenated with high selectivity and high conversation.[1]

Palladium catalysts are preferred for the selective partial hydrogenation of alkynes, they are usually used with a variety of modifiers to improve reaction selectivity. Metal salts, amines, amine oxides, sulfur compounds, hydroxides, and carbon monoxide are among the modifiers used. For heterogeneous systems, the catalyst performance is strongly influenced by (i) the ability to get reactants to the active sites, (ii) to establish the optimum hydrogen to alkyl surface coverage, and (iii) the rapid removal of the hydrogenated products. These constitute the mass-transfer limitations and can have an overriding impact on the ability to achieve selective hydrogenation.[2−4] Many papers in the literature involve the selective hydrogenation of double bonds. However, more challenging, from an academic and industrial point of view, is the selective hydrogenation of alkynes. Many products obtained through this type of reaction are useful in the synthesis of natural products, such as biologically active compounds. The catalysts used must be selective to avoid the total hydrogenation of the alkynes to alkanes.

Flame synthesis is an established commercial process to make nanoparticles in large quantity and low cost.[5] Flame spray pyrolysis (FSP) is a technique that is capable of producing a wide variety of product compositions.[6] In particular, FSP has been demonstrated for the one-step dry synthesis of high-surface-area and highly efficient noble-metal-laden catalysts.[7] Recently, we reported the one-step flame spray synthesis of palladium nanoparticles with an average size of 0.5−3 nm on SiO_2 supports.[8] The as-synthesized FSP-derived catalysts showed higher catalytic activities for the selective hydrogenation of 1-heptyne under mild conditions than the commercial SiO_2 supported Pd catalyst, with no appreciable influence on alkene selectivity.

The objective of this study is to compare the characteristics and catalytic properties of the flame spray-derived Pd/SiO_2 that has been prepared in one step to those prepared on the flame-made SiO_2 via the conventional impregnation technique. The catalysts were characterized by N_2 physisorption, X-ray diffraction (XRD), CO pulse chemisorption, transmission electron spectroscopy (TEM), and X-ray photoelectron spectroscopy (XPS). Their catalytic activities were evaluated in the liquid-phase selective hydrogenation of 1-heptyne under mild conditions.

2. Experimental Section

2.1. Catalyst Synthesis. 2.1.1. Flame Synthesis of Pd/SiO_2. The synthesis of Pd/SiO_2 was conducted using a spray flame reactor.[9] Palladium acetylacetonate (Aldrich) and tetraethylorthosilicate (TEOS; Aldrich) were used as palladium and silicon precursors, respectively. The precursors were prepared by dissolving in xylene (Merck; 99.8 vol %)/acetonitrile (Fluka; 99.5 vol %) mixtures (70/30 vol %) with a total metal concentration that was maintained at 0.5 M. The palladium concentration was in the range of 0−10 wt %. Using a syringe pump, 5 mL/min of precursor solution was dispersed into fine droplets by a gas-assisted nozzle fed by 5 L/min of oxygen (Thai Industrial Gas Limited; purity >99%). The pressure drop at the capillary tip was maintained at 1.5 bar by adjusting the orifice gap area at the nozzle. The spray was ignited by supporting flamelets fed with oxygen (3 L/min) and methane (1.5 L/min), which are positioned in a ring around the nozzle outlet. A sintered metal plate ring (8 mm wide, starting at a radius of 8 mm) provided an additional 10 L/min of oxygen as a sheath for the supporting flame. The product particles were collected

* To whom correspondence should be addressed. Tel. 66-2218-2882. Fax. 66-2218-6877. E-mail: joongjai.p@eng.chula.ac.th.

10.1021/ie8012055 CCC: $40.75
Published on Web 02/03/2009

on a glass fiber filter (Whatman GF/C, 15 cm in diameter) with the aid of a vacuum pump.

2.1.2. Impregnation of Palladium on Flame-Made SiO_2. Silica supports were prepared using a spray flame reactor. A mixture of TEOS and xylene (Merck; 99.8 vol %)/acetonitrile (Fluka; 99.5 vol %) mixtures (70/30 vol %) with a total silicon concentration of 0.5 M was used as the starting precursors. The flame conditions were identical to flame-made Pd/SiO_2 catalyst (explained in Section 2.1.1). The Pd/SiO_2 catalysts were prepared by incipient wetness impregnation of flame-made SiO_2 with a desired amount of an aqueous solution of palladium nitrate [$Pd(NO_3)_2$] (Aldrich). The palladium metal loading of the catalysts was in the range of 0−10 wt %. The catalysts were dried at 110 °C for 24 h and calcined in air at 300 °C for 2 h, using a ramp rate of 1 °C/min.

2.2. Characterization. XRD patterns were recorded with a Siemens Model D5000 system, using nickel-filtered Cu Kα radiation. The crystallite size (d_{XRD}) was determined using the Scherrer equation. The specific surface areas, average pore diameters, and pore size distribution were determined via the physisorption of nitrogen (N_2) using a Micromeritics Model ASAP 2020 apparatus. The palladium oxide particle size and distribution of palladium on silica supported was observed using a JEOL-JEM Model 200CX transmission electron microscopy (TEM) microscope operated at 100 kV. The active sites and the relative percentages dispersion of palladium catalyst were determined by the CO-pulse chemisorption technique, using Micromeritics Model ChemiSorb 2750 equipment.

2.3. Selective Hydrogenation of 1-Heptyne. The catalytic hydrogenation of 1-heptyne (Aldrich) was performed in a magnetically stirred 50-mL stainless steel autoclave reactor. Twenty milligrams of Pd/SiO_2 catalyst was dispersed in 10 mL of 2 vol % 1-heptyne (Fluka) in toluene. The reaction was performed under flowing hydrogen at 1 bar and 30 °C for 5−40 min. The liquid reactants and products were analyzed by a gas chromatography (GC) system that was equipped with a flame ionization detection (FID) detector (Shimadzu, Model GC-14A). Prior the reaction testing, the Pd/SiO_2 catalyst was reduced by hydrogen gas at a flow rate of 50 mL/min at room temperature for 2 h.

3. Results and Discussion

3.1. Catalyst Properties. Figure 1 shows the XRD patterns of all the Pd/SiO_2 catalysts that have palladium loadings of 0.5−10 wt %. The patterns in Figure 1a correspond to the flame-made powder, which has been prepared in one step, while the patterns in Figure 1b are for impregnation-made powder (two-step synthesis). Both flame- and impregnation-made powders for all palladium loadings exhibited the characteristic peaks of the amorphous silica. For the flame-made Pd/SiO_2 powders, an additional peak corresponding to the Pd^0 metal was observed at $2\theta = 41°$ for 10 wt % Pd/SiO_2 catalyst. While the additional peaks corresponding to the PdO phase were observed at $2\theta = 33.8°$ instead for all the impregnation-made catalysts. The broadness of the flame-made Pd phases peaks (a) compared to the impregnation-made material (b) is consistent with smaller primary particles in the flame- than in the wet-made powder. Such result suggests the better dispersion of Pd metal cluster on the silica support was obtained by one-step flame process.

Figure 2 shows the TEM micrographs of flame- and impregnation-made Pd/SiO_2 catalysts with different palladium contents. TEM images of the flame made-powder (see Figures 2a, b, and c) show the aggregation of SiO_2 primary particles. However, the particle areas of SiO_2 cannot be observed clearly. Palladium

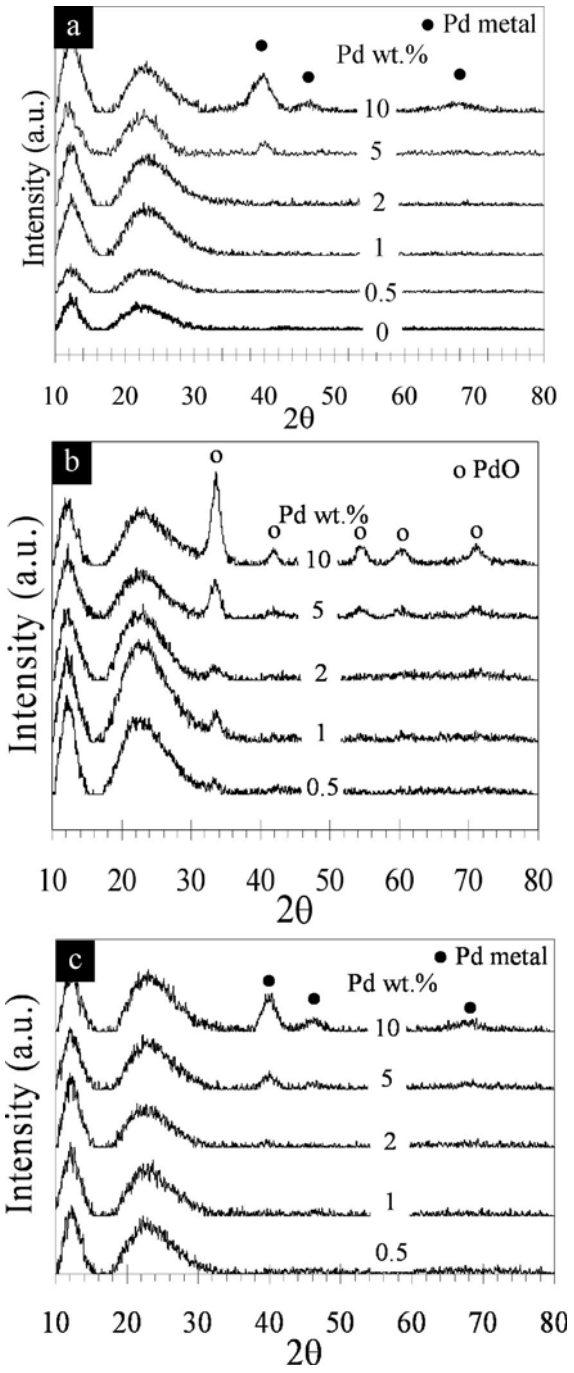

Figure 1. XRD patterns of all Pd/SiO_2 catalyst with palladium loadings in the range of 0−10 wt %: (a) the flame-made catalyst, (b) the impregnation-made catalyst, and (c) the impregnation-made catalyst after reduction.

clusters confined to the surface of SiO_2 particles were determined to have a spherical shape, with an average diameter of 0.5−3 nm with a narrow size distribution. The results were similar to the Pd/Al_2O_3 and Pt/Al_2O_3 catalysts prepared via flame processing.[6,10] It was found that the size of the palladium clusters increased from 0.5 nm to 3 nm as the palladium contents increased from 0.5 wt % to 2 wt % and remained essentially the same size even after increasing the palladium loading to 10 wt %. For the impregnation-made catalysts, the SiO_2 particles were identical to those synthesized in one step. However, the crystallite sizes of PdO were larger and were in the range of 2−10 nm for palladium loadings of 0−10 wt %. The results were in good agreement with the observation by X-ray diffraction (XRD).

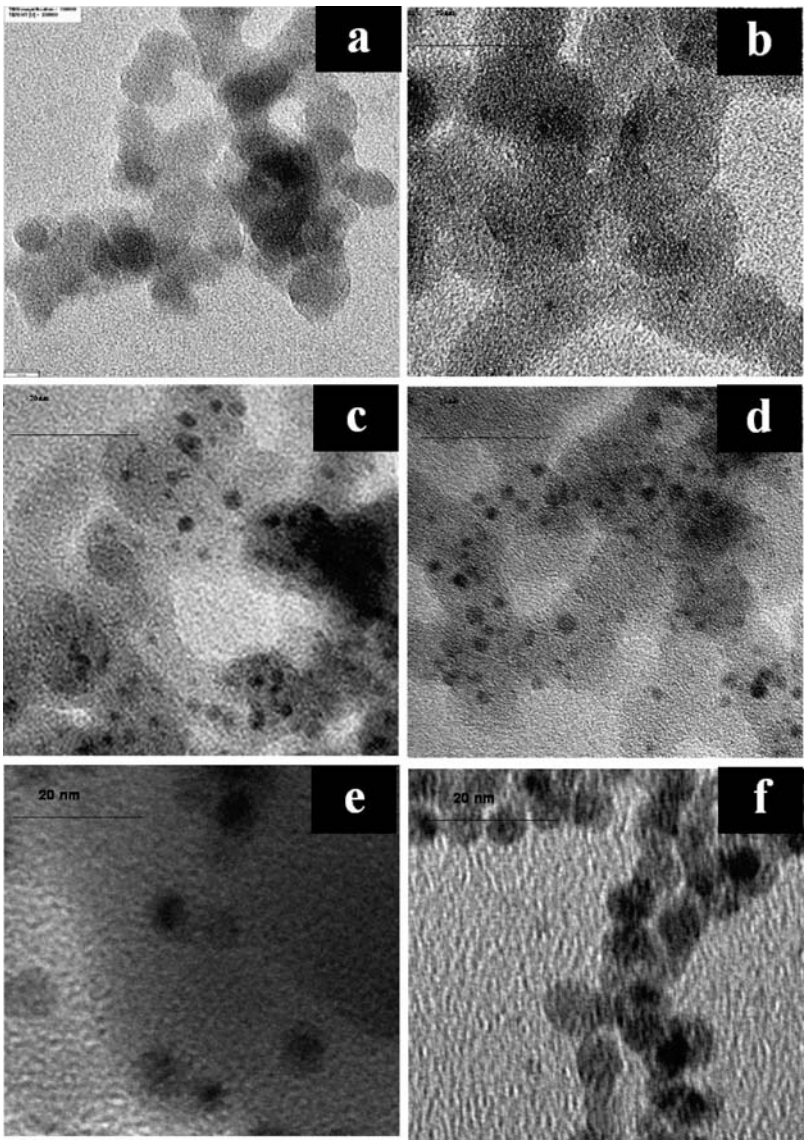

Figure 2. Transmission electron microscopy (TEM) micrographs of flame- and impregnation-made Pd/SiO_2 catalyst with different palladium contents: (a) SiO_2, (b) flame-made with 0.5 wt % palladium, (c) flame-made with 5 wt % palladium, (d) flame-made with 10 wt % palladium, (e) impregnation-made with 5 wt % palladium, and (f) impregnation-made with 10 wt % palladium.

Table 1. Physicochemical Properties of Flame- and Impregnation-Made Pd/SiO_2 Catalysts

		Particle Size (nm)				CO Chemisorption Results		
catalyst	BET surface area (m^2/g)	SiO_2	Pd phase	pore volume (cm^3/g)	average pore size (Å)	CO uptake (molecule CO/g-cat)	%Pd dispersion	Pd^0 particle size, d_P (nm)
Flame-Made Catalysts								
SiO_2	196	14.0	n/a[a]	0.48	90.0	n/a	n/a	n/a
0.5% Pd/SiO_2	246	11.1	n.d.[b]	0.43	67.3	0.97	3.42	33
1% Pd/SiO_2	251	10.9	n.d.[b]	0.46	73.7	1.93	3.40	33
2% Pd/SiO_2	260	10.9	n.d.[b]	0.49	77.6	3.27	2.88	39
5% Pd/SiO_2	306	8.9	n.d.[b]	0.59	76.1	13.38	4.71	24
10% Pd/SiO_2	299	9.1	2.8	0.69	90.9	25.84	4.55	25
Impregnation-Made Catalysts								
0.5% Pd/SiO_2	174	15.7	n.d.[b]	0.91	204.4	3.79	14.6	7.7
1% Pd/SiO_2	171	15.9	n.d.[b]	0.91	193.5	5.02	9.7	11.6
2% Pd/SiO_2	133	20.5	n.d.[b]	0.60	249.1	7.70	7.4	15.2
5% Pd/SiO_2	109	25.0	12.4	0.47	143.5	17.99	7.0	16.1
10% Pd/SiO_2	128	21.3	5.2	0.50	168.2	27.80	5.4	20.8

[a] Not available. [b] Not determined.

Table 1 summarizes the physical and chemical properties of flame- and impregnation-made Pd/SiO_2 catalysts. The Brunauer−Emmett−Teller (BET) surface areas of flame-made catalysts increased from 195 m^2/g to 305 m^2/g as the palladium contents increased from 0 wt % to 5 wt % and became steady when the palladium content as increased to 10 wt %. The pore volumes

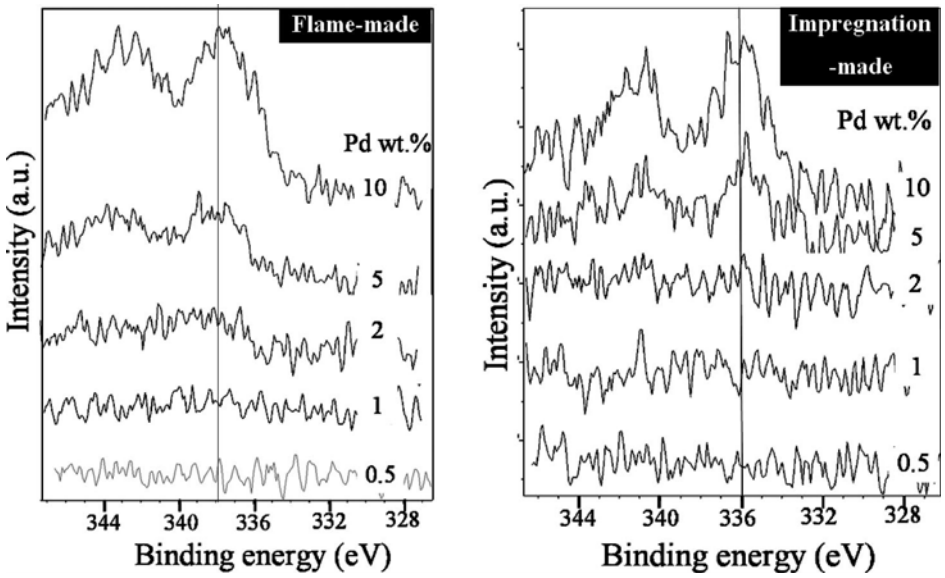

Figure 3. XPS spectra of Pd $3d_{5/2}$ for flame-made and impregnation-made Pd/SiO_2 catalysts.

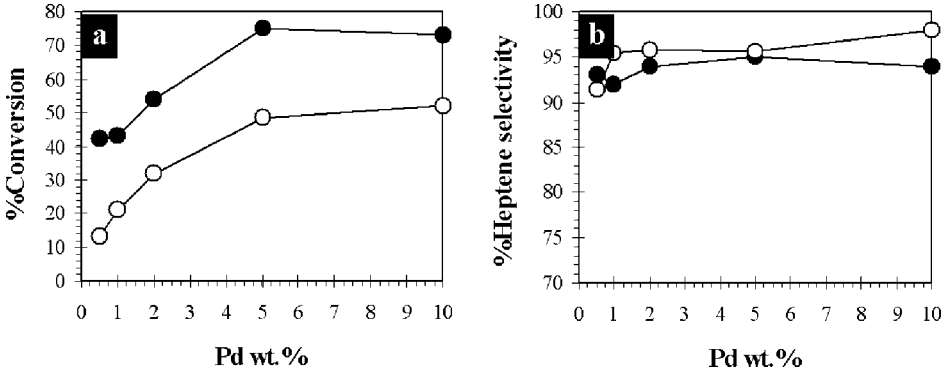

Figure 4. Plots of (a) 1-heptyne conversion and (b) heptene selectivity, relative to the palladium loading (0.5−10 wt %) of flame-made Pd/SiO_2 catalyst (solid circles, ●) and an impregnation-made Pd/SiO_2 catalysts (open circles, ○).

of flame-made catalysts were ca. 0.5 cm^3/g and were not significantly changed as the palladium loading increased. The pore-size distribution patterns of flame-made samples calculated by the Barrett−Joyner−Halenda (BJH) equation exhibited the typical pattern for mesopore structure (not shown). For the impregnation-made catalysts, the BET surface areas gradually decreased from 196 m^2/g to 128 m^2/g as the palladium loading increased from 0 wt % to 10 wt %. A decrease in the BET surface areas with increasing metal loading is typical for supported metal catalysts prepared using a conventional impregnation method. It was probably due to sintering during the calcination process and pore blockage of Pd/PdO clusters. However, increases in the BET surface area with palladium loading is possible for the flame-made Pd/SiO_2 catalysts. Formation of the Pd/SiO_2 nanoparticles by FSP was considered as follows: the sprayed droplets of precursor solution were evaporated and combusted as soon as they met the flame at very high temperature and released the metal atoms, then nucleation and growth of particles by coagulation and condensation occurred along the axial direction of the flame. Comparing to silica, the vapor pressure of Pd/PdO was much higher in the hot flame environment, and consequently SiO_2 particle formation started earlier. Further downstream the flame, at lower temperatures, Pd/PdO started to form small particles and/or deposited directly on the SiO_2 support. This particle formation mechanism was also suggested for Pd/Al_2O_3 and Pt/TiO_2.[10,11] With the addition of palladium, the surface area

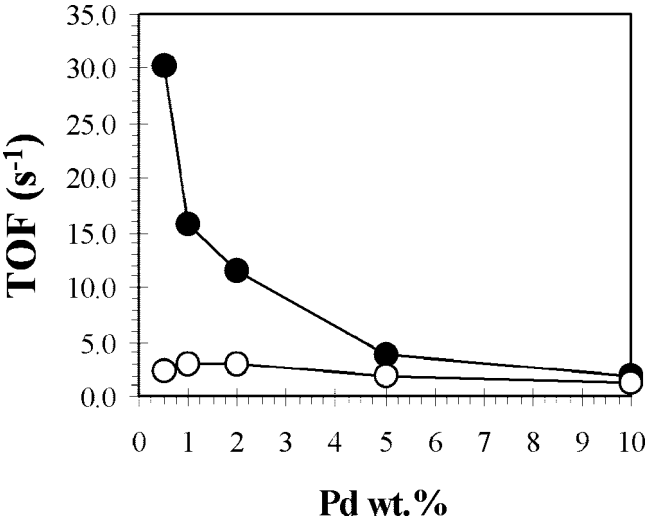

Figure 5. Plots of the turnover frequency (TOF) number, relative to the palladium loading (0.5−10 wt %) of a flame-made Pd/SiO_2 catalyst (solid circle, ●) and an impregnation-made Pd/SiO_2 catalyst (open circle, ○).

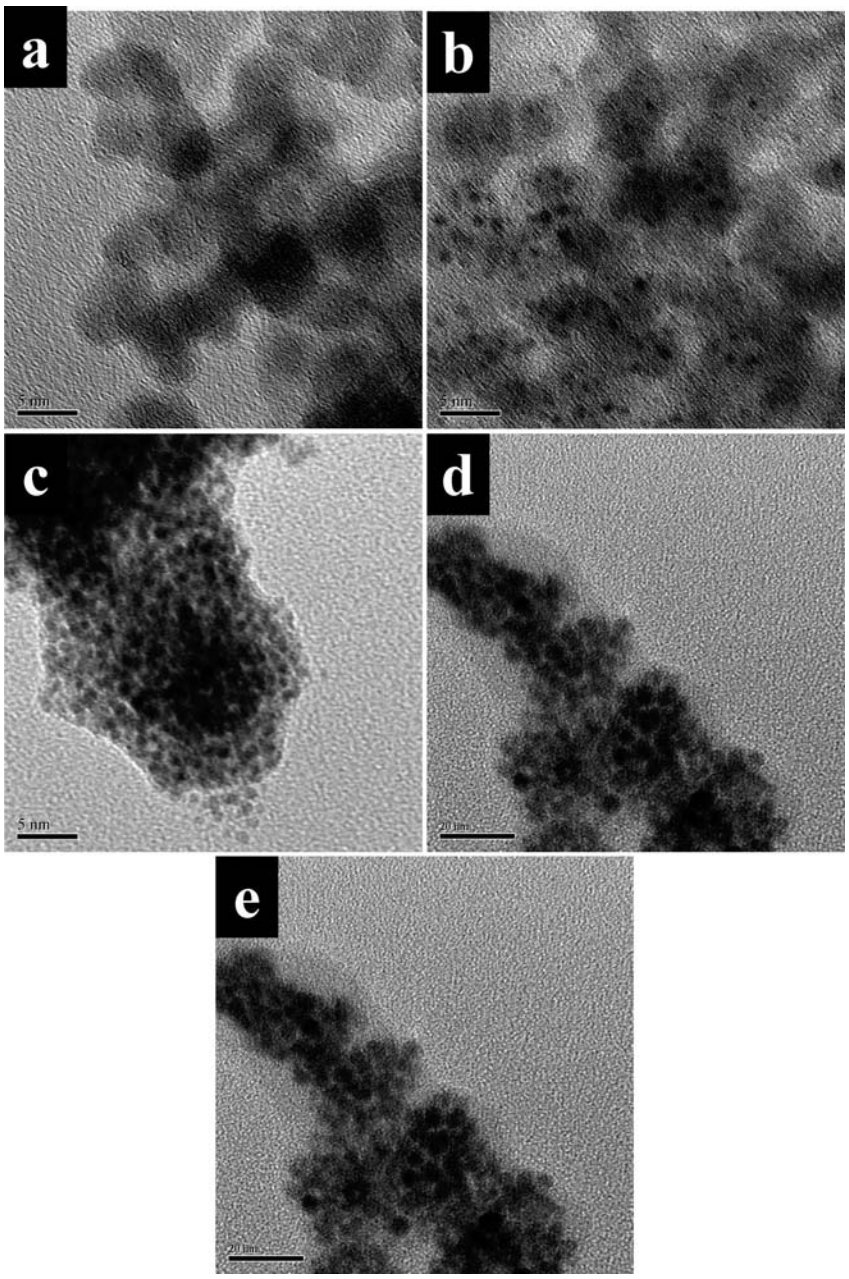

Figure 6. TEM micrographs of flame- and impregnation-made Pd/SiO_2 spent catalyst with different palladium contents; (a) flame-made with 0.5 wt % palladium, (b) flame-made with 5 wt % palladium, (c) flame-made with 10 wt % palladium, (d) impregnation-made with 5 wt % palladium, and (e) impregnation-made with 10 wt % palladium.

of the SiO_2 support increased as the particle size decreased. This suggests that the palladium dopants inhibited the growth of the SiO_2 particles. This result is in good agreement with the flame-synthesized Au−Ag/SiO_2 nanoparticles that were reported by Hannemann et al.[12]

The relative amounts of surface-active palladium metal on the catalyst samples were calculated from CO chemisorption experiments at room temperature, based on the assumption that one carbon monoxide molecule (CO) adsorbs on one palladium (Pd) site.[13,14] The results are also given in Table 1. For the flame-made catalysts, the Pd active sites increased from 0.97 $\times$ 10^{18} sites/g-catalyst to 25.84 $\times$ 10^{18} sites/g-catalyst, corresponding to the increase in palladium metal dispersion from 6.3 to 8.4 as the palladium content increased from 0.5 wt % to 10 wt %. For the impregnated catalysts, the active sites increased from 3.79 $\times$ 10^{18} sites/g-catalyst to 27.8 $\times$ 10^{18} sites/g-catalyst, corresponding to the increase in palladium metal dispersion from 14.5 to 5.4 as the palladium contents increased from 0.5 wt % to 10 wt %. Based on CO chemisorption results, the particle size (d_P) of the impregnated-made Pd^0 was determined to be smaller than that of the FSP-made Pd^0. It is likely that there was an overestimation of the palladium particle size, which would have been attributed to low CO chemsisorption measurement for the flame-made catalysts. The palladium particles on the FSP-made catalysts may be surrounded by a support matrix (i.e., in the form of Si−O group), resulting in the inhibition of CO chemisorption, and/or palladium on the flame-made catalysts that was in a partially oxidized state.

XPS spectra of Pd 3d for the flame- and impregnation-made catalysts are shown in Figure 3. While the binding energies of Pd $3d_{5/2}$ for the flame-made catalysts were observed at 337.4 eV, those of the impregnation-flame-made variety were observed at 335.7 eV. Compared to the binding energy for Pd^0 metal, which is typically ~335.0 eV,[15] it is likely that the FSP may

result in partially oxidized PdO. The results are in good agreement with extended X-ray analysis fine structure (EXAFS) results for other FSP-synthesized supported palladium catalysts reported by Baiker et al.,[16] Pratsinis et al.,[17] and Grunwaldt et al.[18] Such phenomena strongly affected the CO chemisorption results and the dispersion of low-loaded catalysts. Moreover, it is possible that there was stronger interaction between the palladium and the SiO_2 support for the flame-synthesized catalysts, compared to those prepared by conventional impregnation.

3.2. Catalytic Behavior in Liquid-Phase Selective Hydrogenation of 1-Heptyne. Selective hydrogenation reaction of 1-heptyne to 1-heptene was used as the model reaction to investigate the catalytic properties of flame-made and impregnation-made Pd/SiO_2 catalysts. Figure 4 compares the relationship of 1-heptyne conversion and 1-heptene selectivity with palladium loading (expressed as a weight percentage) for the flame-made and impregnation-made Pd/SiO_2 catalysts. For flame-made catalysts, the conversions of 1-heptyne increased from 42% to 75% as the palladium contents increased from 0.5 wt % to 5 wt % and remained constant when the palladium content was increased to 10 wt %. The selectivity for 1-heptene also increased from 92% to 95% as the palladium content increased from 0.5 wt % to 10 wt %. Similar behavior was observed for the impregnation-made catalysts: the conversions of 1-heptyne increased from 13% to 52% as the palladium content increased from 0.5 wt % to 5 wt % and remained constant when the palladium content was increased to 10 wt %. The selectivity for 1-heptene increased from 91% to 98% as the palladium content increased from 0.5 wt % to 10 wt %. The results indicated that the activity and selectivity for the reaction increased as the active size increased, corresponding to the increasing palladium content. However, all the flame-made Pd/SiO_2 powders exhibited higher hydrogenation activity than the impregnation-made Pd/SiO_2 powders. In all cases, the other product besides heptene was heptane.

The activity for 1-heptyne hydrogenation of the catalysts was also expressed in terms of turnover frequency (TOF), which is defined as the number of 1-heptyne molecules converted per atom of exposed palladium on the surface per unit time. The Pd atomic concentrations on the catalyst surface were based on the CO chemisorption results. Figure 5 shows the correlation between TOF and the palladium loading (expressed as a weight percentage) of the flame-made and the impregnation-made Pd/SiO_2 catalysts. The flame-made powders exhibited higher TOF values than the impregnation-made powders. However, the TOF values for flame-made catalysts decreased from 66.2 s^{-1} to 4.3 s^{-1} as the palladium loading (expressed as a weight percentage) increased from 0.5 wt % to 10 wt %, whereas the TOF values of impregnation-made catalysts remained constant at $\sim 1-3$ s^{-1}. In liquid-phase selective hydrogenation, the palladium dispersion (palladium metal size), metal−support interaction, and electronic state of palladium usually have an important role.[19,20] In this paper, the flame-made catalyst with low palladium contents exhibited remarkably high TOF values, compared to the literature and the impregnation-made catalysts. The results reported here were different from the study by Baiker et al.[10] on the enantioselective hydrogenation over noble-metal catalysts, in which larger particles exhibited higher activities. However, it is suggested that the simultaneous formation of palladium nanoparticles in the support matrices during flame spray synthesis could result in the formation of active ensembles for the reaction. Such phenomena was somewhat similar to those of Pd/MCM-41 catalysts prepared via simultaneous synthesis (simultaneous self-assembling of the MCM-41 and Pd incorporation), where remarkably high activities in the alkyne hydrogenation were observed.[21,22]

TEM micrographs of the spent catalysts for both flame- and impregnation-made catalysts are shown in Figure 6. The spherical shape of Pd^0 metal particles was still observed, and there was no significant change in the particle/cluster size of Pd^0 metal after reaction, regardless of the preparation method that was used.

4. Conclusions

Nanocrystalline Pd/SiO_2 catalysts were prepared via one-step flame spray pyrolysis (FSP) and compared to the conventional impregnation of palladium on flame-made SiO_2 (two-step synthesis). The flame-made catalyst powders consisted of polyhedral silica primary particles 10−20 nm in size and nanocrystals of Pd^0 metal with average particle/cluster sizes between 0.5−3 nm for a palladium loading of 0.5−10 wt %. The PdO with average crystallite sizes of 5−12 nm was observed instead for the impregnation-made catalysts. The flame-made catalysts exhibited better catalytic performances for selective hydrogenation of 1-heptyne compared to the impregnation-made catalysts. The remarkably high turnover frequency (TOF) values of the flame-made catalyst were probably due to the formation of active ensembles of palladium nanoparticles in the support matrices during FSP synthesis.

Acknowledgment

The authors would like to thank the Thailand Research Fund (TRF) (through Grant No. RMU-50-80030), Joongjai Panpranot, and the Research and Development Institute of Silpakorn University for their financial support of this project.

Literature Cited

(1) Bailey, S.; King, F. In *Fine Chemicals through Heterogeneous Catalysis*; Sheldon, R. A., van Bekkum, H., Eds.; Wiley−VCH: Weinheim, Germany, 2000; Chapter 8.

(2) L'Argentiere, P. C.; Cagnola, E. A.; Quiroga, M. E.; Liprandi, D. A. A palladium tetra-coordinated complex as catalyst in the selective hydrogenation of 1-heptyne. *Appl. Catal., A* **2002**, *226*, 253.

(3) Cagnola, M. E.; Liprandi, D.; Quiroga, M.; L'Argentiere, P. C. 1-heptyne semihydrogenation catalyzed by $[PdCl_2(NH_2(CH_2)_5CH_3)_2]$. *React. Kinet. Catal. Lett.* **2003**, *80*, 277.

(4) L'Argentiere, P. C.; Quiroga, M. E.; Liprandi, D. A.; Cagnola, E. A.; Roman-Martinez, M. C.; Diaz-Aunon, J. A.; Salinas-Martinez de Lecea, C. Activated-carbon-heterogenized $[PdCl_2(NH_2(CH_2)_{12}CH_3)_2]$ for the selective hydrogenation of 1-heptyne. *Catal. Lett.* **2003**, *87*, 97.

(5) Pratsinis, S. E. Flame aerosol synthesis of ceramic powders. *Prog. Energy Combust. Sci.* **1998**, *24*, 197.

(6) Strobel, R.; Stark, W. J.; Madler, L.; Pratsinis, S. E.; Baiker, A. Flame-made platinum/alumina: structural properties and catalytic behavior in enantioselective hydrogenation. *J. Catal.* **2003**, *213*, 296.

(7) Height, M. J.; Pratsinis, S. E.; Mekasuwandunrong, O.; Praserthdam, P. Ag-ZnO catalysts for UV-photodegradation of methylene blue. *Appl. Catal., B* **2006**, *63*, 305.

(8) Somboonthanakij, S.; Mekasuwandumrong, O.; Panpranot, J.; Nimmanwudtipong, T.; Strobel, R.; Pratsinis, S. E.; Praserthdam, P. Characteristics and catalytic properties of Pd/SiO_2 synthesized by one-step flame spray pyrolysis in liquid-phase hydrogenation of 1-heptyne. *Catal. Lett.* **2007**, *119*, 346.

(9) Mädler, L.; Stark, W. J.; Pratsinis, S. E. Simultaneous deposition of Au nanoparticles during flame synthesis of TiO_2 and SiO_2. *J. Mater. Res.* **2003**, *18*, 115.

(10) Strobel, R.; Krumeich, F.; Stark, W. J.; Pratsinis, S. E.; Baiker, A. Flame spray synthesis of Pd/Al_2O_3 catalysts and their behavior in enantioselective hydrogenation. *J. Catal.* **2004**, *222*, 307.

(11) Teoh, W. Y.; Mädler, L.; Beydoun, D.; Pratsinis, S. E.; Amal, R. Direct (one-step) synthesis of TiO_2 and Pt/TiO_2 nanoparticles for photocatalytic mineralisation of sucrose. *Chem. Eng. Sci.* **2005**, *60*, 5852.

(12) Hannemann, S.; Grunwaldt, J.; Krumeich, F.; Kappen, P.; Baiker, A. Electron microscopy and EXAFS studies on oxide-supported gold-silver nanoparticles prepared by flame spray pyrolysis. *Appl. Surf. Sci.* **2006**, *252*, 7862.

(13) Mahata, N.; Vishwanathan, V. Influence of palladium precursors on structural properties and phenol hydrogenation characteristics of supported palladium catalysts. *J. Catal.* **2000**, *196*, 262.

(14) Ali, S. H.; Goodwin, J. G., Jr. SSITKA Investigation of palladium precursor and support effects on CO hydrogenation over supported Pd catalysts. *J. Catal.* **1998**, *176*, 3.

(15) Wagner, C. D.; Riggs, W. M.; Davis, L. E.; Moulder, J. F. In *Handbook of X-ray Photoelectron Spectroscopy*; Muilenberg, G. E., Ed.; Perkin−Elmer Corporation: Eden Prairie, MN, 1978.

(16) Chiarello, G. L.; Grunwaldt, J.-D.; Ferri, D.; Krumeich, F.; Oliva, C.; Forni, L.; Baiker, A. Flame-synthesized $LaCoO_3$-supported Pd: 1. Structure, thermal stability and reducibility. *J. Catal.* **2007**, *252*, 127.

(17) Strobel, R.; Baiker, A.; Pratsinis, S. E. Aerosol flame synthesis of catalysts. *Adv. Powder Technol.* **2006**, *17*, 457.

(18) Grunwaldt, J.-D.; Kimmerle, B.; Baiker, A.; Boye, P.; Schroer, C. G.; Glatzel, P.; Borca, C. N.; Beckmann, F. Catalysts at work: From integral to spatially resolved X-ray absorption spectroscopy. *Catal. Today* **2009**, in press.

(19) Robles-Dutenhefner, P. A.; Speziali, M. G.; Sousa, E. M. B.; dos Santos, E. N.; Gusevskaya, E. V. Selective hydrogenation of myrcene catalyzed by sol−gel Pd/SiO_2. *Appl. Catal., A* **2005**, *295*, 52.

(20) Lederhos, R. C.; L'Argentiere, P. C.; Fýgoli, N. S. 1-Heptyne selective hydrogenation over Pd supported catalysts. *Ind. Eng. Chem. Res.* **2005**, *44*, 1752.

(21) Dominguez-Dominguez, S.; Berenguer-Murcia, A.; Linares-Solano, A.; Cazorla-Amoros, D. Inorganic materials as supports for palladium nanoparticles: Application in the semi-hydrogenation of phenylacetylene. *J. Catal.* **2008**, *257*, 87.

(22) Papp, A.; Molnar, A.; Mastalir, A. Catalytic investigation of Pd particles supported on MCM-41 for the selective hydrogenations of terminal and internal alkynes. *Appl. Catal., A* **2005**, *289*, 256.

Received for review August 6, 2008
Revised manuscript received January 8, 2009
Accepted January 9, 2009

IE8012055

Catalysis Communications 10 (2009) 1380–1385

Contents lists available at ScienceDirect

Catalysis Communications

journal homepage: www.elsevier.com/locate/catcom

Synthesis of Au–ZnO and Pt–ZnO nanocomposites by one-step flame spray pyrolysis and its application for photocatalytic degradation of dyes

Pongsapak Pawinrat [a], Okorn Mekasuwandumrong [b], Joongjai Panpranot [a,*]

[a] Center of Excellence on Catalysis and Catalytic Reaction Engineering, Department of Chemical Engineering, Faculty of Engineering, Chulalongkorn University, Phayathai Road, Bangkok 10330, Thailand
[b] Department of Chemical Engineering, Faculty of Engineering and Industrial Technology, Silpakorn University, Nakhonphatom 73000, Thailand

ARTICLE INFO

Article history:
Received 25 October 2008
Received in revised form 27 February 2009
Accepted 8 March 2009
Available online 14 March 2009

Keywords:
Pt–ZnO
Au–ZnO
Flame spray pyrolysis
Methylene blue
Photocatalytic activity

ABSTRACT

Au–ZnO and Pt–ZnO nanocomposites have been synthesized by one-step flame spray pyrolysis (FSP) and characterized by X-ray diffraction (XRD), nitrogen adsorption, UV–vis spectroscopy, photoluminescence (PL), and transmission electron microscopy (TEM). The XRD and TEM results revealed that Au and Pt metallic phase were formed late during flame synthesis after ZnO was formed. Their average particle/cluster sizes were ranged between 3 and 7 nm depending on the amount loading (1 and 3 wt%). Although both of the FSP-derived Au–ZnO and Pt–ZnO possessed similar physical properties (i.e., crystallite size and specific surface area), an improvement in photocatalytic degradation of methylene blue in comparison to pure ZnO and commercial titania photocatalysts (JRC-TiO_2 and P-25) was observed only for the Au–ZnO and not for the Pt–ZnO due probably to the different type of Fermi-level equilibration between Au and Pt.

1. Introduction

Wastewater contaminated with residual dyes from textile, paper, and other industries is a source of environmental problems. The photo-assisted catalytic decomposition of organic pollutants employing semiconductors as photocatalysts has been a promising method for the degradation of pollutants in wastewater. Among the semiconductors, TiO_2 is widely employed as a photocatalyst. However, ZnO is a low cost alternative to TiO_2 because it has similar band gap energy (3.2 eV) with relatively large quantum efficiency [1]. Higher photocatalytic efficiencies of ZnO have also been reported especially for degradation of organics in aqueous solutions [2–7].

The combination of semiconductor substrate (i.e. TiO_2 and ZnO) and metal cluster such as Ag, Au, Pd and Pt has been reported to enhance photocatalytic activity by trapping the photo-induced charge carriers, thereby improving the charge transfer processes [8–14]. The noble metals of gold and platinum were used for the metal–ZnO formation because of high electron affinity behavior [15] and the highest Schottky barrier produced among the various metals [14]. For ZnO *n*-type semiconductor (with a work function (ϕ_s) of ~4.3 eV) in contact with noble metals with a work function ϕ_m (Au: 5.1 eV and Pt: 5.65 eV) [9] >ϕ_s, a Schottky barrier will form at the junction, facilitating the electron capture.

Flame aerosol synthesis is used to make commercially available nanoscale materials in bulk quantities at low cost [16], for example, the widely used photocatalyst Degussa P25-TiO_2 is produced by this technique. In particular, flame spray pyrolysis (FSP) has been demonstrated to be an effective and versatile process for one-step, dry synthesis of high surface area noble metal laden catalysts [17]. This method provides good control of particle size, particle crystal structure and also can produce highly pure particles continuously without further subsequent processes such as drying, calcination, and milling. In the present work, Au–ZnO and Pt–ZnO nanocomposites were prepared via one-step flame spray pyrolysis and characterized by X-ray diffraction (XRD), surface area analysis, transmission electron microscopy (TEM), photoluminescence, and UV–vis spectrophotometer. Their photocatalytic activities were evaluated in the degradation of methylene blue (MB) and compared to those of the commercially available TiO_2-P25 and JRC-TiO_2 photocatalysts.

2. Experimental

2.1. Flame-synthesis of Au–ZnO and Pt–ZnO

Synthesis of Au–ZnO powders were carried out using a spray flame reactor [18]. Zinc naphthanate (Aldrich, <50% in mineral spirits) and gold (III) chloride trihydrate (Aldrich, 99.9+%) were used as zinc and gold precursors. The precursors were dissolved in ethanol (J.T. Baker, 99.9%) with total metal concentration maintained at

* Corresponding author. Tel.: +66 2 2186869; fax: +66 2 2186877.
E-mail address: joongjai.p@eng.chula.ac.th (J. Panpranot).

1566-7367/$ - see front matter © 2009 Elsevier B.V. All rights reserved.
doi:10.1016/j.catcom.2009.03.002

0.8 M and the gold concentration ranged between 0 and 5 wt%. Using a syringe pump, 8 mL/min of precursor solution was dispersed into fine droplets by a gas-assist nozzle fed by 3 L/min of oxygen designated as a 8/3 flame. The pressure drop at the capillary tip was maintained at 1.5 bar by adjusting the orifice gap between the nozzle. The reactor was water-cooled to avoid evaporation or decomposition of the precursor within the feed lines. The flame was surrounded and ignited by a concentric premixed methane/oxygen pilot flame (CH_4 1.5 L/min, O_2 3.0 L/min) that was sheathed further by flowing oxygen (25 L/min) through a sintered metal plate ring (8 mm wide, starting at a radius of 8 mm). The powder particles were collected on a glass–fiber filter (GF/D Whatman, 257 mm diameter) with the aid of a vacuum pump.

Pt–ZnO was prepared by the same condition but changed raw materials for preparation of a liquid-phase precursor from gold (III) chloride trihydrate to platinum acetylacetonate (Fluka) and solvent for dissolved platinum acetylacetonate from ethanol to xylene (MERCK, 99.8 vol.%)/acetonitrile (Fluka, 99.5 vol.%) mixtures 70/30 vol.%.

2.2. Characterization

Powder X-ray diffraction was performed by a SIEMENS XRD D5000 using CuKa radiation. The crystallite size (d_{XRD}) was estimated by using the Scherrer equation. The specific surface area was measured by N_2 physisorption using a Micromeritics ASAP 2000 automated system and the Brunauer–Emmet–Teller (BET) method. Each sample was degassed under vacuum at $<1 \times 10^{-5}$ bar in the Micromeritics system at 300 °C for 3 h prior to N_2 physisorption. The particle morphology was observed using JEOL Model JEM-2010 transmission electron microscope operated at 200 keV. PL measurement was carried out on a Fluorescence spectrophotometer (Perkin–Elmer LS-50) using a Xenon lamp as the excitation source at room temperature. The sample was dispersed in ethanol using ultrasonic bath and the excitation wavelength used in PL measurement was 325 m. The UV–vis absorption spectra of the photocatalysts were obtained in the range of 200–900 nm using a UV–vis scanning spectrophotometer (Perkin–Elmer lampda 650).

2.3. Photocatalytic testing

A basic aniline dye, methylene blue (Unilab, Asia Pacific Specialty Chemicals Limited) was used as a probe molecule to evaluate the photocatalytic activities. The photocatalytic reaction was conducted at room temperature under UV light 2×15 W UV tube predominantly emit at 365 nm (Philips) with the average light intensity on the reaction beaker (pyrex) at a distance of 6 cm from the lamp was found to be 4.7×10^{-4} W cm^{-2}. The reaction was carried out with 20 mg of catalyst was dispersed in 200 mL of 10 ppm methylene blue aqueous solution. Prior to irradiation, the suspensions were magnetically stirred in the dark for 15 min to establish the adsorption/desorption equilibrium of methylene blue. Approximately 3.5 mL samples were withdrawn every 10 min. Before analysis, the aqueous samples were centrifuged to remove any suspended solid catalyst particles. The residual concentration of methylene blue was measured at 665 nm using the UV–vis spectrophotometer (Perkin–Elmer lampda 650) in liquid cuvette configuration with de-ionized water as reference. The percentage of degradation was calculated by using the equation given below:

$$\text{Degradation } (\%) = \frac{C_0 - C}{C_0} \times 100 \quad (1)$$

In which C_0 is the initial dye concentration and C is the dye concentration after the treatments. The UV–vis spectra were also collected using an absorbance method.

3. Results and discussion

3.1. Particle characterization

X-ray diffraction was used to investigate the changes of phase structure and crystallite size of the FSP-made Au–ZnO and Pt–ZnO powders. The XRD patterns are shown in Fig. 1. The characteristic peaks of the ZnO wurtzite structure (JCPDS Card File No. 36-1451) were apparent for every sample. For the FSP-made Au–ZnO powders with 3 wt% Au loading, additional peaks corresponding to Au^0 metal ((111), (200), and (220)) were clearly observed at $2\theta = 38$, 44.3 and 64.5°. Similarly, for the FSP-made Pt–ZnO powders with 3 wt% Pt loading, additional peaks corresponding to Pt^0 metal ((111) and (200)) were observed at 39.7 and 46.2°2θ, respectively. Such results suggest that most of the Au and Pt atoms were not incorporated in the ZnO lattice or only to a very small extent. It is likely that Au and Pt metallic phases were formed on the ZnO surface late during flame synthesis after the ZnO particles were already formed, similar to those of Ag–ZnO synthesized by FSP method previously reported by our group [10].

The TEM images of FSP-made Au–ZnO and Pt–ZnO with 1 and 3 wt% metal loadings are shown in Fig. 2. Spherical metal nanoparticles/clusters dispersed on the surface of ZnO were clearly observed as the darker spots. Average diameters of Au particles/clusters deposited on ZnO were determined to be approximately 4.0 and 6.7 nm for 1% Au–ZnO and 3% Au–ZnO, respectively. For similar metal loading, the average particle/cluster size of Pt particles deposited on ZnO was slightly smaller than those of Au–ZnO, e.g., 3.3 nm for 1% Pt–ZnO and 5.0 nm for 3% Pt–ZnO. The corresponding selected-area electron diffraction (SAED) patterns for all the samples (results not shown) illustrated spotty rings patterns, indicating its highly crystalline ZnO wurtzite structure, which was in good agreement with the XRD results.

Table 1 summarizes the physical properties of the FSP-made pure ZnO, Pt–ZnO, and Au–ZnO catalysts. The average crystallite size (d_{XRD}) of ZnO, Au and Pt were calculated from (101), (111) and (111) diffraction peaks of ZnO, Au, and Pt, respectively using Scherrer equation. The d_{XRD} of ZnO for both Au–ZnO and Pt–ZnO catalysts were calculated to be in the range of 34.6–39.8 nm and were not significantly changed as the wt% metal (Au and Pt) content increased. The d_{TEM} data were consistent with the d_{XRD} values indicating that these particles are single crystalline. Addition of Au and Pt during flame synthesis of ZnO did not significantly alter the specific surface area of ZnO.

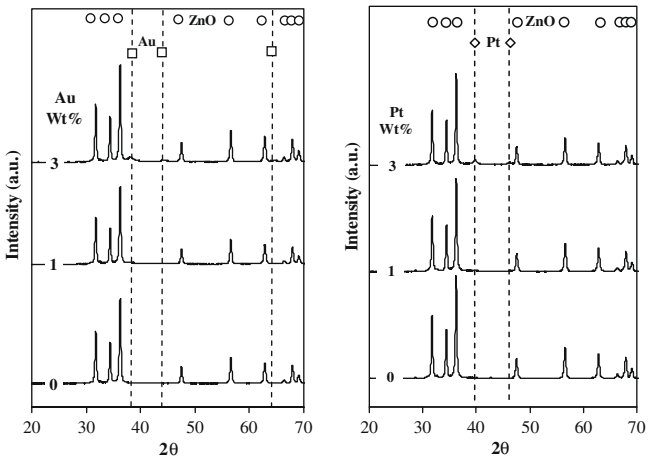

Fig. 1. XRD patterns of flame-made (a) Au–ZnO and (b) Pt–ZnO powders. All powders exhibit the typical pattern for hexagonal zincite (○). (□) and (◇) represent the characteristic pattern of Au and Pt metal, respectively.

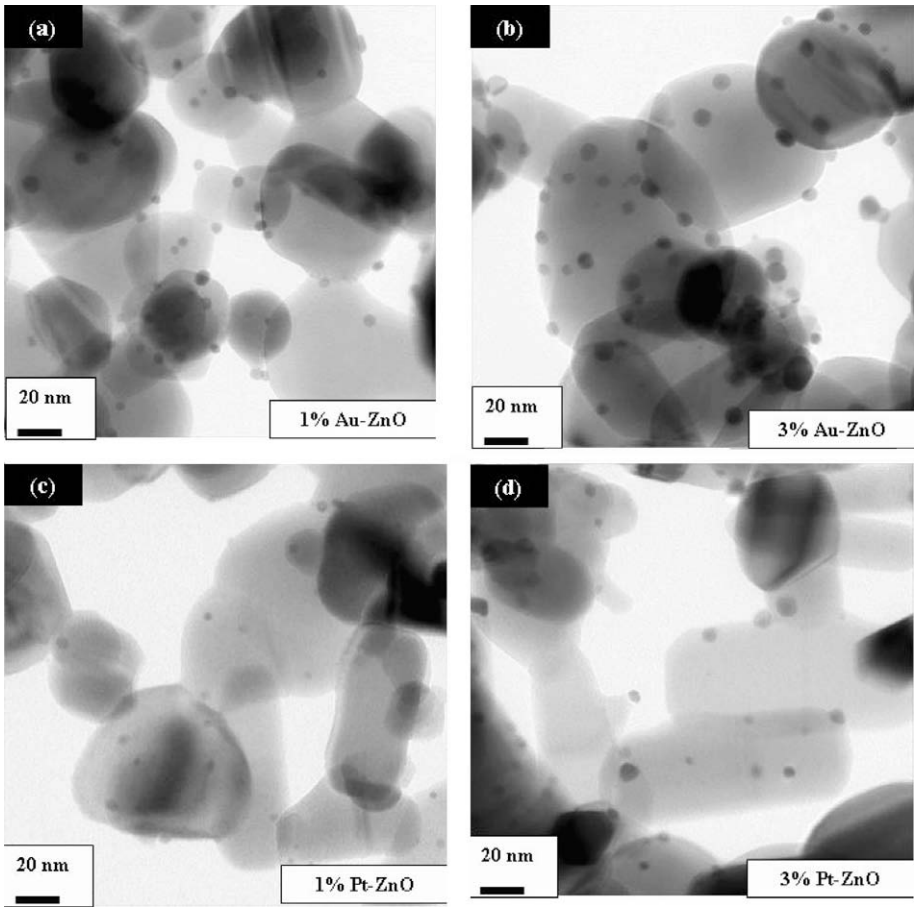

Fig. 2. TEM images of (a) 1% Au–ZnO, (b) 3% Au–ZnO, (c) 1% Pt–ZnO, and (d) 3% Pt–ZnO. The darker spots on the TEM images (a and b) are Au deposits and (c and d) are Pt deposits.

Table 1
Characteristics of the FSP-made pure ZnO, Pt–ZnO, and Au–ZnO catalysts.

Sample	*d*XRD (nm)[a]		*d*TEM (nm)[b]		BET (m^2/g)
	ZnO	Metal	ZnO	Metal	
ZnO	38.3	n.d.[c]	37.7	n.d.	18.6
1% Au–ZnO	37.3	n.d.	37.1	4.0	19.2
3% Au–ZnO	38.9	5.8	38.9	6.7	16.1
1% Pt–ZnO	34.6	n.d.	35.0	3.3	23.9
3% Pt–ZnO	38.9	5.8	36.5	5.0	19.1

[a] Average crystallite size calculated by Scherrer equation.
[b] Calculated from the average size of 40 particles.
[c] n.d. = not determined.

The UV–vis absorbance spectra of FSP-made Au–ZnO and Pt–ZnO powders are shown in Fig. 3. The absorption at visible wavelengths (400–900 nm) of Au–ZnO increased with increasing Au contents due to the surface plasmon resonance of the Au nanoparticles, indicating the presence of Au metal clusters which is in agreement with the XRD and TEM results. The absorption results were also consistent with the visible powder color shift from white, to light purple, and dark purple, with increasing Au loadings from 0 to 3 wt%. Similarly, the UV–vis spectra of flame-made Pt–ZnO powders also show that absorption at visible wavelengths increased with increasing platinum content, consistent with the visible powder color shift from white, to light gray, and gray. It should be noticed that while the absorption at visible wavelengths of the FSP-made Pt–ZnO showed constant absorption, variation absorption was evident for the FSP-made Au–ZnO. It has been reported that if equal sized metal clusters are formed, constant absorption in the visible region corresponding to the excitation from the valence band of ZnO to the unoccupied level of metal cluster will be observed [15].

PL emission spectra are useful to disclose the efficiency of charge carrier trapping, immigration, and transfer, and to understand the fate of electron–hole pairs in semiconductor particles since PL emission results from the recombination of free carriers. In this study, the PL emission spectra of the FSP-made Au–ZnO ant Pt–ZnO with different amounts of metal loading were examined and compared to the pure ZnO with excitation wavelength of 325 nm. The results are shown in Fig. 4. The spectrum of pure ZnO powder mainly consists of two emission bands: one is the UV near-band-edge emission (NBE) at ~385 nm and the other is the visible emission that usually associates with the deep level emission (DLE) in ZnO [19]. The blue emission at ~425 nm and weak blue emission at ~445 nm most likely occurs from the donor level of Zn interstitial to acceptor energy level of Zn vacancy [20]. The blue–green band around 470 nm is induced by radiative transition of electron from shallow donor levels, created by the oxygen vacancy to valence band [21]. The green emission at ~530 is commonly observed for ZnO, and is attributed to the singly ionized oxygen vacancy in ZnO [22]. The UV near-band-edge emission (NBE) spectra of the Pt–ZnO, Au–ZnO and pure ZnO showed similar peak positions, but with different PL intensities. It can be concluded that deposition of Pt and Au on ZnO during flame spray synthesis did not change much the band edge, but resulted in the reduction of PL emission significantly. The decrease of PL intensity for the Au–ZnO and Pt–ZnO nanoparticles may be attributed to the

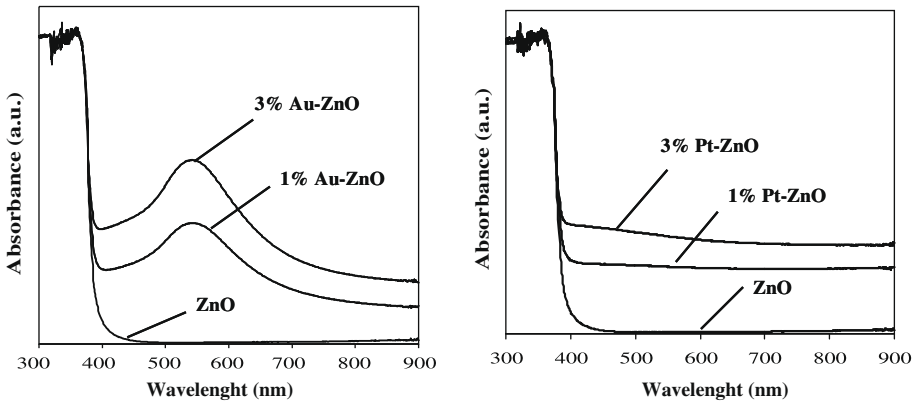

Fig. 3. UV–vis spectra of the flame-made (a) Au–ZnO and (b) Pt–ZnO.

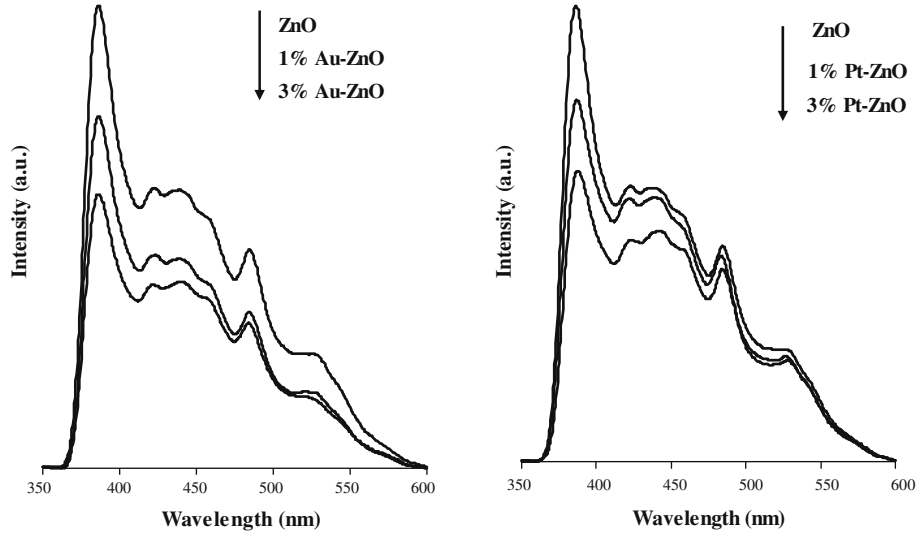

Fig. 4. PL spectra for (a) Au–ZnO and (b) Pt–ZnO with the excitation wavelength of 325 nm.

capture of noble metal ions. The PL emission mainly resulted from the recombination of excited electrons and holes, thus the lower PL intensity indicated the lower recombination rate of electron–holes under irradiation of visible light. In other words, the weaker the excitonic PL spectrum, the higher the separation rate of photo-induced charges carriers [23]. From the figures, the PL emission spectrum of Au–ZnO was lower than that of Pt–ZnO especially at deep level emission. It is likely that the FSP-made Au–ZnO had higher separation rate of photo-induced charges than the FSP-made Pt–ZnO.

3.2. Photocatalytic testing

Fig. 5 shows the catalytic performances for MB photodegradation of the flame-made ZnO, Au–ZnO and Pt–ZnO nanopowders. Irradiation in the absence of photocatalyst for 60 min revealed no change in the MB concentration, confirming that the MB cannot be degraded by 365 nm irradiation alone. For the Au–ZnO powders, the observed photocatalytic activity was enhanced especially with 3% Au–ZnO. The enhancement of photocatalytic activity of pure ZnO by doping with small amount of Au suggests that Au clusters (small size of Au nanoparticles) acted as a separation center. According to Subramanian et al. [8], the photogenerated electrons are stored in the Au nanoparticles and induce a shift of the Fermi-level toward more negative potentials. The transfer of electrons to Au nanoparticles continues until the Fermi level reaches close to the conduction band edge of ZnO. The recombination of the photogenerated electron–hole pairs in the ZnO crystal are thus reduced, and thereby, promoting photocatalytic activity. The photocatalytic activity of the flame-made Au–ZnO showed good agreement with the PL spectra measurement. For the Pt-doped flame-made ZnO, poor photocatalytic activity for MB degradation was observed. The reason for this would be related with nature of the metal nanoparticles brought in contact with the irradiated semiconductor. Pt is ohmic type which differs from the case of FSP-made Au–ZnO. Pt deposited on ZnO neither induced the Fermi-level shift toward more negative potentials nor stored photogenerated electrons in the Pt nanoparticles. On the other hand, it merely facilitated discharge of the photogenerated electrons into the electrolyte. Thus, Pt deposited on ZnO did not produce a longer electron–hole pair separation lifetime and enhance photocatalytic activity. The results were in good agreement with the PL spectra measurement. The Schottky barrier formation in the presence of Au and the ohmic contact in the presence of Pt were found to be in good agreement with the well-established trends in the literature. Subramanian et al. [8] monitored the emission intensity of ZnO nanoparticles during Pt and Au metal ion reduction on a ZnO surface. The results show no significant changes in the emission for Pt–ZnO system suggesting that the contact between ZnO and Pt particles remained ohmic in nature and facilitated discharge of photogenerated elec-

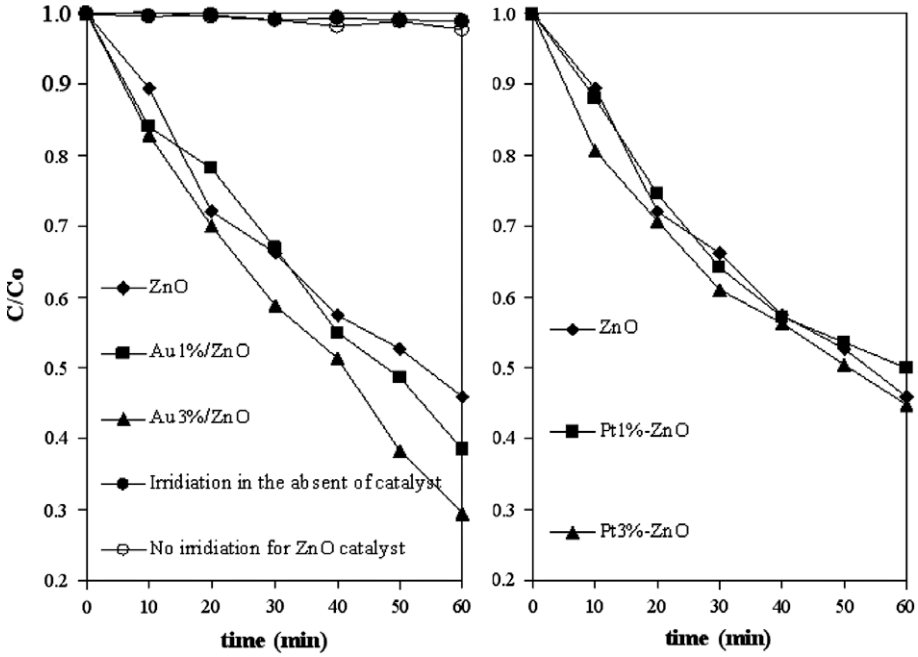

Fig. 5. Photodegradation of MB in the presence of pure ZnO, Au–ZnO, and Pt–ZnO (error of measurement was +/− 2%).

Table 2
Photocatalytic performance in photodegradation of methylene blue for pure ZnO, Au–ZnO, and Pt–ZnO prepared via FSP method in comparison to P-25 and JRC-TiO2 photocatalysts.

Sample	MB conversion after 1 h (%)	Rate constant (h^{-1})
ZnO	54	0.80
Au 1 wt%–ZnO	62	0.89
Au 3 wt%–ZnO	71	1.14
Pt 1 wt%–ZnO	50	0.73
Pt 3 wt%–ZnO	55	0.85
TiO_2 (JRC)	18	0.19
TiO_2 (P25)	57	0.80

trons into the solution. The difference between electron storage behavior for both catalysts has also been suggested by Wood et al. [24].

Based on the MB conversions at 1 h time-on-stream and apparent first-order reaction rate constants of the various photocatalysts (Table 2), the FSP-made Au–ZnO with 3 wt% Au loading showed the highest photocatalytic activity. Compared to the pure ZnO and the commercial Degussa P-25 and JRC-TiO_2 photocatalysts, the percent degradation of MB on 3% Au–ZnO increased by 17%, 14%, and 53%, respectively. In the present study, photocatalytic activity of the Au–ZnO catalysts increased from 0.89 to 1.14 h^{-1} when Au particle size increased from 4.1 to 6.3 nm. The effect of metal size on the photocatalytic activity of metal deposited on photocatalyst has been previously investigated by some researchers. For examples, Wu and Tseng [9] studied the effect of Au metal size on the photocatalytic properties of Au/ZnO catalyst and found that the photocatalytic degradation of methyl orange increased as the Au metal size decreased from 30 to 5 nm. They suggested that charge separation ability of the Au nanoparticles strongly depended on the Au particle size. Subramanian et al. [8] reported the size-dependent shift in the apparent Fermi level of the TiO_2–Au composite 20 mV for 8-nm diameter, 40 mV for 5-nm, and 60 mV for 3-nm Au nanoparticles, respectively. The different trend observed in this study could probably be explained by that in our case the amount of Au loading was increased from 1 to 3 wt% resulting in higher concentration of Au nanoclusters on the ZnO surface (with little changes in Au particle size) whereas in the other studies, the amount of Au loading was kept constant (i.e., at 1 wt%) while varying Au particle size in the colloidal form.

4. Conclusions

FSP is an effective method for one-step synthesis of Au–ZnO and Pt–ZnO nanocomposites. Metallic phase of Au and Pt with average crystallite size between 3 and 7 nm were deposited directly on the ZnO during flame synthesis, no further treatment step is required. When employed as photocatalysts for methylene blue degradation, it was found that 3% Au–ZnO exhibited superior performance than the pure ZnO and the commercially available TiO_2 photocatalysts (Degussa P-25 and JRC-TiO_2). The Au–ZnO showed a stronger absorption of visible light and a lower intensity of PL emission than the undoped ZnO. The presence of discrete Au clusters may retard recombination of the photo-induced electron–hole pairs by shift in the Fermi level and store photogenerated electrons in them. On the other hand, Pt–ZnO did not enhance photocatalytic activity of the ZnO since the ohmic type of Pt may facilitate discharge of the photogenerated electrons into the electrolyte instead.

Acknowledgements

The financial supports from the Thailand Research Fund (RMU-50-Joongjai Panpranot and the Graduate School of Chulalongkorn University) are gratefully acknowledged.

References

[1] M.A. Behnajady, N. Modirshahla, R. Hamzavi, J. Hazard. Mater. B 133 (2006) 226.
[2] K. Tanaka, K. Padermpole, T. Hisanaga, Water Res. 34 (2000) 327.
[3] A. Sharma, P. Rao, R.P. Mathur, S.C. Ameta, J. Photochem. Photobiol. A: Chem. 86 (1995) 197.
[4] A.A. Khodja, T. Sehili, J.F. Pilichowski, P. Boule, J. Photochem. Photobiol. A: Chem. 141 (2001) 231.
[5] A. Akyol, H.C. Yatmaz, M. Bayramoglu, Appl. Catal. B 54 (2004) 19.
[6] R. Kavitha, S. Meghani, V. Jayaram, Mater. Sci. Eng. B 139 (2007) 134.

[7] N. Daneshvar, D. Salari, A.R. Khataee, J. Photochem. Photobiol. A: Chem. 162 (2004) 317.
[8] V. Subramanian, E.E. Wolf, P.V. Kamat, J. Phys. Chem. B 107 (2003) 7479.
[9] J. Wu, C. Tseng, Appl. Catal. B 66 (2006) 51.
[10] M.J. Height, S.E. Pratsinis, O. Mekasuwandumrong, P. Praserthdam, Appl. Catal. B 63 (2006) 305.
[11] L. Jing, D. Wang, B. Wang, S. Li, B. Xin, H. Fu, J. Sun, J. Mol. Catal. A 244 (2006) 193.
[12] C.A.K. Gouvêa, F. Wypych, S.G. Moraes, N. Durán, P.P. Zamora, Chemosphere 40 (2000) 427.
[13] F.B. Li, X.Z. Li, Appl. Catal. A 228 (2002) 15.
[14] F.B. Li, X.Z. Li, Chemosphere 48 (2002) 1103.
[15] S. Sakthivel, M.V. Shankar, M. Palanichamy, Banumathi Arabindoo, D.W. Bahnemanna, V. Murugesan, Water Res. 38 (2004) 3001.
[16] S.E. Pratsinis, Prog. Energy Combust. Sci. 24 (1998) 197.
[17] R. Strobel, F. Krumeich, W.J. Stark, S.E. Pratsinis, A. Baiker, J. Catal. 222 (2004) 307.
[18] T. Tani, L. Mädler, S.E. Pratsinis, J. Nanopart. Res. 4 (2002) 337.
[19] B. Marí, F.J. Manjón, M. Mollar, J. Cembrero, R. Gómez, Appl. Surf. Sci. 252 (2006) 2826.
[20] X.Q. Wei, B.Y. Man, M. Liu, C.S. Xue, H.Z. Zhuang, C. Yang, Phys B 388 (2007) 145.
[21] D. Chu, Y. Zeng, D. Jiang, Mater. Lett. 60 (2006) 2783.
[22] K. Vanheusden, W.L. Warren, C.H. Seager, D.R. Tallant, J.A. Voigt, B.E. Gnade, J. Appl. Phys. 79 (1996) 7983.
[23] J. Liqiang, Q. Yichun, W. Baiqi, L. Shudan, J. Baojiang, Y. Libin, F. Wei, F. Honggang, S. Jiazhong, Solar Energy Mater. Solar Cells 90 (2006) 1773.
[24] A. Wood, M. Giersig, P. Mulvaney, J. Phys. Chem. B 105 (2001) 8810.

Influence of Preparation Method on the Nanocrystalline Porosity of α-Al_2O_3 and the Catalytic Properties of Pd/α-Al_2O_3 in Selective Acetylene Hydrogenation

Sataporn Komhom,[†] Okorn Mekasuwandumrong,[‡] Joongjai Panpranot,*[,†] and Piyasan Praserthdam[†]

Center of Excellence on Catalysis and Catalytic Reaction Engineering, Department of Chemical Engineering, Faculty of Engineering, Chulalongkorn University, Bangkok, 10330 Thailand, and Department of Chemical Engineering, Faculty of Engineering and Industrial Technology, Silpakorn University, Nakhonphatom, 73000 Thailand

Nanocrystalline α-Al_2O_3 powder with average crystallite sizes of 34−68 nm have been synthesized by three different methods, namely, solvothermal, sol−gel, and precipitation. Although the smallest crystallite size of α-Al_2O_3 was obtained via the sol−gel synthesis, the α-Al_2O_3 sol−gel possessed the least amount of specific surface area and pore volume. A narrow pore size distribution with an average pore diameter of 15 nm can be obtained via solvothermal method, whereas the precipitation method yielded α-Al_2O_3 with larger pore size and a wider pore size distribution. When used as a support for palladium catalysts, the α-Al_2O_3 solvothermal provided the highest palladium dispersion and the best catalyst performance in selective hydrogenation of acetylene. The catalytic properties of Pd/α-Al_2O_3 solvothermal were improved, in terms of both acetylene conversion and ethylene selectivity. As shown by temperature program studies, the use of solvothermal-derived α-Al_2O_3 facilitated H_2 reduction at low temperature and the desorption of ethylene and CO.

1. Introduction

Because of their fine particle size, high surface area, high melting point, high purity, good adsorbence, and high catalytic activity, alumina (Al_2O_3) powders find use in a myriad of applications.[1,2] They are well-known to be used as adsorbents, coatings, soft abrasives, ceramic tools, fillers, wear-resistant ceramics, catalysts, and catalyst supports.[3,4] Among the various transition phases of alumina (such as α-, γ-, χ-, δ-, η-, and θ-Al_2O_3), α-Al_2O_3 is the typical support used for the preparation of Pd/Al_2O_3 catalysts for the selective removal of acetylene in ethylene feed streams.

Polymer-grade ethylene has a strict specification of acetylene impurity (∼1 ppm maximum), because acetylene is poison to catalysts for ethylene polymerization.[5,6] Typically, α-Al_2O_3 provides a lower dispersion of active metal than the other transition phases of Al_2O_3, because of its lower surface area, but it is desirable in this reaction, because Pd/α-Al_2O_3 catalysts possess less active sites for direct ethane formation than Pd/γ-Al_2O_3 catalysts.[7] In addition, less oligomer/green oil was formed on Pd/α-Al_2O_3, because α-Al_2O_3 is less acidic than γ-Al_2O_3. The performance of Pd/α-Al_2O_3 in such reactions also is dependent largely on metal dispersion and reducibility of the palladium metal.[8,9] These properties are functions of the nature of the support, which typically is influenced by the preparation method that is used.

Many studies have shown supporting effects for palladium catalysts in selective acetylene hydrogenation.[10−12] However, in those studies, the addition of a second component such as SiO_2, MgO, TiO_2, or Nb_2O_5 was necessary for modification of the catalyst properties. In our previous studies, we have reported the improved catalytic performance of supported palladium catalysts in selective acetylene hydrogenation, using mixed-phase γ-/α-Al_2O_3,[13] nanocrystalline TiO_2,[14,15] and nanocrystalline α-Al_2O_3[16] as palladium catalyst supports. Modification of α-Al_2O_3 with a second metal such as nickel[17] or zinc[18] also resulted in significant improvement of Pd/α-Al_2O_3 catalyst properties in selective acetylene hydrogenation, in terms of both acetylene conversion and selectivity to ethylene. The formation of $NiAl_2O_4$ or $ZnAl_2O_4$ spinels dramatically decreased the acidity of the alumina supports; hence, the catalysts showed less deactivation by coke formation.

Different preparation methods have been proposed for the synthesis of nanocrystalline Al_2O_3, such as solvothermal,[19,20] sol−gel,[21,22] and precipitation.[23] The physical properties such as crystallite size, particle shape, particle size distribution, degree of agglomeration, and porosity can be controlled by adjusting the preparation parameters and conditions. Despite much effort that has been exerted, it is, however, still unclear about the most convenient method, in terms of precursor decomposition and crystal growth.

In this work, nanocrystalline α-Al_2O_3 was prepared via solvothermal, sol−gel, and precipitation methods and then used as supports for palladium catalysts for the selective hydrogenation of acetylene. The catalyst behaviors were determined to be strongly dependent on the porosity of α-Al_2O_3 supports, which itself a function of the preparation method used. Various analytical techniques, such as N_2 physisorption, X-ray diffraction (XRD), CO pulse chemisorption, H_2 temperature-programmed reduction (H_2-TPR), temperature-programmed desorption (C_2H_4-TPD and CO-TPD), infrared spectroscopy (IR), and transmission electron microscopy (TEM) were used to investigate the physicochemical properties of α-Al_2O_3 supports and the corresponding Pd/α-Al_2O_3 catalysts.

2. Experimental Section

2.1. Preparation of α-Al_2O_3. The Al_2O_3 support was prepared via the solvothermal, sol−gel, and precipitation methods. For the solvothermal method, aluminum isopropoxide (AIP,

* To whom correspondence should be addressed. Tel.: 66-2-2186869. Fax: 66-2-2186877. E-mail: joongjai.p@eng.chula.ac.th.

[†] Center of Excellence on Catalysis and Catalytic Reaction Engineering, Department of Chemical Engineering, Faculty of Engineering, Chulalongkorn University.

[‡] Department of Chemical Engineering, Faculty of Engineering and Industrial Technology, Silpakorn University.

10.1021/ie801784f CCC: $40.75
Published on Web 05/29/2009

25 g) was suspended in 100 mL of toluene within a test tube, which was placed in an autoclave and then added with 30 mL of toluene in the gap between the test tube and the autoclave wall. The autoclave was completely purged by nitrogen before heating to 300 °C at a rate of 2.5 °C/min, and the autoclave was kept at that temperature for 2 h. After cooling to room temperature, the resulting product was collected after repeated washing with methanol by centrifugation and air-dried overnight. The obtainable powder was placed into a box furnace and heated to 1150 °C with a rate of 10 °C/min and kept at 1150 °C for 3 h. Finally, a white α-Al_2O_3 powder was obtained.

For the sol−gel method, 24 g of aluminum nitrate was dissolved in 50 mL of ethanol. The experiment was conducted in the reflux−condenser reactor at a temperature of ∼70−80 °C for 18 h. Urea solution, which consists of urea (60 g) and distilled water (50 mL), then was added, to adjust the pH of solution. The mixture was permitted to rest at the same temperature for 24 h, to be gelled under neutral conditions. Then, it was calcined with two steps of heating rate to avoid the overflowing of gel during calcination (i.e., 3 °C/min from room temperature to 500 °C and continue heating at 5 °C/min to 1150 °C). The temperature was held for 3 h.

For the precipitation method, ammonium aluminum sulfate solution was gradually added to an ammonium hydrogen carbonate aqueous solution with a concentration ratio of 0.2: 2.0 mol/L. The experiment was controlled at temperatures in the range of 40−45 °C, a mixing speed of 450 rpm, an addition rate of 3 mL/min, and a constant pH value of 9. The mixture was aged for 15 min to permit crystal growth. The white precipitate that formed was separated from the final solution by centrifugation, repeatedly washed with methanol, and dried in an oven at 110 °C overnight. The obtainable powder was calcined in a depleted-oxygen atmosphere in a box furnace at 1150 °C for 3 h at a rate of 10 °C/min for the obtained α-Al_2O_3.[24]

2.2. Preparation of Pd/α-Al_2O_3 Catalysts. The Al_2O_3 obtained from various methods were used as supports for the preparation of 0.3% Pd/Al_2O_3 catalysts. Palladium was deposited on the alumina by incipient wetness impregnation, using $Pd(NO_3)_2 \cdot x(H_2O)$ as the palladium precursor and deionized water as a solvent. After being allowed to stand at room temperature for 6 h and drying at 110 °C in air overnight, the catalyst was further calcined in a N_2 flow (60 cm^3/min) at a rate of 10 °C/min until the temperature reached 500 °C; then, the environment was switched to an air flow (100 cm^3/min) at 500 °C for 2 h.

2.3. Characterization. The XRD pattern obtained within the range of 20°−80° (2θ), with a resolution of 0.04°, in a Siemens Model XRD D5000 system, with Cu Kα radiation and a nickel filter. The specific surface area of the support with various preparations was measured by adsorption of N_2 at 77 K, using a Micromeritic ASAP 2000 automated system. The functional group in the samples was determined using infrared (IR) spectroscopy (Nicolet Impact 400). Before measurement, the sample was mixed with KBr and then was formed into a thin pellet. The amount of CO chemisorbed on the Pd/Al_2O_3 catalyst was measured using a Micromeritics Model Chemisorb 2750 automated system, in conjunction with ChemiSoft TPx software, at room temperature. Temperature program experiments were conducted in a Micromeritics Model Chemisorb 2750 automated system. The temperature ramping was controlled by a temperature controller (Furnace Power 48 VAC 8A MAX). A mixture of 10% H_2 in argon, with a flow rate of 25 cm^3/min, was used in the TPR experiment. TPR was applied with a constant rate of 10 °C/min from 35 °C to 300 °C. For the C_2H_4-TPD experiment, the sample was prereduced at 150 °C in H_2 for 2 h, followed by cooling to room temperature. Ethylene adsorption then was performed at room temperature for 3 h. TPD was applied with a constant rate of 10 °C/min from 30 °C to 780 °C. For the CO-TPD experiment, the sample was prereduced at 150 °C in H_2 for 2 h (at a flow rate of 50 cm^3/min), followed by cooling to room temperature. CO adsorption then was performed at room temperature by continuous injection until the disappearance of CO adsorption. TPD was applied with a constant rate of 10 °C/min from 35 °C to 800 °C. The amount of desorbed CO was measured by analyzing the effluent gas with a thermal conductivity detector. The distribution of palladium on the catalyst support was observed using a transmission electron microscopy system (JEOL, Model JEM-2010) that was operated at 200 keV.

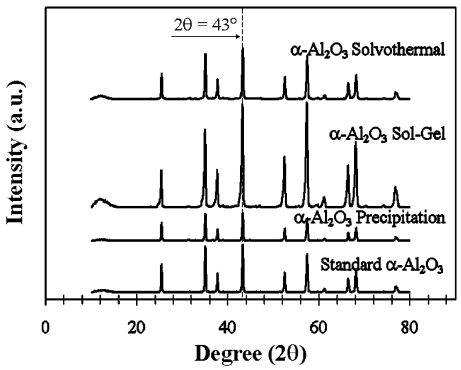

Figure 1. XRD patterns of the α-Al_2O_3 supports: solvothermal, sol−gel, and precipitation method.

2.4. Reaction Study. The catalyst performance in the selective hydrogenation of acetylene was evaluated using a 10-mm (inner diameter (id)) Pyrex reactor. First, the catalyst was reduced in situ with hydrogen by heating from room temperature to 150 °C at a rate of 10 °C/min. The reactor then was purged with argon and cooled to the reaction temperature (80 °C). The reaction was performed using a feed composition of 1.5% C_2H_2 and 1.7% H_2, with the balance being C_2H_4, with various gas hourly space velocities (GHSV = 52580, 32577, 22534, 12385, 9366, 6660, and 4282 h^{-1}). The products and feeds were analyzed by two gas chromatographs: one that was equipped with a flame ionization detection (FID) device (Shimadzu, Model FID GC 9A, carbosieve column S-2) and another that was equipped for thermal conductivity detection (TCD) (Shimadzu, Model TCD GC 8A, molecular sieve-5A).

Acetylene conversion, as used herein, is defined as the number of moles of acetylene converted, with respect to the number of moles of acetylene in the feed. Ethylene selectivity is defined as the percentage of acetylene hydrogenated to ethylene over the total amount of hydrogenated acetylene. The ethylene being hydrogenated to ethane (ethylene loss) is the difference between all the hydrogen consumed and all the acetylene that has been totally hydrogenated.

3. Results and Discussion

3.1. Characteristics of α-Al_2O_3. Figure 1 shows the XRD patterns of Al_2O_3 supports prepared by different preparation methods. The typical characteristic peaks for α-Al_2O_3 were detected for all samples, without any contamination of other transition alumina phases. The IR spectra of as-synthesized and calcined products are shown in Figure 2. In all cases, the strong H_2O peak at a wavenumber of ∼3450 cm^{-1} disappeared after

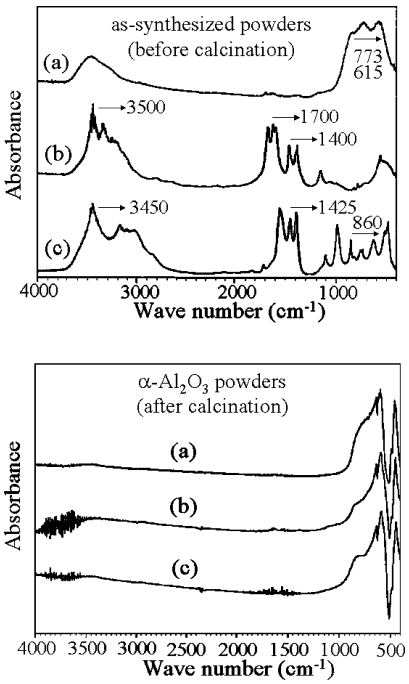

Figure 2. IR spectra of α-Al_2O_3 from (a) solvothermal, (b) sol−gel, and (c) precipitation methods.

calcination, suggesting that moisture that was trapped between crystals was removed by heat treatment. For the α-Al_2O_3 prepared by the precipitation method, absorption bands at 860 and 1425 cm^{-1}, corresponding to organic groups (CO_3^{2-} and NH_4^+), were eliminated during calcination. For the sol−gel α-Al_2O_3, the disappearance of the absorption peaks at 1400, 1700, and 3500 cm^{-1} after calcination indicated that organic groups and the NO_3^- ion have been removed. The characteristic absorption bands of boehmite observed at 773 and 615 cm^{-1} from the as-synthesized solvothermal powder also disappeared after calcination. Boehmite resulted from the presence of a small amount of water, which was byproduct from AIP decomposition.[25] From IR analyses, it is confirmed that the α-Al_2O_3 powders obtained after calcination in all cases were pure Al_2O_3, without residual organic moiety. The calcination conditions were also satisfactory for complete phase transformation or decomposition to α-Al_2O_3.

The BET surface area, pore volume, average pore diameter, and average crystallite size of Al_2O_3 supports are given in Table 1. The average crystallite sizes of α-Al_2O_3 were calculated from XRD results using the Scherrer equation and the characteristic peak of α-Al_2O_3 at $2\theta = 43°$. The crystallite size of sol−gel-derived α-Al_2O_3 support was smallest at 33.8 nm, whereas the solvothermal- and precipitation-derived α-Al_2O_3 supports gave larger crystallite sizes (53 and 67.6 nm, respectively). The specific surface area usually shows a reversed tendency with crystallite size. However, in this study, the α-Al_2O_3 obtained from the sol−gel method not only possessed the smallest crystallite size but also had the minimum value of specific surface area (1.7 m^2/g), compared to those obtained by the solvothermal (19.8 m^2/g) and precipitation (41.2 m^2/g) methods. This could possibly be due to the difference in the degree of agglomeration. From Table 1, the total pore volume of sol−gel-derived α-Al_2O_3 (0.0065 cm^3/g) was much less than those obtained from other preparation methods (0.2020 cm^3/g for the precipitation method and 0.0739 cm^3/g for the solvothermal method). These results indicated that the sol−gel-derived support had the smallest space between particles, compared to the other supports, which prohibited the adsorption of N_2 molecules on the catalyst surface and led to the smallest surface area.

The pore size distribution curves of α-Al_2O_3 supports are shown in Figure 3. While the solvothermal- and precipitation-derived α-Al_2O_3 exhibited the typical characteristic of a mesopore system (having an average pore size of 16−32 nm), the sol−gel-derived α-Al_2O_3 did not show any distinguishing curves. Peak areas under the pore size distribution curves that were directly correlated with the pore volume increased in the following order: precipitation > solvothermal ≫ sol−gel. The nitrogen adsorption isotherms for the α-Al_2O_3 prepared by different methods are shown in Figure 4. It can be seen that the precipitation-derived support represented adsorption isotherms with hysteresis loops with type-A adsorption characteristics, which corresponds to the presence of a two-ended tabular pore structure. However, the solvothemal- and sol−gel-derived alumina exhibited a Type-E hysteresis loop, which is an indication of the presence of a tabular pore structure, through short pores with winded parts of various widths.[26,27] These pores were formed among the primary particles of alumina.

3.2. Physicochemical Properties of Pd/α-Al_2O_3. The CO chemisorption results, such as the number of active Pd atoms, palladium dispersion (%), and average palladium-metal particle size, for the Pd/α-Al_2O_3 catalysts are given in Table 1. The mean stoichiometry of palladium metal to CO molecule ($X_{Pd\text{-}CO}$) was determined by the iterative method, according to those of Lambert et al.[28] A polynomial function was fitted based on the table established by Joyal and Butt,[29] who determined $X_{Pd\text{-}CO}$ as a function of palladium dispersion. The values of $X_{Pd\text{-}CO}$ were determined to be 0.51, 0.34, and 0.29 for palladium catalysts supported on solvothermal-, sol−gel-, and precipitation-derived α-Al_2O_3, respectively. The numbers of active sites of palladium supported on solvothermal-, sol−gel and precipitation-derived α-Al_2O_3 catalysts were 11.5×10^{17}, 3.9×10^{17}, and 2.1×10^{17} sites/g-catalyst, corresponding to palladium dispersions of 7.6%, 2.6%, and 1.4%, respectively. The lower percetnage of palladium dispersion that was obtained for the Pd/sol−gel-derived α-Al_2O_3 would be due to the lower specific surface area and pore volume. On the other hand, the larger pore size of precipitation-derived α-Al_2O_3 could also result in a low percentage of palladium dispersion, because of the agglomeration of palladium particles within the pores. Among the various Pd/α-Al_2O_3 catalysts, the maximum CO chemisorption was obtained on the solvothermal-derived α-Al_2O_3 with medium pore size. In a previous study from our group about palladium dispersed on silica and MCM-41 with various pore sizes, a lower percentage of palladium dispersion was found on the small pore SiO_2, because of the significant amount of palladium being located outside the pores of the supports.[30] A similar result was obtained when palladium was supported on the sol−gel α-Al_2O_3 with a very low amount of porosity.

The TEM micrographs of Pd/α-Al_2O_3 catalysts were also taken to physically measure the size of the palladium oxide particles and/or palladium clusters on the various α-Al_2O_3; these micrographs are shown in Figure 5. The palladium catalyst supported on the sol−gel-derived support consisted of agglomerated particles primarily with irregularly shaped structure, whereas, for those prepared by the solvothermal and precipitation methods, the agglomeration of fingerlike and rodlike particles was observed. The palladium metal cluster size on the various alumina supports increased in the following order:

$$\alpha\text{-}Al_2O_3\ (\text{precipitation}) \approx \alpha\text{-}Al_2O_3\ (\text{sol}-\text{gel}) > \alpha\text{-}Al_2O_3\ (\text{solvothermal})$$

Table 1. Physicochemical Properties of α-Al_2O_3 Various Preparation Methods and 0.3% Pd/Al_2O_3 Catalysts

Pd/Al_2O_3 catalyst	BET surface area[a,b] (m^2/g)	pore volume[b,c] (cm^3/g)	average pore diameter[b,c] (nm)	crystallite size[b,d] (nm)	Pd active sites[e] (× 10^{-17} sites/ g-catalyst)	Pd dispersion[f] (%)	average Pd^0 particle size[g] (nm)
solvothermal-derived	19.8	0.0739	14.9	53	11.5	7.6	14.7
sol−gel-derived	1.7	0.0065	46	33.8	3.9	2.6	43.2
precipitation-derived	41.2	0.2020	26.9	67.6	2.1	1.4	80.2

[a] Error of measurement = 10%. [b] Only catalyst supports were measured. [c] Calculated from the Barrett−Joyner−Halenda (BJH) method. [d] Determined from XRD line broadening. [e] Determined from CO chemisorption. Fraction of Pd active sites = $S_f \times (V_{ads}/V_g) \times (6.02 \times 10^{23})$, where V_{ads} the volume adsorbed, V_g the molar volume of gas at standard temperature and pressure (STP), and S_f the stoichiometry factor for CO on Pd. Error of measurement = ±5%. [f] Based on D = [fraction of Pd active sites × (MW/%M) × 100% × 100%]/(6.02×10^{23}), where D is the fractional metal dispersion, MW the molecular weight of the metal, and %M the percentage of metal. [g] Based on d (nm) = (1.12/D).[40]

Table 2. Consumption of Hydrogen in TPR, and the Amount of Ethylene and CO Desorption

	Temperature at Maximum (°C)								
	Peak 1			Peak 2		Peak 3			
Pd/Al_2O_3 catalyst	H_2-TPR[b]	C_2H_4-TPD[c]	CO-TPD[d]	C_2H_4-TPD[c]	CO-TPD[d]	C_2H_4-TPD[c]	H_2 consumption (μmol)[a]	amount of ethyl ene desorption (μmol)[a]	amount of CO desorption (μmol)[a]
solvothermal-derived	60	90	90	240	230	420	658	131	76
sol−gel-derived	65	100	90	280	230	500	488	75	10
precipitation-derived	70	100	90	260	250	440	610	122	33

[a] Measured using the same weight of catalysts. [b] Based on H_2-TPR results. [c] Based on C_2H_4-TPD results. [d] Based on CO-TPD results.

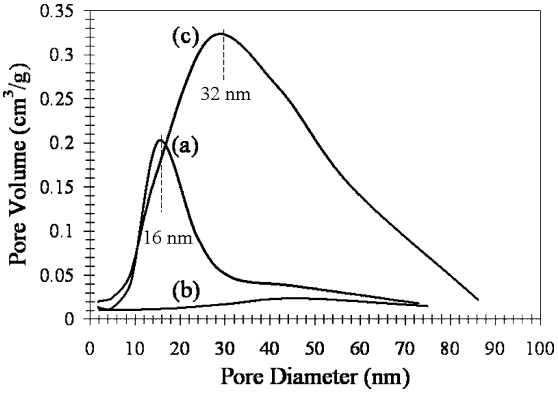

Figure 3. Pore size distribution results of the α-Al_2O_3 supports from (a) solvothermal, (b) sol−gel, and (c) precipitation methods.

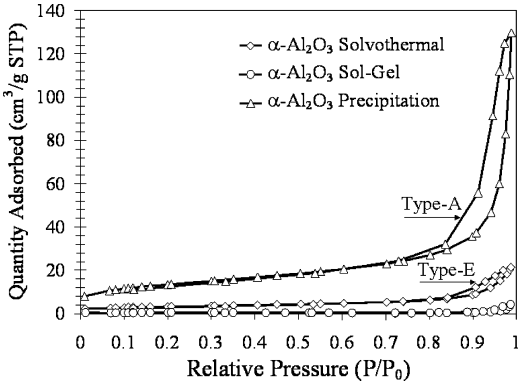

Figure 4. N_2 adsorption isotherms.

The reduction behaviors and reducibility of catalysts were studied by the TPR technique. The TPR profiles of Pd/α-Al_2O_3 catalysts are shown in Figure 6. All the TPR profiles showed a single reduction peak in the range of 60−70 °C, which corresponded to the reduction of PdO to palladium metal.[31−33] This peak was shifted to higher temperature for the catalysts that were supported on sol−gel- and precipitation-derived α-Al_2O_3 by ∼10 °C. The lower reduction temperature of the TPR profile suggested that PdO/Pd supported on the solvothermal-derived α-Al_2O_3 facilitated reduction at lower temperature. The average oxidation states of palladium were calculated

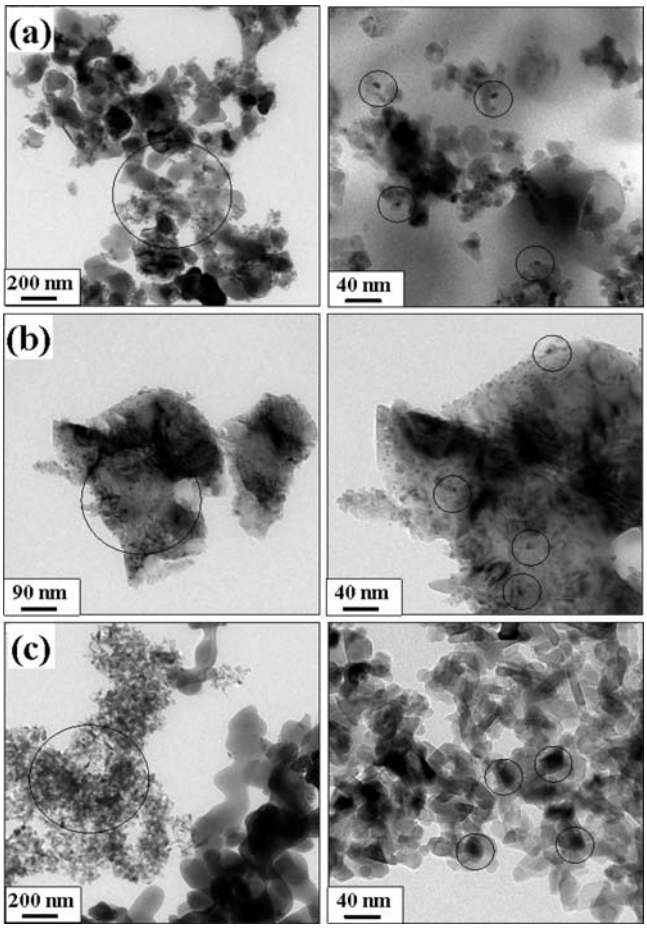

Figure 5. TEM image of the palladium supported by α-Al_2O_3 from (a) solvothermal, (b) sol−gel, and (c) precipitation methods. Characteristic palladium is shown within the circles in the micrographs.

according to the amount of H_2 consumption, and the results are given in Table 2. The solvothermal Pd/Al_2O_3 possessed the highest fraction of Pd active sites, probably because it had the smallest PdO/Pd sizes produced, as determined by TEM measurement.

Ethylene-temperature-programmed desorption (C_2H_4-TPD) was performed to obtain information about the ethylene adsorp-

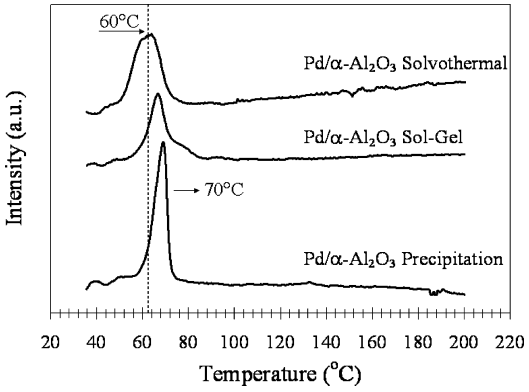

Figure 6. H_2-TPR profiles for the various Pd/α-Al_2O_3 catalysts.

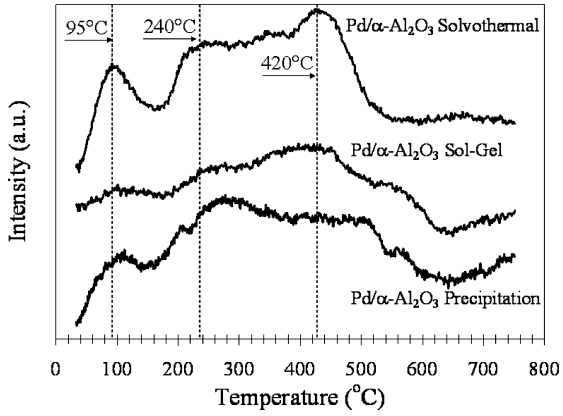

Figure 7. C_2H_4-TPD profiles for the various Pd/α-Al_2O_3 catalysts.

tion behavior on the catalyst surface, and the results are shown in Figure 7. We observed the peak locations and found that it appeared at different temperature ranges, depending on the characteristic modes of the ethylene adsorbed on the surface. All of the catalysts showed that the three major peaks had differences in their temperature positions and peak intensities. According to Shin et al.,[34,35] the first peak, at ~95 °C, was assigned to π-bonded ethylene, which was weakly adsorbed and, consequently, desorbed without decomposition. The peak at ~240 °C was due to di-σ-bonded ethylene, which undergoes decomposition, followed by the recombination of the surface hydrocarbon species with hydrogen to produced ethylene as well as ethane. The last peak, at ~420 °C, was the CH_3 group, because the CH_3 signal was due to the decomposition of C_2 hydrocarbons that were adsorbed on the catalyst (tentatively, ethane or ethylene).[36,37]

It is generally accepted that ethylene adsorption is dependent on palladium particle size; it adsorbs more strongly on larger palladium particles. The results in this study follow the same trend in the literature. The low-temperature ethylene desorption peak decreased and slightly shifted to higher temperature as the palladium particle size increased from 14.7 to 80.2 nm for the α-Al_2O_3 supports prepared by solvothermal, sol−gel, and precipitation, respectively. According to Shaikhutdinov et al.,[38] adsorption of π-bond ethylene occurs at low temperature and then desorbs when the temperature increases without hydrogenation reaction. Small palladium particles favor such a process, whereas, on larger palladium particles, a fraction of ethylene molecules adsorbs as di-σ-bonded ethylene, which can either desorb near room temperature or dehydrogenate, producing surface species such as ethylidyne and atomic hydrogen. The formation of these surface species is believed to be the origin

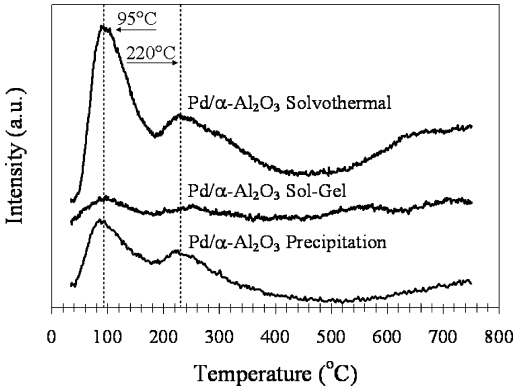

Figure 8. CO-TPD profiles for the various Pd/α-Al_2O_3 catalysts.

for ethane production and carbon deposits during acetylene hydrogenation.

The CO temperature-programmed desorption (CO-TPD) behavior for the palladium catalysts supported on Al_2O_3 from different preparation methods is shown in Figure 8. Two desorption peaks, one with strong intensity at ca. 95 °C and another small peak located at ca. 220 °C, were observed for all the catalysts, which could be attributed to CO adsorption on two adsorptive site groups. The first group gave the strong peak, ranging from 95 to 180 °C, which was weak CO species over the catalyst. The second one was characteristic of the strong chemically adsorbed CO molecules. The amount of chemisorbed CO (see Table 2) on Pd/α-Al_2O_3 (solvothermal-derived support) was 7 and 2 times greater than those on the Pd/α-Al_2O_3 sol−gel-derived support and the Pd/α-Al_2O_3 precipitation-derived support, respectively. The difference may be related to different geometry states of the adsorptive sites on catalysts that may have occurred from the different support configurations of the Pd/α-Al_2O_3 catalysts. Moreover, it has been reported that the activation energy of CO desorption decreased as the size of the palladium particles decreased.[39] The results from this study also show that the Pd/Al_2O_3 solvothermal-derived support with the smallest palladium particle size facilitated CO desorption. The atomic structures of CO and ethylene were similar, in terms of the double bond, which consisted of a π-bond and a σ-bond; thus, both the C_2H_4-TPD and CO-TPD results show the same trend.

3.3. Catalytic Performance in Selective Acetylene Hydrogenation. The effect of nanocrystalline porosity of α-Al_2O_3 obtained from various preparation methods on the catalytic properties of Pd/α-Al_2O_3 was investigated in selective acetylene hydrogenation. The catalyst performances are shown by the plots of acetylene conversion × ethylene selectivity versus the GHSV value in Figure 9. Ethylene yield (%) clearly was improved in the following order of Pd/α-Al_2O_3 catalysts:

Pd/solvothermal-derived α-Al_2O_3 > Pd/sol−gel-derived α-Al_2O_3 > Pd/precipitation-derived α-Al_2O_3

Among the three catalyst systems, the Pd/solvothermal-derived α-Al_2O_3 showed better performance than catalysts supported on the other α-Al_2O_3 supports. Based on our characterization results, Pd/solvothermal-derived α-Al_2O_3 had the appropriate total pore volume, the highest fraction of Pd active sites, and the highest metal dispersion of Pd on Al_2O_3 support; it also facilitated the reduction of PdO at lower temperature, which promoted acetylene conversion. Moreover, the TPD profiles of Pd/solvothermal-derived α-Al_2O_3 suggested that the amount of ethylene adsorbed at low temperature on the catalyst surface

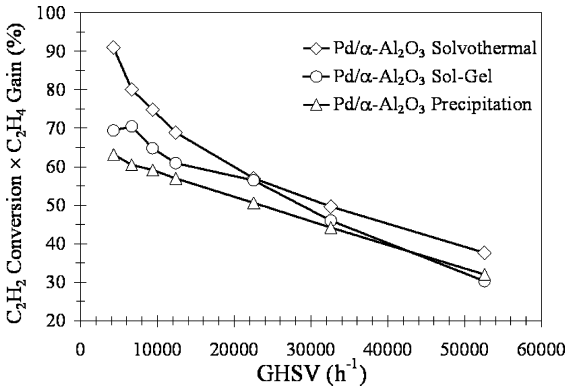

Figure 9. Performance of Pd/α-Al_2O_3 catalysts in selective acetylene hydrogenation.

was highest, which was important for the improvement of ethylene gain, especially at high acetylene conversions.

4. Conclusions

Nanocrystalline porosity of α-Al_2O_3 powders was varied by changing the preparation methods. While the sol−gel method yielded the smallest crystallite size of α-Al_2O_3 with little pore volume and surface area, a mesopore structure with an average pore size of 15−27 nm was obtained via the solvothermal and precipitation methods. Suitable properties of the solvothermal-derived α-Al_2O_3, such as high surface area and narrow pore size distribution, were determined to result in the best catalyst performance of Pd/α-Al_2O_3 catalysts in the selective hydrogenation of acetylene. The solvothermal-derived α-Al_2O_3 not only provided the highest percentage of palladium dispersion and smallest palladium particle size, but it also facilitated H_2 reduction at low temperature and the desorption of ethylene and CO.

Acknowledgment

The financial support from the Thailand Research Fund (TRF) and the National Research Council of Thailand (NRCT) are gratefully acknowledged.

Literature Cited

(1) Pajonk, G.; Teichner, S.; Fricke, J. *Aerogels*; Springer: Berlin, 1986.

(2) Church, J. S.; Cant, N. W.; Trimm, D. L. Stabilisation of Aluminas by Rare Earth and Alkaline Earth Ions. *Appl. Catal., A* **1993**, *101* (1), 105–116.

(3) Misra, C. *Industrial Alumina Chemicals*; ACS Monograph 184; American Chemical Society: Washington, DC, 1986.

(4) Topsoe, H.; Clausen, B. S.; Massoth, F. E. *Hydrotreating Catalysis*; Springer: Berlin, 1996.

(5) Mohundro, E. L. Presented at the American Institute of Chemical Engineers 15th Ethylene Produces Conference, Spring National Meeting, New Orleans, LA, March−April 3, 2003.

(6) Didillon, B.; Cosyns, J.; Cameron, C.; Uzio, D.; Sarazzi, P.; Boitiaux, J. P. Industrial Evaluation of Selective Hydrogenation Catalyst Poisoning. *Stud. Surf. Sci. Catal.* **1997**, *111*, 447–454.

(7) Vincent, M. J.; Gonzalez, R. D. A Langmuir-Hinshelwood Model for a Hydrogen Transfer Mechanism in the Selective Hydrogenation of Acetylene over a Pd/α-Al_2O_3 Catalyst Prepared by the Sol−Gel Method. *Appl. Catal., A* **2001**, *217* (1−2), 143–156.

(8) Zakarina, N. A.; Zakumbaeva, G. D.; Toktabaeva, N. F.; Kuanyshev, A. Sh.; Litvyakova, E. L. Preparation and Properties of High Dispersity Palladium Catalysts. *React. Kinet. Catal. Lett.* **1984**, *26* (3−4), 441–445.

(9) Park, Y. H.; Price, G. L. Promotional Effects of Potassium on Palladium/Alumina Selective Hydrogenation Catalysts. *Ind. Eng. Chem. Res.* **1992**, *31* (2), 469–474.

(10) Hong, J.; Chu, W.; Chen, M.; Wang, X.; Zhang, T. Preparation of Novel Titania Supported Palladium Catalysts for Selective Hydrogenation of Acetylene to Ethylene. *Catal. Commun.* **2007**, *8* (3), 593–597.

(11) Noronha, F. B.; Aranda, D. A. G.; Ordine, A. P.; Schmal, M. The Promoting Effect of Nb_2O_5 Addition to Pd/Al_2O_3 Catalysts on Propane Oxidation. *Catal. Today* **2000**, *57* (3−4), 275–282.

(12) Guimon, C.; Auroux, A.; Romero, E.; Monzon, A. Acetylene Hydrogenation over Ni-Si-Al Mixed Oxides Prepared by Sol−Gel Technique. *Appl. Catal., A* **2003**, *251* (1), 199–214.

(13) Komhom, S.; Mekasuwandumrong, O.; Praserthdam, P.; Panpranot, J. Improvement of Pd/Al_2O_3 Catalyst Performance in Selective Acetylene Hydrogenation Using Mixed Phases Al_2O_3 Support. *Catal. Commun.* **2008**, *10*, 86–91.

(14) Kontapakdee, K.; Panpranot, J.; Praserthdam, P. Effect of Ag Addition on the Properties of Pd-Ag/TiO_2 Catalysts Containing Different TiO_2 Crystalline Phases. *Catal. Commun.* **2007**, *8* (12), 2166–2170.

(15) Panpranot, J.; Kontapakdee, K.; Praserthdam, P. Selective Hydrogenation of Acetylene in Excess Ethylene on Micron-sized and Nanocrystalline TiO_2 Supported Pd Catalysts. *Appl. Catal., A* **2006**, *314* (1), 128–133.

(16) Wongwaranon, N.; Mekasuwandumrong, O.; Praserthdam, P.; Panpranot, J. Performance of Pd Catalysts Supported on Nanocrystalline α-Al_2O_3 and Ni-modified ά-Al_2O_3 in Selective Hydrogenation of Acetylene. *Catal. Today* **2008**, *131* (1−4), 553–558.

(17) Mekasuwandumrong, O.; Wongwaranon, N.; Panpranot, J.; Praserthdam, P. Effect of Ni-modified α-Al_2O_3 Prepared by Sol−Gel and Solvothermal Methods on the Characteristics and Catalytic Properties of Pd/α-Al_2O_3 Catalysts. *Mater. Chem. Phys.* **2008**, *111* (2−3), 431–437.

(18) Chinayon, S.; Mekasuwandumrong, O.; Praserthdam, P.; Panpranot, J. Selective Hydrogenation of Acetylene over Pd Catalysts Supported on Nanocrystalline α-Al_2O_3 and Zn-modified α-Al_2O_3. *Catal. Commun.* **2008**, *9* (14), 2297–2302.

(19) Inoue, M.; Kominami, H.; Inui, T. Thermal Reaction of Aluminum Alkoxide in Glycols. *J. Am. Ceram. Soc.* **1990**, *73* (4), 1100–1102.

(20) Inoue, M.; Kominami, H.; Inui, T. Thermal Transformation of χ-Alumina Formed by Thermal Decomposition of Aluminum Alkoxide in Organic Media. *J. Am. Ceram. Soc.* **1992**, *75* (9), 2597–2598.

(21) Bahlawane, N.; Watanabe, T. New Sol−Gel Route for the Preparation of Pure Alumina at 950 °C. *J. Am. Ceram. Soc.* **2000**, *83* (9), 2324–2326.

(22) Lin, C.-P.; Wen, S.-B.; Lee, T.-T. Preparation of Nanometer-Sized α-Alumina Powders by Calcining an Emulsion of Boehmite and Oleic Acid. *J. Am. Ceram. Soc.* **2002**, *85* (1), 129–133.

(23) Scott, W. B.; Matijevic, E. Aluminum hydrous oxide sols: III. Preparation of Uniform Particles by Hydrolysis of Aluminum Chloride and Perchlorate Salts. *J. Colloid Interface Sci.* **1978**, *66* (3), 447–454.

(24) Kato, S.; Iga, T.; Hatano, S.; Isawa, Y. U.S. Patent 4,053,579, October 11, 1975.

(25) Mekasuwandumrong, O.; Silveston, P. L.; Praserthdam, P.; Inoue, M.; Pavarajarn, V.; Tanakulrungsank, W. Synthesis of Thermally Stable Micro Spherical χ-Alumina by Thermal Decomposition of Aluminum Isopropoxide in Mineral Oil. *Inorg. Chem. Commun.* **2003**, *6* (7), 930–934.

(26) Lippens, B. C.; de Boer, J. H. Studies on Pore Systems in Catalysts I. The Adsorption of Nitrogen; Apparatus and Calculation. *J. Catal.* **1964**, *3* (1), 32–37.

(27) Lippens, B. C.; de Boer, J. H. Studies on Pore Systems in Catalysts: V. The *t* Method. *J. Catal.* **1965**, *4* (3), 319–323.

(28) Lambert, S.; Cellier, C.; Grange, P.; Pirard, J. P.; Heinrichs, B. Synthesis of Pd/SiO_2, Ag/SiO_2, and Cu/SiO_2 cogelled xerogel catalysts: study of metal dispersion and catalytic activity. *J. Catal.* **2004**, *221* (2), 335–346.

(29) Joyal, C. L. M.; Butt, J. B. Chemisorption and Disproportionation of Carbon Monoxide on Palladium/Silica Catalysts of Differing Percentage Metal Exposed. *J. Chem. Soc., Faraday Trans. I* **1987**, *83* (9), 2757–2764.

(30) Panpranot, J.; Pattamakomsan, K.; Goodwin, J. G.; Praserthdam, P. A. Comparative Study of Pd/SiO_2 and Pd/MCM-41 Catalysts in Liquid-Phase Hydrogenation. *Catal. Commun.* **2004**, *5* (10), 583–590.

(31) Figoli, N. S.; Largentiere, P. C.; Arcoya, A.; Seoane, X. L. Modification of the Properties and Sulfur Resistance of a Pd/SiO_2 Catalyst by La Addition. *J. Catal.* **1995**, *155* (1), 95–105.

(32) Seoane, X. L.; Figoli, N. S.; L'Argentiere, P. C.; González, J. A.; Arcoya, A. Palladium-Lanthanum Interaction Phenomena in Pd-$LaCl_3$/SiO_2 and Pd-La_2O_3/SiO_2 Catalysts. *Catal. Lett.* **1997**, *47* (3−4), 213–220.

(33) Yang, C.; Ren, J.; Sun, Y. Role of La_2O_3 in Pd-Supported Catalysts for Methanol Decomposition. *Catal. Lett.* **2002**, *84* (1−2), 123–129.

(34) Shin, E. W.; Kang, J. H.; Kim, W. J.; Park, J. D.; Moon, S. H. Performance of Si-modified Pd Catalyst in Acetylene Hydrogenation: The

Origin of the Ethylene Selectivity Improvement. *Appl. Catal., A* **2002**, *223* (1−2), 161–172.

(35) Kang, J. H.; Shin, E. W.; Kim, W. J.; Park, J. D.; Moon, S. H. Selective Hydrogenation of Acetylene on Pd/SiO_2 Catalysts Promoted with Ti, Nb and Ce Oxides. *Catal. Today* **2000**, *63* (2−4), 183–188.

(36) Tsuchiya, S.; Nakamura, M. Study of Chemisorption and Hydrogenation of Ethylene on Platinum by Temperature-Programmed Desorption. *J. Catal.* **1977**, *50* (1), 1–7.

(37) Park, Y. H.; Price, G. L. Temperature-Programmed-Reaction Study on the Effect of Carbon Monoxide on the Acetylene Reaction over Palladium/Alumina. *Ind. Eng. Chem. Res.* **1991**, *30* (8), 1700–1707.

(38) Shaikhutdinov, Sh.; Heemeier, M.; Bäumer, M.; Lear, T.; Lennon, D.; Oldman, R. J.; Jackson, S. D.; Freund, H.-J. Structure-Reactivity Relationships on Supported Metal Model Catalysts: Adsorption and Reaction of Ethene and Hydrogen on $Pd/Al_2O_3/NiAl(110)$. *J. Catal.* **2001**, *200* (2), 330–339.

(39) Matolin, V. Rheed and TPD Studies of the Effect of Particle Size on CO Desorption from Al_2O_3 Supported Pd and Rh Model Catalysts. *Fiz. A* **1995**, *4* (2), 181–189.

(40) Mahata, N.; Vishwanathan, V. Influence of Palladium Precursors on Structural Properties and Phenol Hydrogenation Characteristics of Supported Palladium Catalysts. *J. Catal.* **2000**, *196* (2), 262–270.

Received for review November 21, 2008
Revised manuscript received March 23, 2009
Accepted May 8, 2009

IE801784F

React Kinet Catal Lett (2009) 97:115–123
DOI 10.1007/s11144-009-0010-8

Effect of Fe-modified α-Al_2O_3 on the properties of Pd/α-Al_2O_3 catalysts in selective acetylene hydrogenation

Tatiya Sangkhum · Okorn Mekasuwandumrong · Piyasan Praserthdam · Joongjai Panpranot

Received: 5 November 2008 / Accepted: 10 February 2009 / Published online: 17 June 2009

Abstract The use of nanocrystalline Fe-modified α-Al_2O_3 prepared by sol–gel and solvothermal method as supports for Pd catalysts resulted in an improved catalyst performance in selective acetylene hydrogenation. Moreover, the amount of coke deposits was reduced due to lower acidity of the Fe-modified α-Al_2O_3 supports.

Keywords Fe-modified Al_2O_3 · Selective acetylene hydrogenation

Introduction

Selective hydrogenation of acetylene using supported Pd-based catalysts is an important process in the polyethylene industry because acetylene contaminant in ethylene feedstock poisons the polymerization catalyst. It is of particular challenge to produce an effective catalyst that can remove trace amounts of acetylene in ethylene feedstock while ethylene remains inactive during hydrogenation to prevent ethylene loss. Because Pd catalysts have poor selectivity at high acetylene conversion and oligomer formation on the catalysts, which lessens the catalyst lifetime, promotion with a second component such as Ag [1, 2], Si [3], K [4], Au [5], and TiO_2 [6] has often been employed in order to improve the catalyst performance. Besides Pd/Al_2O_3, new, efficient catalyst systems for selective hydrogenation of acetylene have been continuingly developed including Pd on nano-sized TiO_2 [7–10] and zeolite-supported Pd–Ag catalysts [11, 12].

T. Sangkhum · P. Praserthdam · J. Panpranot (✉)
Department of Chemical Engineering, Faculty of Engineering, Center of Excellence on Catalysis and Catalytic Reaction Engineering, Chulalongkorn University, Bankok 10330, Thailand
e-mail: joongjai.p@eng.chula.ac.th

O. Mekasuwandumrong
Department of Chemical Engineering, Faculty of Engineering and Industrial Technology, Silpakorn University, Nakorn Pathom 73000, Thailand

Recently, our studies showed that the use of nanocrystalline α-Al_2O_3 prepared by sol–gel and solvothermal method as supports for Pd catalysts yielded superior catalyst performance compared to those on commercial α-Al_2O_3 [13]. Moreover, modification of α-Al_2O_3 with a second metal such as Ni [14] and Zn [15] has been shown to result in significant improvement of Pd/α-Al_2O_3 catalyst properties in selective acetylene hydrogenation in terms of both acetylene conversion and selectivity to ethylene. Formation of $NiAl_2O_4$ or $ZnAl_2O_4$ spinels dramatically decreased the acidity of the alumina supports hence the catalysts showed less deactivation by coke formation.

The present paper is our follow-up effort to produce a highly effective catalyst for purification of ethylene feed stream in polyethylene production. The effect of Fe-modified α-Al_2O_3 on the properties of Pd/α-Al_2O_3 catalyst in selective acetylene hydrogenation is focused. The Fe-substituted alumina is interesting as a catalyst support due to its improved stability and high resistance to oxidation [16, 17]. The catalyst performances were correlated with the catalyst characterization results from N_2 physisorption, CO chemisorption, X-ray diffraction (XRD), ammonia temperature program desorption (NH_3-TPD), and thermal gravimetric and differential temperature analysis (TG/DTA).

Experimental

Preparation of α-Al_2O_3 and Fe-modified α-Al_2O_3

The nanocrystalline α-Al_2O_3 was prepared by solvothermal and sol–gel method according to that of Panpranot and co-workers [13]. The iron precursors used for the preparation of Fe-modified α-Al_2O_3 by solvothermal and sol–gel method were iron (II) acetylacetonate ($(C_5H_8O_2)_3Fe$) and ferric nitrate nonahydrate ($FeN_3O_9{\cdot}9H_2O$), respectively. The Pd/Fe-modified α-Al_2O_3 catalysts were prepared by incipient wetness impregnation of support with a desired amount of an aqueous solution of palladium (II) nitrate hydrate (Aldrich) to obtain the final Pd loading of ca. 0.3 wt%. The catalysts were dried overnight at 110 °C and then calcined in N_2 flow (60 cm^3/min) with a heating rate of 10 °C/min until the temperature reached 500 °C and then in air flow (100 cm^3/min) at 500 °C for 2 h.

Catalyst characterization

X-ray diffraction patterns were recorded between 20° and 80° (2θ) with a SIEMENS D5000 X-ray diffractometer using Cu K_α radiation with a Ni filter. Specific surface areas were measured using nitrogen adsorption with a Micromeritic Chemisorb 2750 system. Prior to measurements, the samples were degassed at 200 °C for 2 h. Metal active sites were measured using CO chemisorption technique at room temperature in a Micromeritic Chemisorb 2750 automated system attached with ChemiSoft TPx software. Before chemisorption measurement, the sample was reduced in a H_2 flow at 150 °C for 2 h then cooled down to ambient temperature in a He flow. NH_3-TPD was also performed in the Micromeritic Chemisorb 2750

automated system attached with ChemiSoft TPx software. The distribution of palladium on catalyst supports were characterized using a JEOL 2010 transmission electron microscope operated at 2,000 kV. Thermal gravimetric analysis (TGA) thermograms were performed using a SDT Analyzer Model Q600 from TA Instruments, USA.

Reaction study

The selective hydrogenation of acetylene was performed in a quartz tube reactor. Prior to the start of the reaction, the catalyst was reduced in H_2 at 150 °C for 2 h. Then the reactor was purged with argon and cooled down to the reaction temperature. The feed gas was composed of 1.5% C_2H_2, 1.7% H_2, and balanced C_2H_4 (TIG Co., Ltd.). The composition of product and feed stream were analyzed by a Shimadzu GC 8A equipped with TCD and FID detectors (molecular sieve-5A and carbosieve S2 columns, respectively). Acetylene conversion as used herein is defined as moles of acetylene converted with respect to acetylene in feed. Ethylene selectivity is defined as the percentage of acetylene hydrogenated to ethylene over totally hydrogenated acetylene.

Results and discussion

The XRD patterns of Pd/α-Al_2O_3 and Pd/Fe-modified α-Al_2O_3 are shown in Fig. 1. For all the samples, the characteristic peaks of α-Al_2O_3 were evident while the diffraction lines of iron, iron oxides, iron aluminate, palladium or palladium oxide

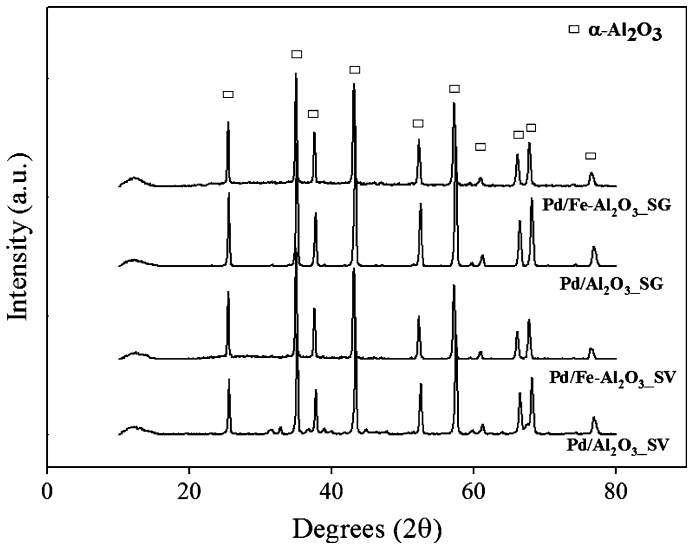

Fig. 1 XRD patterns of the Pd/α-Al_2O_3 and Pd/Fe-modified α-Al_2O_3 prepared by sol–gel (SG) and solvothermal (SV) methods

Table 1 Physicochemical properties of Pd/Al_2O_3 and $Pd/Fe\text{-}Al_2O_3$ catalysts

	BET surface area (m^2/g)	Avg. crystallite size[a] (nm)	CO chemisorption ($\times 10^{17}$ site/g cat.)	% Pd dispersion	d_p Pd^0 (nm)
$Pd/Al_2O_3\_SG$	1.0	46	10.0	8.4	13
$Pd/Fe\text{–}Al_2O_3\_SG$	1.4	62	4.1	2.7	42
$Pd/Al_2O_3\_SV$	5.1	52	11.0	7.2	16
$Pd/Fe\text{–}Al_2O_3\_SV$	3.9	63	7.8	5.1	22

[a] Average crystallite size of $\alpha\text{-}Al_2O_3$ supports determined from XRD results using Scherrer equation

were not apparent due probably to the very low amount present. The average crystallite sizes of $\alpha\text{-}Al_2O_3$ were calculated from the full width at half maximum of the XRD peaks at $2\theta = 43°$ using the Scherrer equation; the results are shown in Table 1. The average crystallite sizes of $\alpha\text{-}Al_2O_3$ and Fe-modified $\alpha\text{-}Al_2O_3$ prepared by sol-gel and solvothermal method were ranged between 46 and 63 nm. The corresponding surface areas of the catalysts were 1–5 m^2/g which were quite low

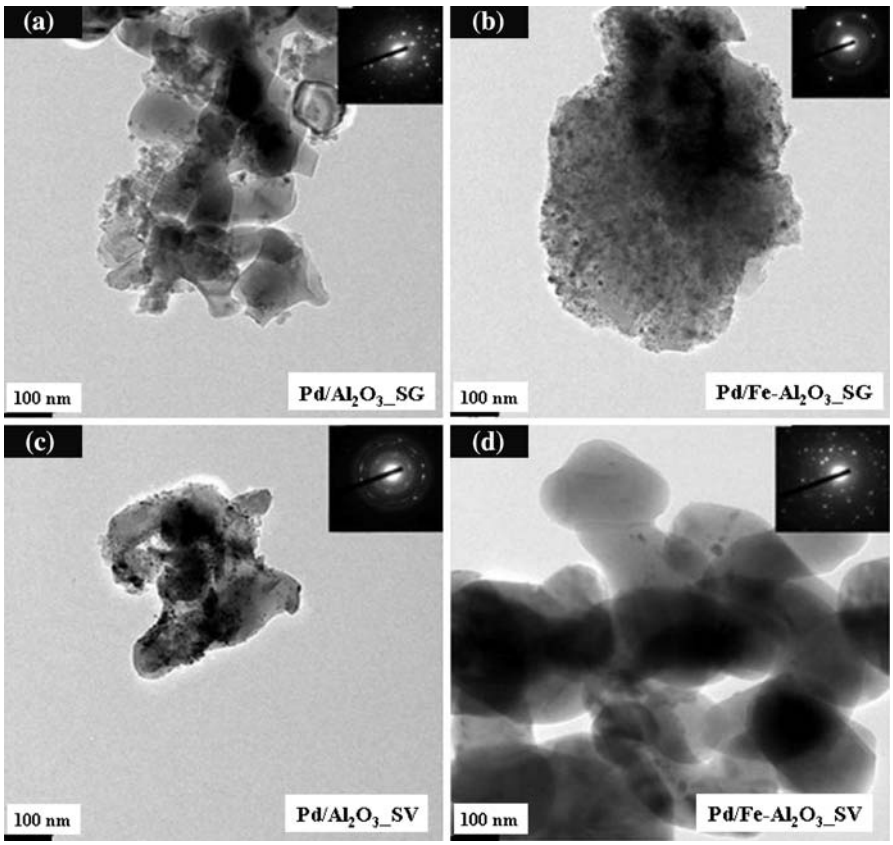

Fig. 2 TEM micrographs of $Pd/\alpha\text{-}Al_2O_3$ and Pd/Fe-modified $\alpha\text{-}Al_2O_3$ catalysts

probably due to high agglomeration of these nanocrystalline particles during calcination at high temperature. In a previous study, we have shown that sol–gel Al_2O_3 possessed much less pore volume than the samples prepared by the solvothermal method, as a consequence lower surface area was obtained [15].

Figure 2 shows the TEM micrographs with SAED patterns of Pd/α-Al_2O_3 and Pd/Fe-modified α-Al_2O_3 prepared by sol–gel and solvothermal methods. Palladium particles/clusters with average particle size ≤10 nm were found to be deposited on both of the alumina supports. The metal active sites, the Pd dispersion, and the average Pd metal particle sizes were also determined from CO chemisorption experiment and are summarized in Table 1. The technique is based on the assumption that only one CO molecule adsorbed on one metal active site and CO did not chemisorb on Al_2O_3 support [18]. It is clearly seen that when the catalysts were supported on Fe-modified α-Al_2O_3, Pd dispersion decreased. The larger crystallite size of α-Al_2O_3 resulted in larger Pd particle size being formed and lower Pd dispersion. Moreover, Pd catalyst supported on Fe-modified α-Al_2O_3 prepared by sol–gel method showed lower Pd dispersion than that prepared by solvothermal due probably to more agglomeration of the α-Al_2O_3 support as also noticed from TEM measurements.

NH_3 temperature program desorption is a commonly used technique for the titration of surface acid sites [19]. The strength of an acid site can be related to the corresponding desorption temperature, while the total amount of ammonia desorption after saturation coverage permits quantification of the number of acid sites at the surface. The temperature-programmed desorption profiles for the nanocrystalline α-Al_2O_3 and Fe-modified α-Al_2O_3 supports are shown in Fig. 3. It was found that modification of Al_2O_3 with small amounts of Fe considerably changed its acid properties, i.e., reduction in the number of strong acid sites [20].

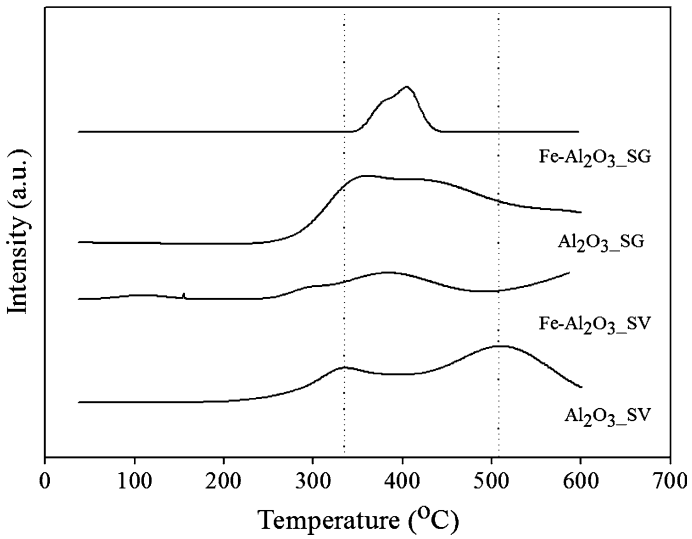

Fig. 3 NH_3 temperature program desorption profiles for α-Al_2O_3 and Fe-modified α-Al_2O_3 supports

The catalytic properties of Pd/α-Al_2O_3 and Pd/Fe-modified α-Al_2O_3 catalysts were evaluated in the selective hydrogenation of acetylene using a fixed bed flow reactor with a GHSV of 16,901 h^{-1}. A study of the temperature dependence of acetylene conversion and selectivity toward ethylene on Pd/α-Al_2O_3 and Pd/Fe-modified α-Al_2O_3 catalysts is shown in Fig. 4 in the temperature range between 40 and 100 °C. In all cases, acetylene conversion increases with increasing temperature while ethylene selectivity decreases due to the fact that the ethylene is produced as an intermediate in acetylene hydrogenation reaction. Ethylene selectivity at relatively high acetylene conversion (>80%) improved in the order: Pd/Fe-modified

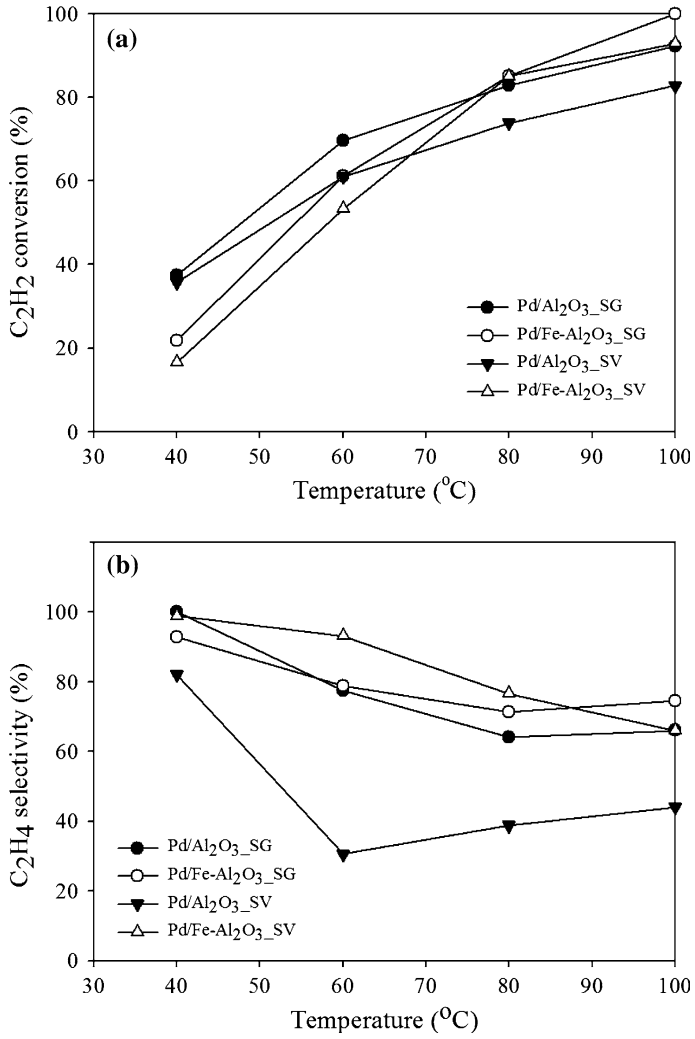

Fig. 4 Temperature dependence of the catalytic performance of Pd/α-Al_2O_3 and Pd/Fe-modified α-Al_2O_3 catalysts; **a** % conversion of C_2H_2, **b** % selectivity of C_2H_4

α-Al_2O_3-sol–gel > Pd/Fe-modified α-Al_2O_3-solvothermal ≈ Pd/α-Al_2O_3-sol–gel > Pd/α-Al_2O_3-solvothermal. It was also found that acetylene hydrogenation activity depended on Pd particle size in which the activity increased with increasing Pd particle size. A similar trend has been observed for supported Pd catalysts in other selective hydrogenation reactions [21–24].

After reaction, the amounts of carbonaceous deposits on the catalyst samples were measured by thermal gravimetric analysis and the results are shown in Fig. 5. The weight loss at around 200–400 °C was due to oxidation of the carbonaceous deposited on the surface of used catalysts [25]. As shown by the exothermic peaks in

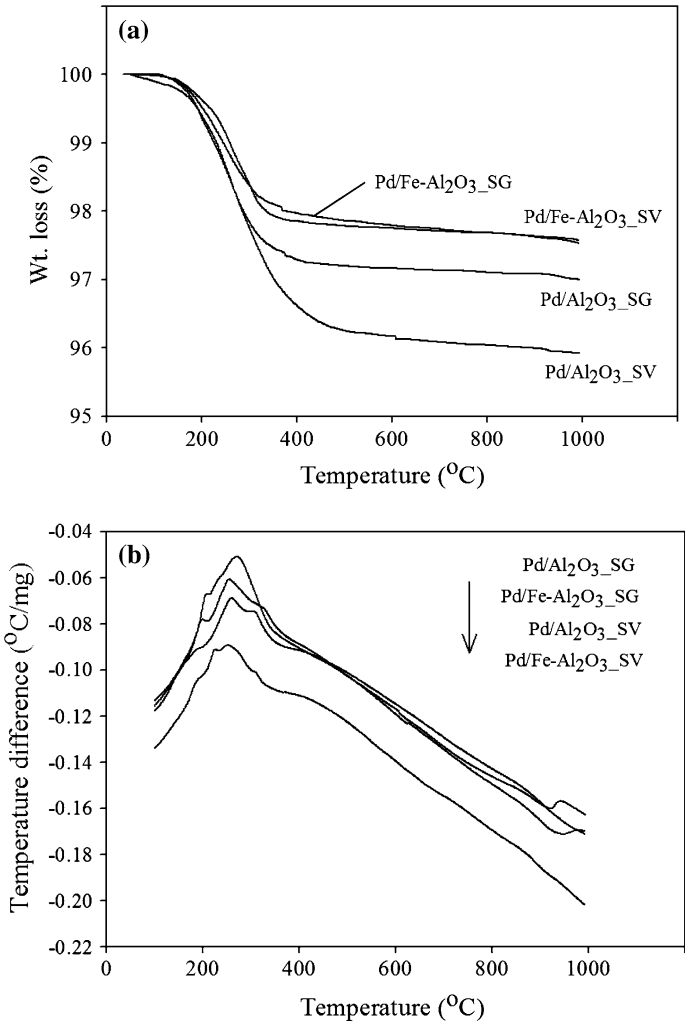

Fig. 5 Thermal gravimetric and differential temperature analysis (TG/DTA) of Pd/α-Al_2O_3 and Pd/Fe-modified α-Al_2O_3 catalysts after reaction; **a** in terms of temperature (°C) and weight loss (%), **b** in terms of temperature (°C) and temperature difference (°C/mg)

Fig. 5b, the type of coke species occurred during reaction was probably "soft coke" similar to those suggested by Xiangjing et al. [26]. Based on TGA results, the amount of coke deposits on the catalysts on Fe-modified α-Al_2O_3 prepared by sol–gel or solvothermal method was lower than those on the unmodified ones. The results were in good agreement with acidity of the Al_2O_3 supports measured from NH_3 TPD technique.

Acknowledgments The financial supports from the Thailand Research Fund (TRF) and the National Research Council of Thailand (NRCT) for the author J.P. are gratefully acknowledged.

References

1. Zhang, Q., Li, J., Liu, X., Zhu, Q.: Synergetic effect of Pd and Ag dispersed on Al_2O_3 in the selective hydrogenation of acetylene. Appl. Catal. A **197**, 221–228 (2000)
2. Jin, Y., Datye, A.K., Rightor, E., Gulotty, R., Waterman, W., Smith, M., Holbrook, M., Maj, J., Blackson, J.: The influence of catalyst restructuring on the selective hydrogenation of acetylene to ethylene. J. Catal. **203**, 292–306 (2001)
3. Shin, E.W., Choi, C.H., Chang, K.S., Na, Y.H., Moon, S.H.: Properties of Si-modified Pd catalyst for selective hydrogenation of acetylene. Catal. Today **44**, 137–143 (1998)
4. Park, Y.H., Price, G.L.: Promotional effects of potassium on palladium/alumina selective hydrogenation catalysts. Ind. Eng. Chem. Res. **31**, 469–474 (1992)
5. Sarkany, A., Horvath, A., Beck, A.: Hydrogenation of acetylene over low loaded Pd and Pd-Au/SiO_2 catalysts. Appl. Catal. A **229**, 117–125 (2002)
6. Jung, H.K., Eun, W.S., Woo, J.K., Jae, D.P., Sang, H.M.: Selective hydrogenation of acetylene on TiO_2-added Pd catalysts. J. Catal. **208**, 310–320 (2002)
7. Shi, C., Hoisington, R., Jang, B.W.-L.: Promotion effects of air and H_2 nonthermal plasmas on TiO_2 supported Pd and Pd-Ag catalysts for selective hydrogenation of acetylene. Ind. Eng. Chem. Res. **46**, 4390–4395 (2007)
8. Panpranot, J., Nakkararuang, L., Ngamsom, B., Praserthdam, P.: Promotion effects of air and H_2 nonthermal plasmas on TiO_2 supported Pd and Pd-Ag catalysts for selective hydrogenation of acetylene. Catal. Lett. **103**, 53–58 (2005)
9. Panpranot, J., Kontapakdee, K., Praserthdam, P.: Selective hydrogenation of acetylene in excess ethylene on micron-sized and nanocrystalline TiO_2 supported Pd catalysts. Appl. Catal. A **314**, 128–133 (2006)
10. Hong, J., Chu, W., Chen, M., Wang, X., Zhang, T.: Preparation of novel titania supported palladium catalysts for selective hydrogenation of acetylene to ethylene. Catal. Commun. **8**, 593–597 (2007)
11. Huang, W., McCormick, J.R., Lobo, R.F., Chen, J.G.: Selective hydrogenation of acetylene in the presence of ethylene on zeolite-supported bimetallic catalysts. J. Catal. **246**, 40–51 (2007)
12. Huang, W., Pyrz, W., Lobo, R.F., Chen, J.G.: Selective hydrogenation of acetylene in the presence of ethylene on K^+-β-zeolite supported Pd and PdAg catalysts. Appl. Catal. A **333**, 254–263 (2007)
13. Wongwaranon, N., Mekasuwandumrong, O., Praserthdam, P., Panpranot, J.: Performance of Pd catalysts supported on nanocrystalline α-Al_2O_3 and Ni-modified α-Al_2O_3 in selective hydrogenation of acetylene. Catal. Today **131**, 553–558 (2008)
14. Mekasuwandumrong, Wongwaranon, N., Panpranot, J., Praserthdam, P.: Preparation of novel titania supported palladium catalysts for selective hydrogenation of acetylene to ethylene. Mater. Chem. Phys. **111**, 431–437 (2008)
15. Chinayon, S., Mekasuwandumrong, O., Praserthdam, P., Panpranot, J.: Preparation of novel titania supported palladium catalysts for selective hydrogenation of acetylene to ethylene. Catal. Commun. **9**, 2297–2302 (2008)
16. Huang, Y.L., Xue, D.S., Zhou, P.H., Ma, Y., Li, F.S.: α-Fe-Al_2O_3 nanocomposites prepared by sol-gel method. Mater. Eng. A **359**, 332–337 (2003)
17. Ladavos, A.K., Bakas, T.V.: The Al_2O_3-Fe_2O_3 mixed oxidic system, I. Preparation and characterization. React. Kinet. Catal. Lett. **73**, 223–228 (2001)

18. Heinrichs, B., Delhez, P., Schoebrecht, J.-P., Pirard, J.-P.: Palladium-silver sol-gel catalysts for selective hydrodechlorination of 1,2-dichloroethane into ethylene. J. Catal. **172**, 322–335 (1997)
19. Kung, M.C., Kung, H.H.: IR studies of NH_3, pyridine, CO, and NO adsorbed on transition metal oxides. Catal. Rev. Sci. Eng. **27**, 425–460 (1985)
20. Kania, W., Jurczyk, K.: Acid-base properties of modified γ-alumina. Appl. Catal. **34**, 1–12 (1987)
21. Ryndin, Y.A., Stenin, M.V., Boronin, A.I., Bukhtiyarov, V.I., Zaikovskii, V.I.: Effect of Pd/C dispersion on its catalytic properties in acetylene and vinylacetylene hydrogenation. Appl. Catal. **54**, 277–288 (1989)
22. Dominguez-Dominguez, S., Berenguer-Murcia, A., Linares-Solano, A., Cazorla-Amoros, D.: Inorganic materials as supports for palladium nanoparticles: application in the semi-hydrogenation of phenylacetylene. J. Catal. **257**, 87–95 (2008)
23. Panpranot, J., Phandinthong, K., Sirikajorn, T., Arai, M., Praserthdam, P.: Impact of palladium silicide formation on the catalytic properties of Pd/SiO_2 catalysts in liquid-phase semihydrogenation of phenylacetylene. J. Mol. Catal. A **261**, 29–35 (2007)
24. Semagina, N., Renken, A., Kiwi-Minsker, L.: Palladium nanoparticle size effect in 1-hexyne selective hydrogenation. J. Phys. Chem. C **111**, 13933–13937 (2007)
25. Soares, R.W., Menezes, V.J., Fonseca, M.V.A., Dweck, J.: Characterization of carbonaceous products by TG and DTA. J. Therm. Anal. **49**, 657–661 (1997)
26. Xiangjing, Z., Yan, W., Feng, X.: Coke deposition and characterization on titanium silicalite-1 catalyst in cyclohexanone ammoximation. Appl. Catal. A **307**, 222–230 (2006)

Korean J. Chem. Eng., **24**(3), 397-402 (2007)

Synthesis of nanocrystalline alumina by thermal decomposition of aluminum isopropoxide in 1-butanol and their applications as cobalt catalyst support

Kamonchanok Pansanga, Okorn Mekasuwandumrong*, Joongjai Panpranot and Piyasan Praserthdam†

Center of Excellence on Catalysis and Catalytic Reaction Engineering, Department of Chemical Engineering, Faculty of Engineering, Chulalongkorn University, Bangkok 10330, Thailand
*Department of Chemical Engineering, Faculty of Engineering and Industrial Technology, Silpakorn University, Nakorn Pathom 73000, Thailand
(*Received 21 August 2006 • accepted 13 November 2006*)

Abstract−Nanocrystalline alumina powders were prepared by thermal decomposition of aluminum isopropoxide (AIP) in 1-butanol at 300 °C for 2 h and employed as cobalt catalyst supports. The crystallization of alumina was found to be influenced by the concentration of AIP in the solution. At low AIP content, wrinkled sheets-like structure of γ-Al_2O_3 was formed, while at high AIP concentrations, fine spherical particles of χ-Al_2O_3 were obtained. It was found that using these fine particles alumina as cobalt catalyst supports resulted in much higher amounts of cobalt active sites measured by H_2 chemisorption and higher CO hydrogenation activities.

Key words: Nanocrystalline Alumina, Thermal Decomposition, Cobalt Catalyst, Solvothermal Method, CO Hydrogenation

INTRODUCTION

Alumina powders are very interesting crystalline materials with broad applicability as adsorbents, coatings, soft abrasives, ceramic tools, fillers, wear-resistant ceramics, catalysts, and catalyst supports [1,2]. Because of their fine particle size, high surface area, high melting point (above 2,000 °C), high purity, good adsorbent, and high catalytic activity, they have been employed in a wide range of large-scale technological processes [3,4].

Various transition aluminas (α, γ, χ, δ, η and θ) have been prepared by different methods, such as sol-gel synthesis [5,6], hydrothermal synthesis [7], microwave synthesis [8], emulsion evaporation [9], plasma technique [10], and solvothermal synthesis [11-18]. Among these methods, solvothermal synthesis attracts the most attention because it gives the products with small uniform morphology, well-controlled chemical composition, and narrow size distribution. Furthermore, the desired shape and size of particles can be produced by controlling process conditions such as solute concentration, reaction temperature, reaction time, and the type of solvent [19,20]. For example, Berntsen et al. [21] described a simple route to high surface area nanostructured MoS_2 based on the decomposition of cluster-based precursor $(NH_4)_2Mo_3S_{13}\cdot xH_2O$ in toluene at 380 °C. It was found that solvothermal decomposition resulted in nanostructured material distinct from that obtained by decomposition of the precursor in sealed quartz tubes at the same temperature. Wang et al. [22] prepared nanocrystalline titania in alcohols under solvothermal conditions at 100 °C for 24 h. The selection of crystal structures, grain sizes, and morphologies was achieved by simply varying the alcohols and other reaction conditions.

Alumina prepared by the solvothermal method is considered high thermal stability. In our recent works [23-26], nanocrystalline transition alumina with micro spherical particles and high thermal stability has been synthesized by decomposition of aluminum isopropoxide (AIP) under solvothermal conditions. The mechanism of the process involves the formation of amorphous complexes before further decomposition takes place. Inoue et al. [27] prepared silica-modified alumina by the reaction of AIP and tetraethyl orthosilicate (TEOS) in 1,4-butanediol at 300 °C. The products were found to maintain large surface areas after calcination at high temperature.

In this study, the influence of concentration of aluminum isopropoxide in 1-butanol used in the preparation of nanocrystalline alumina by solvothermal method on the properties of alumina powders and alumina supported cobalt catalysts was investigated by using various characterization techniques such as XRD, BET analysis, TEM, SEM, EDX, H_2 chemisorption, and temperature-programmed reduction. The catalytic activity of the catalysts was tested in carbon monoxide hydrogenation at 220 °C and atmospheric pressure.

EXPERIMENTAL

1. Catalyst Preparation

1-1. Preparation of Nanocrystalline Al_2O_3

A selected amount of aluminum isopropoxide (Aldrich) (10-35 g) was suspended in 100 ml of 1-butanol (Ajax Finechem) in a test tube, which was then placed in a 300 ml autoclave. In the gap between the test tube and the autoclave wall, 30 ml of 1-butanol was added. The atmosphere inside the autoclave was purged completely with nitrogen. The mixture was heated to 300 °C at a heating rate of 2.5 °C/min and was kept at that temperature for 2 h. After cooling to room temperature, the resulting powders were collected after repeated washing with acetone by centrifugation. They were then air-dried. The calcination of the products was carried out in a box furnace by heating up to 600 °C at a rate of 10 °C/min and held at that temperature for 1 h.

1-2. Preparation of Al_2O_3-Supported Co Catalysts

The Co/Al_2O_3 catalysts were prepared by incipient wetness impregnation of Al_2O_3 with a desired amount of an aqueous solution

†To whom correspondence should be addressed.
E-mail: piyasan.p@chula.ac.th

of cobalt nitrate [$Co(NO_3)_2 \cdot 6H_2O$] (Aldrich). The final loading of the catalysts was determined by atomic absorption spectroscopy (Varian Spectra A800) to be ca. 10 wt% cobalt. The catalysts were dried at 110 °C for 24 h and calcined in air at 300 °C for 2 h using a ramp rate of 1 °C/min.

2. Catalyst Nomenclature

In this study, alumina and alumina-supported cobalt catalysts are referred to as Al-x and Co/Al-x, where x is the amount (g) of AIP used in the preparation of alumina powders. For example, Al-10 and Co/Al-10 refer to Al_2O_3 and Co/Al_2O_3 catalyst prepared with 10 g AIP.

3. Catalyst Characterization

XRD patterns of the samples were collected with a SIEMENS D-5000 X-ray diffractometer with Cu K_α radiation (λ=1.54439 Å). The spectra were scanned at a rate of 0.04°/step from 2θ=15° to 80°. BET surface areas were calculated by using the BET-single point method at liquid N_2 temperature. Transmission electron microscopy (TEM) was performed with a JEOL JEM1220. SEM and EDX were performed with a JEOL JSM-35CF scanning electron microscope in the back scattering electron (BSE) mode at 20 kV. EDX was performed by using Link Isis 300 software. Static H_2 chemisorption was carried out on the reduced cobalt catalyst samples at 100 °C according to the method described by Reuel and Bartholomew [28] by using a Micromeritics Pulse Chemisorb 2700 system. Prior to H_2 chemisorption, the catalyst samples were reduced at 350 °C in flowing H_2 for 3 h. Temperature-programmed reduction (TPR) was performed by using an in-house system. Approximately 0.1 g of the catalyst was placed in the middle of a stainless steel reactor. A temperature ramp from 35 to 600 °C at a ramp rate 5 °C/min and the reduction gas 5% H_2 in Ar were used. A thermal conductivity detector (TCD) was used to determine the amount of hydrogen consumed. A cold trap was placed before the detector to remove water produced during the reduction. The hydrogen consumption was calibrated by using TPR of silver oxide (Ag_2O) at the same conditions.

4. Reaction

CO hydrogenation was carried out in a fixed-bed quartz reactor under differential reaction conditions (<10% conversion) at 220 °C, 1 atm total pressure, and H_2/CO=10/1. The total flow rate of H_2/CO/Ar was 80/8/32 cc/min. Typically, 0.1 g of the catalyst sample was reduced *in situ* in flowing H_2 (50 cc/min) at 350 °C for 3 h prior to CO hydrogenation. After the startup, samples were taken in 1-h interval and analyzed by gas chromatography. Steady state was reached within 6 h in all cases.

RESULTS AND DISCUSSION

1. Effect of AIP Concentration on the Properties of Al_2O_3

Fig. 1 shows the XRD patterns of various alumina powders obtained from thermal decomposition of AIP in 1-butanol after calcination at 600 °C for 1 h. XRD patterns of Al_2O_3 show strong diffraction peaks at 31°, 33°, 38°, 43°, 47.5°, and 68° (according to the JCPDSs database). It was found that when lower amounts of AIP were used, only γ-alumina was formed as seen by the XRD characteristic peaks at 2θ=33° according to the JCPDSs database. The XRD characteristic peaks of χ-alumina were observed at 2θ=42.5° for the ones prepared with AIP 25 and 35 g. The intensity of χ-alumina peaks became stronger with increasing amount of AIP content. It is indicated that increasing AIP content during the synthesis resulted in formation of mixed phase between γ-alumina and χ-alumina. The crystallization process of alumina was probably affected by the amounts of AIP in 1-butanol.

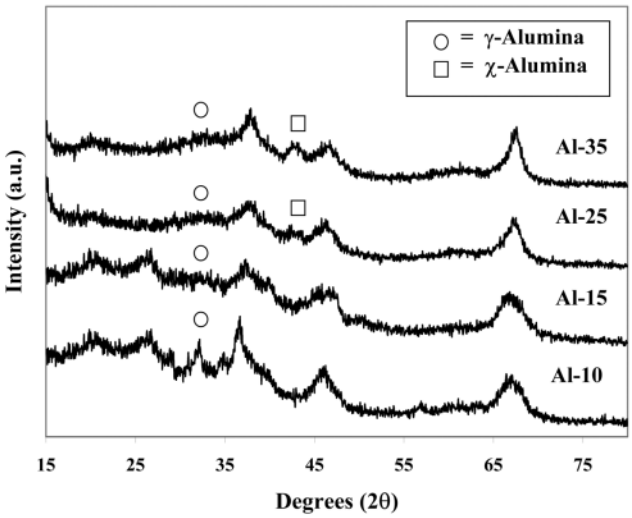

Fig. 1. XRD patterns of various nanocrystalline alumina prepared by the reaction of AIP in 1-butanol at 300 °C for 2 h (after calcinations at 600 °C for 1 h).

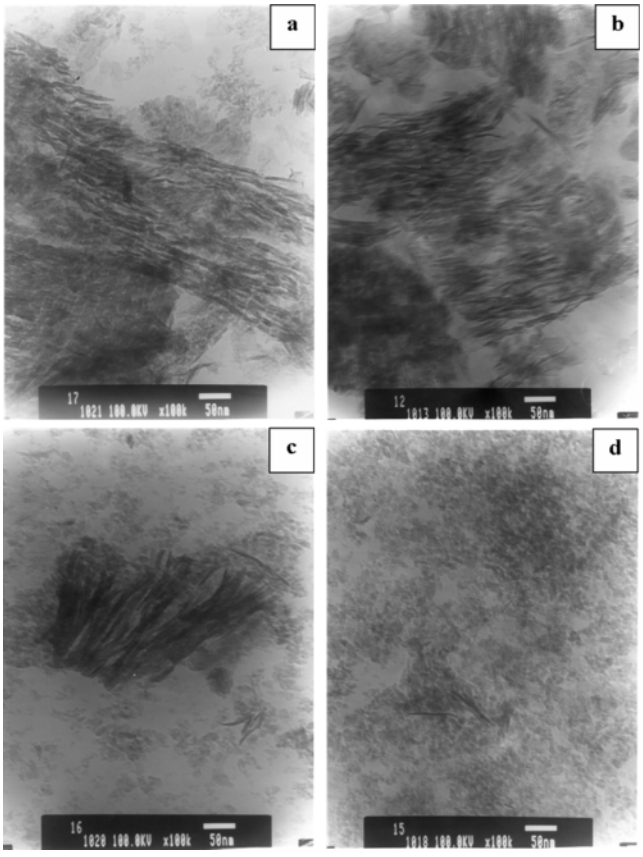

Fig. 2. TEM images of alumina obtained by the reaction of AIP in 1-butanol at 300 °C for 2 h with different amounts of AIP (a) Al-10 (b) Al-15 (c) Al-25 (d) Al-35.

Table 1. The physical and chemical properties of Al_2O_3 supports

Samples	Amounts of AIP (g)	Surface area (m^2/g)[a]	Bulk density (g/cm^3)[a]	Morphology
Al-10	10	70	0.3824	Wrinkled sheets
Al-15	15	120	0.3858	High amount of wrinkled sheets
Al-25	25	139	0.3928	Wrinkled sheets and small amount of spherical particles
Al-35	35	145	0.5358	Small amount of wrinkled sheets and high amount of spherical particles

[a]Error of measurement=±5%

TEM images of alumina powders prepared with different amounts of AIP are shown in Fig. 2. For the ones prepared with lower amounts of AIP, Al-10 and Al-15, the wrinkled sheets morphology was observed. They were found to be similar to those obtained from the formation of γ-alumina by decomposition of glycol or alkyl derivatives on boehmite [26,27]. As the amounts of AIP increased, the wrinkled sheets morphology became less apparent and spherical particles were observed. The presence of spherical particles was probably due to the formation of χ-alumina, which is normally formed by thermal decomposition reaction of AIP in inert organic solvents at 300 °C [23-26]. TEM results were in good agreement with the XRD patterns that a mixture of γ-alumina and χ-alumina was observed when AIP concentration increased.

The physical properties of the alumina products are summarized in Table 1. The BET surface areas increased with increasing AIP concentration as a result of morphology changing from wrinkled sheets structure to small spherical particles. BET surface area of the Al-35 (145 m^2/g) was found to be twice of that of Al-10 (70 m^2/g). Similar trend was observed for the bulk density of the alumina powders. The bulk density increased with increasing AIP contents.

Mechanism of thermal decomposition of AIP in alcohol has been proposed in our previous works [23,26] involving three competitive reactions. First, AIP reacted with 1-butanol yielding aluminum butoxide, which decomposed further to give the alkyl (butyl) derivative of boehmite. Second, 1-butanol can be dehydrated to give water which then hydrolyzes aluminum isopropoxide or butoxide yielding pseudoboehmite. Finally, the direct decomposition of aluminum alkoxide in organic solvent, which proceeded slowest, gave χ-alumina. In the present work, at low AIP content, boehmite was probably the main product and γ-alumina was obtained after calcination at 600 °C for 1 h. The morphology of the boehmite products obtained via solvothermal reaction was wrinkled sheets [23,26], which was also similar to those of γ-alumina decomposed from. However, when the amounts of AIP in 1-butanol increased, formation of χ-alumina from direct decomposition of AIP in the solvent occurred as the main reaction.

2. Characteristics of Co/Al_2O_3 Catalysts

The XRD patterns of cobalt catalysts supported on alumina prepared with various amounts of AIP are shown in Fig. 3. The XRD patterns of the Co/Al_2O_3 catalysts were not significantly different from those of alumina supports. No XRD peaks of Co_3O_4 or other Co compounds were detected. This indicates that cobalt was present in a highly dispersed form on alumina even for cobalt loading as high as 10 wt% [29].

SEM and EDX were performed in order to study the morphology and elemental distribution of the catalyst samples, respectively. Typical SEM micrographs of Co/Al_2O_3 catalysts are shown in Fig. 4. There was no significant change in morphology of the catalyst samples due to the effect of AIP concentrations in 1-butanol used in the preparation process. The white or light spots observed in all figures can be attributed to the cobalt patches distributed on the external surface of catalyst granules. Fig. 5 shows the SEM micrographs and the EDX mapping of the cross-sectioned Co/Al-35 catalyst granule. The distribution of cobalt was found to be well dispersed throughout the catalyst granule.

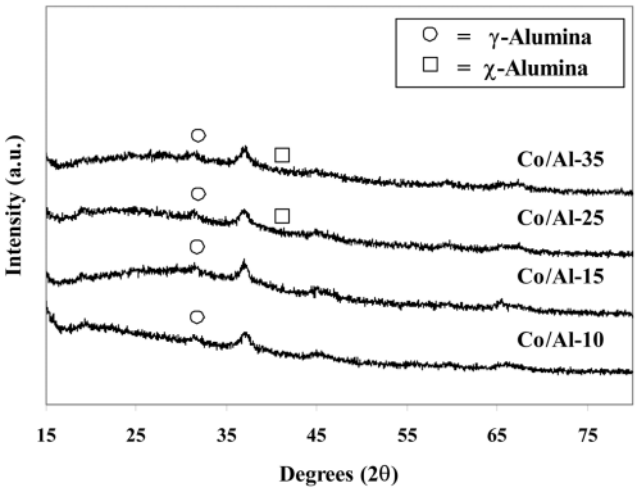

Fig. 3. XRD patterns of Co/Al_2O_3 catalysts with different amounts of AIP.

The relative amounts of active surface cobalt on the catalyst samples were calculated from H_2 chemisorption experiments at 100 °C according to Reuel and Bartholomew [28]. It is known that only surface cobalt metal atoms are active for CO hydrogenation, not its oxide or carbide [30]. The H_2 chemisorption results are reported in Table 2. The amounts of H_2 chemisorption increased from 0.90 to 20.65 μmol/g cat., with increasing amount of AIP in 1-butanol used in the preparation of the alumina supports from 10 to 35 g. It is likely that the increase in the relative amounts of active cobalt metals was due to the formation of the small spherical particles of χ-alumina. As also seen in the Table 2, the amount of H_2 chemisorption of Co/Com-Al (13.38 μmol/g cat.), prepared from the commercial γ-alumina which the crystal shape of alumina was spherical (the results was not shown), was better than solvothermal-made Co/γ-alumina (0.90 μmol/g cat.) but lower than Co/χ-alumina (20.65 μmol/g cat.).

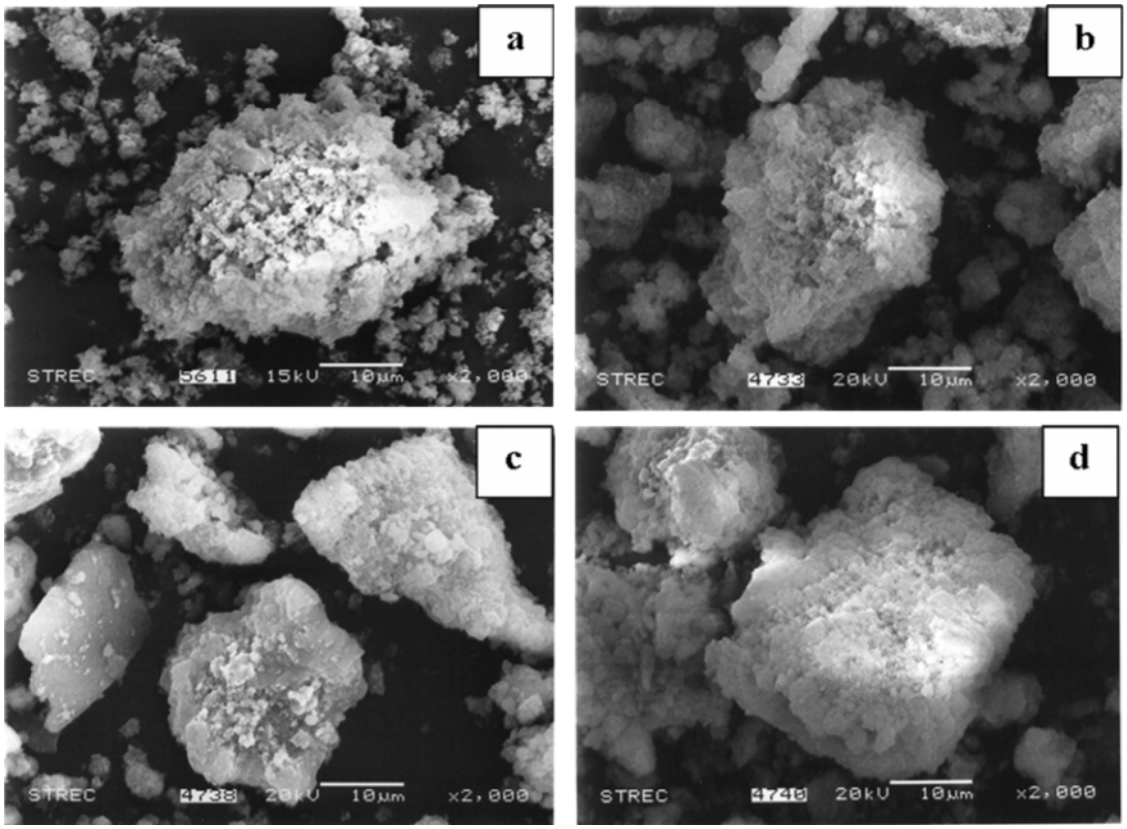

Fig. 4. SEM micrographs of (a) Co/Al-10, (b) Co/Al-15, (c) Co/Al-25, and (d) Co/Al-35.

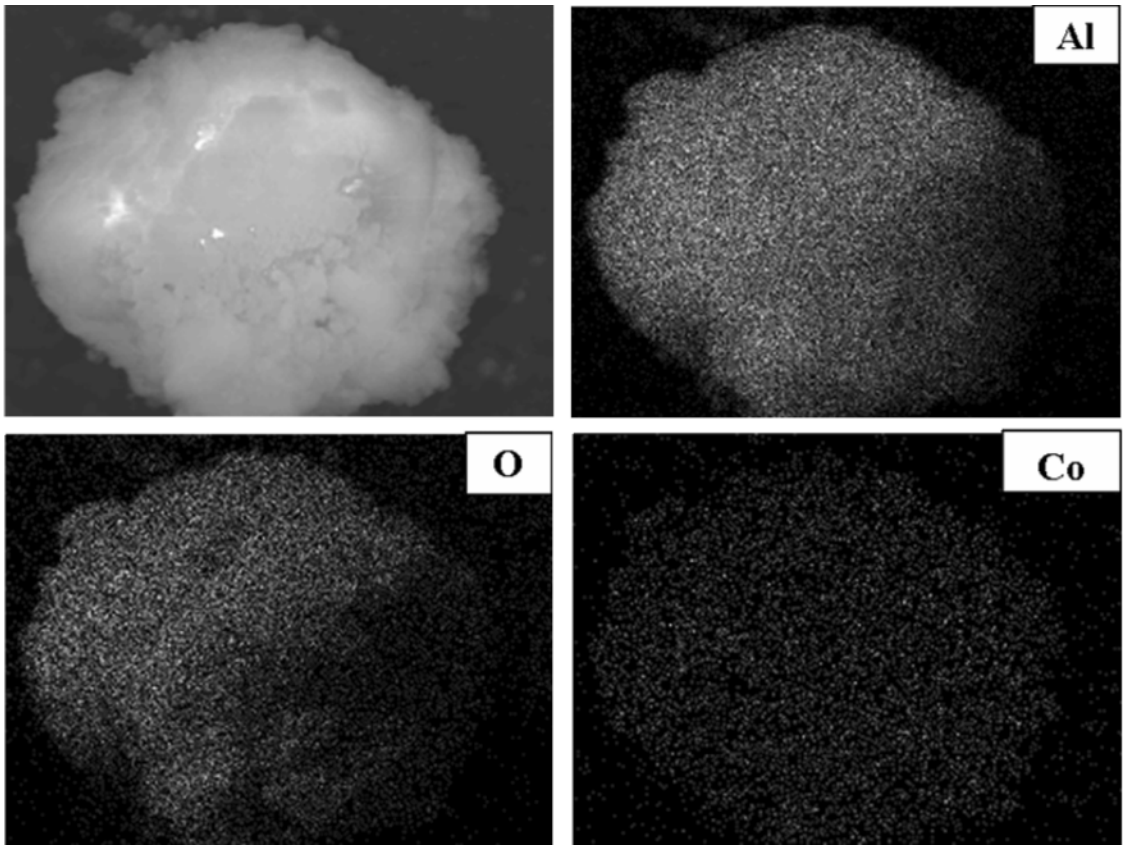

Fig. 5. SEM micrograph and EDX mapping of cross-sectioned Co/Al-35 catalyst granule.

It was again confirmed that the spherical morphology of the alumina support is important in achieving a higher amount of active cobalt metal.

3. Reduction and Catalytic Behaviors of Co/Al_2O_3 Catalysts

Temperature program reduction (TPR) is a powerful tool for studying the reduction behavior of the catalysts. The TPR profiles of various nanocrystalline alumina supported cobalt catalysts are shown in Fig. 6. All the catalyst samples exhibited two main reduction peaks which could be assigned to the two-step reduction of Co_3O_4: first reduction of Co_3O_4 to CoO and then the subsequent reduction of CoO to Co^0 [31]. The two reduction steps may not always be observed as separate peaks in TPR profile [32], as seen in the Co/Al-35 sample. A wide range of variables such as metal particle size and metal-support interaction have an influence on the reduction behavior of cobalt catalysts resulting in the observation of different locations of the TPR peaks. The TPR profiles for all the catalysts except Co/Al-35 appeared to be not significantly different, suggesting that the AIP content had little impact on the interaction of cobalt and alumina supports. Thus, high dispersion of cobalt obtained on Co/Al-35 was rather to be due to the formation of small spherical particles alumina and not to the change in reducibility of the catalysts.

Table 2. The characteristics and H_2 chemisorption of cobalt catalyst

Catalyst samples	Surface area (m^2/g)[a]	Amount of H_2 chemisorption ($\mu mol/g$ cat.)[a]
Co/Al-10	61	0.90
Co/Al-15	87	2.29
Co/Al-25	108	7.58
Co/Al-35	114	20.65
Co/Com-Al*	145	13.38

[a]Error=±5%, as determined directly.
*Commercial γ-alumina, BET surface area of alumina 230 m^2/g.

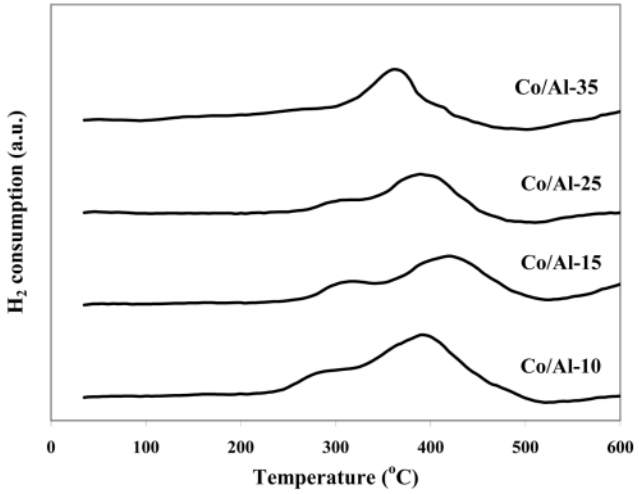

Fig. 6. TPR profiles of the catalyst samples.

CO hydrogenation reaction was carried out as a test reaction to determine the catalytic activity of the catalyst samples. The results are shown in Table 3. It is clearly seen that alumina prepared with higher amounts of AIP in 1-butanol resulted in much higher CO hydrogenation activities and CH_4 selectivities. The reaction results confirm the amount of surface cobalt metals measured by H_2 chemisorption.

CONCLUSIONS

Nanocrystalline alumina powders were prepared by thermal decomposition of AIP in 1-butanol with various AIP contents. The concentration of AIP in 1-butanol had a significant impact on the properties of alumina and alumina supported cobalt catalysts. Increasing amounts of AIP in the solution resulted in the transformation of wrinkled sheet γ-alumina to fine spherical particles of χ-alumina. It also gave rise to the cobalt active sites and CO hydrogenation activities when employed as supports for preparation of Co/Al_2O_3 catalysts.

ACKNOWLEDGMENTS

The authors would like to thank the Thailand Research Fund (TRF) for the financial support of this project.

REFERENCES

1. J. S. Church, N. W. Cant and D. L. Trimm, *Appl. Catal. A*, **101**(1), 105 (1993).
2. G. Pajonk and S. Teichner, *Aerogels*, Spinger, Berlin (1986).
3. C. Misra, *Industrial alumina chemicals*, ACS Monograph 184, Washington (1986).

Table 3. Reaction rate and selectivity for CO hydrogenation on catalyst samples

Catalyst samples	CO conversion (%)[a]		Rate ($\times 10^2$ gCH_2 $gcat^{-1}h^{-1}$)[b]		CH_4 selectivity (%)	
	Initial[c]	SS[d]	Initial	SS	Initial	SS
Co/Al-10	1.92	0.54	5.76	1.62	13	11
Co/Al-15	2.63	0.75	7.89	2.25	49	47
Co/Al-25	5.45	3.02	16.35	9.06	56	54
Co/Al-35	8.49	4.03	25.47	12.09	70	67

[a]CO hydrogenation was carried out at 220 °C, 1 atm, and H_2/CO/Ar=80/8/32.
[b]Error±5%, as determined directly.
[c]After 20 min of reaction.
[d]After 6 h of reaction.

4. H. Topsoe, B. S. Clausen and F. E. Massoth, *Hydrotreating catalysis*, Springer, Berlin (1996).
5. C. J. Brinker and G. W. Scherrer, *Sol-gel science*, Academic Press, San Diego (1990).
6. K.-C. Song, K.-J. Woo and Y. Kang, *Korean J. Chem. Eng.*, **16**, 75 (1999).
7. W. H. Dawson, *Am. Ceram. Soc. Bull.*, **67**, 1673 (1988).
8 S. G. Deng and Y. S. Lin, *Sci. Lett.*, **16**, 1291 (1997).
9. Y. Sarikaya, I. Sevinc and M. Akinc, *Powder Technol.*, **116**(1), 109 (2001).
10. S.-M. Oh and D.-W. Park, *Korean J. Chem. Eng.*, **17**, 299 (2000).
11. M. Inoue, H. Kominami and T. Inui, *J. Am. Ceram. Soc.*, **73**, 1100 (1990).
12. M. Inoue, H. Kominami and T. Inui, *J. Chem. Soc. Dalton Trans.*, 3331 (1991).
13. M. Inoue, H. Kominami and T. Inui, T. *J. Am. Ceram. Soc.*, **75**, 2597 (1992).
14. M. Inoue, H. Kominami and T. Inui, *Appl. Catal. A*, **97**, L25 (1993).
15. M. Inoue, H. Kominami and T. Inui, *Appl. Catal. A*, **121**, L1 (1995).
16. M. Inoue, H. Kominami and T. Inui, *J. Am. Ceram. Soc.*, **75**, 2597 (1996a).
17. M. Inoue, Y. Kondo and T. Inui, *Inorg. Chem.*, **27**, 215 (1988).
18. M. Inoue, H. Otsu, H. Kominami and T. Inui, *Ind. Eng. Chem. Res.*, **35**, 295 (1996b).
19. Y. Deng, G-D. Wei and C.-W. Nan, *Chem. Phys. Lett.*, **368**(5-6), 639 (2003).
20. Y. Deng, X.-S. Zhou, G-D. Wei, J. Liu, C.-W. Nan and S.-J. Zhao, *J. Phys. Chem. Solids*, **63**(11), 2119 (2002).
21. N. Berntsen, T. Gutjahr, L. Loeffler, J. R. Gomm, R. Seshadri and W. Tremel, *Chem. Mater.*, **15**(23), 4498 (2003).
22. C. Wang, Z.-X. Deng, G. Zhang, S. Fan and Y. Li, *Powder Technol.*, **125**(1), 39 (2002.
23. O. Mekasuwandumrong, H. Kominami, P. Praserthdam and M. Inoue, *J. Am. Ceram. Soc.*, **87**(8), 1543 (2004a).
24. O. Mekasuwandumrong, P. Praserthdam, M. Inoue, V. Pavarajarn and W. Tanakulrungsank, *J. Mater. Sci.*, **39**, 2417 (2004b).
25. O. Mekasuwandumrong, P. L. Silveston, P. Praserthdam, M. Inoue, V. Pavarajarn and W. Tanakulrungsank, *Inorg. Chem. Commu.*, **6**(7), 930 (2003).
26. P. Praserthdam, M. Inoue, O. Mekasuvandumrong, W. Tanakulrungsank and S. Phatanasri, *Inorg. Chem. Commu.*, **3**(11), 671 (2000).
27. M. Inoue, H. Otsu, H. Kominami and T. Inui, *Ind. Eng. Chem. Res.*, **35**, 295 (1996c).
28. R. C. Reuel and C. H. Bartholomew, *J. Catal.*, **85**, 63 (1984).
29. B. Jongsomjit, J. Panpranot and J. G. Goodwin Jr., *J. Catal.*, **215**(1), 66 (2003).
30. R. B. Anderson, *The Fischer-Tropsch synthesis*, Academic Press, San Diego (1984).
31. Y. Zhang, D. Wei, S. Hammache and J. G. Goodwin Jr., *J. Catal.*, **188**(2), 281 (1999).
32. B. Ernst, S. Libs, P. Chaumette and A. Kiennemann, *Appl. Catal. A*, **186**(1-2), 145 (1999).

Available online at www.sciencedirect.com
ScienceDirect
Applied Catalysis A: General 332 (2007) 130–137
APPLIED CATALYSIS A: GENERAL
www.elsevier.com/locate/apcata

Copper-modified alumina as a support for iron Fischer–Tropsch synthesis catalysts

Kamonchanok Pansanga [a], Nattaporn Lohitharn [b], Andrew C.Y. Chien [b], Edgar Lotero [b], Joongjai Panpranot [a], Piyasan Praserthdam [a], James G. Goodwin Jr. [b,*]

[a] *Center of Excellence on Catalysis and Catalytic Reaction Engineering, Department of Chemical Engineering, Faculty of Engineering, Chulalongkorn University, Bangkok 10330, Thailand*

[b] *Department of Chemical and Biomolecular Engineering, Clemson University, Clemson, SC 29634, USA*

Received 2 May 2007; received in revised form 31 July 2007; accepted 4 August 2007
Available online 9 August 2007

Abstract

In the present study, the effect of Cu-modified Al_2O_3 on the properties of Al_2O_3-supported Fe catalysts in the Fischer–Tropsch synthesis was investigated. Ten weight percent Cu was first impregnated into γ-alumina to produce Cu-modified Al_2O_3 supports; then 20 wt.% of Fe and (in some cases) 1 wt.% Cu were added to the supports by the sequential impregnation method. Two different pretreatment methods (drying or drying and calcining) were employed after each metal impregnation. It was found that the use of Cu-modified Al_2O_3 supports increased significantly the overall activity of the Fe/Al_2O_3 catalysts. Addition of 1% Cu as a reduction promoter to the Cu-modified supported Fe catalysts was not necessary since it did not further enhance the activity of the catalysts. There were no changes in FT product selectivity, chain growth probability (α), or olefin selectivity due to any effect of the Cu-modified Al_2O_3 or Cu-promotion. However, the more calcination steps used during preparation, the higher the catalyst activity obtained. Cu-modification of the alumina most probably diminished the interaction/reaction of the Fe with the support, thereby improving its chemisorption and catalytic properties.

Keywords: Iron catalysts; Alumina-supported catalysts; Copper modification; Fischer–Tropsch synthesis

1. Introduction

Due to depletion of oil reserves and increased cost of petroleum, alternative methods for synthesizing hydrocarbon fuels such as the Fischer–Tropsch synthesis (FTS) have again received considerable attention. FTS is an important technology in the production of liquid fuels and chemicals from syngas derived from coal, natural gas, or other carbon-containing materials. Several metal catalysts can be used for the FTS, however, only iron and cobalt catalysts appear to be economically feasible on an industrial scale [1]. Co catalysts yield mainly straight-chain hydrocarbons [2–4] while Fe catalysts are more useful when the H_2/CO ratio is low (because of the water–gas-shift activity of Fe) or for the production of alkenes, oxygenates, and branched hydrocarbons, which depends on the promoters and process conditions employed [2,5]. Many inorganic oxides such as Al_2O_3 [6–9], SiO_2 [10], TiO_2 [7,11] and ZrO_2 [7,12] have been studied as supports for Fe catalysts. However, Fe can easily react with the supports to form compounds [10,12,13] and is often difficult to reduce when highly dispersed on refractory oxides. For example, Zhang et al. [10] investigated the iron–silica interaction of a silica-supported iron FTS catalyst and found that nanoparticles of iron oxide mixtures existed in the as-prepared catalyst while wüstite and iron silicate were the main phases after reduction. The formation of these nanoparticles and the presence of metastable phases resulted in lower FTS activity and production of more gaseous hydrocarbons. Thus, the use of supported Fe catalysts has been limited and bulk Fe catalysts usually show superior properties [2,14,15].

Development of highly active supported Fe catalysts, however, would be useful since it could reduce catalyst density and make catalyst application in fluidized/slurry reactors easier. Most of the studies reported have attempted to improve catalyst

* Corresponding author. Fax: +1 864 656 0784.
E-mail address: james.goodwin@ces.clemson.edu (J.G. Goodwin Jr.).

0926-860X/$ – see front matter © 2007 Elsevier B.V. All rights reserved.
doi:10.1016/j.apcata.2007.08.006

performance by promoting with additives such as K [11,16,17], Mn [11,18], Cr [11], Ru [19], and Pd [16–20]. Cu is usually present in bulk Fe catalysts as a reduction promoter [19,21–23]. It facilitates reduction of iron oxide to metallic iron during hydrogen activation by lowering the reduction temperature which, in turn, reduces sintering of the metallic iron that is formed [24]. However, to the best of our knowledge, the effect of Cu to modify the metal oxide support for supported iron catalyst in FTS has never been reported. Cu is more interesting than many other transition metals since it does not alloy with Fe. This means there is less chance that desired Fe catalytic properties would be altered.

The purpose of this study was to investigate the effect of Cu-modified Al_2O_3 on the properties of Al_2O_3-supported Fe catalysts. A series of Cu-modified alumina supported Fe catalysts were prepared by the sequential impregnation method followed by different pretreatments (either drying or drying and calcining). The catalysts were then characterized by N_2 physisorption, CO chemisorption, X-ray diffraction, scanning electron microscopy, and FTS.

2. Experimental

2.1. Catalyst preparation

For preparation of the reference 1% Cu on Fe/Al_2O_3 catalyst, a solution of iron(III) nitrate nonahydrate (Alfa Aesar) was first impregnated into the γ-Al_2O_3 support (Johnson Matthey, specific surface area of 100 m^2/g) using the incipient wetness method to give a final catalyst composition of ca. 20 wt.% Fe. The impregnated catalyst was dried at 110 °C for 24 h followed by calcination in air at 350 °C for 3 h. Then, 1 wt.% Cu was impregnated into the sample using a solution of copper(II) nitrate trihydrate (Acros Organics) and incipient wetness (IW). The catalyst was dried at 110 °C for 24 h and then calcined again in air at 460 °C for 3 h.

The 10% Cu-modified Al_2O_3 supports were prepared by the incipient wetness impregnation of the γ-Al_2O_3 with a solution of copper(II) nitrate trihydrate. The samples were dried at 110 °C for 24 h and then calcined (in some cases) in air with ramping of the temperature at 10 °C/min up to 300 °C and holding for 1 h. The temperature was thereafter increased by 10 °C/min up to 500 °C and held for 6 h. Then a solution of iron(III) nitrate nonahydrate was used to impregnate (by IW) the Cu-modified Al_2O_3 supports to produce 20 wt.% Fe catalysts followed by drying and where indicated calcining at 350 °C. A solution of copper(II) nitrate trihydrate was finally impregnated (by IW) where indicated to produce 1 wt.% Cu, followed by drying and in some cases calcining at 460 °C.

2.2. Catalyst nomenclature

The catalyst nomenclature, the compositions, and the preparation conditions of the various Al_2O_3 supported Fe catalysts are given in Table 1. The Fe catalysts prepared basically had three metal components in addition to the Al_2O_3 support. The base catalyst was 1% Cu promoted 20% Fe/Al_2O_3. All the other catalysts were prepared on 10% Cu-modified Al_2O_3 supports. The catalysts were either dried (D) or dried and calcined (C) after each metal loading step. The nomenclature used for these catalysts consists of five components. For examples, the base catalyst is referred to as ''1-0-*CC'', where the first number ''1'' referred to 1% Cu promoted 20% Fe/Al_2O_3 and the second number ''0'' referred to 0% Cu added to the Al_2O_3 support. The symbol and the letters ''*CC'' indicate the pretreatment used in each metal loading step. The asterisk (*) means that there was no pretreatment for the first stage since no Cu was added to the Al_2O_3 support in this sample but the catalysts were dried and calcined after Fe and Cu loadings. The catalyst designated ''1-10-DDC'' indicates that it was 1% Cu promoted 20% Fe catalyst on 10% Cu-modified Al_2O_3 support. The Cu-modified Al_2O_3 support was dried only (designated by the first D) but not calcined prior to Fe impregnation. The 20% Fe on 10% Cu-modified Al_2O_3 was then dried again (designated by the second D) but not calcined prior to the addition of 1% Cu. After the final impregnation step, the catalyst was then dried and calcined (designated by the third C).

2.3. Reaction

Steady-state FTS reaction rates and selectivities were measured in a stainless steel fixed-bed reactor under differential

Table 1
Catalyst nomenclatures and the preparation conditions

Catalyst	Metal loading (wt.%)			Pretreatment after each metal impregnation		
	Cu	Fe	Cu on Al_2O_3	1st (10% Cu on Al_2O_3)	2nd (20% Fe)	3rd (1% Cu)
1-0-*CC[a]	1	20	0	None	C	C[b]
1-10-CCC	1	20	10	C	C	C
1-10-CDC	1	20	10	C	D[c]	C
1-10-DDC	1	20	10	D	D	C
1-10-DDD	1	20	10	D	D	D
0-10-CC*	0	20	10	C	C	None
0-10-CD*	0	20	10	C	D	None
0-10-DC*	0	20	10	D	C	None

[a] 1% Cu-promoted 20% Fe/Al_2O_3 is the reference catalyst.
[b] C: dried in air at 110 °C for 24 h followed by calcination in air at desired temperature and holding time for each metal.
[c] D: dried in air at 110 °C for 24 h.

reaction conditions at 280 °C and 1.8 atm total pressure. The H_2/CO ratio used was 2/1. Typically, 0.1 g of the catalyst sample was pretreated *in situ* in flowing H_2 (50 ml/min) at 460 °C for 16 h prior to reaction. After pretreatment the reaction mixture containing 5 ml/min of CO, 10 ml/min of H_2, and 45 ml/min of He was then introduced into the reactor at 280 °C. The system pressure used was 1.8 atm. Product samples were taken at 1.5-h intervals and analyzed by gas chromatography. Analysis of hydrocarbons was carried out with a AT-Q 30 m × 0.53 mm Heliflex capillary column using a flame ionization detector. Analysis of CO and CO_2 were performed in a Carbosphere 80/100 6 ft × 1/8 in. × 0.085 in. SS packed column using a thermal conductivity detector. Steady-state was reached within 6 h in all cases.

2.4. Catalyst characterization

The BET surface area, pore volume, and average pore size were measured by N_2 physisorption at liquid N_2 temperature (−196 °C) using a Micromeritics ASAP 2020 automated system. The samples were degassed under vacuum at 100 °C for 1 h and then the temperature was increased by 10 °C/min to 300 °C and the samples were held at that temperature for 2 h prior to each measurement. X-ray diffraction patterns of the catalysts were collected with a Scintag 2000 X-ray diffractometer, using monochromatized Cu Kα radiation (40 kV, 40 mA), a Ge detector, and a step scan mode. The samples were scanned at a scan rate of 0.04° (2θ) per second from 2θ = 10° to 80°. SEM and EDX were carried out using a JEOL JSM-35CF scanning electron microscope in the back scattering electron (BSE) mode at 20 kV. EDX was performed using Link Isis 300 software. Pulse CO chemisorption was measured for the catalyst samples at 50 °C. Approximately, 0.1 g of catalyst was put in a quartz tube, placed in a temperature-controlled oven, and connected to a thermal conductivity detector (TCD). The carrier gas used was helium. Prior to CO chemisorption, the catalyst samples were pretreated in flowing (50 ml/min) H_2 at 460 °C for 16 h with a ramping rate of 10 °C/min. Afterwards, the sample was purged with helium for 20 min and finally cooled down to 50 °C. Carbon monoxide was pulsed at 50 °C over the reduced catalyst until the TCD signal was constant. Temperature-programmed reduction (TPR) was performed to study the reduction behaviors of the catalysts using a Micromeritics Pulse Chemisorb 2750 system. Approximately 0.1 g of the catalyst was placed in the quartz tube. A temperature ramp from 35 to 800 °C at a ramp rate 5 °C/min and the reduction gas 10% H_2 in Ar were used. A thermal conductivity detector (TCD) was used to determine the amount of hydrogen consumed. A cold trap was placed before the detector to remove water produced during the reduction.

3. Results and discussion

The catalytic activities and selectivities for Fischer–Tropsch synthesis of the various Cu-modified Fe/Al_2O_3 catalysts are shown in Table 2. It can be seen that all the catalysts with Cu-modified Al_2O_3 supports exhibited higher hydrocarbon formation rates than the base Cu-promoted Fe/Al_2O_3 catalyst (1-0-*CC), regardless of the addition of 1% Cu as a promoter. The steady-state rates for CO_2 formation were also higher for the catalysts prepared with Cu-modified Al_2O_3 supports. For a similar catalyst system (1% Cu-promoted or non-promoted Fe/Cu-modified Al_2O_3 catalysts), the more calcination steps used during preparation, the higher the FTS activity. Hence, among the catalysts studied, the 1-10-CCC catalyst gave the highest hydrocarbon formation activity. Neither the addition of 10% Cu to the Al_2O_3 support nor the pretreatment during preparation appeared to have much effect on the FTS product selectivity, the Anderson–Schulz–Flory (ASF) chain growth probability (α), or the olefin selectivity, at least under the reaction conditions used. No oxygenated hydrocarbon products were observed in this study due to such compounds not being major products and to the fact that differential conversion was used (<10%). The reaction results are consistent with those reported by Coville and co-workers [25] that Cu promotion enhances activity of supported Fe

Table 2
FTS reaction rate and selectivity

Catalyst	Metal loading (wt.%)			SS rate of CO_2 formation[a,b] (μmol/g cat./s)	SS rate of total HC formation[a,b] (μmol of CO converted/g cat./s)	TOF (s^{-1})[c]	% Selectivity[b]							% Olefin (C_2–C_4)[b]	α (C_3–C_6)[b]
	Cu	Fe	Cu on Al_2O_3				C_1	C_2	C_3	C_4	C_5	C_6	C_{7+}		
1-0-*CC	1	20	0	Nil	0.50	0.42	41.0	29.1	20.5	6.4	2.0	0.7	0.2	67	0.33
1-10-CCC	1	20	10	0.31	0.90	0.04	45.5	26.1	19.4	6.2	1.8	0.8	0.2	55	0.35
1-10-CDC	1	20	10	0.34	0.86	0.08	49.8	25.6	17.9	4.3	1.6	0.6	0.2	54	0.32
1-10-DDC	1	20	10	0.35	0.71	0.10	45.9	26.4	19.1	6.0	1.8	0.6	0.2	58	0.31
1-10-DDD	1	20	10	0.32	0.63	0.63	44.5	26.9	19.3	6.1	1.9	0.9	0.4	61	0.35
0-10-CC*	–	20	10	0.30	0.89	0.06	46.5	25.9	19.2	5.5	1.8	0.8	0.2	58	0.34
0-10-CD*	–	20	10	0.24	0.74	0.15	44.6	26.7	19.8	6.1	1.8	0.8	0.2	63	0.34
0-10-DC*	–	20	10	0.07[d]	0.81	0.12	43.4	27.0	20.1	6.4	2.0	0.9	0.3	58	0.35

[a] FTS reaction was carried out at 280 °C, 1.8 atm total pressure, and H_2/CO ratio used = 2/1. Rate of hydrocarbon formation is in μmol of CO converted/g cat./s. The reaction reached steady-state product formation before 6 h TOS, so all steady-state data is for that TOS.
[b] Error of measurement = ± 5% as determined directly.
[c] Based on pulse CO chemisorption (see Table 3). Error of measurement = ± 10%.
[d] Repeatability for two times. Error of measurement = ± 2% as determined directly.

catalysts but does not have an effect on FT product selectivity. The results from this study reveal that the effect of the Cu-modified Al_2O_3 support on the catalytic properties of Fe/Al_2O_3 catalysts is similar in nature to the addition of Cu as a second metal promoter. Moreover, the catalyst that had never been calcined in any preparation step (1-10-DDD) exhibited the lowest FTS activity among the various Fe catalysts prepared with the Cu-modified Al_2O_3 support. Therefore, the calcination step appears to be very important in producing highly active catalysts.

Some physicochemical properties of the Al_2O_3 support and the various Al_2O_3 supported Fe catalysts are shown in Table 3. It was found that BET surface areas, pore volumes, and pore sizes of the 1% Cu promoted Fe on Cu-modified Al_2O_3 catalysts prepared with calcination pretreatment after the last metal impregnation (all of the 1–10 catalysts except 1-10-DDD) were in the range of 107–113 m^2/g and were not significant different from the base 1-0-*CC catalyst (115 m^2/g). On the other hand, for the 0–10 catalysts (the catalysts without 1% Cu as a second metal promoter) and the catalysts prepared with only drying after the last metal impregnation (prior to reduction), the BET surface areas were higher (130–147 m^2/g) with 0-10-CD* showed the highest BET surface area. Since the average pore sizes and pore volumes of all the catalysts were smaller than those of the alumina support, some of the active metal probably was deposited in the pores of the alumina. XRD patterns of the Al_2O_3, the 10 wt.% Cu/Al_2O_3 (dried and calcined), and the various catalysts are shown in Fig. 1. The γ-Al_2O_3 exhibited strong diffraction peaks at $2\theta = 31^\circ$, 33°, 38°, 39.7°, 43°, 46°, and 68° (based on the JCPDS database). For the 10% Cu/Al_2O_3 catalyst, it was found that Cu was in the form of CuO, as indicated by its characteristic peaks at $2\theta = 35.5^\circ$ and 39°. It has been reported that interaction between CuO and Al_2O_3 occurs readily at calcination temperatures close to 600 °C, yielding $CuAl_2O_4$ [26]. Moreover, the extent of solid–solid interaction between oxides involved in aluminate formation increases on increasing the calcination temperature from 600 to 800 °C. It is likely that in this study $CuAl_2O_4$ was not formed at the calcination temperature used (460 °C) since no XRD peaks for $CuAl_2O_4$ were detected. The XRD patterns for all the supported Fe catalysts do not show any characteristic peaks of Fe_2O_3 or any other Fe compound suggesting that Fe was present in a highly dispersed form. Except for the catalysts that were only dried after the last metal impregnation, all the catalysts exhibited XRD patterns similar to the base catalyst where only the major peaks for γ-Al_2O_3 were found. For the 1-10-DDD and 0-10-CD* catalysts which were only dried after the last metal impregnation, additional diffraction peaks at $2\theta = 12.9^\circ$, 20.9°, and 25.8° can be seen in the XRD patterns. These peaks are attributed to the presence of residual Fe nitrate of Cu nitrate in the catalysts. These catalysts were less active than those prepared with calcination pretreatment after impregnation of the metal(s), perhaps due to a greater difficulty in reducing the Fe oxide to Fe metal during reduction of the catalysts with H_2.

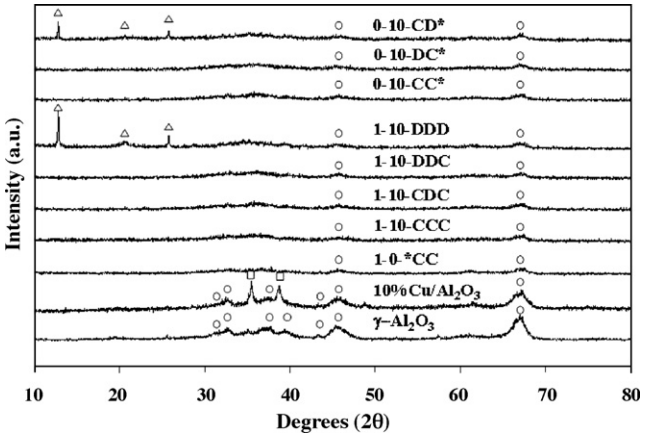

Fig. 1. XRD patterns of the γ-Al_2O_3 support, the 10 wt.% Cu/Al_2O_3 support (dried and calcined), the Al_2O_3-supported Fe catalysts and Cu-modified Al_2O_3-supported Fe catalysts. (○) γ-Al_2O_3; (□) CuO; (△) Nitrate species.

SEM and EDX were also performed in order to study the morphology and elemental distribution of the catalyst samples. The alumina and Cu-modified alumina supports consisted of irregular shaped particles/granules formed by agglomeration of nanocrystalline alumina (results not shown). There were no differences in the cluster size and morphology of the various alumina-supported Fe catalysts, as seen in Fig. 2. An SEM micrograph with EDX elemental mapping (for Al, O, Fe, and Cu) of the 1-10-CCC catalyst is shown in Fig. 3. It can be seen

Table 3
Catalyst characteristics

Catalyst	Metal loading (wt.%)			BET surface area (m^2/g cat.)[a]	Average pore volume (cm^3/g cat.)[a]	Average pore size (nm)[a]	CO chemisorption (μmol/g cat.)[b]
	Cu	Fe	Cu on Al_2O_3				
γ-Al_2O_3	0	0	0	100.0	0.68	27.2	–
1-0-*CC	1	20	0	114.8	0.37	12.9	1.2
1-10-CCC	1	20	10	107.4	0.36	13.4	24.8
1-10-CDC	1	20	10	113.1	0.35	12.5	11.2
1-10-DDC	1	20	10	108.6	0.35	12.9	6.9
1-10-DDD	1	20	10	145.7	0.35	9.7	1.0
0-10-CC*	0	20	10	130.4	0.36	11.0	15.2
0-10-CD*	0	20	10	146.7	0.32	8.8	4.8
0-10-DC*	0	20	10	130.4	0.35	10.8	6.8

[a] Using N_2 physisorption at 77 K. Error of measurement = ± 10%.
[b] Error of measurement = ± 5%.

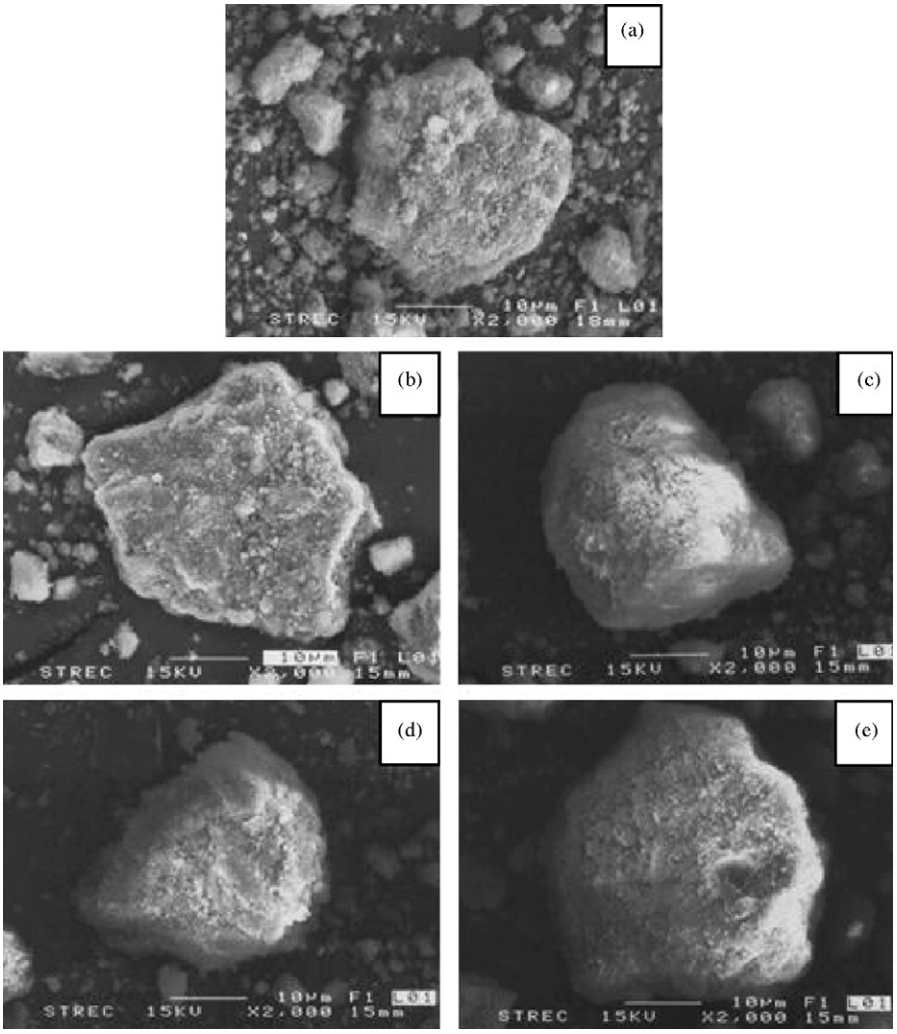

Fig. 2. SEM micrographs of the catalysts. (a) 1-0-*CC, (b) 1-10-CCC, (c) 1-10-DDC, (d) 1-10-DDD and (e) 0-10-CC*.

that all of elements in the catalyst were well dispersed and distributed throughout the catalyst granules. Similar results were also obtained for other Cu-modified alumina-supported Fe catalysts.

The reduction behavior of the catalysts was studied by H_2 temperature program reduction (TPR). The TPR profiles of the Fe/Al_2O_3 catalyst and the variously Cu-modified Fe/Al_2O_3 catalysts are shown in Fig. 4. TPR profile of the alumina support (not shown) exhibited no reduction peak under the TPR conditions used. For the Fe/Al_2O_3 catalyst, only one reduction peak located at ca. 165–400 °C (maximum at 265 °C) was observed. TPR profiles for the Cu-modified Fe/Al_2O_3 catalysts were similar to that of Fe/Al_2O_3 with only a single reduction peak being observed. The reduction peaks of the Cu-modified Fe/Al_2O_3 catalysts (except 1-10-DDD and 0-10-CD*) were located at ca. 105–345 °C (maximum at 230 °C). While, the reduction peak of the 1-10-DDD and 0-10-CD* catalysts were located at ca. 200–400 °C (maximum at 330 °C). The maximum in the reduction peak at ca. 265 °C for the Fe/Al_2O_3 catalyst was shifted about 35 °C lower when there was a presence of Cu in the alumina support as seen for the Cu-modified Fe/Al_2O_3 catalysts (except 1-10-DDD and 0-10-CD*). The shift of the reduction peak maximum to a lower temperature indicates a greater ease of reduction that can be due in part to a weaker interaction between iron and alumina. For the Cu-modified Fe/Al_2O_3 catalysts with drying pretreatment after the final impregnation (1-10-DDD and 0-10-CD*), the TPR peak maximum was about 65 °C higher (at ca. 330 °C). The shift of a reduction peak to higher temperature suggests a stronger interaction between iron and the alumina support. It can be seen that the reduction temperature decreased significantly for the Cu-modified alumina supported iron catalysts with calcining pretreatments after the final impregnation step. However, the one prepared with only a drying pretreatment after the final impregnation resulted in an increased reduction temperature. This may be due in large part to the presence of residual nitrate species in the catalysts.

Pulse CO chemisorption was performed in order to determine the relative amounts of active iron on the catalyst samples. The results are shown in Table 3. The amounts of CO chemisorption on the Cu-modified Fe/Al_2O_3 catalysts varied in the range of 1.0–24.8 μmol/g cat. and were higher than that of the Fe/Al_2O_3 base catalyst. The presence of the Cu-modified alumina support resulted in an increase in the relative amounts of surface-exposed active iron metal. Each additional calcina-

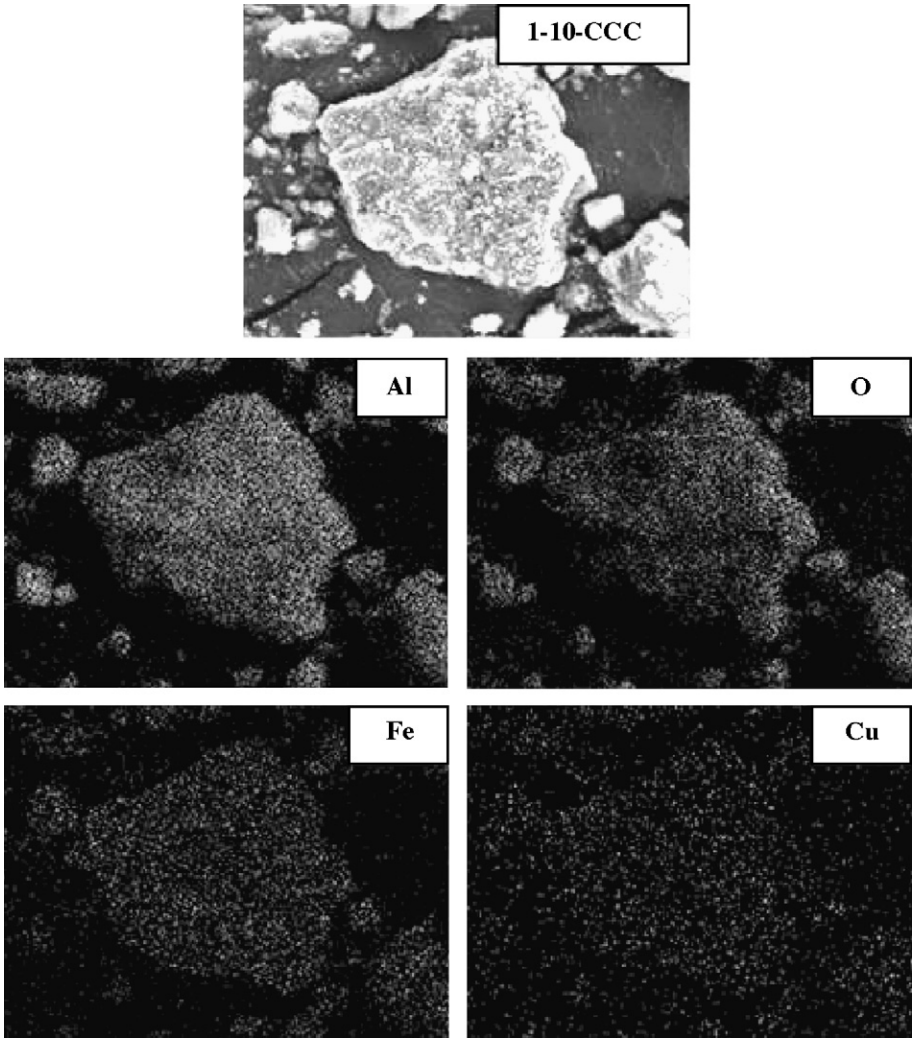

Fig. 3. SEM micrograph and EDX mapping of a cross-sectioned 1-10-CCC catalyst granule.

tion led to increased CO chemisorption, as shown in Fig. 5 for the Cu-modified Fe/Al_2O_3 catalysts. The CO chemisorption results suggest an increased Fe dispersion after multiple calcinations. However, CO is also known to adsorb somewhat on Cu oxide surfaces [27,28]; thus, some of the increase in CO chemisorption may have been due to CO adsorbing on Cu oxide entities/particles on the catalyst surface.

Fig. 6 shows the effect of the number of calcinations on the steady-state hydrocarbon synthesis rate. It can be seen that there was a significant increase in the steady-state hydrocarbon

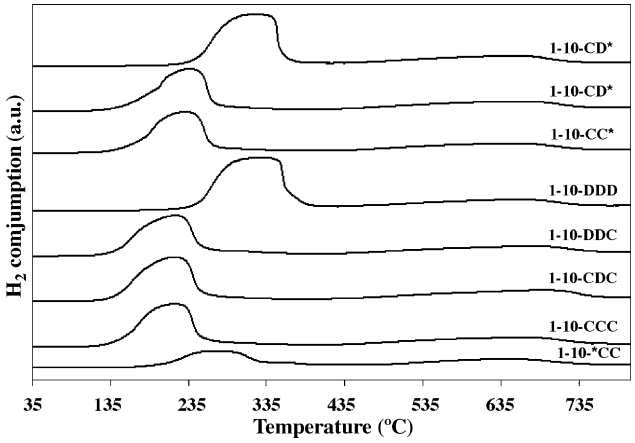

Fig. 4. TPR profiles of the catalyst samples.

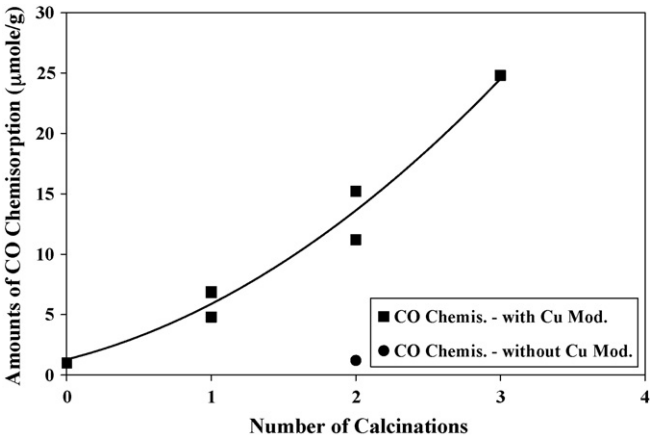

Fig. 5. Effect of number of calcinations on CO chemisorption.

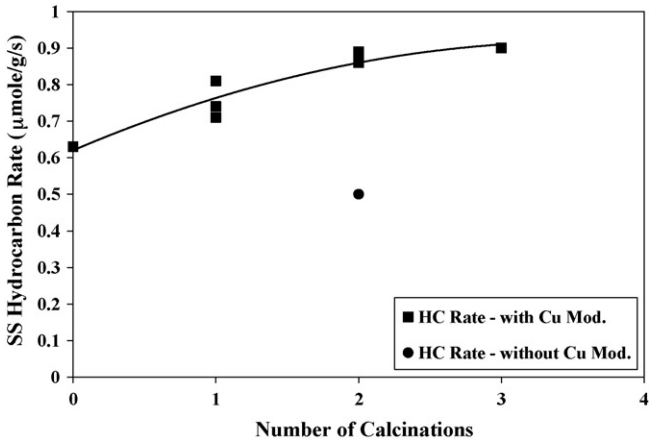

Fig. 6. Effect of number of calcinations on steady-state of total hydrocarbon rate.

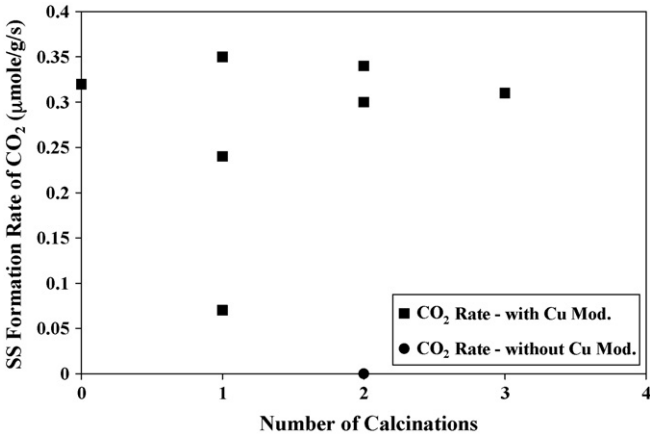

Fig. 7. Effect of number of calcinations on steady-state formation rate of CO_2.

synthesis rate with the number of calcinations. However, there was little (or no) effect of calcinations on the rate of CO_2 formation, although Cu-modification significantly increased water–gas-shift reaction on the catalysts (Fig. 7). The relationship between the steady-state hydrocarbon synthesis rate and CO chemisorption is illustrated in Fig. 8. It can be observed that while the rate of hydrocarbon formation

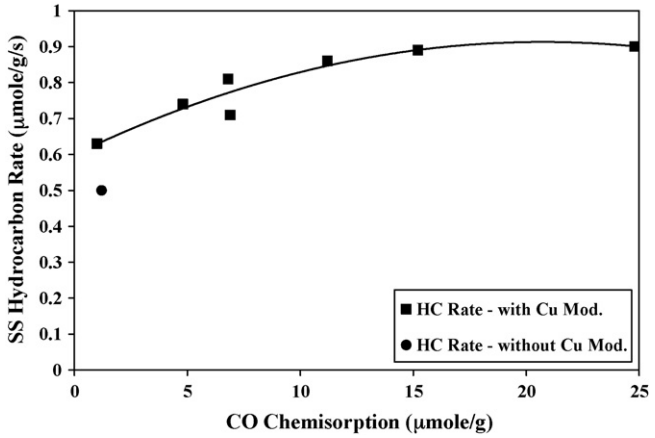

Fig. 8. Steady-state hydrocarbon synthesis rate vs. CO chemisorption.

increased with CO chemisorption, there was only a weak dependence, supporting the suggestion given above that some of the additional CO chemisorption took place on Cu oxide entities. The results of this study, however, clearly indicate that the number of calcinations during preparation is an important variable besides Cu-modification of the support in affecting the hydrogenation activity of Fe/Al_2O_3 catalysts. Multiple calcinations can perhaps (a) decrease the contamination of the surface by nitrate species, (b) increase Fe reducibility, and/or (c) produce larger Fe particles which are easier to reduce (although this is not able to be verified by XRD).

4. Conclusions

This study explored the effect of copper-modified alumina on the activity and selectivity of alumina-supported iron catalysts for the FTS reaction. It was found that the Fe catalysts supported on 10 wt.% Cu-modified alumina exhibited significantly higher activities than those of a 1 wt.% Cu-promoted Fe/Al_2O_3 catalyst. There was, however, little effect on FT product selectivity, chain growth probability (α), or olefin selectivity. Moreover, calcination after impregnation of each metal during catalyst preparation is important for producing highly active catalysts. It is likely that Cu-modification acts to restrict interaction of Fe with the alumina support, known to decrease the activity of Fe for FTS. Use of the Cu-modified support increased both the CO chemisorption and the ease of reduction provided the catalyst was calcined after preparation.

Acknowledgments

The authors would like to thank the Thailand Research Fund (TRF) for the financial support of this project. We also would like to thank NASEO-STAC (Contract no. DE-FC36-03GO13026) for partial funding of the research carried out in the U.S.

References

[1] V.U.S. Rao, G.J. Stiegel, G.J. Cinquegrane, R.D. Srivastava, Fuel Process. Technol. 30 (1992) 83.
[2] R.J. O'Brien, L. Xu, R.L. Spicer, S. Bao, D.R. Milburn, B.H. Davis, Catal. Today 36 (1997) 325.
[3] A.A. Adesina, Appl. Catal. A 138 (1996) 345.
[4] J. Panpranot, S. Kaewkun, P. Praserthdam, J.G. Goodwin Jr., Catal. Lett. 91 (2003) 95.
[5] G.A. Mills, Catalysts for Fuels from Syngas, IEA Coal Research, London, 1988, pp. 34–44.
[6] M.L. Cubeiro, H. Morales, M.R. Goldwasser, M.J. Perez-Zurita, F. Gonzalez-Jimenez, C.U. de N, Appl. Catal. A 189 (1999) 87.
[7] Z.H. Suo, Y. Kou, J.Z. Niu, W.Z. Zhang, H.L. Wang, Appl. Catal. A 148 (1997) 301.
[8] T. Riedel, M. Claeys, H. Schulz, G. Schaub, S.S. Nam, K.W. Jun, M.J. Choi, G. Kishan, K.W. Lee, Appl. Catal. A 186 (1999) 201.
[9] M.L. Cubeiro, F. Gonzalez-Jimenez, M.R. Goldwasser, M.J. Perez-Zurita, E. Pietri, L. Garcia, Hyperfine Interact. 134 (2001) 13.
[10] C.H. Zhang, H.J. Wan, Y. Yang, H.W. Xiang, Y.W. Li, Catal. Commun. 7 (2006) 733.
[11] D.J. Duvenhage, N.J. Coville, Catal. Lett. 104 (2005) 129.
[12] K. Chen, Y. Fan, Q. Yan, J. Catal. 167 (1997) 573.

[13] H.J. Wan, B.S. Wu, C.H. Zhang, H.W. Xiang, Y.W. Li, B.F. Xu, F. Yi, Catal. Commun. 8 (2007) 1538.
[14] A.F.H. Wielers, A.J.H.M. Kock, C.E.C.A. Hop, J.W. Geus, A.M. v d Kraan, J. Catal. 117 (1989) 1.
[15] L. Guczi, Catal. Rev. Sci. Eng. 35 (1993) 1.
[16] Y. Yang, H.W. Xiang, Y.Y. Xu, L. Bai, Y.W. Li, Appl. Catal. A 266 (2004) 181.
[17] M. Luo, R.J. O'Brien, S. Bao, B.H. Davis, Appl. Catal. A 239 (2003) 111.
[18] T. Li, Y. Yang, C. Zhang, X. An, H. Wan, Z. Tao, H. Xiang, Y. Li, F. Yi, B. Xu, Fuel 86 (2007) 921.
[19] S. Li, S. Krishnamoorthy, A. Li, G.D. Meitzner, E. Iglesia, J. Catal. 206 (2002) 202.
[20] M. Luoa, R. O'Briena, B.H. Davis, Catal. Lett. 98 (2004) 17.
[21] S. Li, A. Li, S. Krishnamoorthy, E. Iglesia, Catal. Lett. 77 (2001) 197.
[22] H. Storch, N. Golumbic, R.B. Anderson, Fischer–Tropsch and Related Synthesis, Wiley, New York, NY, 1951.
[23] J. Xu, C.H. Bartholomew, J. Phys. Chem. B 109 (2005) 2392.
[24] M.E. Dry, in: J.R. Anderson, M. Boudart (Eds.), Catalysis Science and Technology, 1, Springer-Verlag, New York, 1981, p. 159.
[25] M.C. Bahome, L.L. Jewell, D. Hildebrandt, D. Glasser, N.J. Coville, Appl. Catal. A 287 (2005) 60.
[26] H.G. El-Shobaky, M. Mokhtar, G.A. El-Shobaky, Appl. Catal. A 180 (1999) 335.
[27] J.W. London, A. Bell, J. Catal. 31 (1973) 32.
[28] Y.A. Lokhov, A.A. Davydov, Kinetika I kataliz 20 (1979) 1498.

Available online at www.sciencedirect.com
ScienceDirect
Catalysis Communications 9 (2008) 207–212
CATALYSIS COMMUNICATIONS
www.elsevier.com/locate/catcom

Effect of mixed γ- and χ-crystalline phases in nanocrystalline Al_2O_3 on the dispersion of cobalt on Al_2O_3

Kamonchanok Pansanga [a], Joongjai Panpranot [a], Okorn Mekasuwandumrong [b], Chairit Satayaprasert [a], James G. Goodwin [c], Piyasan Praserthdam [a,*]

[a] Center of Excellence on Catalysis and Catalytic Reaction Engineering, Department of Chemical Engineering, Faculty of Engineering, Chulalongkorn University, Bangkok 10330, Thailand
[b] Department of Chemical Engineering, Faculty of Engineering and Industrial Technology, Silpakorn University, Nakorn Pathom 73000, Thailand
[c] Department of Chemical and Biomolecular Engineering, Clemson University, Clemson, SC, 29634, USA

Received 10 January 2007; received in revised form 22 May 2007; accepted 22 May 2007

Abstract

This paper reports the results of a study into the effect of mixed γ and crystalline phases in Al_2O_3 on the characteristics and catalytic activities for CO hydrogenation of Co/Al_2O_3 catalysts. The catalysts were characterized by X-ray diffraction, N_2 physisorption, transmission electron microscopy, and H_2 chemisorption. Increasing Co loading from 5 to 20 wt% for the mixed phase Al_2O_3-supported Co catalysts resulted in a constant increase in both the number of cobalt metal active sites and the hydrogenation activities. However, for those supported on γ-Al_2O_3, Co dispersion increased up to 15 wt%Co and declined at 20 wt%Co loading. It is suggested that the spherical-shape like morphology of the χ-phase Al_2O_3 prevented agglomeration of Co particles, especially at high Co loadings.

Keywords: Nanocrystalline alumina; Crystalline phase; Cobalt catalyst; CO hydrogenation; χ-Alumina; γ-Alumina

1. Introduction

Alumina is one of the most common commercial carriers used to disperse catalytic materials because of its excellent thermal stability, high mechanical resistance, and wide range of chemical, physical, and catalytic properties. In general, acidic, high surface area alumina hydrates are produced at relatively low temperatures by precipitation from either acidic or basic solutions and then are transformed to "transition" β-, γ-, η-, χ-, κ-, δ-, α-, and α-Al_2O_3 by dehydration and treatment at high temperatures [1].

Despite a wide range of crystalline structures, only γ- and α-Al_2O_3 have been studied often as catalyst supports. Typically, γ-Al_2O_3 provides a better dispersion of catalytically active metals than α-Al_2O_3 due to its higher surface area. Only a few publications have reported the effect of other crystalline phases of alumina on the properties of alumina-supported catalysts. For example, Chary et al. [2] reported that dispersion of vanadium oxide on alumina as well as its catalytic activities in partial oxidation decreased with increasing calcination temperature due to the transformation of γ-alumina into θ-alumina, δ-alumina, and α-alumina phases. Recently, Moya et al. [3] studied silver nanoparticles supported on α-, η-, and δ-Al_2O_3 prepared by a colloidal processing route. It was found that silver particle sizes varied between 1 and 100 nm depending on the alumina phase. To our knowledge, the effect of mixed γ- and χ-Al_2O_3 phases on the properties of Al_2O_3 as a catalyst support has never been reported.

In this study, nanocrystalline transition Al_2O_3 (γ-Al_2O_3 and mixed γ- and χ-Al_2O_3) were synthesized by decomposition of aluminum isopropoxide (AIP) under solvothermal conditions. The advantages of the solvothermal method are

* Corresponding author. Tel.: +66 2218 2882; fax: +66 2218 6877.
E-mail address: piyasan.p@chula.ac.th (P. Praserthdam).

1566-7367/$ - see front matter © 2007 Elsevier B.V. All rights reserved.
doi:10.1016/j.catcom.2007.05.042

that it gives products with uniform morphology, well-controlled chemical composition, and narrow particle size distribution [4–8]. Furthermore, desired shapes and sizes of particles can be tailored by controlling process conditions such as solute concentration, reaction temperature, reaction time, and the type of solvent [9,10]. The effects of mixed crystalline phases of Al_2O_3 on the dispersion of cobalt on Al_2O_3 and the resulting catalytic activity for CO hydrogenation were investigated.

2. Experimental

2.1. Preparation of alumina

Nanocrystalline transition Al_2O_3 was prepared by the solvothermal method according to the procedure described in Ref. [11]. The desired amount of aluminum isopropoxide (AIP) (Aldrich) (10, 15, 25, or 35 g) was suspended in 100 ml of 1-butanol (Ajax Finechem) in a beaker, which was then placed in a 300 ml autoclave. In the gap between the beaker and the autoclave wall, 30 ml of 1-butanol was added. After the atmosphere inside the autoclave was purged completely with nitrogen, the mixture was heated to 300 °C at a heating rate of 2.5 °C/min and was kept at that temperature for 2 h. After cooling to room temperature, the resulting powders were collected after repeated washing with acetone and were then air-dried. The calcination of the products was carried out in a box furnace by heating up to 600 °C at a rate of 10 °C/min and held at that temperature for 1 h.

2.2. Catalyst preparation

The Al_2O_3-supported cobalt catalysts with different Co loadings (5, 10, 15, and 20 wt%) cobalt were prepared by incipient wetness impregnation of alumina with a desired amount of an aqueous solution of cobalt nitrate [$Co(NO_3)_2 \cdot 6H_2O$] (Aldrich). After impregnation, the catalysts were dried at 110 °C for 24 h and calcined in air at 300 °C for 2 h using a ramp rate of 1 °C/min.

2.3. Catalyst characterization

X-ray diffraction patterns of the samples were collected using a SIEMENS D-5000 X-ray diffractometer with Cu Kα radiation ($\lambda = 1.54439$ Å). The spectra were scanned at a rate of 0.04°/step from $2\theta = 15°$ to 80°. The composition of each crystalline phase has been calculated from the calibration of X-ray diffraction peak areas of the mixtures between each pure phase (physically mixed). BET surface areas of the sample were calculated using the BET-single point method at liquid N_2 temperature. Transmission electron microscopy was performed to study the morphologies of the catalyst samples and the dispersion of cobalt oxide species on the alumina supports using a JEOL JEM 1230. The number of surface cobalt metal atoms was determined by pulse H_2 chemisorption at 100 °C on the reduced cobalt catalysts based on the static method described by Reuel and Bartholomew [12] using a Micromeritics Pulse Chemisorb 2750 system. Prior to H_2 chemisorption, the catalyst samples were reduced at 350 °C in flowing H_2 for 3 h. The X-ray photoelectron spectroscopy (XPS) analysis was performed using an AMICUS photoelectron spectrometer equipped with a Mg Kα X-ray as a primary excitation and a KRATOS VISION2 software. XPS elemental spectra were acquired with 0.1 eV energy step at a pass energy of 75 kV. The C 1s line was taken as an internal standard at 285.0 eV.

2.4. Reaction study

CO hydrogenation was carried out at 220 °C and 1 atm total pressure in a fixed-bed quartz reactor under differential reaction conditions. The H_2/CO ratio used was 10/1. Typically, 0.1 g of the catalyst sample was reduced *in situ* in flowing H_2 (50 cc/min) at 350 °C for 3 h prior to reaction. After the start up, samples were taken at 1-h intervals and analyzed by gas chromatography. Steady state was reached within 6 h in all cases.

3. Results and Discussion

In this study, nanocrystalline alumina powders were prepared by thermal decomposition of AIP in 1-butanol with various AIP content. XRD patterns of these alumina samples after calcination at 600 °C for 1 h are shown in Fig. 1. The XRD patterns of transition Al_2O_3 were observed at degree $2\theta = 31°$, 33°, 38°, 43°, 47.5°, and 68°. It was found that when lower amounts of AIP were used (10 and 15 g in 100 cm^3 of 1-butanol), only γ-Al_2O_3 was formed by calcination, as seen by the XRD characteristic peaks at $2\theta = 33°$ according to the JCPDSs database.

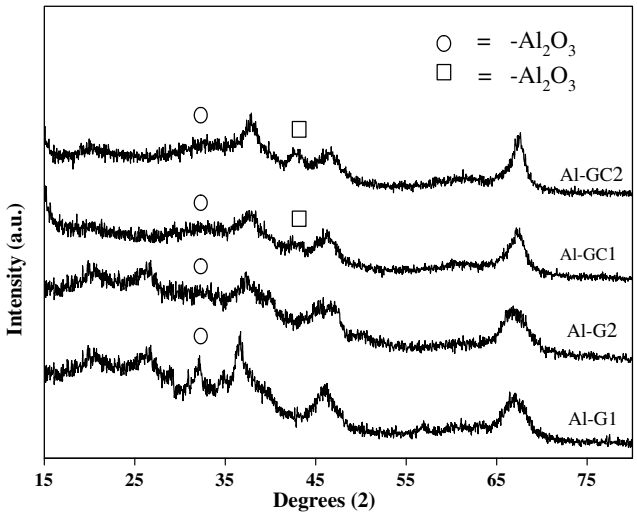

Fig. 1. XRD patterns of the various nanocrystalline alumina prepared by the reaction of AIP in 1-butanol at 300 °C for 2 h (after calcination at 600 °C for 1 h).

Table 1
Properties of the various nanocrystalline Al_2O_3 samples prepared by the reaction of AIP in 1-butanol at 300 °C for 2 h

Samples	Amounts of AIP (g)	Amounts of χ-phase (%)	Surface area (m^2/g)[a]	Bulk density (g/cm^3)[a]	Morphology [27]
Al-G1	10	–	70	0.38	Wrinkled sheets
Al-G2	15	–	120	0.38	High amount of wrinkled sheets
Al-GC1	25	33	139	0.39	Wrinkled sheets and small amount of spherical particles
Al-GC2	35	57	145	0.53	Small amount of wrinkled sheets and high amount of spherical particles
Al-C[b]	25	100	180	0.56	Spherical particles

[a] Error of measurement = 5%.
[b] Pure χ-Al_2O_3.

These γ-Al_2O_3 samples are denoted hereafter as Al-G1 and Al-G2, respectively. The XRD characteristic peak of χ-alumina was observed at $2\theta = 42.5°$ for the supports prepared with higher amounts of AIP (25 and 35 g in 100 cm^3 1-butanol). The mixed γ- and χ-crystalline phase samples containing χ-phase of ca. 33% and 57% were denoted as Al-GC1 and Al-GC2, respectively. Pure χ-alumina prepared by reaction of AIP in toluene was used as the reference sample and denoted as Al–C. The intensity of χ-Al_2O_3 peaks became stronger with increasing amount of AIP content during preparation, indicating that increasing AIP content during the solvothermal synthesis resulted in formation of alumina giving rise to mixed phases of γ-Al_2O_3 and χ-Al_2O_3 after calcination. The physical properties of the various Al_2O_3 samples are shown in Table 1. The BET surface area of the Al-GC2 (145 m^2/g) was found to be twice of that of Al-G1 (70 m^2/g). A similar trend was observed for the bulk density of the Al_2O_3 powders. The bulk density increased with increasing amount of AIP used during preparation (from 0.38 g/cm^3 to 0.54 g/cm^3). The BET surface areas also increased with increasing AIP concentration, probably as a result of morphology changing from a wrinkled sheet structure to small spherical particles (see Fig. 3). These results were confirmed by Al-C with highest BET surface area (180 m^2/g), highest bulk density (0.56 g/cm^3) and complete spherical particle morphologies. From results such as these, it has been proposed that for preparation with low AIP contents, boehmite is the main product resulting in γ-alumina after calcination at 600°C for 1 h. The morphology of the boehmite products obtained via the solvothermal reaction has been shown to be wrinkled sheets [13,14]. The precursor to spherical-shaped χ-Al_2O_3 was formed by direct decomposition of AIP in the solvent and appeared to increase with increasing AIP concentration.

Fig. 2 shows the IR spectra of alumina supports after calcination at 600 °C for 1 h. The IR peaks assigned to OH stretching were observed at around 3730 and broad peak between 3200 and 3600 cm^{-1}. According to Peri's model [15], the features at 3791, 3730, and 3678 cm^{-1} are assigned to surface isolated hydroxyl groups. The broader peak at 3589 cm^{-1} is due to the vibration of associated hydroxyl groups of aluminum oxide. The spectra which assigned to OH groups of all samples were nearly identical. Therefore, the amounts and nature of OH groups of all supports were essentially same.

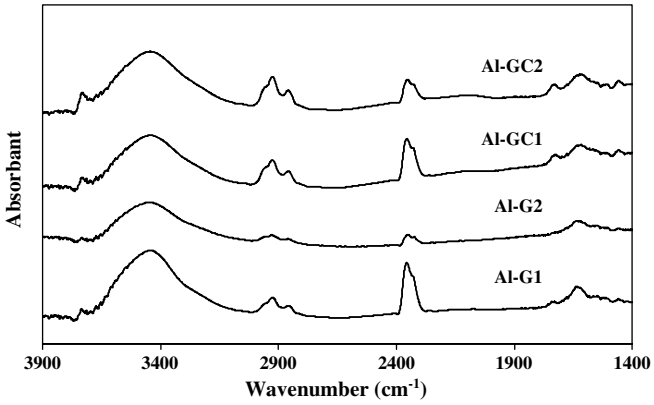

Fig. 2. IR spectra of various alumina supports.

The nanocrystalline γ-Al_2O_3 and mixed γ- and χ-Al_2O_3 were then employed as catalyst supports for Co catalysts. The Co/Al_2O_3 catalysts were prepared using the incipient wetness impregnation method with cobalt loadings of 5, 10, 15, and 20 wt% in order to investigate the effect of mixed crystalline phases of Al_2O_3 on the dispersion of Co and its catalytic activity for CO hydrogenation. The XRD patterns of the various Co/Al_2O_3 catalysts after calcination at 300°C were not significantly different from those of the Al_2O_3 supports (results not shown). No XRD characteristic peaks of Co_3O_4 and/or other Co compounds were detected for all the catalyst samples. This suggests that the crystallite size of cobalt oxide on Al_2O_3 was probably below the lower limit for XRD detectability (3–5 nm). Such results also indicate that cobalt oxide species were present in a highly dispersed form on these nanocrystalline Al_2O_3 even for cobalt loadings as high as 20 wt%.

The morphology and distribution of cobalt oxide particles on the Al_2O_3 supports were investigated by transmission electron microscopy (TEM). The typical TEM micrographs of 20 wt% of cobalt on alumina supports

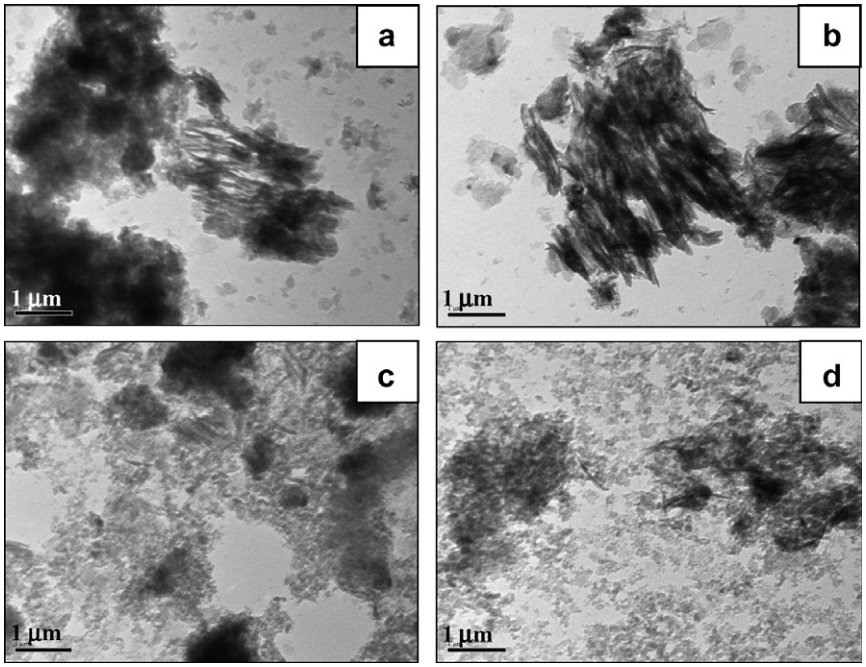

Fig. 3. TEM micrographs of the various 20 wt%Co/Al_2O_3 catalysts (a) 20Co/Al-G1 (b) 20Co/Al-G2 (c) 20Co/Al-GC1 (d) 20Co/Al-GC2.

containing different compositions of γ and χ phases are shown in Fig. 3. In all the TEM figures, the darker spots on the catalyst granules represent a high concentration of cobalt and its compounds while the lighter areas indicate the support with minimal or no cobalt present. It was found that the wrinkled sheets-like structure of γ-Al_2O_3 was maintained after impregnation and calcination for both 20Co/Al-G1 and 20Co/Al-G2 catalysts (Figs. 2a and b). The mixed structure between spherical particles of χ-Al_2O_3 and wrinkled sheets of γ-Al_2O_3 were also observed for 20Co/Al-GC1 and 20Co/Al-GC2 samples (Figs. 2c and d). However, cobalt oxide species appeared to be more agglomerated on the γ-Al_2O_3 supports than on the mixed γ- and χ-ones as shown by the appearance of larger cobalt oxide particles/granules.

Static H_2 chemisorption on the reduced cobalt catalyst was used to determine the number of active surface cobalt metal atoms [16]. The H_2 chemisorption results for all the catalyst samples are reported in Table 2. The overall dispersion of reduced Co and crystal size of Co^0 in the catalyst samples based on the H_2 chemisorption results is also given. In order to distinguish the effect of mixed γ- and χ-crystalline phases of Al_2O_3 and the effect of BET surface area, we also report the H_2 chemisorption results in terms of the amount of H_2 chemisorption per total specific surface area of the catalyst (see Fig. 4). For the Co/Al-G1 and Co/Al-G2 catalysts in which the Al_2O_3 contained only the γ-phase, the number of active surface cobalt metal atoms per unit surface area increased with increasing Co loading up to 15 wt%. Further increase of the amount of Co loading to 20 wt% resulted in both a lower cobalt dispersion and fewer exposed surface cobalt metal atoms (Table 2), even taking into account BET surface area (Fig. 4). This is typical for supported Co Fischer–Tropsch catalysts. Dispersion usually decreases with increasing Co loading beyond a certain point [17–

Table 2
H_2 chemisorption results

Catalyst samples	Amounts of H_2 chemisorption (μmol/g cat.)[a]				%Co dispersion[b]				dp Co^0 (nm) (96.2/D%)			
	5%Co	10%Co	15%Co	20%Co	5%Co	10%Co	15%Co	20%Co	5%Co	10%Co	15%Co	20%Co
Co/Al-G1	0	0.9	9.2	3.3	0	0.1	0.7	0.2	0	962	137	481
Co/Al-G2	0.9	2.3	14.9	10.9	0.2	0.3	1.2	0.6	481	321	80	160
Co/Al-GC1	5.6	7.6	18.9	19.5	1.1	1.1	1.5	1.5	87	87	64	64
Co/Al-GC2	5.8	20.7	21.4	24.6	1.3	1.7	1.7	1.8	74	57	57	53
Co/Al-C[c]	–	–	16.8	–	–	–	1.3	–	–	–	74	–

[a] Error = ±5 %, as determined directly.
[b] %Co dispersion = [2 × (total H_2 chemisorption/g cat.) / (no. of μmol of Co total/g cat.)] × 100%
[c] Co/Al_2O_3 prepared from pure χ-Al_2O_3 support.

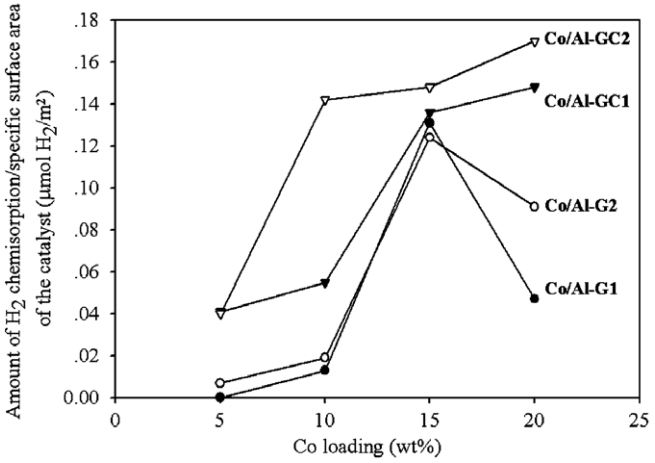

Fig. 4. The amount of H_2 chemisorption/specific surface area of the Co/Al_2O_3 catalysts as a function of cobalt loading.

21]. On the contrary, the amounts of H_2 chemisorption per unit surface area of the mixed γ- and χ-crystalline phases Al_2O_3 supported Co catalysts (Co/Al-GC1 and Co/Al-GC2) constantly increased with increasing Co loading from 5 to 20 wt% (Table 2, Fig. 4). To study the effect of phase composition on active sites of Co catalyst, 15%Co/pure χ-alumina catalyst was characterized to compare with 15%Co deposited on pure γ-Al_2O_3 and mix phase supports. The amounts of H_2 chemisorption increased from 9.2 to 21.4 μmol/g catalyst as the χ-phase contents increased from 0% to 57%. While the amounts of H_2 chemisorption of Co/pure χ-alumina catalyst ranged around 16.8 μmol/g catalyst. It is suggested that the presence of χ-phase in γ-Al_2O_3 may prevent agglomeration of Co particles especially at high Co loadings, resulting in the maintenance of high Co dispersion. Because of its surface sensitivity, XPS is used to identify the surface compositions of the catalysts as well as the interaction between Co and the alumina supports. The results are given in Table 3. It was found that the ratio of Al/O atomic concentration was slightly increased while that of Co/Al decreased with the presence of χ-phase in γ-Al_2O_3 suggesting higher dispersion of Co on the mixed phase Al_2O_3 supports. There was also a slight shift of Co 2p binding energy to higher values for the 15Co/Al-GC1 and 15Co/Al-GC2 catalysts compared to those supported on γ-Al_2O_3 (Al-G1 and Al-G2). Such results suggest stronger interaction between Co and the mixed phases γ- and χ-Al_2O_3.

Table 3
Surface compositions based on XPS results for 15 wt%Co/Al_2O_3 catalysts

Sample	Binding energy (eV)			Atomic concentration (%)	
	Co 2p	O 1s	Al 2s	Al/O	Co/Al
15Co/Al-G1	782.4	533.1	120.9	0.29	0.026
15Co/Al-G2	782.4	533.1	120.6	0.33	0.027
15Co/Al-GC1	782.8	533.1	121.0	0.34	0.015
15Co/Al-GC2	782.9	532.9	120.3	0.40	0.019

CO hydrogenation was carried out in a fixed-bed quartz reactor under differential reaction conditions in order to determine the catalytic activity of the catalyst samples. The reaction results in terms of CO conversion, hydrogenation rate, and the turnover frequency (TOF) per exposed Co atom calculated using the hydrogen chemisorption data are given in Table 4. The catalytic activities increased with increasing Co loading in general (at least to 15 wt%Co). For a similar Co loading, Co catalysts supported on the mixed crystalline phases Al_2O_3 exhibited higher CO hydrogenation activities compared to those supported on the ones containing only γ-phase Al_2O_3. The TOFs of the cobalt catalysts in which the Al_2O_3 support contained only the γ-phase decreased with increasing Co loading, suggesting perhaps an underestimation of exposed Co metal atoms by H_2 chemisorption. However, the TOFs for the mixed crystalline phases Al_2O_3 did not significantly change regardless of cobalt loading percentage. The reaction results are in a good agreement with the H_2 chemisorption results since CO hydrogenation is usually considered to be a structure insensitive reaction [22–26]. Thus, higher dispersion of Co yields higher hydrogenation activity.

4. Conclusions

Nanocrystalline γ-Al_2O_3 and mixed γ- and χ-Al_2O_3 were obtained by decomposition of AIP in 1-butanol by varying the amounts of AIP used under the solvothermal conditions. For a similar Co loading, the presence of χ-phase in γ-Al_2O_3 support resulted in higher dispersion of Co as

Table 4
Reaction rate for CO hydrogenation on Co/Al_2O_3 catalysts

Catalyst samples	CO conversion (%)[a]				Rate (μmol g cat^{-1} s^{-1})[b]				TOF(s^{-1})[b,c]			
	5%Co	10%Co	15%Co	20%Co	5%Co	10%Co	15%Co	20%Co	5%Co	10%Co	15%Co	20%Co
Co/Al-G1	0.5	1.9	8.8	2.1	0.3	1.1	5.2	1.3	–	0.6	0.3	0.2
Co/Al-G2	1.1	2.6	10.0	4.0	0.7	1.6	6.0	2.4	0.4	0.3	0.2	0.1
Co/Al-GC1	2.9	5.5	10.2	7.3	1.7	3.3	6.1	4.3	0.2	0.2	0.2	0.1
Co/Al-GC2	4.0	8.5	10.6	10.7	2.4	5.1	6.3	6.3	0.2	0.1	0.1	0.2

[a] CO hydrogenation was carried out at 220 °C, 1 atm, and H_2/CO/Ar = 80/8/32.
[b] Error of measurement = ±5% as determined directly.
[c] Based on H_2 chemisorption.

well as higher CO hydrogenation activities of the Co/Al_2O_3 catalysts. It is suggested that the spherical-shape like morphology of the χ-phase Al_2O_3 provide better stability of the Co particles, especially for those with high Co loadings.

Acknowledgment

The authors would like to thank the Thailand Research Fund (TRF) for the financial support of this project.

References

[1] R.J. Farrauto, C.H. Bartholomew, Fundamentals of Industrial Catalytic Processes, Blackie Academic & Professional, London, 1997.
[2] K.V.R. Chary, G. Kishan, C.P. Kumar, G.V. Sagar, Appl. Catal. A 246 (2003) 335.
[3] A. Esteban-Cubillo, C. Diaz, A. Fernandez, L.A. Diaz, C. Pecharroman, R. Torrcillas, J.S. Moya, J. Eur. Ceram. Soc. 26 (2006) 1–7.
[4] M. Inoue, H. Kominami, T. Inui, J. Am. Ceram. Soc. 73 (1990) 1100.
[5] M. Inoue, H. Kominami, T. Inui, J. Chem. Soc., Dalton Trans. 12 (1991) 3331.
[6] M. Inoue, H. Kominami, T. Inui, J. Am. Ceram. Soc. 75 (1992) 2597.
[7] M. Inoue, H. Kominami, T. Inui, Appl. Catal. A 77 (1993) L25.
[8] M. Inoue, Y. Kondo, T. Inui, Inorg. Chem. 27 (1988) 215.
[9] Y. Deng, X. Zhou, G. Wei, J. Liu, C.W. Nan, S. Zhao, J. Phys. Chem. Solids 63 (2002) 2119.
[10] Y. Deng, G.D. Wei, C.W. Nan, Chem. Phys. Lett. 368 (2003) 639.
[11] O. Mekasuwandumrong, P.L. Silveston, P. Praserthdam, M. Inoue, V. Pavarajarn, W. Tanakulrungsank, Inorg. Chem. Commun. 6 (2003) 930.
[12] R.C. Reuel, C.H. Bartholomew, J. Catal. 85 (1984) 63.
[13] M. Inoue, H. Otsu, H. Kominami, T. Inui, Ind. Eng. Chem. Res. 35 (1995) 295.
[14] P. Praserthdam, M. Inoue, O. Mekasuvandumrong, W. Tanakulrungsank, S. Phatanasri, Inorg. Chem. Commun. 3 (2000) 671.
[15] J.B. Peri, J. Phys. Chem. 69 (1965) 211.
[16] B. Jongsomjit, T. Wongsalee, P. Praserthdam, Mater. Chem. Phys. 92 (2005) 572.
[17] L.B. Backman, A. Rautiainen, A.O.I. Krause, M. Lindblad, Catal. Today 43 (1998) 11.
[18] L.B. Backman, A. Rautiainen, M. Lindblad, A.O.I. Krause, Appl. Catal. A 191 (2000) 55.
[19] G. Jacobs, T.K. Das, Y. Zhang, J. Li, G. Racoillet, B.H. Davis, Appl. Catal. A 223 (2002) 263.
[20] A. Martinez, C. Lopez, F. Marquez, I. Diaz, J. Catal. 220 (2003) 486.
[21] S.A. Hosseini, A. Taeb, F. Feyzi, Catal. Commun. 6 (2005) 233.
[22] V. Ragaini, R. Carli, C.L. Bianchi, D. Lorenzetti, G. Predieri, P. Moggi, Appl. Catal. A 139 (1996) 31.
[23] J. Panpranot, J.G. Goodwin Jr., A. Sayari, Catal. Today 77 (2002) 269.
[24] B.G. Johnson, C.H. Bartholomew, D.W. Goodman, J. Catal. 128 (1991) 231.
[25] E. Iglesia, Appl. Catal. A 161 (1997) 59.
[26] N. Tsubaki, S. Sun, K. Fujimoto, J. Catal. 199 (2001) 236.
[27] K. Pansanga, O. Mekasuwandumrong, J. Panpranot, P. Praserthdam, Korean J. Chem. Eng. 24 (2007) 397.

Dependence of Quenching Process on the Photocatalytic Activity of Solvothermal-Derived TiO_2 with Various Crystallite Sizes

Piyawat Supphasrirongjaroen, Wilasinee Kongsuebchart, Joongjai Panpranot, Okorn Mekasuwandumrong, Chairit Satayaprasert, and Piyasan Praserthdam*

Center of Excellence on Catalysis and Catalytic Reaction Engineering, Department of Chemical Engineering, Faculty of Engineering, Chulalongkorn University, Bangkok, 10330 Thailand

In the present work, the effect of quenching on surface defect and photocatalytic activity of the solvothermal-derived nanocrystalline TiO_2 with average crystallite sizes between 9 and 13 nm was extensively studied. On the basis of CO_2-TPD (TPD = temperature-programmed desorption) and XPS (XPS = X-ray photoelectron spectroscopy) results, it was found that the amount of Ti^{3+} surface defects and photocatalytic activities of the prepared TiO_2 depended strongly on the type of quenching media used in the following order: H_2O_2-RT > H_2O_2-373K > H_2O-RT > H_2O-373K > air-RT > air-373K, where RT = room temperature. However, the TiO_2 sample that was slowly cooled after calcination (the nonquenched sample) also possessed a significant amount of Ti^{3+} surface defects and high photocatalytic activity to a degree similar to that quenched in H_2O-RT. The effect of quenching was more pronounced on the smaller crystallite size TiO_2 than on the larger ones due probably to its higher surface energy so that oxygen atoms were released more easily.

1. Introduction

Titanium(IV) dioxide or titania (TiO_2) has been the focus of many research interests during the past decade due to its scientific and technological importance. It is a low-cost, widely available, nontoxic, and biocompatible substance that is widely used in domestic applications (e.g., increasing paint durability, cleaning wastewaters, etc.).[1−2] It has been demonstrated to be useful in various areas because of its versatile properties such as catalytic activity,[3] photocatalytic activity for pollutant removal,[4] good stability toward adverse environment,[5] sensitivity to humidity and gas,[6] dielectric character,[7] photoelectrochemical conversion,[8] nonlinear optics,[9] and photoluminescence.[10] TiO_2 has been an important component for cosmetics, pigments, filter coating, gas and humidity sensors, dielectric ceramics, catalyst support, solar cells, and so on.[11] Its performance in these applications depends to a large extent on its physical and chemical properties which are related to the synthetic conditions. These conditions dictate the properties such as crystal structure, morphology, grain size, thermal stability, and surface structure of the TiO_2 products.

The photocatalytic activity of TiO_2 is greatly influenced by its crystal structure, particle size, surface area, incident light intensity, and porosity. Among these factors, crystal structure and crystallinity of TiO_2 are considered the important factors. Amorphous titania has negligible photocatalytic activity because of the recombination between the pair of photoexcited electron and hole in the amorphous structure.[12] Anatase crystalline TiO_2 is generally accepted to have significant photocatalytic activity. However, much effort indicates that rutile TiO_2 and metal-doped rutile TiO_2 also exhibit high photocatalytic activity especially under visible light irradiation.[13−15] With the decrease in particle size of powder to nanometer scale, the catalytic activity of titania is enhanced because the optical band gap is widened due to surface defect[16,17] and an increased in surface area.[18,19]

Many methods have been proposed to synthesize nanaocrystalline TiO_2 in anatase polymorph such as sol−gel[20] and hydrothermal method.[21] Although the sol−gel method is widely used to prepare nanosized TiO_2, calcination of the gel inevitably causes the grain growth and reduction in the specific surface area of the TiO_2 particles and even induces phase transformation. Solvothermal synthesis, in which chemical reactions can occur in aqueous or organic media under the self-produced pressure at low temperature (usually lower than 250 °C), can solve those problems encountered during the sol−gel process.[22] This method has been used to successfully synthesize various types of nanosized metal oxides with large surface area, high crystallinity, and high thermal stability.[23−24]

In the present work, nanocrystalline TiO_2 powders with various crystallite sizes (9−13 nm) were prepared by the solvothermal method using titanium butoxide as the precursor. Then the TiO_2 products were subjected to a rapid quenching process in various quenching media such as air, water, and hydrogen peroxide at two different temperatures (303 and 373 K). The quenching process has shown to result in a variety of surface defects, strains, and reconstructions of materials.[25] It is believed that surface defects on the TiO_2 samples as well as their photocatalytic acitivity can be modified by rapid quenching process. The properties of TiO_2 samples were characterized using various analytical methods such as X-ray diffraction (XRD), N_2 physisorption, CO_2-temperature programmed desorption (CO_2-TPD), and X-ray photoelectron spectroscopy (XPS). Photocatalytic activity of the TiO_2 was tested in gas-phase decomposition of ethylene under UV irradiation.

2. Experimental Section

2.1. Preparation of Nanocrystalline TiO_2. Nanocrystalline TiO_2 was prepared using the solvothermal method according to that of Payakgul et al.[26] using titanium(IV) *n*-butoxide (TNB) as starting material. In general, an amount of 15−25 g of TNB was suspended in 100 cm^3 of toluene in a test tube, which was then placed in a 300 cm^3 autoclave. The gap between the test tube and the autoclave wall was filled with 30 cm^3 of the same solvent used in the test tube. The autoclave was purged completely by nitrogen before heating up to the desired temperature, in the range of 573−593 K at a rate of 2.5 K/min.

* To whom all correspondence should be addressed. Tel.: 66-2218-6883. Fax: 66-2218-6877. E-mail: piyasan.p@chula.ac.th.

10.1021/ie070705a CCC: $40.75
Published on Web 01/10/2008

Table 1. Phase Compositions and Structural Properties of the TiO_2 Synthesized by Solvothermal Method after Quenching in Various Media

synthesis conditions	quenching medium	crystallite size (nm)	S_{BET} (m^2/g)	sample nomenclature
TNB, 15 g	air at 373 K	8.6	96	9A
toluene, 100 mL	air at RT*	9.4	94	9B
temp, 573 K	H_2O at 373 K	9.0	99	9C
holding time, 30 min	H_2O at RT	8.9	104	9D
	H_2O_2 at 373 K	10.0	92	9E
	H_2O_2 at RT	10.5	91	9F
TNB, 25 g	air at 373 K	9.6	85	11A
toluene, 100 mL	air at RT	10.6	93	11B
temp, 573 K	H_2O at 373 K	10.4	95	11C
holding time, 2 h	H_2O at RT	10.5	112	11D
	H_2O_2 at 373 K	13.2	90	11E
	H_2O_2 at RT	13.3	94	11F
TNB, 15 g	air at 373 K	10.4	60	13A
toluene, 100 mL	Air at RT	13.4	67	13B
temp, 593 K	H_2O at 373 K	13.4	67	13C
holding time, 6 h	H_2O at RT	13.2	69	13D
	H_2O_2 at 373 K	14.6	61	13E
	H_2O_2 at RT	14.7	63	13F

Autogenously pressure during the reaction gradually increased as the temperature was raised. Once the prescribed temperature was reached, the temperature was held constant for 0.5−6 h. After the system was cooled down, the resulting powders were repeatedly washed with methanol and dried in air.

2.2. Quenching Process. Prior to quenching, the synthesized TiO_2 was dried in air atmosphere at 573 K with a heating rate of 10 K/min for 1 h, and then it was taken out and immediately quenched in various quenching media. In this study, both liquid-phase and gas-phase media were employed. For quenching in gas-phase media, air at room temperature and 373 K were used (samples A and B). For quenching in liquid-phase media, hydrogen peroxide at room temperature and 373 K (samples C and D) and water at room temperature and 373 K (samples E and F) were used. After the samples were quenched in the media for 30 min, all the TiO_2 samples were dried in air at room temperature and stored in a desiccator.

2.3. Characterization. The XRD patterns of the TiO_2 samples were recorded using a SIEMENS D5000 X-ray diffractometer using Cu Kα radiation with a Ni filter in the range of 20−80° 2θ. The crystallite size of TiO_2 was determined from half-height width of the 101 diffraction peak of anatase using the Scherrer equation. The specific surface area (S_{BET}) was calculated using BET single-point method on the basis of nitrogen (N_2) uptake measured at 77 K in a Micromeritics ASAP 2000. Temperature-programmed desorption using CO_2 as a probe molecule was performed to determine the Ti^{3+} site existing on the surface of TiO_2 particle.[27] It was carried out using 0.05 g of a TiO_2 sample. TiO_2 was dosed by 1 vol % CO_2 in helium for 1 h and then desorbed from 143 to 273 K with the rate of 21.5 K/min. The XPS measurement was carried out using an AMICUS photoelectron spectrometer equipped with an Mg Kα X-ray as a primary excitation and KRATOS VISION2 software. XPS elemental spectra were acquired with 0.1 eV energy step at a pass energy of 75 kV. All the binding energies were referenced to the C 1s peak at 285.0 eV of the surface adventitious carbon.

2.4. Photocatalytic Activity Measurement. Catalytic decomposition of ethylene was carried out in order to determine photocatalytic activity of the TiO_2 using a horizontal quartz fixed bed reactor. High purity grade air containing 0.1 vol % ethylene was continuously fed at a constant flow rate with a gas hourly space velocity (GHSV) of 120 h^{-1}. An air stream with 0.1 vol % ethylene was first passed through the reactor without irradiation until reaching gas−solid adsorption equilibrium.

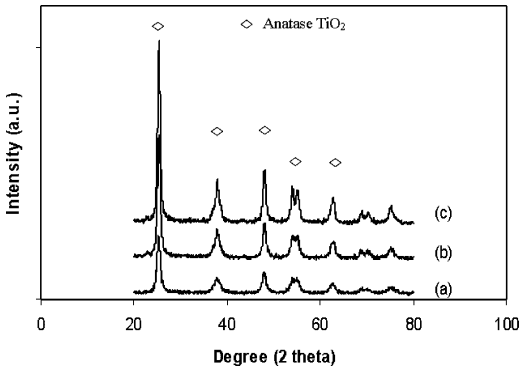

Figure 1. The XRD patterns of the various TiO_2 samples after quenching in air at room temperature: (a) 9 nm, (b) 11 nm, (c) 13 nm.

Then, UV light was irradiated on the surface of the catalyst using a 500 W mercury lamp (Philips, HPL-N). The outlet gas was taken every 30 min. Its composition was analyzed using a Shimadzu GC-14B gas chromatograph equipped with the flame-ionized detector until the reaction reached steady state.

3. Results and Discussion

3.1. Structure and Surface Properties of TiO_2 Quenched in Different Media. In this study, the effects of quenching medium as well as quenching temperature on the properties of nanocrystalline TiO_2 synthesized by solvothermal method are extensively investigated. Quenching process was applied as a postsynthesis treatment with the aims being to create more defects on the TiO_2 surface and, as a consequence, improve their photocatalytic activities. Physical properties of the various TiO_2 such as the BET surface areas and the average TiO_2 crystallite sizes after quenching in different media are shown in Table 1. Due to the different preparation conditions, the TiO_2 samples possessed different crystallite sizes and specific surface areas. The average crystallite size of TiO_2 samples increased from 9 to 13 nm as the BET surface area of the TiO_2 samples decreased from ca. 95 to 65 m^2/g. Quenching treatment, however, did not significantly alter the specific surface area and the average crystallite size of the TiO_2. The anatase TiO_2 crystalline phase was preserved after quenching. All the TiO_2 samples consisted of only pure anatase phase TiO_2 (major XRD peaks at 25.36, 37.82, and 48.18° 2θ). XRD patterns of the TiO_2 with various crystallite sizes after quenching in air at room temperature are shown in Figure 1. The crystallite sizes of the TiO_2 from XRD are in good agreement with those observed from the TEM micrographs of the samples (Figure 2).

The surface structure of TiO_2 was characterized by temperature-programmed desorption of CO_2. All the TiO_2 samples exhibited two main desorption peaks at temperatures ca. 145 and 170 K which could be attributed to adsorption of CO_2 on two different structures of TiO_2 surface.[27] For example, the CO_2-TPD profiles of TiO_2 samples with average crystallite size of 11 nm after quenching in various media are shown in Figure 3. The desorption peak at ca. 145 K was attributed to CO_2 molecules binding to the regular five-coordinate Ti^{4+} site which was considered as the perfected TiO_2 structure. The second peak at ca. 170 K has been considered as desorption of CO_2 molecules binding to Ti^{3+} defect sites of TiO_2. On the basis of the CO_2-TPD results, it was found that, for a given TiO_2 crystallite size, the peak areas for CO_2 desorption at ca. 170 K (representing the amount of Ti^{3+} defective sites) depended on the type of quenching media employed in the following order: air at 373 K < air at RT < H_2O at 373 K < H_2O at RT < H_2O_2 at 373

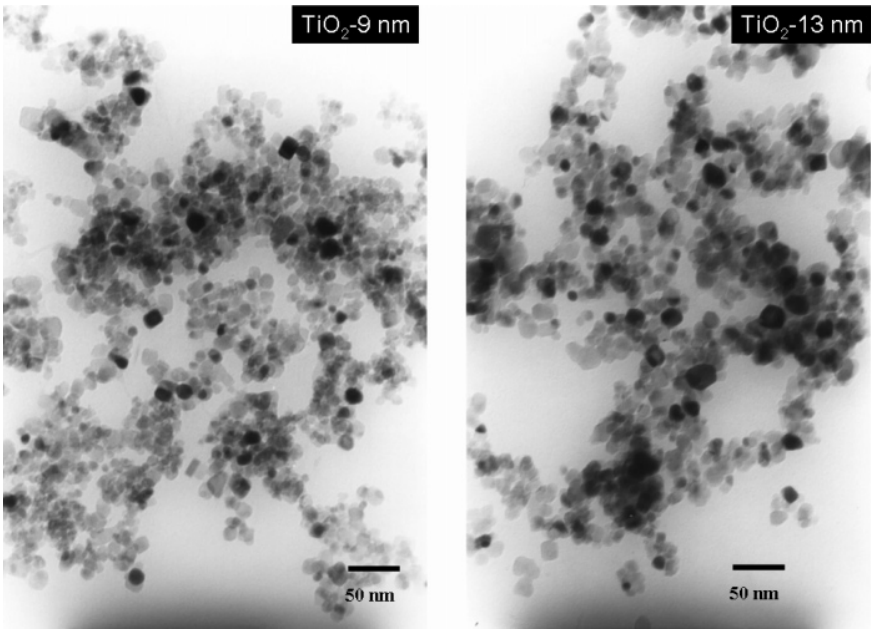

Figure 2. TEM micrographs of TiO_2-9 nm and TiO_2-13 nm (nonquenched).

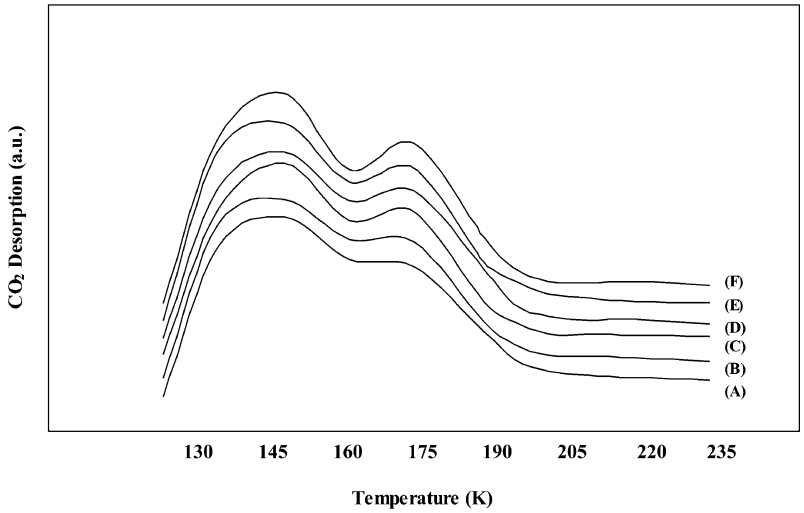

Figure 3. CO_2-temperature-programmed desorption results of the TiO_2-11 nm quenched in different media: (A) air at 373 K, (B) air at RT, (C) H_2O at 373 K, (D) H_2O at RT, (E) H_2O_2 at 373 K, and (F) H_2O_2 at RT (RT = room temperature).

K < H_2O_2 at RT. It is known that quenching treatment of a metal can create nucleation of dislocations, surface defect, and concentration of stress on the metal surface.[28] The results in this study have shown that quenching process can be applied as a postsynthesis treatment for controlling the amount of surface defects on nanocrystalline TiO_2. The Ti^{3+}/Ti^{4+} ratios calculated from CO_2-TPD results of the various quenched TiO_2 samples and the nonquenched one are illustrated in Figure 4. It was found that the nonquenched sample also possessed a significant amount of Ti^{3+} to a degree similar to that quenched in H_2O at room temperature. However, when compared with the TiO_2 sample quenched in H_2O_2 and H_2O, it is noticed that the TiO_2 sample quenched in liquid-phase media that contained more -OH group in molecules exhibited higher Ti^{3+}/Ti^{4+} and higher photocatalytic activity. Recently, Xiao-Quan et al.[29] reported that the trapping site of photogenerated holes or the surface -OH is also an important factor affecting photocatalytic reaction besides the surface Ti^{3+}.

The presence of Ti^{3+} on the TiO_2 samples was also studied by X-ray photoelectron spectroscopy. For example, high-resolution XPS spectra of Ti 2p and O 1s recorded from the TiO_2 samples quenched in H_2O_2 at room temperature are shown in Figure 5. The Ti 2p spectrum can be fitted with Gaussian−Lorentzian functions into two spin−orbit components at binding energies of 457.2, and 459.2 eV, corresponding to Ti_2O_3 (Ti^{3+}) and TiO_2 (Ti^{4+}) fractions on the TiO_2 surface, respectively. The component binding energy values are in agreement with those reported in the literature.[30] The O 1s peak is often believed to be composed of three to five different oxygen species such as Ti−O bonds in TiO_2 and Ti_2O_3, hydroxyl groups, C−O bonds, and adsorbed H_2O. It is shown that the O 1s peak is asymmetric, suggesting that at least three peaks related to three different chemical states of oxygen are present. The binding energies of each individual component are 530.8 (Ti^{4+}−O), 531.8 (Ti^{3+}−O), and 533.3 eV (O−H).[31−32] The shapes of the XPS spectra of Ti 2p and O 1s for all the TiO_2 samples are quite similar,

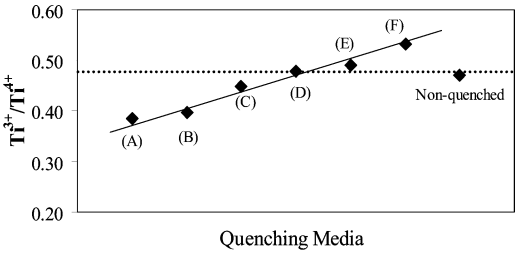

Figure 4. Ti^{3+}/Ti^{4+} ratios calculated from CO_2−TPD results of the TiO_2-11 nm quenched in different media: (A) air at 373 K, (B) air at RT, (C) H_2O at 373 K, (D) H_2O at RT, (E) H_2O_2 at 373 K, and (F) H_2O_2 at RT (RT = room temperature).

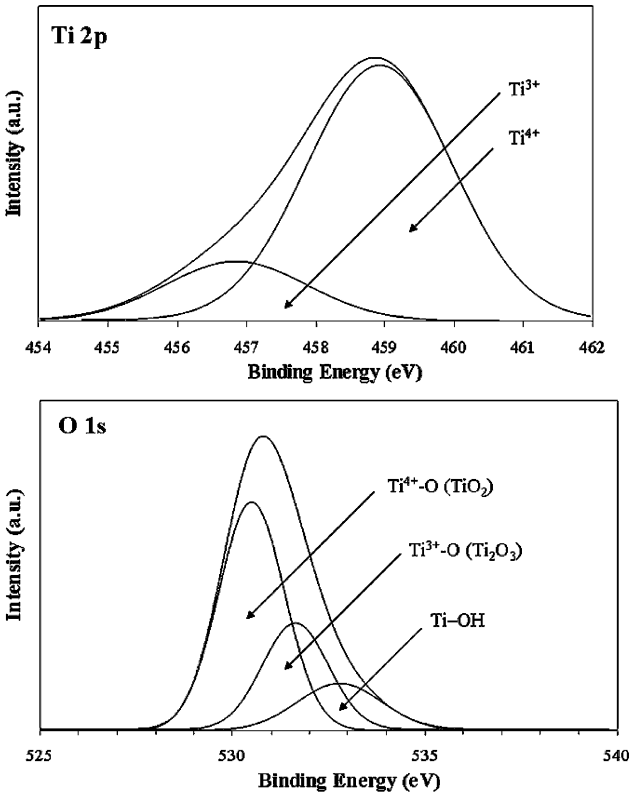

Figure 5. XPS spectra of Ti 2p and O 1s for TiO_2-11 nm quenched in H_2O_2 at room temperature.

and it was found that the amount of surface Ti^{3+} sites increased in a trend similar to those observed from CO_2- TPD results.

In photocatalysis, defect sites on the surface of TiO_2 are known as adsorption sites,[33,34] electronic promoters,[35] or electron traps.[36,37] In general, light irradiation of TiO_2 powder with photon energy larger than the band gap energy produces electrons (e^-) and holes (h^+) in the conduction band and the valence band, respectively.[38,39] These electrons and holes are thought to have the respective abilities to reduce and oxidize chemical species adsorbed on the surface of TiO_2 particles. For a photocatalyst to be most efficient, different interfacial electron processes involving e^- and h^+ must compete effectively with the major deactivation processes involving e^-−h^+ recombination. Surface Ti^{3+} defect sites (oxygen vacancies) are the sites that oxygen adsorption occurs as well as that the photogenerated electrons are trapped,[40−42] so they are effective sites for interface electron transferring. The relationship between the amount of Ti^{3+} defects on TiO_2 surface and their photocatalytic activities has been reported by many authors.[43−46]

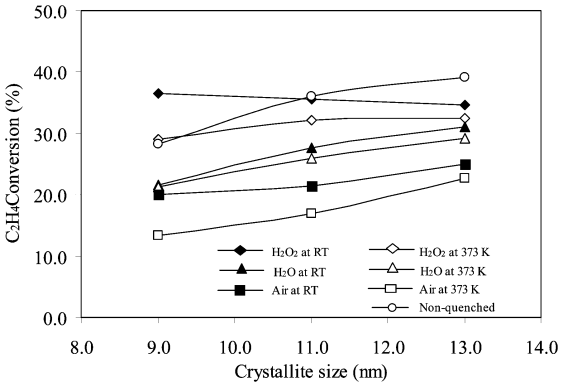

Figure 6. Results of the photocatalytic activities of TiO_2 samples quenched in different media.

3.2. Photocatalytic Activity of the TiO_2 Quenched in Different Media. Photocatalytic activities of the TiO_2 samples with various crystallite sizes after quenching in different media were evaluated in the decomposition of ethylene in gas-phase and the results are shown in Figure 6. Ethylene conversions at steady state (after 180 min of run) for the quenched TiO_2 samples with various crystallite sizes were ranged from ca. 20−37%, while that of TiO_2 Degussa P25 under similar reaction conditions gave ca. 30% ethylene conversion. It was found that, for a given TiO_2 crystallite size, ethylene conversions were strongly dependent on the quenching media and were found to be in the following order: H_2O_2 at RT > H_2O_2 at 373 K > H_2O at RT > H_2O at 373 K > air at RT > air at 373 K. Such results were in good agreement with the amount of Ti^{3+} surface defect on the TiO_2 samples in which those with higher amounts of Ti^{3+} surface defect exhibited higher photocatalytic activities for ethylene decomposition. For a similar quenching medium, the TiO_2 quenched at low temperature resulted in a larger amount of Ti^{3+} and exhibited higher photocatalytic activity compared to those quenched at high temperature. This can probably be explained by a thermal shock effect that a large difference in temperature of the TiO_2 surface and quenching medium can create more surface defects. However, compared to the TiO_2 sample that was slowly cooled down after calcination (the nonquenched sample), only the smaller crystallite size TiO_2 (TiO_2, 9 nm) that quenched in H_2O_2 exhibited higher photocatalytic activities. The effect of quenching was less pronounced on the larger TiO_2 crystallite size and the nonquenched samples showed higher activities.

4. Conclusions

The surface properties and photocatalytic activities of nanosized TiO_2 powders synthesized by solvothermal method with various crystallite sizes (9−13 nm) were significantly influenced by quenching media and quenching conditions. For the use of similar quenching media, the TiO_2 quenched in a low-temperature medium has been shown to result in more Ti^{3+} surface defects on the TiO_2 surface and consequently higher photocatalytic activity than those quenched in a high-temperature one. The amount of Ti^{3+} and photocatalytic activity of the quenched samples depended on the type of quenching medium in the following order: H_2O_2 > H_2O > air. Compared to the nonquenched sample (the one slowly cooled after calcination), quenching in H_2O_2 has shown to result in higher Ti^{3+} and photocatalytic activity of the TiO_2 with small crystallite size (9 nm). There was less effect of quenching on larger crystallite size TiO_2.

Acknowledgment

Financial support from the Thailand Research Fund (TRF) and the Graduate School of Chulalongkorn University is gratefully acknowledged. The authors also thank the Cooperative Research Network (CRN) of the Thai Ministry of Education for the scholarship for P.S.

Literature Cited

(1) Chen, C. H.; Kelder, E. M.; Schoonman, J. Electrostatic sol-spray deposition (ESSD) and characterization of nanostructured TiO_2 thin films. *Thin Solid Films* **1999**, *342*, 35.

(2) Ollis, D. E., Al-Ekabi, H., Eds. *Photocatalitic Purification and Treatment of Water and Air*; Elsevier: Amsterdam, 1993.

(3) Tsubota, S.; Nakamura, T.; Tanaka, K.; Haruta, M. Effect of calcination temperature on the catalytic activity of Au colloids mechanically mixed with TiO_2 powder for CO oxidation. *Catal. Lett.* **1998**, *56*, 131.

(4) Senogles, P.-J.; Scott, J. A.; Shaw, G.; Stratton, H. Photocatalytic degradation of the cyanotoxin cylindrospermopsin, using titanium dioxide and UV irradiation. *Water Res.* **2001**, *35*, 1245.

(5) Tonejc, A. M.; Goti, M.; Grŵeta, B.; Musicì, S.; Popovi, S.; Trojko, R.; Turkovi, A.; MuSêvicì, I. Transmission electron microscopy studies of nanophase TiO_2. *Mater. Sci. Eng. B* **1993**, *40* 177.

(6) Traversa, E.; Gnappi, G.; Montenero, A.; Gusmano, G. Ceramic thin films by sol-gel processing as novel materials for integrated humidity sensors. *Sens. Actuators B* **1996**, *31*, 59.

(7) Ohtani, B.; Nishimoto, S.-I; Effect of surface adsorptions of aliphatic alcohols and silver ion on the photocatalytic activity of TiO_2 suspended in aqueous solutions. *J. Phys. Chem*. **1993**, *97*, 920.

(8) Raja, K. S.; Mahajan, V. K.; Misra, M. Determination of photo conversion efficiency of nanotubular titanium oxide photo-electrochemical cell for solar hydrogen generation. *J. Power Sources* **2006**, *159*, 1258.

(9) O'Regan, B.; Grätzel, M. A low-cost, high-efficiency solar cell based on dye-sensitized colloidal TiO_2 films. *Nature* **1991**, *353*, 737.

(10) Fujihara, K.; Izumi, S.; Ohno, T.; Matsumura, M. Time-resolved photoluminescence of particulate TiO_2 photocatalysts suspended in aqueous solutions. *J. Photochem. Photobiol., A* **2000**, *132*, 99.

(11) Ha, H. Y.; Nam, S. W.; Lim, T. H.; Oh, I.-H.; Hong, S.-A. Properties of the TiO_2 membranes prepared by CVD of titanium tetraisopropoxide. *J. Membr. Sci.* **1996**, *111*, 81.

(12) Ohtani, B.; Ogawa, Y.; Nishimoto, S.-I. Photocatalytic activity of amorphous-anatase mixture of titanium(IV) oxide particles suspended in aqueous solutions. *J. Phys. Chem. B* **1997**, *101*, 3746.

(13) Liu, H.; Gao, L. Co-doped rutile TiO_2 as a new photocatalyst for visible light irradiation *Chem. Lett.* **2004**, *33*, 730.

(14) Sopyan, I.; Watanabe, M; Murasawa, S; Hashimoto, K.; Fujishima, A. Efficient TiO_2 powder and film photocatalysts with rutile crystal structure *Chem. Lett.* **1996**, *25*, 69.

(15) Liu, H. Y.; Gao, L. Synthesis and properties of CdSe-sensitized rutile TiO_2 nanocrystals as a visible light-responsive photocatalyst. *J. Am. Ceram. Soc.* **2005**, *88*, 1020.

(16) Shifu, C.; Gengyu, C. The effect of different preparation conditions on the photocatalytic activity of TiO_2·SiO_2/beads. *Surf. Coat. Technol.* **2006**, *200*, 3637.

(17) Suriye, K.; Praserthdam, P.; Jongsomjit, B. Impact of Ti^{3+} present in titania on characteristics and catalytic properties of the Co/TiO_2 catalyst. *Ind. Eng. Chem. Res.* **2005**, *44*, 6599.

(18) Madhusudan Reddy, K.; Gopal Reddy, C. V.; Manorama, S. V. Preparation, characterization, and spectral studies on nanocrystalline anatase TiO_2. *J. Solid State Chem.* **2001**, *158*, 180.

(19) Toyoda, T.; Kawano, H.; Shen, Q.; Kotera, A.; Ohmori, M. Characterization of electronic states of TiO_2 powders by photoacoustic spectroscopy. *Jpn. J. Appl. Phys., Part 1* **2000**, *39*, 3160.

(20) Alam, M. J.; Cameron, D. C. Preparation and characterization of TiO_2 thin films by sol-gel method. *J. Sol-Gel Sci. Technol.* **2002**, *25*, 137.

(21) Kolen'ko, Y. V.; Burukhin, A. A.; Churagulov, B. R.; Oleynikov, N. N. Synthesis of nanocrystalline TiO_2 powders from aqueous $TiOSO_4$ solutions under hydrothermal conditions. *Mater. Lett.* **2003**, *57*, 1124.

(22) Carp, O.; Huisman, C. L.; Reller, A. Photoinduced reactivity of titanium dioxide. *Prog. Solid State Chem.* **2004**, *32*, 33.

(23) Kongwudthiti, S.; Praserthdam, P.; Silveston, P. L.; Inoue, M. Influence of synthesis conditions on the preparation of zirconia powder by the glycothermal method. *Ceram. Int.* **2003**, *29*, 807.

(24) Mekasuwandumrong, O.; Silveston, P. L.; Praserthdam, P.; Inoue, M.; Pavarajarn, V.; Tanakulrungsank, W. Synthesis of thermally stable micro spherical χ-alumina by thermal decomposition of aluminum isopropoxide in mineral oil. *Inorg. Chem. Commun.* **2003**, *6*, 930.

(25) Henderson, M. A. An HREELS and TPD study of water on TiO_2-(110): The extent of molecular versus dissociative adsorption. *Surf. Sci.* **1996**, *355*, 151.

(26) Payakgul, W.; Mekasuwandumrong, O.; Pavarajarn, V.; Praserthdam, P. Effects of reaction medium on the synthesis of TiO_2 nanocrystals by thermal decomposition of titanium (IV) n-butoxide. *Ceram. Int.* **2005**, *31*, 391.

(27) Thompson, T. L.; Diwald, O.; Yates, J. T., Jr. CO_2 as a probe for monitoring the surface defects on TiO_2(110)-temperature-programmed desorption. *J. Phys. Chem. B* **2003**, *107*, 11700.

(28) Watson, S. S.; Beydoun, D.; Scott, J. A.; Amal, R. The effect of preparation method on the photoactivity of crystalline titanium dioxide particles. *Chem. Eng. J.* **2003**, *95*, 213.

(29) Xiao-Quan, C.; Huan-Bin, L.; Guo-Bang, G., Preparation of nanometer crystalline TiO_2 with high photocatalytic activity by pyrolysis of titanyl organic compounds and photo-catalytic mechanism. *Mater. Chem. Phys.* **2005**, *91*, 317.

(30) Kumar, P. M.; Badrinarayanan, S.; Sastry, M. Nanocrystalline TiO_2 studied by optical, FTIR and X-ray photoelectron spectroscopy: Correlation to presence of surface states. *Thin Solid Films* **2000**, *358*, 122.

(31) Yu, J.; Zhao, X.; Zhao, Q. Effect of surface structure on photocatalytic activity of TiO_2 thin films prepared by sol-gel method. *Thin Solid Films* **2000**, *379*, 7.

(32) Pouilleau, J.; Devilliers, D.; Groult, H.; Marcus, P. Surface study of a titanium-based ceramic electrode material by X-ray photoelectron spectroscopy. *J. Mater. Sci.* **1997**, *32*, 5645.

(33) Diebold, U. The surface science of titanium dioxide. *Surf. Sci. Rep.* **2003**, *48*, 53.

(34) Sorescu, D. C.; Yates, Jr., J. T. First principles calculations of the adsorption properties of CO and NO on the defective TiO_2(110) surface. *J. Phys. Chem. B* **2002**, *106*, 6184.

(35) Liu, G.; Rodriguez, J. A.; Hrbek, J.; Long, B. T.; Chen, D. A. Interaction of thiophene with stoichiometric and reduced rutile TiO_2(110) surfaces: Role of Ti^{3+}sites in desulfurization activity. *J. Mol. Catal. A* **2003**, *202*, 215.

(36) Sakai, N.; Fujishima, A.; Watanabe, T.; Hashimoto, K. Enhancement of the photoinduced hydrophilic conversion rate of TiO_2 film electrode surfaces by anodic polarization. *J. Phys. Chem. B* **2001**, *105*, 3023.

(37) Park, D.- R.; Zhang, J.; Ikeue, K.; Yamashita, H.; Anpo, M.; Photocatalytic oxidation of ethylene to CO_2 and H_2O on ultrafine powdered TiO_2 photocatalysts in the presence of O_2 and H_2O. *J. Catal.* **1999**, *185*, 114

(38) Schwitzgebel, J.; Ekerdt, J. G.; Gerischer, H.; Heller, A. Role of the oxygen molecule and of the photogenerated electron in TiO_2-photocatalyzed air oxidation reactions. *J. Phys. Chem.* **1995**, *95*, 5633.

(39) Brinkley, D.; Engel, T. Active site density and reactivity for the photocatalytic dehydrogenation of 2-propanol on TiO_2 (110). *Surf. Sci.* **1998**, *415*, 1001.

(40) Diebold, U.; Lehman, J.; Mahmoud, T.; Kuhn, M.; Leonardelli, G.; Hebenstreit, W.; Schmid, M.; Varga, P. Intrinsic defects on a TiO_2-(110)(1 × 1) surface and their reaction with oxygen: A scanning tunneling microscopy study. *Surf. Sci.* **1998**, *411*, 137.

(41) Schaub, R.; Thostrup, P.; Lopez, N.; Lægsgaard, E.; Stensgaard, I.; Nørskov, J. K.; Besenbacher, F. Oxygen vacancies as active sites for water dissociation on rutile TiO_2(110). *Phys. Rev. Lett.* **2001**, *87*, 2661041.

(42) Schaub, R.; Wahlström, E., Rønnau, A., Lægsgaard, E.; Stensgaard, I.; Besenbacher, F. Oxygen-mediated diffusion of oxygen vacancies on the TiO_2(110) surface. *Science* **2003**, *299*, 377.

(43) Li, F. B.; Li, X. Z. Photocatalytic properties of gold/gold ion-modified titanium dioxide for wastewater treatment. *Appl. Catal. A-Gen.* **2002**, *228*, 15.

(44) Li, F. B.; Li, X. Z.; Ao, C. H.; Lee, S. C.; Hou, M. F. Enhanced photocatalytic degradation of VOCs using Ln^{3+}-TiO_2 catalysts for indoor air purification. *Chemosphere* **2005**, *59*, 787.

(45) Kongsuebchart, W.; Praserthdam, P.; Panpranot, J.; Sirisuk, A.; Supphasrirongjaroen, P.; Satayaprasert, C. Effect of crystallite size on the surface defect of nano-TiO_2 prepared via solvothermal synthesis. *J. Cryst. Growth* **2006**, *297*, 234.

(46) Suriye, K.; Praserthdam, P.; Jongsomjit, B. Control of Ti^{3+} surface defect on TiO_2 nanocrystal using various calcination atmospheres as the first step for surface defect creation and its application in photocatalysis. *Appl. Surf. Sci.* **2007**, *253*, 3849.

Received for review May 17, 2007
Revised manuscript received September 5, 2007
Accepted October 17, 2007

IE070705A